UNIVERSITY OF CALIFORNIA SAN DIEGO

Discovery of pH-Dependent Protease Cleavage Properties leads to the Rational Design of Neutral pH-Selective Inhibitor of Cathepsin B involved in Human Diseases

A Dissertation submitted in partial satisfaction of the requirements
for the degree Doctor of Philosophy

in

Biomedical Sciences

by

Michael C. Yoon

Committee in charge:

Professor Vivian Hook, Chair
Professor Anthony J. O'Donoghue, Co-Chair
Professor Michael D. Burkart
Professor Michael K. Gilson
Professor Gentry N. Patrick

2022

The Dissertation of Michael C. Yoon is approved, and it is acceptable in quality and form for publication on microfilm and electronically.

University of California San Diego

2022

DEDICATION

This dissertation is dedicated to my parents, brother, friends, and wife.

Thank you all for your support.

EPIGRAPH

Trust in the Lord with all your heart,
and do not lean on your own understanding.
In all your ways acknowledge him,
and he will make straight your paths.

Proverbs 3:5-6

TABLE OF CONTENTS

LIST OF FIGURES

LIST OF TABLES

ACKNOWLEDGEMENTS

I would like to thank my PhD advisors, Drs. Vivian Hook and Anthony O'Donoghue for their mentorship, guidance, and support. I have been fortunate to be co-mentored by two advisors with expertise in their fields of neuroscience and enzymology, respectively. I am especially grateful for them for their approachability and encouragement for me to persevere during the difficulties of my PhD journey.

I would also like to thank my current and former colleagues: Zhenze Jiang, Christopher Lietz, Sonia Podvin, Charles Mosier, Von Phan, and Tom Toneff for helping me learn basic skills in the laboratory to start off my research. Special thanks to Zhenze and Christopher for helping me understand the difficult concepts of mass spectrometry and helping me with writing valuable scripts that has made it easier for me to process the enormous amounts of data generated from my research.

Next, I would like to thank our collaborators, William Gerwick, Mitchell Christy, Dennis Wolan, and Angelo Solania. Their expertise in molecular docking and chemical synthesis really helped drive my project forward.

Most importantly, I would like to thank my wife, Stephanie Yoon, and church family for providing me the emotional and spiritual support to help me endure throughout the rigorous PhD and PharmD program here at UC San Diego.

And finally, this dissertation would not have been possible without the financial support from NIH grants (R01NS109075 and T32GM067550) and the scholarships generously provided by the UC San Diego Skaggs School of Pharmacy and Pharmaceutical Sciences PharmD/PhD program. I am also grateful for the UC San Diego Biomedical Sciences Graduate Program that provided me the resources and environment to successfully complete the requirements of the PhD.

Chapter 2, in full, is a reprint of the material as it appears in ACS Chemical Biology 2021 coauthored with Yoon MC, Solania A, Jiang Z, Christy MP, Podvin S, Mosier C, Lietz CB, Ito G, Gerwick WH, Wolan DW, Hook G, O'Donoghue AJ, Hook V. The dissertation author was the primary researcher and author of this material.

Chapter 3, in full, is a reprint of the material as it appears in ACS Biochemistry 2022 coauthored with Yoon MC, Christy MP, Phan VV, Gerwick WH, Hook G, O'Donoghue AJ, Hook V. The dissertation author was the primary researcher and author of this material.

Chapter 4, in full, is a reprint of the material as it appears in ACS Biochemistry 2022 coauthored with Yoon MC, Hook V, O'Donoghue AJ. The dissertation author was the primary researcher and author of this material.

Chapter 5, in full, is a reprint of the material as it appears in ACS Chemical Neuroscience 2021 coauthored with Jiang Z, Lietz CB, Podvin S, Yoon MC, Toneff T, Hook V, O'Donoghue AJ. The dissertation author was the co-author of this material.

Chapter 6, in full, is a reprint of the material as it appears in ACS Chemical Neuroscience 2022 coauthored with Yoon MC, Ames J, Mosier C, Jiang Z, Podvin S, O'Donoghue AJ, Hook V. The dissertation author was the primary researcher and author of this material.

VITA

2008 – 2012 Bachelor of Science in Chemistry, summa cum laude, Stony Brook University

2017 – 2022 Doctor of Philosophy in Biomedical Sciences, University of California San Diego

PUBLICATIONS

Colbert J, McBane S, Lam MS, Blaj A, Zimmers B, **Yoon MC**, Park B, Le T, Dinh H, Wang J; Assessing the Acceptance of the Pay-For-Performance Model in a Segment of California Pharmacists. *Journal of Contemporary Pharmacy Practice* 2018, 65 (3): 37–42. Jun 1.

Gauglitz JM, Aceves CM, Aksenov AA, Aleti G, Almaliti J, Bouslimani A, Brown EA, Campeau A, Caraballo-Rodríguez AM, Chaar R, da Silva RR, Demko AM, Di Ottavio F, Elijah E, Ernst M, Ferguson LP, Holmes X, Jarmusch AK, Jiang L, Kang KB, Koester I, Kwan B, Li J, Li Y, Melnik AV, Molina-Santiago C, Ni B, Oom AL, Panitchpakdi MW, Petras D, Quinn R, Sikora N, Spengler K, Teke B, Tripathi A, Ul-Hasan S, van der Hooft JJJ, Vargas F, Vrbanac A, Vu AQ, Wang SC, Weldon K, Wilson K, Wozniak JM, **Yoon MC**, Bandeira N, Dorrestein PC. Untargeted mass spectrometry-based metabolomics approach unveils molecular changes in raw and processed foods and beverages. *Food Chem*. 2020 Jan 1;302:125290. PMID: 31404873.

Hook V, **Yoon MC**, Mosier C, Ito G, Podvin S, Head BP, Rissman R, O'Donoghue AJ, Hook G. Cathepsin B in neurodegeneration of Alzheimer's disease, traumatic brain injury, and related brain disorders. *Biochim Biophys Acta Proteins Proteom*. 2020 Aug;1868(8):140428. PMID: 32305689.

Mellott DM, Tseng CT, Drelich A, Fajtová P, Chenna BC, Kostomiris DH, Hsu J, Zhu J, Taylor ZW, Kocurek KI, Tat V, Katzfuss A, Li L, Giardini MA, Skinner D, Hirata K, **Yoon MC**, Beck S, Carlin AF, Clark AE, Beretta L, Maneval D, Hook V, Frueh F, Hurst BL, Wang H, Raushel FM, O'Donoghue AJ, de Siqueira-Neto JL, Meek TD, McKerrow JH. A Clinical-Stage Cysteine Protease Inhibitor blocks SARS-CoV-2 Infection of Human and Monkey Cells. *ACS Chem Biol.* 2021 Apr 16;16(4):642-650. doi: 10.1021/acschembio.0c00875. Epub 2021 Mar 31. PMID: 33787221.

Ashhurst AS, Tang AH, Fajtová P, **Yoon MC**, Aggarwal A, Bedding MJ, Stoye A, Beretta L, Pwee D, Drelich A, Skinner D, Li L, Meek TD, McKerrow JH, Hook V, Tseng CT, Larance M, Turville S, Gerwick WH, O'Donoghue AJ, Payne RJ. Potent Anti-SARS-CoV-2 Activity by the Natural Product Gallinamide A and Analogues via Inhibition of Cathepsin L. *J Med Chem.* 2022 Feb 24;65(4):2956-2970. doi: 10.1021/acs.jmedchem.1c01494. Epub 2021 Nov 3. PMID: 34730959.

Jiang Z, Lietz CB, Podvin S, **Yoon MC**, Toneff T, Hook V, O'Donoghue AJ. Differential Neuropeptidomes of Dense Core Secretory Vesicles (DCSV) Produced at Intravesicular and Extracellular pH Conditions by Proteolytic Processing. *ACS Chem Neurosci.* 2021 Jul 7;12(13):2385-2398. doi: 10.1021/acschemneuro.1c00133. Epub 2021 Jun 21. PMID: 34153188.

Yoon MC, Solania A, Jiang Z, Christy MP, Podvin S, Mosier C, Lietz CB, Ito G, Gerwick WH, Wolan DW, Hook G, O'Donoghue AJ, Hook V. Selective Neutral pH Inhibitor of Cathepsin B Designed Based on Cleavage Preferences at Cytosolic and Lysosomal pH Conditions. *ACS Chem Biol*. 2021 Sep 17;16(9):1628-1643. doi: 10.1021/acschembio.1c00138. Epub 2021 Aug 20. PMID: 34416110.

Yoon MC, Ames J, Mosier C, Jiang Z, Podvin S, O'Donoghue AJ, Hook V. Distinct Dibasic Cleavage Specificities of Neuropeptide-Producing Cathepsin L and Cathepsin V Cysteine Proteases Compared to PC1/3 and PC2 Serine Proteases. *ACS Chem Neurosci.* 2022 Jan 19;13(2):245-256. doi: 10.1021/acschemneuro.1c00653. Epub 2022 Jan 5. PMID: 34986304.

Yoon MC, Christy MP, Phan VV, Gerwick WH, Hook G, O'Donoghue AJ, Hook V. Molecular Features of CA-074 pH-Dependent Inhibition of Cathepsin B. *Biochemistry*. 2022 Feb 15;61(4):228-238. doi: 10.1021/acs.biochem.1c00684. Epub 2022 Feb 4. PMID: 35119840.

Phan VV, Mosier C, **Yoon MC**, Glukhov E, Caffrey CR, O'Donoghue AJ, Gerwick WH, Hook V. Discovery of pH-Selective Marine and Plant Natural Product Inhibitors of Cathepsin B Revealed by Screening at Acidic and Neutral pH Conditions. *ACS Omega.* 2022 Jul 12;7(29):25346-25352. doi: 10.1021/acsomega.2c02287. PMID: 35910167.

Yoon MC, Hook V, O'Donoghue AJ. Cathepsin B Dipeptidyl Carboxypeptidase and Endopeptidase Activities Demonstrated across a Broad pH Range. *Biochemistry*. 2022 Aug 18. doi: 10.1021/acs.biochem.2c00358. Epub ahead of print. PMID: 35981509.

Yoon MC, Hook V, O'Donoghue AJ. Multiplex Substrate Profiling by Mass Spectrometry of Cysteine Proteases Identifies Unique Cleavage Specificities of Cathepsin B, V, L, K, S, and X. In preparation

ABSTRACT OF THE DISSERTATION

Discovery of pH-Dependent Protease Cleavage Properties leads to the Rational Design of Neutral pH-Selective Inhibitor of Cathepsin B involved in Human Diseases

by

Michael C. Yoon

Doctor of Philosophy in Biomedical Sciences

University of California San Diego, 2022

Professor Vivian Hook, Chair
Professor Anthony J. O'Donoghue, Co-Chair

Cathepsin B (CatB) is a cysteine protease that is abundant in the lysosome of cells and is responsible for degradation of proteins to maintain cellular homeostasis. However, in certain pathogenic conditions such as cancer, neurodegenerative brain disorders, autoinflammatory, and pathogen-induced pyroptosis, CatB can be found outside the lysosome. Most lysosomal enzymes are optimally active at the acidic pH of lysosomes and become inactivated at neutral pH outside the lysosome. However, CatB retains good stability and catalytic activity at extra-lysosomal pH conditions such as the cytosol where it has been shown to participate in cellular apoptotic and inflammatory pathways. This has led to the hypothesis that translocation of CatB from the

lysosome to either the cytosol, nucleus, or extracellular environment contributes to the pathogenesis of various diseases. To investigate such hypothesis, we sought to develop inhibitor probes of CatB that are selective for this protease at either neutral pH or acidic pH. In parallel, we aimed to develop inhibitor probes that are specific to CatB over related cathepsins. We found that established inhibitors such as E64c target CatB but also potently inhibit other cysteine cathepsins. CA-074 is an established selective inhibitor for CatB but we discovered that it is over 100-fold more potent at pH 4.6 than pH 7.2. We then proposed that it is possible to develop an inhibitor that is the converse of CA-074—being more potent at pH 7.2 than pH 4.6. This is based on the hypothesis that CatB may have distinct substrate and inhibitor interactions at different pH conditions. To evaluate this hypothesis, we profiled the cleavage specificity of CatB at pH 4.6 and pH 7.2, along with other related cathepsins, and developed substrates that are cleaved by CatB better at neutral pH than at acidic pH and not cleaved by other related cathepsins. We then modified the substrate with a cysteine reactive warhead to successfully develop a novel inhibitor that potently and selectively inhibits CatB at neutral pH to be used as a molecular probe for the investigation of extra-lysosomal CatB pathogenic role in various cell-death and inflammatory pathways of human diseases.

CHAPTER 1 – INTRODUCTION

1.1 Need for Uncovering Novel Pathogenic Mechanisms of Alzheimer's Disease, Traumatic Brain Injury, and other related human diseases

Alzheimer disease (AD) is an age-related form of dementia that affects tens of millions of patients in the US and is the 6th leading cause of death. (1) There is a critical need for more effective therapeutic drugs to treat AD as well as AD-related dementia (ADRD) including traumatic brain injury (TBI). A notable risk factor for AD is TBI, as there is a greater propensity for patients with TBI to develop AD behavioral dysfunctions and neurodegeneration. (2,3) This suggests that TBI and AD shares a common underlying disease pathogenesis (4) involving cell death, neuroinflammation (5–8) and synaptic dysfunction. (9) My dissertation addresses the critical need to uncover novel pathogenic mechanisms of AD, TBI, and other related diseases, which will be achieved through the development of a neutral pH selective inhibitor of cathepsin B (CatB) to be used a molecular probe for the investigation of extra-lysosomal CatB's involvement and mechanistic role in the pathogenesis of brain disorders such as AD and TBI (Figure 1.0).

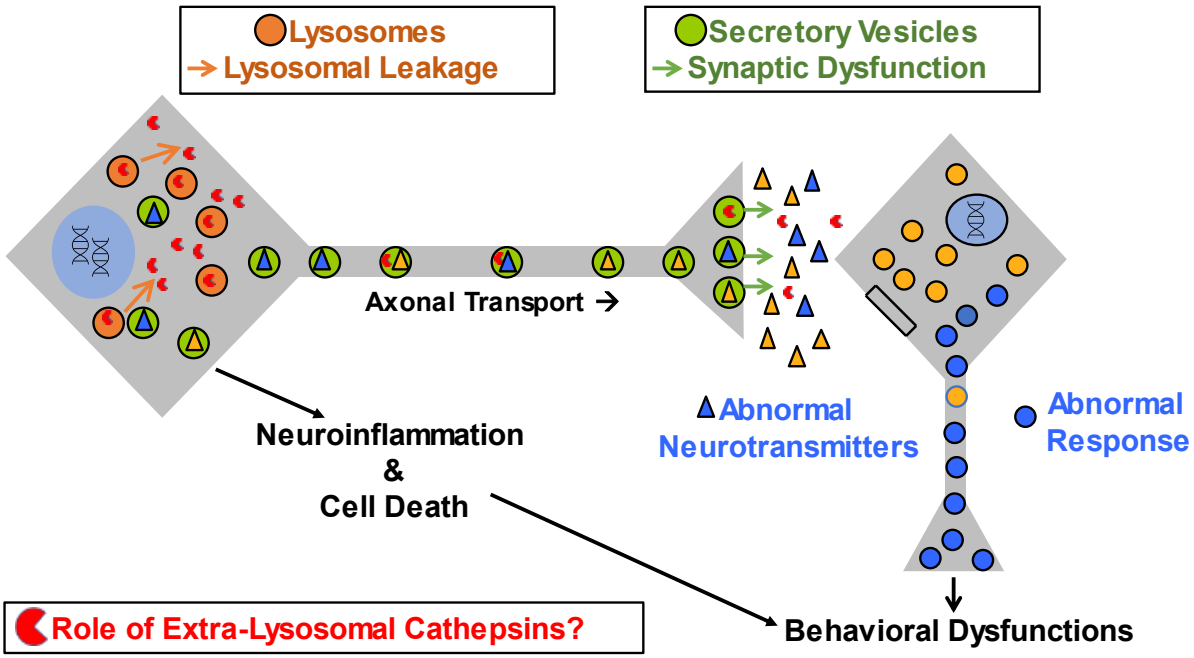

Figure 1.0 Lysosomal Leakage Hypothesis in Brain Disorders (AD, TBI) leading to Neuroinflammation, Cell Death, and Synaptic Dysfunction

Additionally, the scope of this project can be broadly expanded to other diseases that may also involve extra-lysosomal CatB in their disease pathogenesis.

1.2 Lysosomal Proteases and Extra-lysosomal CatB's involvement of Cell Death and Inflammatory Pathways of Alzheimer's disease, TBI, and other diseases

The lysosome contains more than 60 proteases (10) of which cathepsins are the most abundant type of lysosomal proteases. (11) The cathepsin family consists of serine proteases (cathepsins A and G), aspartic proteases (cathepsins D and E), and cysteine proteases (cathepsins B, C, F, H, K, O, S, V, X, and W). (11,12) Of these proteases, cathepsin B (CatB) and cathepsin L are the most abundantly expressed cathepsins in cells. (11,13,14) Most cathepsins are reported to have the highest activity at its native acidic environment of the lysosome where they function to digest peptides. (12) They can also be found in acidic secretory vesicles for the processing of neuropeptides. (15,16) However, some cathepsins can be found outside the acidic environment and can function in neutral pH environments such as in the nucleus, (17,18) cytosol (19,20) and extracellular matrix, (21) possibly due to lysosomal leakage. (22) Extra-lysosomal cathepsins have been implicated in inflammatory or cell death pathways in diseases such as cancer, (23) neurodegenerative conditions such as AD and TBI, (24–26) autoinflammatory, (27–29) and pathogen-induced pyroptosis (30) due to its retained proteolytic activity at neutral pH, (31,32) combined with evidence of elevation of CatB in diseases associated in those inflammatory pathways (33,34) with CatB gene knockout studies in animal models of diseases alleviating the outcome of the diseases, confirming CatB's role in disease pathogenesis. (4,35,36) However, verification of CatB's mechanistic role in disease pathogenesis requires selective inhibition of CatB. To distinguish lysosomal CatB from extra-lysosomal CatB and from other related cathepsins, my dissertation focused on rationally designing a pH-dependent selective inhibitor for

specific CatB inhibition at neutral pH by taking advantage of distinct, pH dependent substrate specificities of CatB, as discussed next.

1.3 Identifying of CatB's Distinct Substrate Specificity at Acidic and neutral pH for Design of Selective Inhibitor at Neutral pH

CatB substrate and inhibitor specificity has been extensively studied in the past and found to have similar specificities to other cathepsins. (37,38) This represents a challenge for designing selective substrates and/or inhibitors for targeting specific cathepsins. For example, the supposedly selective cathepsin L inhibitors such as K-777 and Gallinamide A can still potently inhibit other cathepsins B, V, K, and S (39,40) due to these cathepsins having similar substrate specificities. (37,38) However, overlapping of crystal structures of cathepsin B, K, L and S (41) has revealed that there are unique structural features of CatB, which may be exploited to develop substrates that can be selectively cleaved by CatB. Others have taken advantage of these unique features of CatB (42–44) to successfully discover substrates (45,46) and inhibitors (47–49) selective for CatB.

Another unique feature of CatB is its activity across a broad pH range with evidence of pH dependent substrate specificity. (42,45) This adds another layer of complexity for designing selective inhibitors of CatB, as its effectiveness may also be pH dependent. For instance, the exopeptidase substrate Abz-GIVRAK(Dnp)-OH is more effectively cleaved by CatB at acidic pH and minimally cleaved by CatB at neutral pH. (45) Conversely, the endopeptidase substrate Z-RR-AMC is more effectively cleaved by CatB at neutral pH than at acidic pH. (42) Because of these findings, the current understanding in the field is that CatB transitions from an exopeptidase at acidic pH to an endopeptidase at neutral pH. (42) This is evident when we evaluate the pH dependent potency of the inhibitor CA-074—a well establish potent and selective inhibitor of CatB that was designed to take advantage of CatB exopeptidase activity through its interaction with the occluding loop. (48) As such, we correctly predicted that CA-074 would lose potency at neutral

pH, and indeed, we found that its potency at pH 7.2 is over 100-fold weaker compared to lysosomal pH 4.6. (31) Thus, it is not ideal to use the established inhibitor CA-074 to specifically investigate the role of CatB located at neutral pH compartments of cells. For such purpose, it would be better to use an inhibitor with converse properties of CA-074 that can more potently and selectively inhibit CatB at neutral pH. We proposed that we can develop such inhibitor using a substrate-based inhibitor design approach, described next.

1.4 Strategy for Development of neutral pH-selective inhibitors of CatB

Due to the evidence for CatB for having distinct substrates and/or inhibitors at different pHs, we proposed that extensively profiling CatB, along with other related cathepsins, at neutral pH versus acidic pH would allow for the development of substrates that have the desired property of being better cleaved by CatB at neutral pH than at acidic pH, without being cleaved by other cathepsins. Various proteases were investigated, and their substrate specificities were profiled at acidic pH and neutral pH using multiplex substrate profiling by mass spectrometry (MSP-MS). From the distinct cleavage profiles of different proteases revealed by MSP-MS (Chapters 5 and 7), it is clear that CatB has the unique property of having both pH-dependent substrate specificity (Chapters 2, 4, and 7) that is also distinct from other cathepsins (Chapters 4 and 7). From this, we designed substrates that are cleaved by CatB and not by other cathepsins (Chapter 2) with the additional desired property of being better cleaved by CatB at neutral pH 7.2 over acidic pH 4.6 and vice versa (Chapters 2 and 4). We then modified this substrate into an inhibitor with the desired properties retained from the substrate via attachment of an acyloxymethyl ketone (AOMK) warhead. We demonstrated the success of this strategy in Chapter 2, by developing the substrate Z-Arg-Lys-AMC that is cleaved well by CatB at neutral pH over acidic pH without being cleaved by other cathepsins and then successfully developed the inhibitor Z-Arg-Lys-AOMK that potently

inhibited CatB at neutral pH 7.2 without inhibiting other cathepsins. During this process, we uncovered interesting structural properties of CatB that confers it pH dependent properties.

1.5 Structural features unique to CatB confers pH dependent properties

In Chapters 2 and 3, we uncovered that the unique structural properties of CatB (Glu245 and occluding loop)—not found in other cathepsins—is the reason why CatB has unique pH dependent substrate and inhibitor preferences at different pH. For example, we found that the neutral pH selective inhibitor Z-Arg-Lys-AOMK is both specific for CatB and neutral pH selective due to the more favorable interaction with Arg on the inhibitor and Glu245 residue near the active site pocket of the enzyme at neutral pH than at acidic pH (Chapter 2). Conversely, the inhibitor CA-074 is both specific for CatB and acid pH selective due to the C-terminal carboxylate on the inhibitor interacting more favorably with the His110/His111 residues on the occluding loop at acidic pH than at neutral pH (Chapter 3). Although we have discovered these structural insights into why CatB has pH dependent properties after-the-fact from our original strategic approach of substrate-based inhibitor design, structure-based inhibitor design approach is now a possibility for future strategies involving inhibitor modifications in case there are unforeseen issues with our newly designed inhibitor Z-Arg-Lys-AOMK in cellular biological studies.

1.6 Lysosomal leakage impacts normal cell biology and synaptic function in synaptic vesicles and synapses where proteases function in neurotransmission

Healthy neurons communicate with one another by using neurotransmitters in synapses. (50) Neurotransmitters, along with proteases, are stored and processed within secretory vesicles of neurons, to be eventually released to the synapse. (15,51) However, in neurodegenerative conditions such as in AD and TBI, this communication method between neurons may be disrupted. (52–58) We hypothesized that the cause for such synaptic dysfunction observed in neurodegenerative conditions is lysosomal leakage (Figure 1.0), (59) as the proteases involved in

the normal processing of pro-neuropeptides are disrupted, which may impact synaptic transmission leading to abnormal response between cells. However, the mechanism linking lysosomal leakage and synaptic dysfunction is not clear. In Chapters 5 and 6, we laid the groundwork to establish such connection as we profiled groups of proteases found in secretory vesicles to understand the function of these proteases in relationship to its processing of neurotransmitters in normal conditions. We discovered that these proteases had pH-dependent cleavage properties that was distinct at secretory vesicle pH 5.5 and extracellular pH 7.2. In Chapter 5, we showed that dense core secretory vesicles (DCSV) contain various cathepsins and then we profiled the DCSV contents using MSP-MS at secretory vesicle pH 5.5 and extracellular pH 7.2 to reveal distinct cleavage patterns generated at these different pH conditions, implicating that neuropeptides may be processed differently at different cellular compartments due to different pHs. In Chapter 6, we further profiled the individual proteases Cathepsin L, V, PC1 and PC2 found in secretory vesicles to show that they have distinct cleavage profiles, indicating that these proteases are needed to serve distinct roles in processing pro-neuropeptides to active neuropeptides, which may mean that any dysregulation of these proteases due to lysosomal leakage may result in abnormal neuropeptide processing. Chapters 5 and 6 serves as the starting point for future studies investigating how lysosomal leakage is linked to synaptic dysfunction in neurodegenerative conditions (Figure 1.0).

1.7 Normal biology and diseases involve proteases at different pH locations

Overall, this dissertation demonstrates that different pH environment of proteases must be considered when evaluating their function in normal and in disease conditions. We also demonstrate that it is indeed possible to rationally design a selective inhibitor of CatB that is more potent at neutral pH than acidic pH, without inhibiting other related cathepsins. We identified that CatB has pH dependent substrate specificity, which is clearly distinct from other related cathepsins and uncovered structural reasons for why CatB has such unique properties. CatB at neutral pH

may represent a distinct, pathogenic form, and our successful development of Z-Arg-Lys-AOMK—the neutral pH selective inhibitor of CatB—will allow for future studies regarding CatB's normal and/or pathogenic role in neutral pH environments such as the nucleus, cytosol, and extracellular matrix.

1.8 References

1. Tu S, Okamoto S, Lipton SA, Xu H. Oligomeric Aβ-induced synaptic dysfunction in Alzheimer's disease. Mol Neurodegener. 2014 Nov 14;9:48.

2. 2021 Alzheimer's disease facts and figures. Alzheimer's and Dementia. 2021 Mar 1;17(3):327–406.

3. Hicks AJ, James AC, Spitz G, Ponsford JL. Traumatic Brain Injury as a Risk Factor for Dementia and Alzheimer Disease: Critical Review of Study Methodologies. Vol. 36, Journal of Neurotrauma. Mary Ann Liebert Inc.; 2019. p. 3191–219. Hicks AJ, James AC, Spitz G, Ponsford JL. Traumatic Brain Injury as a Risk Factor for Dementia and Alzheimer Disease: Critical Review of Study Methodologies. J Neurotrauma. 2019 Dec 1;36(23):3191-3219.

4. Sivanandam TM, Thakur MK. Traumatic brain injury: A risk factor for Alzheimer's disease. Vol. 36, Neuroscience and Biobehavioral Reviews. 2012. p. 1376–81. Sivanandam TM, Thakur MK. Traumatic brain injury: a risk factor for Alzheimer's disease. Neurosci Biobehav Rev. 2012 May;36(5):1376-81.

5. Hook V, Yoon M, Mosier C, Ito G, Podvin S, Head BP, Rissman R, O'Donoghue AJ, Hook G. Cathepsin B in neurodegeneration of Alzheimer's disease, traumatic brain injury, and related brain disorders. Biochim Biophys Acta Proteins Proteom. 2020 Aug;1868(8):140428.

6. Carlesimo GA, Oscar-Berman M. Memory deficits in Alzheimer's patients: a comprehensive review. Neuropsychol Rev. 1992 Jun;3(2):119-69.

7. Malpas CB, Saling MM, Velakoulis D, Desmond P, O'Brien TJ. Tau and amyloid-β cerebrospinal fluid biomarkers have differential relationships with cognition in mild cognitive impairment. Journal of Alzheimer's Disease. 2015 Aug 11;47(4):965–75.

8. Kim S, Swaminathan S, Shen L, Risacher SL, Nho K, Foroud T, Shaw LM, Trojanowski JQ, Potkin SG, Huentelman MJ, Craig DW, DeChairo BM, Aisen PS, Petersen RC, Weiner MW, Saykin AJ; Alzheimer's Disease Neuroimaging Initiative. Genome-wide association study of CSF biomarkers Abeta1-42, t-tau, and p-tau181p in the ADNI cohort. Neurology. 2011 Jan 4;76(1):69-79.

9. Han SD, Gruhl J, Beckett L, Dodge HH, Stricker NH, Farias S, et al. Beta amyloid, tau, neuroimaging, and cognition: Sequence modeling of biomarkers for Alzheimer's Disease. Brain Imaging and Behavior. 2012 Dec 1;6(4):610–20.

10. Xu H, Ren D. Lysosomal physiology. Annu Rev Physiol. 2015;77:57-80.

11. Yadati T, Houben T, Bitorina A, Shiri-Sverdlov R. *The Ins and Outs of Cathepsins*: Physiological Function and Role in Disease Management. Cells. 2020 Jul 13;9(7):1679.

12. Turk V, Stoka V, Vasiljeva O, Renko M, Sun T, Turk B, et al. Cysteine cathepsins: From structure, function and regulation to new frontiers. Biochimica et Biophysica Acta - Proteins and Proteomics. 2012;1824(1):68–88.

13. Xing R, Addington AK, Mason RW. Quantification of cathepsins B and L in cells. Biochem J. 1998 Jun 1;332 (Pt 2)(Pt 2):499-505.

14. Turk B, Turk D, Turk V. Lysosomal cysteine proteases: more than scavengers. Biochim Biophys Acta. 2000 Mar 7;1477(1-2):98-111.

15. Jiang Z, Lietz CB, Podvin S, Yoon MC, Toneff T, Hook V, et al. Differential Neuropeptidomes of Dense Core Secretory Vesicles (DCSV) Produced at Intravesicular and Extracellular pH Conditions by Proteolytic Processing. ACS Chemical Neuroscience. 2021 Jul 7;12(13):2385–98.

16. Yoon M, Ames J, Mosier C, Jiang Z, Podvin S, O'Donoghue A, et al. Distinct Dibasic Cleavage Specificities of Neuropeptide-Producing Cathepsin L and Cathepsin V Cysteine Proteases Compared to PC1/3 and PC2 Serine Proteases. ACS Chemical Neuroscience. 13(2):245–56.

17. Meng J, Liu Y, Xie Z, Qing H, Lei P, Ni J. Nucleus distribution of cathepsin B in senescent microglia promotes brain aging through degradation of sirtuins. Neurobiology of Aging. 2020 Dec 1;96:255–66.

18. Goulet B, Sansregret L, Leduy L, Bogyo M, Weber E, Chauhan SS, et al. Increased expression and activity of nuclear cathepsin L in cancer cells suggests a novel mechanism of cell transformation. Molecular Cancer Research. 2007 Sep 1;5(9):899–907.

19. Talukdar R, Sareen A, Zhu H, Yuan Z, Dixit A, Cheema H, et al. Release of Cathepsin B in Cytosol Causes Cell Death in Acute Pancreatitis. Gastroenterology. 2016 Oct 1;151(4):747-758.e5.

20. Oberle C, Huai J, Reinheckel T, Tacke M, Rassner M, Ekert PG, et al. Lysosomal membrane permeabilization and cathepsin release is a Bax/Bak-dependent, amplifying event of apoptosis in fibroblasts and monocytes. Cell Death and Differentiation. 2010 Jul;17(7):1167–78.

21. Fonović M, Turk B. Cysteine cathepsins and extracellular matrix degradation. Biochim Biophys Acta. 2014 Aug;1840(8):2560-70.

22. Wang F, Gómez-Sintes R, Boya P. Lysosomal membrane permeabilization and cell death. Traffic. 2018 Dec;19(12):918-931.

23. Buck MR, Karustis DG, Day NA, Honn K v., Sloane BF. Degradation of extracellular-matrix proteins by human cathepsin B from normal and tumour tissues. Biochemical Journal. 1992;282(1):273–8.

24. Amritraj A, Peake K, Kodam A, Salio C, Merighi A, Vance JE, et al. Increased activity and altered subcellular distribution of lysosomal enzymes determine neuronal vulnerability in Niemann-Pick type C1-deficient mice. American Journal of Pathology. 2009;175(6):2540–56.

25. Freeman D, Cedillos R, Choyke S, Lukic Z, McGuire K, Marvin S, et al. Alpha-Synuclein Induces Lysosomal Rupture and Cathepsin Dependent Reactive Oxygen Species Following Endocytosis. PLoS ONE. 2013 Apr 25;8(4).

26. Dong H, Qin Y, Huang Y, Ji D, Wu F. Poloxamer 188 rescues MPTP-induced lysosomal membrane integrity impairment in cellular and mouse models of Parkinson's disease. Neurochemistry International. 2019 Jun 1;126:178–86.

27. Fujisawa A, Kambe N, Saito M, Nishikomori R, Tanizaki H, Kanazawa N, Adachi S, Heike T, Sagara J, Suda T, Nakahata T, Miyachi Y. Disease-associated mutations in CIAS1 induce cathepsin B-dependent rapid cell death of human THP-1 monocytic cells. Blood. 2007 Apr 1;109(7):2903-11.

28. Rajamäki K, Lappalainen J, Oörni K, Välimäki E, Matikainen S, Kovanen PT, Eklund KK. Cholesterol crystals activate the NLRP3 inflammasome in human macrophages: a novel link between cholesterol metabolism and inflammation. PLoS One. 2010 Jul 23;5(7):e11765.

29. Gonzalez EA, Martins GR, Tavares AMV, Viegas M, Poletto E, Giugliani R, et al. Cathepsin B inhibition attenuates cardiovascular pathology in mucopolysaccharidosis I mice. Life Sciences. 2018 Mar 1;196:102–9.

30. Bergsbaken T, Fink SL, Cookson BT. Pyroptosis: host cell death and inflammation. Nat Rev Microbiol. 2009 Feb;7(2):99-109.

31. Yoon M, Christy M, Phan V, Gerwick W, Hook G, O'Donoghue A, et al. Molecular Features of CA-074 pH-Dependent Inhibition of Cathepsin B. Biochemistry. 61(4):228–38.

32. Yoon M, Solania A, Jiang Z, Christy M, Podvin S, Mosier C, et al. Selective Neutral pH Inhibitor of Cathepsin B Designed Based on Cleavage Preferences at Cytosolic and Lysosomal pH Conditions. ACS Chemical Biology. 16(9):1628–43.

33. Luo CL, Chen XP, Yang R, Sun YX, Li QQ, Bao HJ, et al. Cathepsin B contributes to traumatic brain injury-induced cell death through a mitochondria-mediated apoptotic pathway. Journal of Neuroscience Research. 2010 Oct;88(13):2847–58.

34. Aggarwal N, Sloane BF. Cathepsin B: multiple roles in cancer. Proteomics Clin Appl. 2014 Jun;8(5-6):427-37.

35. Ni J, Lan F, Xu Y, Nakanishi H, Li X. Extralysosomal cathepsin B in central nervous system: Mechanisms and therapeutic implications. Brain Pathol. 2022 Apr 12:e13071.

36. Kindy MS, Yu J, Zhu H, El-Amouri SS, Hook V, Hook GR. Deletion of the cathepsin B gene improves memory deficits in a transgenic alzheimer's disease mouse model expressing AβPP containing the wild-type β-secretase site sequence. Journal of Alzheimer's Disease. 2012;29(4):827–40.

37. Choe Y, Leonetti F, Greenbaum DC, Lecaille F, Bogyo M, Brömme D, et al. Substrate profiling of cysteine proteases using a combinatorial peptide library identifies functionally unique specificities. Journal of Biological Chemistry. 2006 May 5;281(18):12824–32.

38. Ashhurst AS, Tang AH, Fajtová P, Yoon MC, Aggarwal A, Bedding MJ, et al. Potent Anti-SARS-CoV-2 Activity by the Natural Product Gallinamide A and Analogues via Inhibition of Cathepsin L. Journal of Medicinal Chemistry. 2022 Feb 24;65(4):2956–70.

39. Mellott DM, Tseng C te, Drelich A, Fajtová P, Chenna BC, Kostomiris DH, et al. A Clinical-Stage Cysteine Protease Inhibitor blocks SARS-CoV-2 Infection of Human and Monkey Cells. ACS Chemical Biology. 2021 Apr 16;16(4):642–50.

40. Caracelli I, Maganhi SH, de Oliveira Cardoso J, Cunha RLOR, Vega-Teijido MA, Zukerman-Schpector J, et al. Crystallographic and docking (Cathepsins B, K, L and S) studies on bioactive halotelluroxetanes. Zeitschrift fur Kristallographie - Crystalline Materials. 2018 Feb 23;233(2):113–24.

41. Vizovišek M, Vidmar R, van Quickelberghe E, Impens F, Andjelković U, Sobotič B, et al. Fast profiling of protease specificity reveals similar substrate specificities for cathepsins K, L and S. Proteomics. 2015 Jul 1;15(14):2479–90.

42. Polgár L, Csoma C. Dissociation of ionizing groups in the binding cleft inversely controls the endo- and exopeptidase activities of cathepsin B. J Biol Chem. 1987 Oct 25;262(30):14448-53.

43. Illy C, Quraishi O, Wang J, Purisima E, Vernet T, Mort JS. Role of the occluding loop in cathepsin B activity. J Biol Chem. 1997 Jan 10;272(2):1197-202.

44. Hasnain S, Hirama T, Huber CP, Mason P, Mort JS. Characterization of cathepsin B specificity by site-directed mutagenesis. Importance of Glu245 in the S2-P2 specificity for arginine and its role in transition state stabilization. Journal of Biological Chemistry. 1993;268(1):235–40.

45. Cotrin SS, Puzer L, de Souza Judice WA, Juliano L, Carmona AK, Juliano MA. Positional-scanning combinatorial libraries of fluorescence resonance energy transfer peptides to define substrate specificity of carboxydipeptidases: Assays with human cathepsin B. Analytical Biochemistry. 2004 Dec 15;335(2):244–52.

46. Poreba M, Groborz K, Vizovisek M, Maruggi M, Turk D, Turk B, et al. Fluorescent probes towards selective cathepsin B detection and visualization in cancer cells and patient samples. Chemical Science. 2019;10(36):8461–77.

47. Katunuma N. Structure-based development of specific inhibitors for individual cathepsins and their medical applications. Proceedings of the Japan Academy Series B: Physical and Biological Sciences. 2011;87(2):29–39.

48. Towatari T, Nikawa T, Murata M, Yokoo C, Tamai M, Hanada K, Katunuma N. Novel epoxysuccinyl peptides. A selective inhibitor of cathepsin B, in vivo. FEBS Lett. 1991 Mar 25;280(2):311-5.

49. Murata, M.; Miyashita, S.; Yokoo, C.; Tamai, M.; Hanada, K.; Hatayama, K.; Towatari, T.; Nikawa, T.; Katunuma, N. Novel epoxysuccinyl peptides. Selective inhibitors of cathepsin B, in vitro. FEBS Lett. 1991, 280, 307−10.

50. Cotman CW, McGaugh JL. Synaptic Transmission. Behavioral Neuroscience. 1980;151–208.

51. Yasothornsrikul S, Greenbaum D, Medzihradszky KF, Toneff T, Bundey R, Miller R, Schilling B, Petermann I, Dehnert J, Logvinova A, Goldsmith P, Neveu JM, Lane WS, Gibson B, Reinheckel T, Peters C, Bogyo M, Hook V. Cathepsin L in secretory vesicles functions as a prohormone-processing enzyme for production of the enkephalin peptide neurotransmitter. Proc Natl Acad Sci U S A. 2003 Aug 5;100(16):9590-5.

52. Chen Y, Fu AKY, Ip NY. Synaptic dysfunction in Alzheimer's disease: Mechanisms and therapeutic strategies. Pharmacol Ther. 2019 Mar;195:186-198.

53. Taoufik E, Kouroupi G, Zygogianni O, Matsas R. Synaptic dysfunction in neurodegenerative and neurodevelopmental diseases: an overview of induced pluripotent stem-cell-based disease models. Open Biol. 2018 Sep;8(9):180138.

54. Pei YA, Davies J, Zhang M, Zhang HT. The Role of Synaptic Dysfunction in Alzheimer's Disease. J Alzheimers Dis. 2020;76(1):49-62.

55. Marsh J, Alifragis P. Synaptic dysfunction in Alzheimer's disease: the effects of amyloid beta on synaptic vesicle dynamics as a novel target for therapeutic intervention. Neural Regen Res. 2018 Apr;13(4):616-623.

56. Li L, Liang J, Fu H. An update on the association between traumatic brain injury and Alzheimer's disease: Focus on Tau pathology and synaptic dysfunction. Neurosci Biobehav Rev. 2021 Jan;120:372-386.

57. Jamjoom AAB, Rhodes J, Andrews PJD, Grant SGN. The synapse in traumatic brain injury. Brain. 2021 Feb 12;144(1):18-31.

58. Hoffe B, Holahan MR. Hyperacute Excitotoxic Mechanisms and Synaptic Dysfunction Involved in Traumatic Brain Injury. Front Mol Neurosci. 2022 Feb 24;15:831825.

59. Rebiai R, Givogri MI, Gowrishankar S, Cologna SM, Alford ST, Bongarzone ER. Synaptic Function and Dysfunction in Lysosomal Storage Diseases. Front Cell Neurosci. 2021 Mar 4;15:619777.

CHAPTER 2 – Selective Neutral pH Inhibitor of Cathepsin B Designed Based on Cleavage Preferences at Cytosolic and Lysosomal pH Conditions

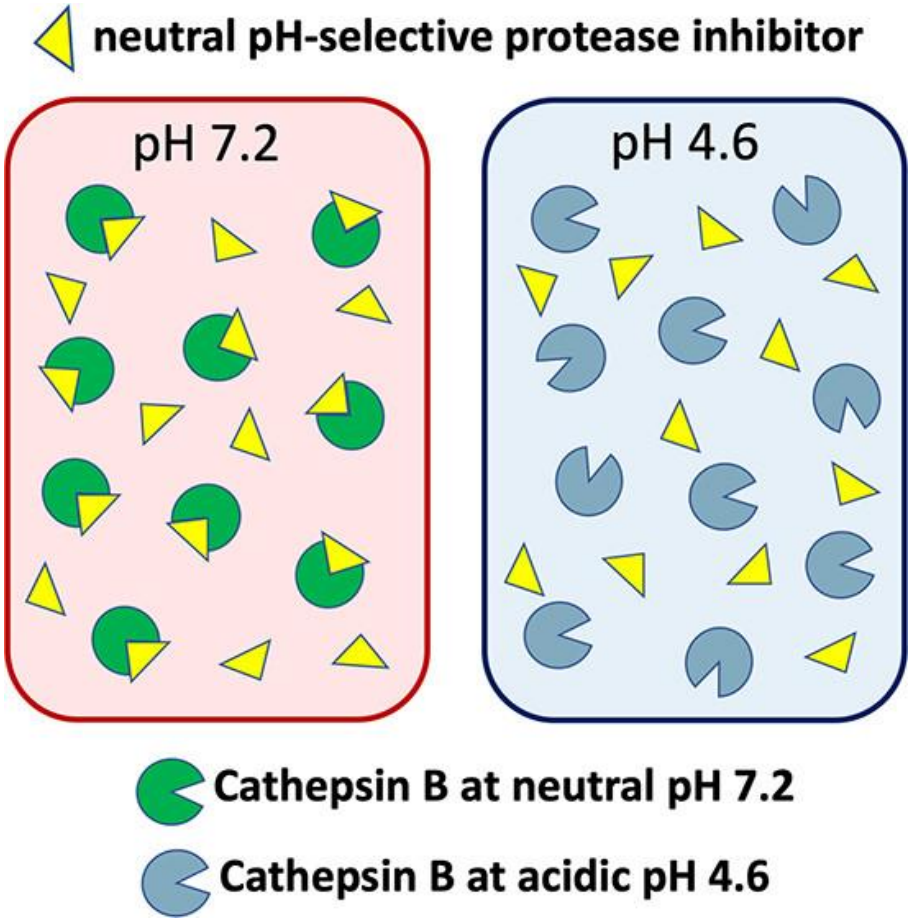

Chapter 2 Graphical Abstract. Cathepsin B is a cysteine protease that normally functions within acidic lysosomes for protein degradation, but in numerous human diseases, cathepsin B translocates to the cytosol having neutral pH where the enzyme activates inflammation and cell death. Cathepsin B is active at both the neutral pH 7.2 of the cytosol and the acidic pH 4.6 within lysosomes. We evaluated the hypothesis that cathepsin B may possess pH-dependent cleavage preferences that can be utilized for design of a selective neutral pH inhibitor by (1) analysis of differential cathepsin B cleavage profiles at neutral pH compared to acidic pH using multiplex substrate profiling by mass spectrometry (MSP-MS), (2) design of pH-selective peptide–7-amino-4-methylcoumarin (AMC) substrates, and (3) design and validation of Z-Arg-Lys-acyloxymethyl ketone (AOMK) as a selective neutral pH inhibitor. Cathepsin B displayed preferences for cleaving peptides with Arg in the P2 position at pH 7.2 and Glu in the P2 position at pH 4.6, represented by its primary dipeptidyl carboxypeptidase and modest endopeptidase activity. These properties led to design of the substrate Z-Arg-Lys–AMC having neutral pH selectivity, and its modification with the AOMK warhead to result in the inhibitor Z-Arg-Lys–AOMK. This irreversible inhibitor displays nanomolar potency with 100-fold selectivity for inhibition of cathepsin B at pH 7.2 compared to pH 4.6, shows specificity for cathepsin B over other cysteine cathepsins, and is cell permeable and inhibits intracellular cathepsin B. These findings demonstrate that cathepsin B possesses pH-dependent cleavage properties that can lead to development of a potent, neutral pH inhibitor of this enzyme.

2.1 Introduction

Cathepsin B functions in lysosomes for protein degradation and maintenance of cellular homeostasis. (1−3) Cathepsin B is a member of the family of cysteine cathepsin proteases that participate in lysosomal protein degradation, together with aspartyl and serine cathepsins. (4,5) Cathepsin B normally functions within the acidic pH 4.6 environment in lysosomes. (6−8) However, significant cathepsin B activity occurs at the neutral pH 7.2 of the cytosol and other cellular compartments as well as extracellular locations. (9−11)

Evidence for neutral pH locations of cathepsin B functions (12−15) suggests the hypothesis that differential cleavage properties of this enzyme at neutral compared to acidic pH conditions may provide the basis for design and development of a neutral pH-selective inhibitor, which represents the purpose of this study. In numerous disease conditions, cathepsin B functions in the cytosol at neutral pH, rather than in lysosomes. Lysosomal leakage of cathepsin B to the neutral cytosol occurs in numerous brain disorders, including Alzheimer's disease, (12−17) traumatic brain injury (TBI), (12,18,19) and neurodegenerative conditions, (20−25) & in autoinflammatory and infectious diseases. (26−32) Cytosolic cathepsin B initiates apoptotic cell death (33−36) and activates inflammatory IL-1β production. (31,37−39) Cathepsin B participates in behavioral deficits, demonstrated by cathepsin B gene knockout and inhibitor studies in animal models of TBI, AD, ischemia, and related disorders. (12,40,41) This enzyme also functions at the neutral pH of the extracellular environment in cancer (42−46) and rheumatoid arthritis, (47) as well as at other neutral pH locations including nuclei. (48−50) The prevalence of cathepsin B functions at neutral pH locations emphasizes the critical importance of this study to gain an understanding of its neutral pH properties compared to its normal acidic lysosomal features.

Cathepsin B is active at the neutral pH 7.2 (9,10) of the cytosol, (51,52) as well as at the acidic pH 4.6 (6−8) within lysosomes. (4) The 400-fold difference in proton concentration at pH 4.6 compared to pH 7.2 alters the charge state of cathepsin B (12) and its substrates. These distinct pH conditions lead to the hypothesis that cathepsin B may possess different substrate cleavage preferences at cytosolic neutral pH compared to lysosomal acidic pH. We tested this hypothesis by comparing the substrate cleavage properties of cathepsin B at both pH conditions by global multiplex substrate profiling by mass spectrometry (MSP-MS) using a peptide substrate library consisting of 228 peptides designed to contain diverse protease cleavage sites. (53,54) Furthermore, MSP-MS directly assesses the location of each cleavage site and can, therefore, distinguish aminopeptidase, (55,56) endopeptidase, (57,58) and carboxypeptidase activities. (53,59) Results showed that cathepsin B displays pH-selective cleavage properties represented by its prominent dipeptidyl carboxypeptidase activity and modest endopeptidase activity.

Based on the distinct cathepsin B cleavage properties at neutral pH compared to acidic pH conditions, peptide–AMC substrates and novel peptidic–AOMK inhibitors of cathepsin B were designed and evaluated for pH selectivity. Notably, Z-Arg-Lys–AOMK was revealed as a potent and selective inhibitor of neutral pH 7.2 cathepsin B activity. This inhibitor displayed high specificity for cathepsin B compared to other lysosomal cysteine cathepsins. These results demonstrate that the unique pH-dependent cleavage properties of cathepsin B provide the basis for design of Z-Arg-Lys–AOMK as a neutral pH inhibitor of cathepsin B. These findings suggest that neutral pH cathepsin B represents a unique form of the enzyme compared to the normal lysosomal cathepsin B.

2.2 Results

2.2.1 Strategy to Assess Cleavage Properties of Cathepsin B for Design of a Neutral pH-Selective Inhibitor

The workflow used to analyze cathepsin B cleavage properties for development of a neutral pH inhibitor is illustrated in Figure 2.1. Unbiased MSP-MS assays evaluated the cleavage properties of cathepsin B at neutral pH 7.2 and acidic pH 4.6 using a peptide library consisting of 228 peptide substrates (14 residues in length) containing 2964 diverse cleavage sites. Cathepsin B cleavage products were identified and quantified by nano-liquid chromatography tandem mass spectrometry (nano-LC-MS/MS) to determine the frequencies of amino acid residues adjacent to cleavage sites at P1-↓P1′ residues. Preferred residues at the P2 and P1 positions were utilized for design of dipeptide fluorogenic substrates. Substrate sequences that were selectively hydrolyzed by cathepsin B at pH 7.2 or 4.6 were synthesized with the acyloxymethyl ketone (AOMK) warhead to generate peptidic inhibitors.

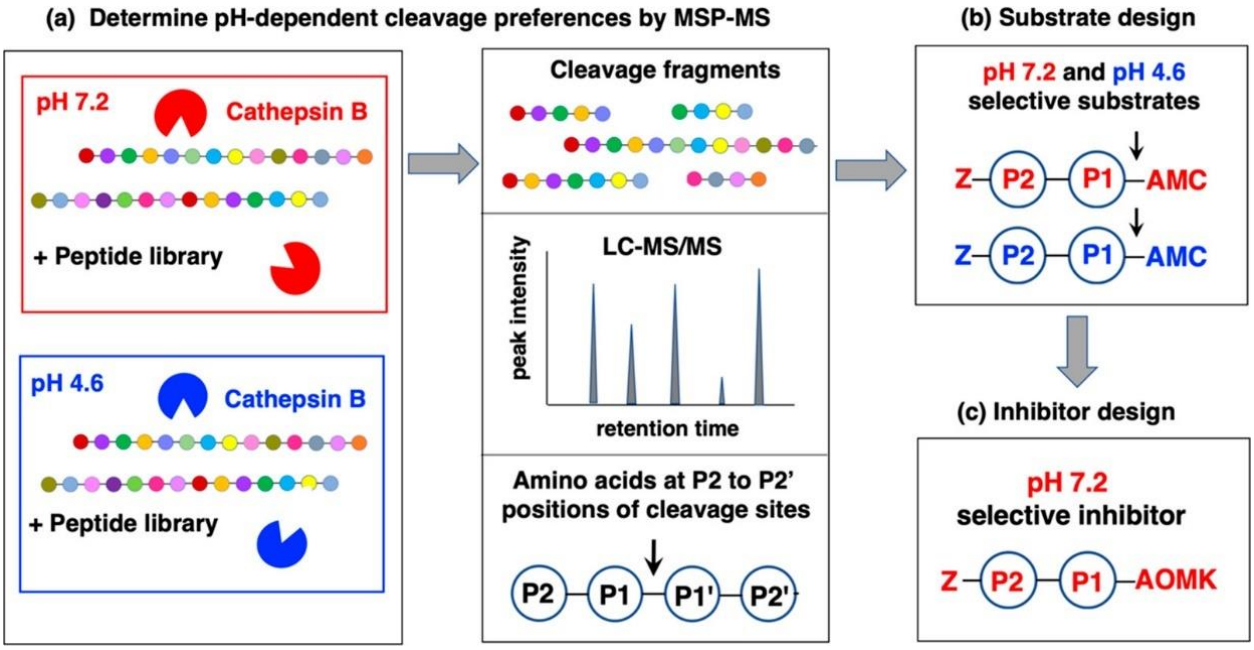

Figure 2.1 Workflow to analyze cathepsin B substrate cleavage site preferences for design of pH-selective inhibitors. (a) Cathepsin B substrate cleavage properties assessed at pH 7.2 and pH 4.6 by multiplex substrate profiling by mass spectrometry (MSP-MS) analyses. The substrate cleavage profiles of cathepsin B at pH 7.2 and pH 4.6 were assessed by MSP-MS analyses. Cathepsin B was incubated (at RT, for 15 and 60 min) at pH 7.2 and pH 4.6 with the peptide library consisting of 228 14-mer peptides designed to contain all neighbor and near-neighbor amino acid combinations. Peptide cleavage products were identified and quantitated by LC-MS/MS analyses. The frequencies of amino acid residues at the P2 to P2′ positions of the P1–↓P1′ cleavage sites were assessed. (b) Design of pH-selective peptide–AMC substrates. Substrates representing the preferred residues at P1 and P2 positions at pH 7.2 and pH 4.6 were utilized for development of pH-selective peptide–AMC substrates of cathepsin B. These substrates contained a C-terminal 7-amino-4-methylcoumarin (AMC) reporter group and an N-terminal carboxybenzyl (Z) group. (c) Design of pH-selective peptidic inhibitors. Peptide–AOMK inhibitors were synthesized based on the AMC substrates that have high selectivity for cleavage at either pH 7.2 or pH 4.6.

2.2.2 Cathepsin B Stability at Neutral pH 7.2 and Acidic pH 4.6

Prior to determining the substrate cleavage profiles of cathepsin B, we evaluated enzyme stability at pH 7.2 and pH 4.6 by preincubating the enzyme for up to 4 h at RT (RT, 27 °C) and at 37 °C, followed by assays with Z-Phe-Arg–AMC substrate. After 1 h of preincubation, the relative activity at each pH and temperature was above 50% and decreased with longer preincubation times (Figure 2.2). We, therefore, performed the MSP-MS cleavage assays at RT for up to 1 h to generate

data for active enzyme. These in vitro assays show that cathepsin B is active at both pH 7.2 and pH 4.6 and represent a model for studying cathepsin B activity.

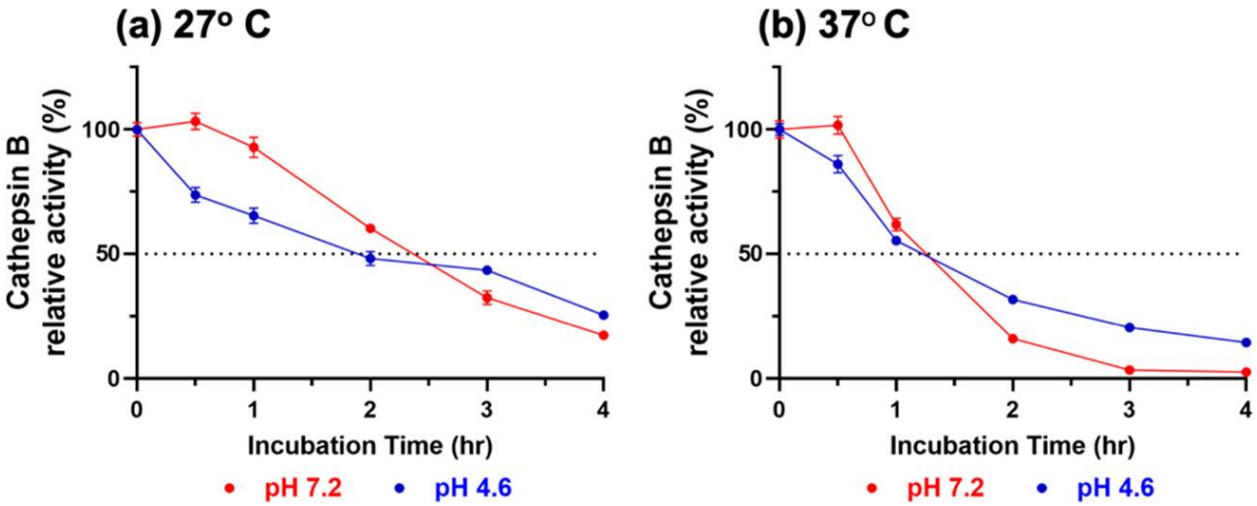

Figure 2.2 Cathepsin B activity at pH 7.2 and pH 4.6. Cathepsin B was preincubated at pH 7.2 or pH 4.6 at RT (27 °C) or at 37 °C for 30 min to 4 h. Z-Phe-Arg–AMC substrate (40 μM) was then added and proteolytic activity was monitored by measurement of AMC fluorescence. Activity is expressed relative to control cathepsin B with no preincubation (100%); data are displayed as the mean ± SEM (n = 4).

2.2.3 Substrate Cleavage Profiling of Cathepsin B Demonstrates Strong Dipeptidyl Carboxypeptidase Specificity

Human recombinant cathepsin B was incubated with the 228 14-mer library for 60 min followed by nano-LC-MS/MS and PEAKS bioinformatics to quantify peptide products. At pH 7.2, cathepsin B cleaved 66 peptide bond sites, and at pH 4.6, the enzyme cleaved 142 sites (Figure 2.S1). Cleavage was defined by peptide products having intensity values that were at least 8-fold above that in the denatured enzyme control, based on the criteria to minimize false positive rate (Figure 2.S2). The distribution of cleavages at each of the 13 peptide bonds among the peptide substrates was quantified, and proteolysis was found to occur primarily at position no. 12 indicating dipeptidyl carboxypeptidase activity (Figure 2.3a). Cleavage at position no. 10 was also prevalent. Fewer numbers of cleavages occurred at position nos. 7–9 and 11, which may represent endopeptidase cleavages, and no cleavages were observed at position nos. 1–6.

The presence of prominent dipeptidyl carboxypeptidase activity suggested that sequential cleavage at position 12 followed by cleavage at position 10 may occur in a time-dependent manner. Evaluation of the number of cleavages occurring at position 10 at 15 and 60 min found that increases occurred in a time-dependent manner (Figure 2.3b), consistent with dipeptidyl carboxypeptidase processing at position 12 followed by such cleavages at position 10 (Table 2.S1). These findings illustrate the primary exopeptidase activity of cathepsin B as a dipeptidyl carboxypeptidase, with low endopeptidase activity, in both neutral and acidic pH conditions.

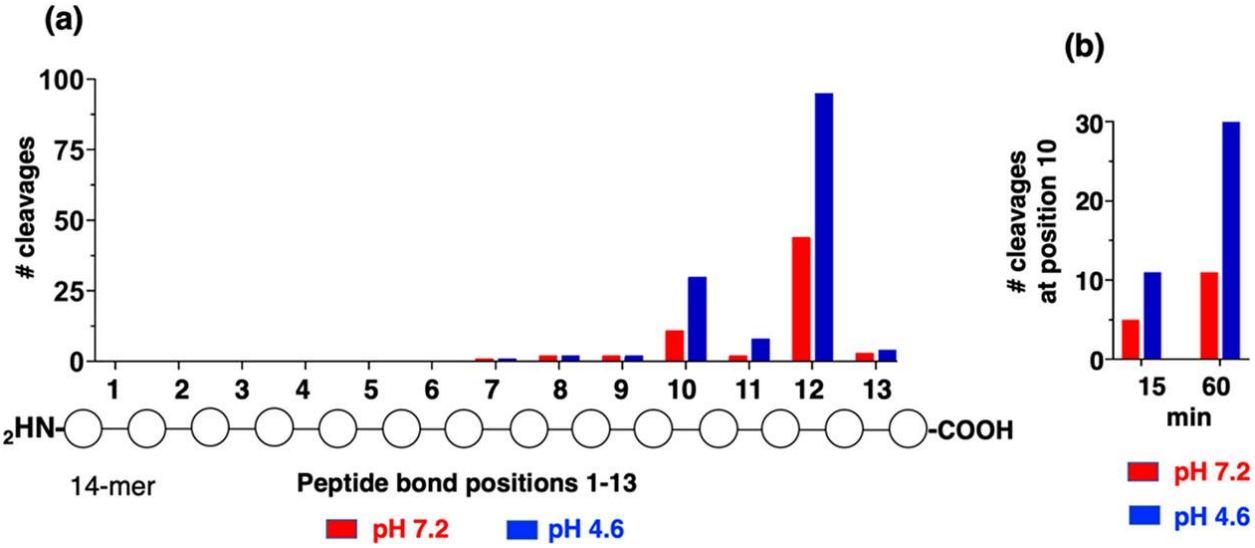

Figure 2.3 Cathepsin B peptide cleavage analyses illustrate major dipeptidyl carboxypeptidase activity at pH 7.2 and pH 4.6, demonstrated by MSP-MS. (a) Cleavage at peptide bonds no. 1–13 of 14-mer peptide library substrates by cathepsin B. Cathepsin B cleavage of the 228 14-mer peptide library at pH 7.2 and pH 4.6 was evaluated as the number of cleavages occurring at each of the peptide bonds no. 1–13, that were generated at pH 7.2 and pH 4.6. (b) Time-dependent cleavage at position 10 of peptide substrates at pH 7.2 and pH 4.6. The number of cleavages by cathepsin B at peptide bond no. 10 at 15 and 60 min incubation is shown. The time-dependent increase in the number of cleavages at position no. 10 may be consistent with sequential dipeptidyl carboxypeptidase cleavages.

2.2.4 pH-Dependent Cleavage Properties of Cathepsin B

Cathepsin B displayed differences in cleavage preferences at pH 7.2 compared to pH 4.6. The frequencies of amino acid residues located at positions P2-P1-↓P1′-P2′ to generate cleaved peptide products were analyzed by MSP-MS for the major cleavages occurring as dipeptidyl

carboxypeptidase cleavages at position 12. IceLogo schematically illustrates the relative frequency of amino acid residues occurring at P2-P1-↓P1′-P2′ residues at pH 7.2 and 4.6 (Figure 2.4a,b).

At the P1 position, cathepsin B at pH 7.2 preferred the basic residues Arg and Lys, along with norleucine and Tyr (Figure 2.4a). At pH 4.6, the P1 positions displayed preferences for the noncharged Thr and Gly residues, as well as the basic residue Arg (Figure 2.4b).

At the P2 position, differences in the preferences for negative and positive residues were observed at pH 7.2 and pH 4.6 (Figure 2.4a,b). At pH 4.6, the acidic Glu residue was a preferred residue at the P2 position, as well as hydrophobic Val. In contrast, at pH 7.2, the basic residues Arg, Lys, and His were preferred at the P2 position, as well as Trp. These preferred P2 residues appear consistent with the presence of Glu245 in the S2 pocket of the protease that interacts with the P2 residue of the cathepsin B substrate. (60) At pH 4.6, the uncharged Glu245 could interact with the uncharged Glu as the P2 residue, while at neutral pH 7.2, the negatively charged Glu245 would be amenable to interacting with the positively charged P2 basic Arg or Lys residues. These preferred residues at the P2 positions may be informative for design of pH-selective substrates of cathepsin B.

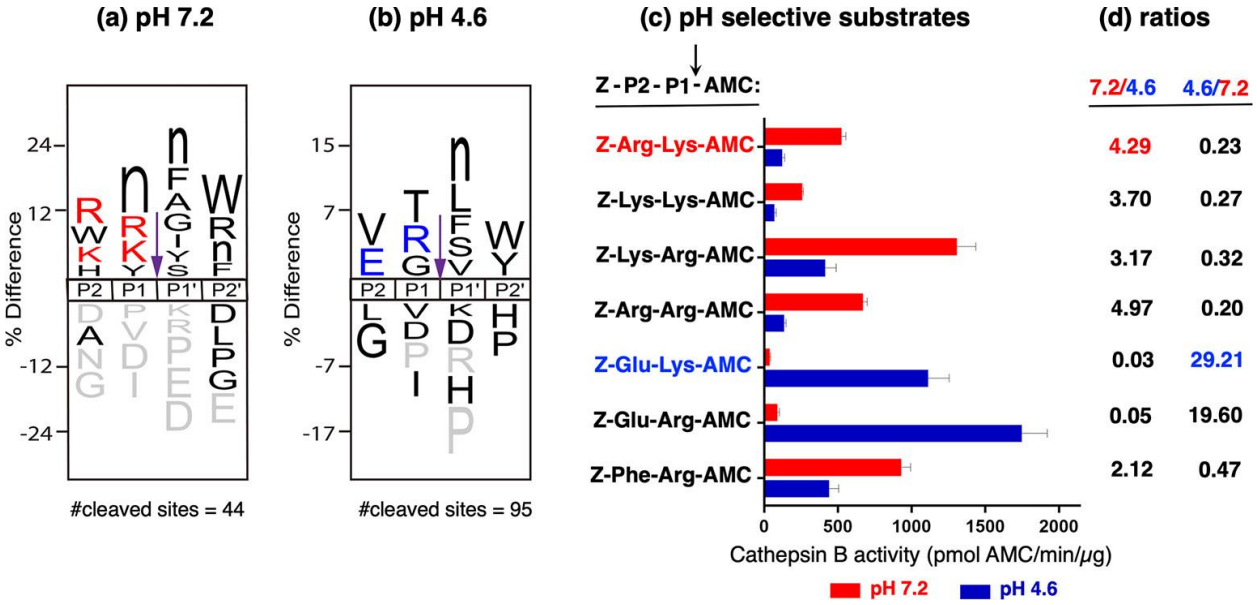

Figure 2.4 Differential cathepsin B substrate cleavage preferences at neutral pH 7.2 compared to acidic pH 4.6. (a) pH-dependent cleavage preferences of cathepsin B at pH 7.2 illustrated by IceLogo. IceLogo analysis demonstrates the relative frequency of amino acids at the P2, P1, P1′, and P2′ positions that surround the cleavage site (purple arrow). Residues shown in gray were not found at the indicated position. The amino acid described with lowercase "n" corresponds to norleucine, a sulfur-free isostere of methionine. Residues colored in red or blue were used in design of selective dipeptide–AMC substrates for pH 7.2 and pH 4.6, respectively. (b) pH-dependent cleavage preferences at pH 4.6 illustrated by IceLogo. IceLogo shows the preferred residues for the P2 to P2′ positions for cleavages occurring at pH 4.6. IceLogo features are described in the panel a description. (c) Dipeptide–AMC substrates selective for cathepsin B activity at pH 7.2 or pH 4.6. Based on MSP-MS peptide cleavage data for the preferred P2 and P1 residues adjacent to cleavage sites, peptide–AMC substrates selective for pH 7.2 and for pH 4.6 were designed and synthesized. Cathepsin B specific activities with each of the peptide–AMC substrates (40 μM final concentration) were assessed at pH 7.2 (red bars) and pH 4.6 (blue bars). (d) Ratios of cathepsin B specific activities at pH 7.2 and pH 4.6. The ratios of cathepsin B specific activity for pH 7.2/pH 4.6 and for pH 4.6/pH 7.2 are shown. Peptide–AMC substrates with a high ratio of pH 7.2/pH 4.6, and high ratio of pH 4.6/pH 7.2, were selected for modification by AOMK for inhibitor development.

2.2.5 Development of pH-Selective Peptide–AMC Substrates for Cathepsin B

The MSP-MS substrate profiling results provided the basis for design of pH-selective dipeptide–AMC substrates (Figure 2.4c). A series of pH 7.2 selective substrates were designed with basic residues at the P2 position, consisting of Z-Arg-Lys–AMC, Z-Lys-Lys–AMC, Z-Lys-Arg–AMC, and Z-Arg-Arg–AMC. At pH 4.6, the preference for Glu at the P2 position was used for design of the pH 4.6 selective substrates Z-Glu-Lys–AMC and Z-Glu-Arg–AMC.

Evaluation of pH substrate selectivity found that dipeptide substrates with basic residues at both P2 and P1 positions were more rapidly cleaved at neutral pH 7.2 than at pH 4.6 by cathepsin B; these substrates consisted of Z-Arg-Lys–AMC, Z-Lys-Lys–AMC, Z-Lys-Arg–AMC, and Z-Arg-Arg–AMC (Figure 2.4c). Z-Arg-Lys–AMC and Z-Arg-Arg–AMC had the highest ratio of pH 7.2/pH 4.6 activities (Figure 2.4d). Furthermore, acid pH preferring substrates consisted of Z-Glu-Lys–AMC and Z-Glu-Arg–AMC with Glu at the P2 position (Figure 2.4c). Z-Glu-Lys–AMC displayed the highest ratio of pH 4.6/pH 7.2 activities, indicating preference for pH 4.6 cathepsin B activity (Figure 2.4d).

Substrate concentration studies showed that at pH 7.2, cathepsin B displayed preference for the Z-Arg-Lys–AMC substrate, shown by the greater rate of hydrolysis of this substrate at pH 7.2 compared to pH 4.6, as illustrated by kcat/Km values (Figure 2.5a). At pH 4.6, cathepsin B preferred the Z-Glu-Lys–AMC substrate (Figure 2.5b), shown by the more rapid rate of hydrolysis at pH 4.6 over pH 7.2. In contrast, Z-Phe-Arg–AMC was hydrolyzed at similar rates by cathepsin B at both pH 4.6 and 7.2 (Figure 2.5c).

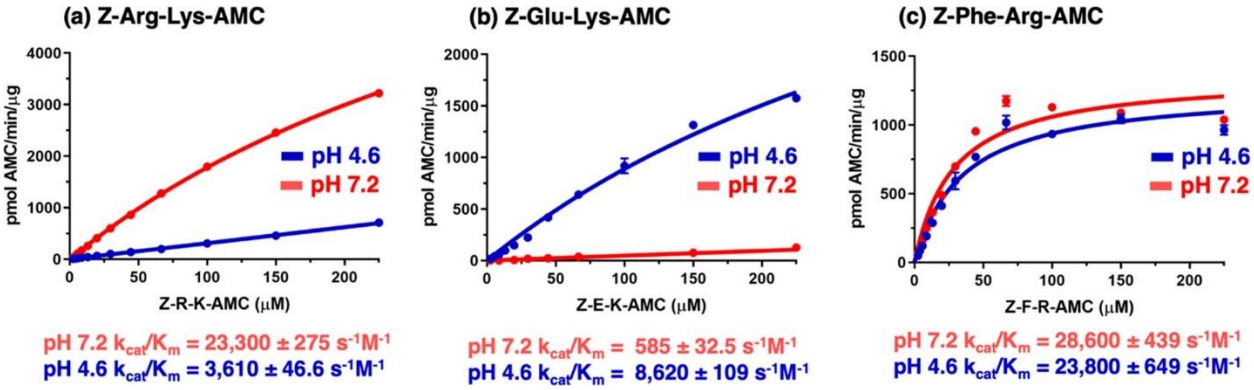

Figure 2.5 Dipeptide–AMC substrates that selectively monitor cathepsin B activity at neutral pH 7.2 compared to acidic pH 4.6, illustrated by kcat/Km values. (a) Z-Arg-Lys–AMC, pH 7.2 selective substrate. Cathepsin B activity with Z-Arg-Lys–AMC substrate at pH 7.2 and pH 4.6 was evaluated over a concentration range of 2.6 µM to 225 µM. (b) Z-Glu-Lys–AMC, pH 4.6 selective substrate. Cathepsin B activity was assessed with Z-Glu-Lys–AMC substrate at pH 7.2 and pH 4.6. (c) Z-Phe-Arg–AMC, substrate for both pH 7.2 and pH 4.6. Cathepsin B activity with Z-Phe-Arg–AMC substrate, a commonly used substrate, (77−79) at pH 7.2 and pH 4.6.

The complete pH profiles were assessed for the pH-selective substrates Z-Arg-Lys–AMC and Z-Glu-Lys–AMC and the non-pH-selective substrate Z-Phe-Arg–AMC (Figure 2.6). Hydrolysis of Z-Arg-Lys–AMC was maximal at pH 7.8, with >50% activity occurring between pH 6.2 to pH 8.5, indicating that Z-Arg-Lys–AMC is a selective neutral pH substrate of cathepsin B. In contrast, Z-Glu-Lys–AMC was optimally hydrolyzed at pH 4.6, with >50% activity occurring at pH 3.6 to pH 5.6, indicating that Z-Glu-Lys–AMC is a selective acidic pH substrate. Z-Phe-Arg–AMC was hydrolyzed across a wide pH range with 50% of the maximum activity occurring between pH 3.8 and 8.6. These data clearly show that cathepsin B has distinct enzymatic properties at pH 4.6 and pH 7.2, and these differences can be exploited by rational design of pH-selective substrates.

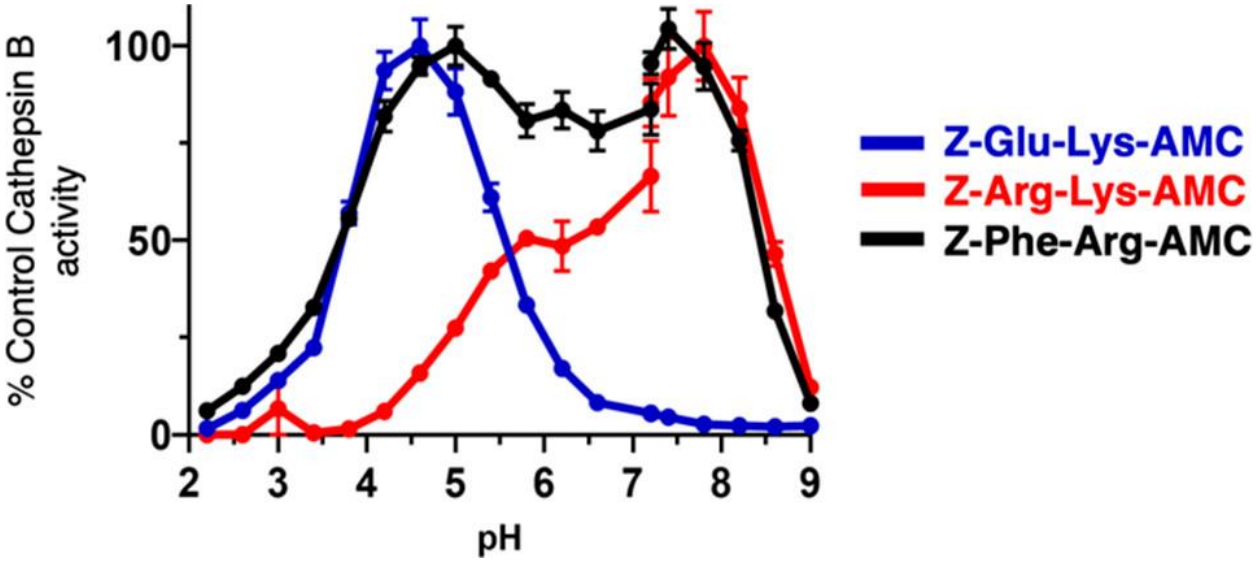

Figure 2.6 Cathepsin B pH-selective substrates Z-Arg-Lys–AMC and Z-Glu-Lys–AMC and the non-pH-selective substrate Z-Phe-Arg–AMC. The pH profiles cathepsin B activity with the substrates Z-Arg-Lys–AMC, Z-Glu-Lys–AMC, and Z-Phe-Arg–AMC were assessed at pH 2 to 9, with substrate concentrations at 60 μM. Data points are shown as the mean ± SEM (n = 3). The pH curves are also illustrated for cathepsin B activity expressed as AMC RFU/s (Figure S3).

The peptidic substrates were assessed for specificity for related lysosomal cysteine cathepsin proteases. Z-Arg-Lys–AMC selectively monitored cathepsin B activity primarily at pH 7.2 and showed no activity for cathepsin L or cathepsin V at pH 7.2 (Figure 2.S4). Z-Glu-Lys–

AMC was selective for cathepsin B activity at pH 4.6 and displayed no activity for cathepsins L or V. In contrast, Z-Phe-Arg–AMC was hydrolyzed by cathepsin B at both pH conditions, and this substrate was also cleaved by cathepsins L and V at pH 4.6.

2.2.6 Z-Arg-Lys–AOMK and Z-Glu-Lys–AOMK Inhibitors of Cathepsin B

The strategy to incorporate the AOMK warhead to replace the AMC group of the peptide–AMC substrates (56,61−63) was utilized to design and synthesize the Z-Arg-Lys–AOMK and Z-Glu-Lys–AOMK peptidic inhibitors (Figure 2.S5).

Z-Arg-Lys–AOMK displayed selective inhibition of cathepsin B at pH 7.2 compared to pH 4.6 (Figure 2.7a and Table 2.1). Determination of kinetic constants showed that Z-Arg-Lys–AOMK was a potent inhibitor with K_I value of 130 nM at pH 7.2 but was less effective at pH 4.6 with a K_I of 15000 nM at pH 4.6 (Table 2.1). The K_I values show that this inhibitor displays 115-fold greater potency at pH 7.2 compared to pH 4.6. The k_{inact}/K_I constant was 1.1×10^5 M^{-1} s^{-1} at pH 7.2 and 1.8×10^3 M^{-1} s^{-1} at pH 4.6 (Table 2.1). The inhibitory effectiveness of Z-Arg-Lys–AOMK was also illustrated by its low IC50 value of 20 nM, compared to its lower effectiveness at pH 4.6 with IC50 value of 1500 nM. These kinetic studies illustrate that Z-Arg-Lys–AOMK is a potent neutral pH inhibitor of cathepsin B.

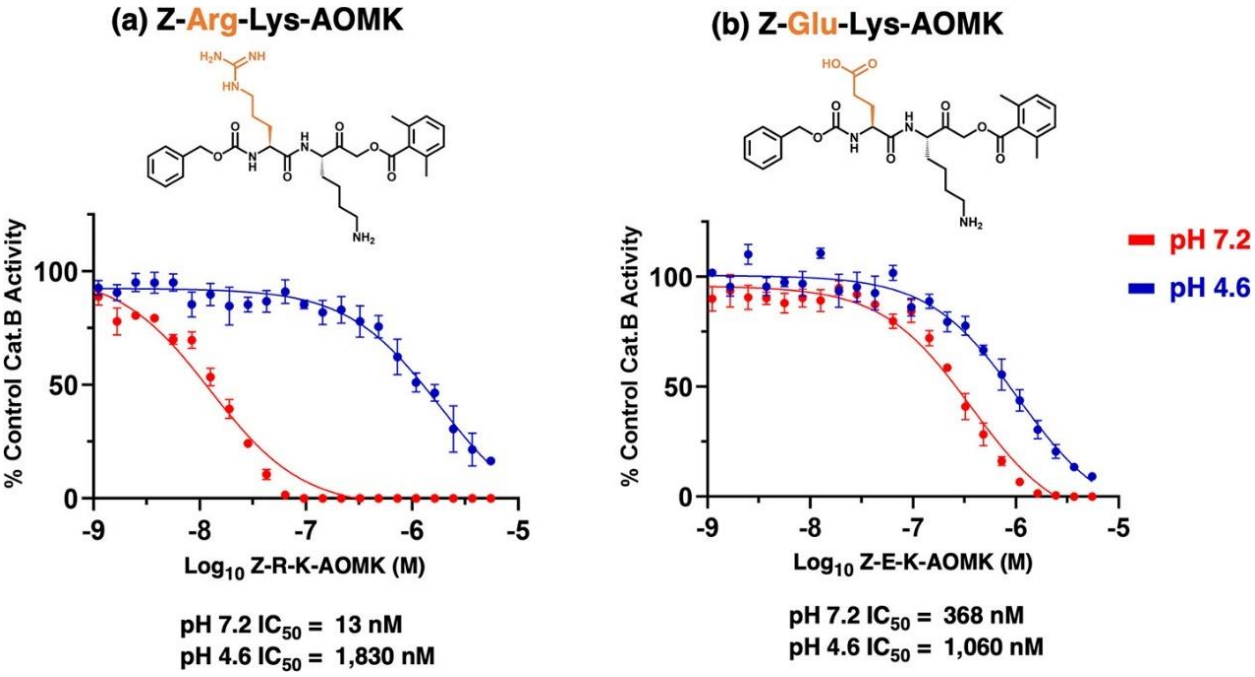

Figure 2.7 Z-Arg-Lys–AOMK and Z-Glu-Lys–AOMK inhibitors of cathepsin B at neutral pH compared to acidic pH conditions. (a) Z-Arg-Lys–AOMK inhibitor. Z-Arg-Lys–AOMK inhibition of cathepsin B was assessed at different inhibitor concentrations to determine IC50 values at pH 7.2 and pH 4.6. Z-Phe-Arg–AMC was used as substrate for cathepsin B assays. (b) Z-Glu-Lys–AOMK inhibitor. The inhibitor Z-Glu-Lys–AOMK at different concentrations was assessed for IC50 values at pH 4.6 and pH 7.2.

Table 2.1 Kinetic Properties of Z-Arg-Lys–AOMK and Z-Glu-Lys–AOMK Inhibitors[a]

	Z-Arg-Lys−AOMK		Z-Glu-Lys−AOMK	
kinetic constant	**pH 4.6**	**pH 7.2**	**pH 4.6**	**pH 7.2**
K_I (nM)	15000 ± 6000	130 ± 50	7900 ± 830	2300 ± 620
k_{inact}/K_I (M^{-1} s^{-1})	1.8×10^3	110×10^3	2.0×10^3	8.2×10^3
IC_{50} (nM)	1500 ± 650	20 + 8.3	1100 ± 480	320 ± 45

[a]K_I, k_{inact}/K_I, and IC_{50} values for the irreversible inhibitors of cathepsin B were determined as explained in the methods; k_{obs} values were determined by plots of cathepsin B activity in time courses with different inhibitor concentrations with curve fitting $Y = Y_0\, e^{(-kobsX)}$, where Y_0 is the activity for the control with no inhibitor condition, Y is the activity in the presence of inhibitor, and X is time. K_I and k_{inact} values were calculated from k_{obs} values with the equation $k_{obs} = k_{inact}[I]/(K_I + [I])$ (graphs shown in Figure 2.S6), where [I] is inhibitor concentration, K_I is the inhibitor concentration (x-axis) at which $y = k_{inact}/2$, and k_{inact} is the maximum rate of inactivation at saturating inhibitor concentrations. K_I and IC_{50} values are expressed as the mean ± SD (n = 4, n = 6, respectively)

Compared to Z-Arg-Lys–AOMK, Z-Glu-Lys–AOMK displayed less effective inhibition of cathepsin B at both pH 7.2 and pH 4.6 (Figure 2.7b and Table 2.1). Kinetic analyses showed that Z-Glu-Lys–AOMK had K_I values of 2300 nM and 7900 nM at pH 7.2 and pH 4.6, respectively (Table 2.1). The k_{inact}/K_I values for this inhibitor were 8.2×10^3 M^{-1} s^{-1} and 2.0×10^3 M^{-1} s^{-1} at pH 7.2 and pH 4.6, respectively (Table 2.1). These data showed that Z-Glu-Lys–AOMK was about 3.5-fold more potent at pH 7.2 compared to pH 4.6, with KI values for both pHs at micromolar levels. IC50 values of 320 nM and 1100 nM for pH 7.2 and 4.6, respectively, were of similar orders of magnitude. The micromolar levels of Z-Glu-Lys–AOMK for inhibition at both pHs were less effective than the nanomolar levels of Z-Arg-Lys–AOMK for neutral pH inhibition of cathepsin B.

2.2.7 Neutral pH-Selective Inhibition of Peptide Library Cleavages by Z-Arg-Lys–AOMK

To further validate the neutral pH selectivity of Z-Arg-Lys–AOMK inhibition, cathepsin B was preincubated with this inhibitor at 64 nM at pH 7.2 and pH 4.6, and proteolytic activity was assessed using the 228-member peptide library in MSP-MS assays. The 64 nM concentration of Z-Arg-Lys–AOMK was chosen because it reduced cathepsin B activity with Z-Phe-Arg–AMC as substrate by 93% at pH 7.2 and by 5% at pH 4.6 (Figure 2.8). At pH 7.2, Z-Arg-Lys–AOMK completely inhibited peptide cleavages by cathepsin B after 1 h incubation (Figure 2.8a). However, at pH 4.6, Z-Arg-Lys–AOMK (64 nM) did not inhibit cathepsin B formation of peptide products (Figure 2.8b). These findings show that Z-Arg-Lys–AOMK selectively inhibits cathepsin B cleavage of peptides at neutral cytosolic pH compared to acidic lysosomal pH conditions.

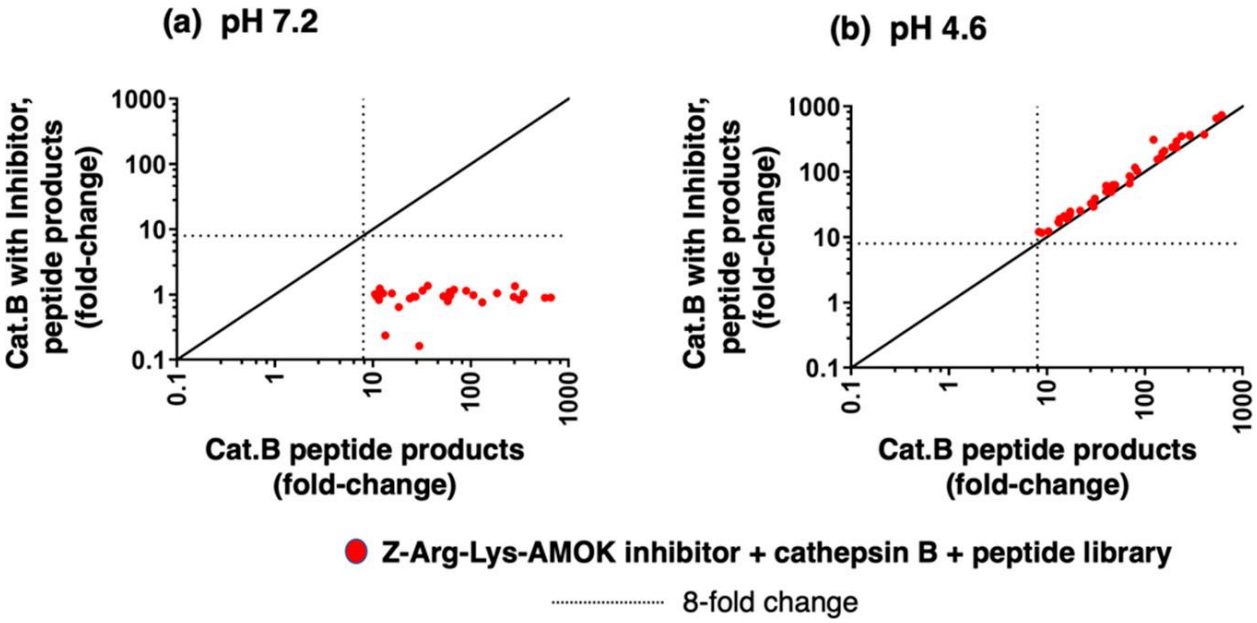

Figure 2.8 Z-Arg-Lys–AOMK selectively inhibits cathepsin B cleavage of peptide substrates at pH 7.2 compared to pH 4.6, assessed by MSP-MS. (a) Z-Arg-Lys–AOMK (64 nM) at pH 7.2 inhibits cathepsin B cleavage of peptide library substrates assessed by MSP-MS. The inhibitor concentration was selected for ~90% inhibition at pH 7.2 (using Z-F-R–AMC substrate), which consisted of 64 nM Z-Arg-Lys–AOMK (93% inhibition at pH 7.2). MSP-MS assays analyzed the cleavage products generated from the peptide library by LC-MS/MS identification and quantification. The relative quantities of each peptide product generated in the absence of inhibitor or in the presence of inhibitor were plotted as the fold-change of each peptide product relative to no enzyme activity control. (b) Z-Arg-Lys–AOMK (64 nM) at pH 4.6 does not inhibit cathepsin B cleavage of peptide library substrates assessed by MSP-MS. Cathepsin B was incubated without and with the inhibitor at pH 4.6 for MSP-MS analyses of peptide products. The MSP-MS procedure and inhibitor concentrations are described in the panel a description.

2.2.8 Irreversible Mechanism of Z-Arg-Lys–AOMK and Z-Glu-Lys–AOMK Inhibitors

The irreversible mechanism of the inhibitors was demonstrated by preincubation of each inhibitor with cathepsin B, followed by dilution and activity measurements (Figure 2.S7). Control enzyme without inhibitor displayed a linear time-dependent progression of proteolytic activity. Preincubation with Z-Arg-Lys–AOMK or Z-Glu-Lys–AOMK at pH 7.2 and pH 4.6, respectively, resulted in no cathepsin B activity after dilution of the inhibitors, indicating the irreversible mechanism of these inhibitors.

2.2.9 Z-Arg-Lys–AOMK and Z-Glu-Lys–AOMK Specifically Inhibit Cathepsin B Compared to Other Cysteine Cathepsins

At pH 7.2, Z-Arg-Lys–AOMK inhibited cathepsin B with an IC50 of 20 nM, which was more potent by 22-fold, 110-fold, and 43-fold than cathepsin V (IC50 = 440 nM), cathepsin S (IC50 = 2200 nM), and cathepsin C (IC50 = 850 nM) inhibition (Table 2.2). At pH 7.2, cathepsins K and H were minimally inhibited by Z-Arg-Lys–AOMK at 16 μM. At pH 4.6, Z-Arg-Lys–AOMK inhibited cathepsin B with IC50 of 1500 nM, and at 16 μM, this inhibitor showed minimal inhibition of cathepsins L, V, S, X, and C, and no inhibition of cathepsin K or cathepsin H.

Table 2.2 Specificity of Z-Arg-Lys–AOMK and Z-Glu-Lys–AOMK for Inhibition of Cathepsin B Compared to Other Cysteine Cathepsins[a]

	Z-Arg-Lys–AOMK IC_{50} (nM)		Z-Glu-Lys–AOMK IC_{50} (nM)	
protease	**pH 4.6**	**pH 7.2**	**pH 4.6**	**pH 7.2**
cathepsin B	1500	20	1100	320
cathepsin C	>16000 (6%)	850	8600	12000
cathepsin H	b	>16000 (29%)	b	b
cathepsin K	b	>16000 (31%)	>16000 (10%)	b
cathepsin L	>16000 (32%)	c	>16000 (23%)	c
cathepsin S	>16000 (13%)	2200	>16000 (26%)	>16000 (30%)
cathepsin V	>16000 (63%)	440	1900	>16000 (10%)
cathepsin X	>16000 (21%)	c	b	c

[a]Inhibitors were evaluated for protease specificity among the 8 cysteine cathepsins, achieved by monitoring the activity of each enzyme in the presence of a range of inhibitor concentrations from 0.5 nM to 16 μM (without preincubation). IC_{50} values were generated for the inhibitors Z-Arg-Lys–AOMK and Z-Glu-Lys–AOMK for each of the cysteine cathepsin enzymes. IC_{50} values are indicated as >16000 nM when partial inhibition was observed (% inhibition is shown in parentheses).
[b]No inhibition at 16000 nM inhibitor.
[c]Enzyme had no activity at the indicated pH.

Z-Glu-Lys–AOMK also demonstrated specific inhibition of cathepsin B compared to other cysteine cathepsins (Table 2.2). At pH 7.2, the inhibitor was 38-fold more potent for cathepsin B (IC50 = 320 nM) than cathepsin C (IC50 = 12000 nM). At pH 4.6, weak inhibition of cathepsin V (IC50 = 1900 nM) and cathepsin C (IC50 = 8600 nM) occurred, while the other cathepsin enzymes tested were minimally inhibited or not inhibited by Z-Glu-Lys–AOMK (at 16 μM) at either pH condition.

These data illustrate the high specificity of Z-Arg-Lys–AOMK and Z-Glu-Lys–AOMK inhibitors for cathepsin B over other members of the cysteine cathepsin family.

2.2.10 Molecular Docking of Z-Arg-Lys–AOMK to Cathepsin B at Neutral pH 7.2: Interaction of Glu245 of the Enzyme with P2 Arg

Modeling of Z-Arg-Lys–AOMK binding interactions to cathepsin B was assessed by the Molecular Operating Environment (MOE) software. (64,65) MOE generated a representation of inhibitor binding to the active site of human cathepsin B (PDB: 1QDQ) (60) at pH 7.2 consisting of P2 and P1 residues of the peptidic inhibitor interacting with the S2 and S1 subsites of the enzyme, according to the Schechter–Berger nomenclature (66) (Figure 2.9). The P2 Arg residue of the Z-Arg-Lys–AOMK shows a strong polar interaction with the carboxylate of Glu245 in the S2 subsite of the enzyme. Glu245 at pH 7.2 is negatively charged (based on its pKa of 5.1) (67) and is predicted to interact with the positively charged P2 Arg of the inhibitor at neutral pH. The P1 Lys residue of the inhibitor interacts with Glu122 and Asn72 of the enzyme S1 pocket. (60,68) The AOMK warhead occupies the S1′ region near the occluding loop; furthermore, the AOMK carbon atom resides less than 3.4 Å from the catalytic Cys29 nucleophile, suggesting a binding mode for irreversible inhibition. The Z group (benzyloxycarbonyl) appears partially solvent exposed and extended from the S2 region. In contrast, a pH 4.6 model of Z-Arg-Lys–AOMK docking to cathepsin B showed a lack of Glu245 interaction with the Arg moiety of this inhibitor

(Figure 2.S8). These features illustrate a model of Z-Arg-Lys–AOMK binding to the active site of cathepsin B at neutral pH.

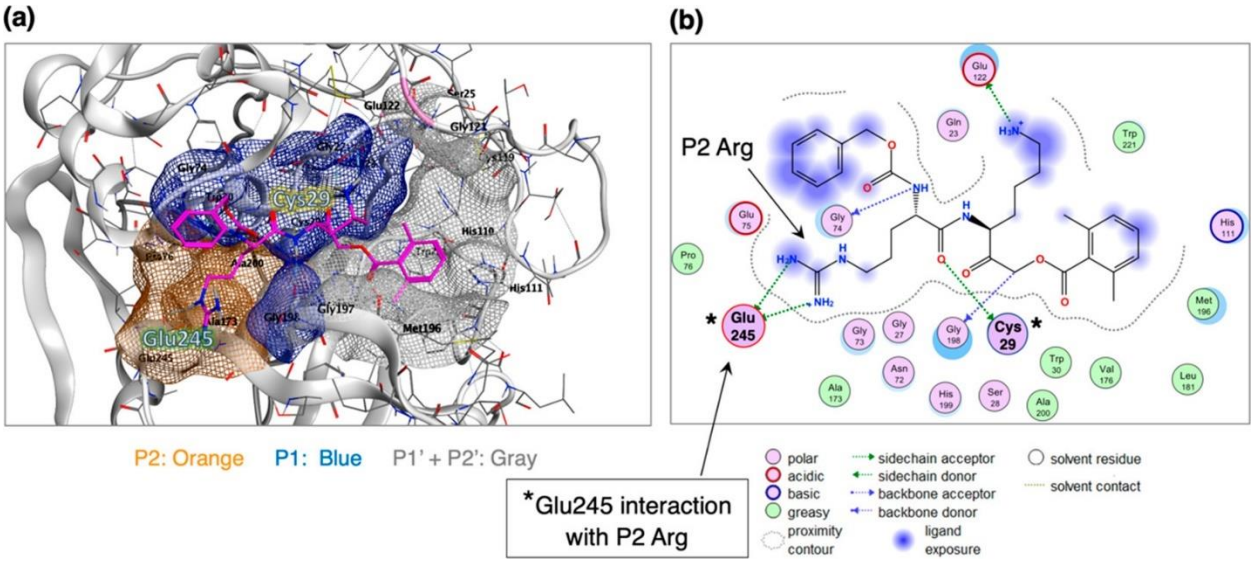

Figure 2.9 Model of Z-Arg-Lys–AOMK binding to cathepsin B at neutral pH 7.2: interaction of enzyme Glu245 with P2 Arg. (a) Model of the Z-Arg-Lys–AOMK inhibitor docking to cathepsin B at pH 7.2. Modeling of Z-Arg-Lys–AOMK binding to the active site of the cathepsin B structure is illustrated, achieved by the MOE software using the cathepsin B structure of PDB 1QDQ as template for analyses at pH 7.2. (60) The P1 Lys residue of Z-Arg-Lys–AOMK interacts with the enzyme S1 subsite, shown in the blue region. The P2 Arg residue of the inhibitor interacts with the enzyme S2 subsite region, shown in orange. The inhibitor AOMK warhead docking to the enzyme region corresponds to the S1′ and S2′ subsites, shown in gray. (b) Two-dimensional illustration of Z-Arg-Lys–AOMK and cathepsin B binding interactions at pH 7.2. The peptidic Z-Arg-Lys–AOMK inhibitor interacts with the active site of cathepsin B, modeled by MOE. The P2 Arg residue of the Z-Arg-Lys–AOMK shows a strong polar interaction with the Glu245 carboxylate of the S2 pocket of the enzyme. The P1 Lys and P2 Arg residues of the inhibitor interact with the corresponding S1 and S2 subsites of the cathepsin B enzyme. The P1 Lys interacts with Glu122 and Asn72 of the S1 subsite. (60,68) The AOMK warhead resides within 3.75 Å from the catalytic Cys29 nucleophile, suggesting a binding mode for irreversible inhibition; the AOMK group occupies the S1′ region near the occluding loop. The Z group (benzyloxycarbonyl) appears partially solvent exposed and extended from the S2 region.

At pH 4.6, Z-Arg-Lys–AOMK docking by MOE modeling showed no interactions of Glu245 (of the enzyme) with the Arg of this inhibitor (Figure 2.S9), which contrasts with Glu245 interactions with Arg of Z-Arg-Lys–AOMK at pH 7.2. MOE modeling suggests Glu245

interaction with Z-Arg-Lys–AOMK at pH 7.2 but no interaction with Z-Glu-Lys–AOMK. MOE calculations of the inhibitor binding energies to cathepsin B at pH 7.2 and pH 4.6 show more favorable interactions of Z-Arg-Lys–AOMK at pH 7.2 compared to pH 4.6 (Table 2.3). These binding energies were estimated based on interactions of enzyme active site residues with the inhibitors.

Table 2.3 Binding Energies of Z-Arg-Lys–AOMK and Z-Glu-Lys–AOMK to Cathepsin B at Neutral pH 7.2 and Acidic pH 4.6[a]

	binding energy (kcal/mol)	
inhibitor	**pH 7.2**	**pH 4.6**
Z-Arg-Lys−AOMK	−55.5	−26.2
Z-Glu-Lys−AOMK	−52.3	−55.9

[a]For Z-Arg-Lys–AOMK, the more negative binding energy calculated for pH 7.2 compared to pH 4.6 indicates a more favorable interaction of this inhibitor to cathepsin B at pH 7.2. These calculations are made with Glu245 protonated at pH 4.6. For Z-Glu-Lys–AOMK, the equivalent binding energies calculated for pH 7.2 and pH 4.6 indicate a similar interaction of this inhibitor to cathepsin B at these two pH conditions.

With respect to Z-Glu-Lys–AOMK, MOE shows that Z-Glu-Lys–AOMK lacks interactions with the Glu245 of the S2 pocket of cathepsin B (Figure 2.S9). Furthermore, similar binding energies were calculated at pH 7.2 and pH 4.6 for Z-Glu-Lys–AOMK (Table 2.3), suggesting that this inhibitor was not pH-selective. This lack of pH selectivity is supported by our inhibition studies (Table 2.1). The MOE modeling implicates the importance of Glu245 of cathepsin B for effectiveness of the neutral pH inhibitor Z-Arg-Lys–AOMK.

2.2.11 Z-Arg-Lys–AOMK Inhibition of Intracellular Cathepsin B and Cell Permeability

Z-Arg-Lys–AOMK was evaluated for its ability to inhibit cathepsin B activity in human neuroblastoma cell lysate using Z-Arg-Arg–AMC substrate. Proteolytic activity in the cell lysate was completely inhibited by Z-Arg-Lys–AOMK (1 μM) and by CA-074 (1 μM), a specific

inhibitor of cathepsin B (69) (Figure 2.10a). These data show that Z-Arg-Lys–AOMK and CA-074 inactivate cathepsin B.

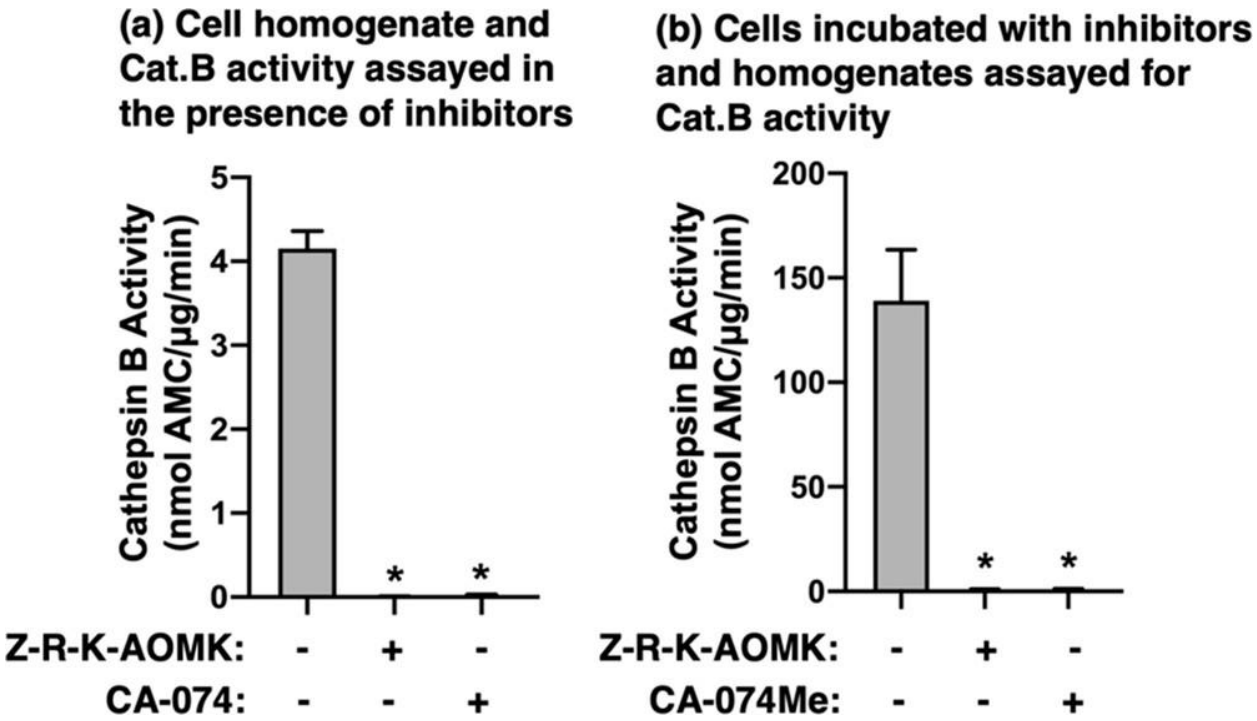

Figure 2.10 Z-Arg-Lys–AOMK inhibition of cathepsin B in human neuroblastoma cells. (a) Cell homogenates assayed for cathepsin B activity in the presence of inhibitors. Homogenates of SHSY5Y human neuroblastoma cells were prepared as described in the Methods and Materials. Cathepsin B activity in the homogenate was assayed with Z-Arg-Arg–AMC substrate in the presence of Z-Arg-Lys–AOMK or CA-074 (1 μM each). Assays were conducted at high concentrations of inhibitors to completely inhibit activity; assays were conducted at pH 5.5 because this is a routine pH used to assay this enzyme in the literature. (71,72) Cathepsin B activity was expressed as nmol AMC/(μg/min), mean ± SD (*$p < 0.05$ by Student's t test, $n = 3$). (b) Cells incubated with inhibitors and assay of cathepsin B activity. Human neuroblastoma cells were incubated with Z-Arg-Lys–AOMK or CA-074Me (50 μM each) for 6 h at 37 °C. Cells were homogenized as described in the Methods and Materials, and cathepsin B was assayed with Z-Arg-Arg–AMC substrate. Cathepsin B activity was expressed as nmol AMC/(μg/min) and shown as mean + SD (*$p < 0.05$ by Student's t test, $n = 6$).

The cell permeability of Z-Arg-Lys–AOMK was evaluated by incubation of neuroblastoma cells with this inhibitor (50 μM) for 6 h. Cells were also incubated with CA-074Me (50 μM); CA-074Me is known to enter cells and be converted by esterases to the potent CA-074 inhibitor of cathepsin B. (70) After incubation, cells were washed, and homogenates were assayed for cathepsin B activity with Z-Arg-Arg–AMC substrate. Z-Arg-Lys–AOMK and CA-074Me

completely inhibited cellular cathepsin B activity (Figure 2.10b). These results demonstrate that the Z-Arg-Lys–AOMK is cell permeable and inhibits intracellular cathepsin B.

2.3 Discussion

In this study, we designed and developed a neutral pH-selective inhibitor, Z-Arg-Lys–AOMK, of cathepsin B based on the enzyme's distinct substrate cleavage properties observed at neutral pH 7.2 compared to acidic pH 4.6. Cathepsin B functions at the neutral pH locations of the cytosol and extracellular environments in brain disorders (12−25) and human diseases of different physiological systems, (26−32) which contrasts with the normal location of cathepsin B in lysosomes of acidic pH. Development of the neutral pH inhibitor was based on the hypothesis that the unique pH-dependent cleavage properties of cathepsin B may provide the basis for the design of selective neutral pH inhibitors. Specifically, the differential cleavage properties of cathepsin B at neutral pH compared to acidic pH were revealed by MSP-MS substrate profiling, which utilizes a peptide library containing all neighbor and near-neighbor amino acid combinations. MSP-MS assays revealed preferences of cathepsin B for residues at the P2 and P1 positions of the cleavage site (P1-↓P1′). The P2 position prefers Glu (E) at acidic pH, but prefers a basic residue Arg (R) at neutral pH. At the P1 position, basic residues are preferred at both neutral and acidic pHs. These cleavage properties led to the design of Z-Arg-Lys–AMC as a neutral pH 7.2 selective substrate and Z-Glu-Lys–AMC as an acidic pH 4.6 selective substrate. Inhibitors were generated by synthesis of these dipeptide substrates with the AOMK (acyloxymethyl ketone) warhead. Z-Arg-Lys–AOMK was found to be an effective irreversible inhibitor of cathepsin B at neutral pH with nanomolar potency. Z-Arg-Lys–AOMK displays 100-fold more potent inhibition of cathepsin B at neutral pH compared to acidic pH. These findings indicate that Z-Arg-Lys–AOMK is a neutral pH inhibitor of cathepsin B, thus validating our hypothesis that substrate specificity differences

can be utilized for rational design of pH-selective inhibitors. Surprisingly, Z-Glu-Lys–AOMK was not selective for inhibition at acid pH; thus, addition of reactive warheads to peptide substrates may not always retain pH selectivity. Nonetheless, these findings demonstrate that pH-selective inhibitors of cathepsin B can be developed based on its pH-dependent cleavage properties.

A notable finding of this study is that cathepsin B displays similar stability at both neutral pH 7.2 and acidic pH 4.6 conditions. While cathepsin B normally functions at the acidic pH 4.6 within lysosomes, we show that cathepsin B has similar stability at both neutral and acidic pH conditions. Cathepsin B was more stable at pH 7.2 than at pH 4.6 for up to 2 h at RT (RT). Using conditions that maintain stability, cathepsin B activity in this study was conducted with RT incubation up to 60 min for MSP-MS assays and up to 30 min for fluorogenic assays. Studies at 37 °C were also conducted and showed similar stability of cathepsin B activity at pH 7.2 and pH 4.6. These stability studies complement reports in the field that cathepsin B becomes inactivated with time at neutral and alkaline conditions of pH 7.0–9.5. (51,73−75) Our data provides new information that similar stability and inactivation properties of cathepsin B are observed at pH 7.2 and pH 4.6.

Cathepsin B is known to cleave folded protein substrates such as MARCKS, collagen, and thyroglobulin (48,76−78) via its endopeptidase activity. Using a substrate library of synthetic peptides that lack secondary structure, we can detect both endoprotease and exoprotease activity for any protease. We show that cathepsin B is primarily a dipeptidyl carboxypeptidase enzyme, and sequential removal of dipeptides from the C-terminus was evident. Detection of dipeptidyl carboxypeptidase activity of protein substrates using traditional gel shift assays is difficult as the molecular weight changes are minor. However, using mass spectrometry, hydrolysis of peptide substrates into shorter products can be readily detected and quantified.

The role of the occluding loop for exopeptidase compared to endopeptidase activities of cathepsin B has been demonstrated by deletion mutagenesis of the loop domain, which resulted in the absence of exopeptidase activity and the presence of only endopeptidase activity. (79) Furthermore, site-directed mutagenesis of selected residues within the occluding loop resulted in increased endopeptidase activity. (80) These studies indicate that the occluding loop regulates the exopeptidase and endopeptidase activities of cathepsin B.

Cathepsin B activity is typically monitored with Z-Phe-Arg–AMC and Z-Arg-Arg–AMC fluorogenic substrates for endopeptidase activity. (81−83) However, use of extended peptide substrates that can be cleaved by either endopeptidases or exopeptidases in the MSP-MS cleavage analyses illustrated the predominant exopeptidase activity of cathepsin B at both neutral and acidic pHs. These data demonstrate that these commonly used peptide–AMC substrates monitor both the dipeptidyl carboxypeptidase and endopeptidase activities of cathepsin B.

The differential cleavage profiles of cathepsin B at neutral pH 7.2 and acidic pH 4.6 conditions by MSP-MS provided the basis for development of pH-selective peptide–AMC substrates. At the P2 position, cathepsin B demonstrated preference for Glu at pH 4.6, but at pH 7.2, the enzyme preferred basic residues of Arg and Lys. At the P1 position, cathepsin B showed preference for basic residues Arg or Lys residues at acidic and neutral pH conditions. Prior studies of cathepsin B cleavage properties at pH 5.5 (71,72) showed that the enzyme prefers P2 residues of Arg and Lys, but not Glu, and prefers P1 residues of Arg and Lys. These findings suggest that the cleavage specificity of cathepsin B at pH 5.5 (71,72) resembles that of cathepsin B at pH 7.2. But cathepsin B at pH 5.5 did not display the pH 4.6 preference of the enzyme for Glu as the P2 residue found in this study. These findings together demonstrate pH-dependent cleavage specificities of cathepsin B.

The differential P2 and P1 residue preferences of cathepsin B were utilized to design and assess pH-selective peptide–AMC substrates. The Z-Arg-Lys–AMC substrate displayed high preference for neutral pH cathepsin B compared to several related substrates tested. The presence of Glu at the P2 position of Z-Glu-Lys–AMC was the rationale for its function as a selective substrate for acidic pH 4.6 cathepsin B. These findings demonstrate that the pH-dependent cleavage properties can provide the basis for design of pH-selective substrates of cathepsin B.

Significantly, design and synthesis of the Z-Arg-Lys–AOMK inhibitor resulted in selective and potent inhibition of neutral pH cathepsin B activity; this inhibitor was designed based on the neutral pH-selective Z-Arg-Lys–AMC substrate. At pH 7.2, the Z-Arg-Lys–AOMK inhibitor displayed potent inhibition with a low K_I of 130 nM, but it was less effective at pH 4.6 with a higher K_I of 15000 nM. These results show that Z-Arg-Lys–AOMK is 115 times more potent at neutral pH 7.2 compared to acidic pH 4.6. Z-Arg-Lys–AOMK was shown to be an irreversible inhibitor with specificity for inhibition of cathepsin B over other cysteine cathepsins (cathepsins L, V, S, X, K, C, and H). Docking of Z-Arg-Lys–AOMK to cathepsin B at pH 7.2 was modeled by MOE, which illustrated the active site binding features of the inhibitor. The model featured the ionic interaction of the positively charged P2 Arg residue of the peptidic inhibitor with the negatively charged Glu245 residue of the S2 subsite of cathepsin B at pH 7.2, which was absent at pH 4.6. This proposed interaction is consistent with studies showing the importance of Glu245 for interactions of the enzyme with the P2 residue of peptides. (60,68) Future studies of inhibitor and enzyme binding interactions can be gained through in-depth structural and computational investigation. Importantly, the findings of this study demonstrate Z-Arg-Lys–AOMK as a novel inhibitor that selectively and potently inhibits cathepsin B at neutral pH.

The Z-Glu-Lys–AOMK inhibitor displayed inhibition of neutral and acidic cathepsin B at micromolar levels of inhibitor with only a 3-fold difference in potency, even though the substrate Z-Glu-Lys–AMC preferentially detected acidic pH cathepsin B activity (rather than neutral pH activity). It appears that substitution of AOMK for the AMC of the Glu-Lys dipeptide removed its pH selectivity. It is noted that Lys at the P1 position is preferred for neutral pH cathepsin B activity, and thus, the Lys at P1 may influence the inhibitor properties of Z-Glu-Lys–AOMK. These data show that a pH-selective peptide–AMC substrate may not always lead to a pH-selective peptidic AOMK inhibitor. Nonetheless, Z-Glu-Lys–AOMK represents a novel inhibitor of cathepsin B.

The neutral, cytosolic pH functions of cathepsin B due to lysosomal leakage occur in brain disorders and in numerous human diseases involving physiological organ systems. (12−32) Lysosomal leakage results in translocation of cathepsin B from the lysosome to the cytosol where cathepsin B initiates apoptotic cell death (33−36) and activates IL-1β production in inflammation. (31,37−39) Cathepsin B leakage to the cytosol occurs in brain disorders: AD, (14−17) TBI and ischemia, (18−21) Parkinson's disease (22,23), Niemann–Pick disease and lysosomal storage disorders, (24,25) and pneumococcal meningitis. (84) These neurodegenerative disorders also involve calpain in membrane permeabilization of lysosomes, allowing cathepsin B to exit the lysosome and enter the cytosol, known as the calpain–cathepsin hypothesis. (85,86) Other human diseases that involve lysosomal leakage of cathepsin B include autoinflammatory disease, (26,27) atherosclerosis, (28,29) and pancreatitis. (30) In addition to the pathogenic function of cathepsin B in the cytosol, cathepsin B also functions at neutral pH in extracellular locations in cancer (42−46) and rheumatoid arthritis (47) and nuclear locations in thyroid carcinoma, (49) in chromosome segregation, (50) and in the thyroid follicle. (48) In cancer, the tumor environment has been found to be at pH 6.8 due to the Warburg effect for tumor

acidosis; (87,88) the Z-Arg-Lys–AOMK inhibitor was also found to be effective at pH 6.8 with an IC_{50} value of 22 nM (Figure 2.S10). Overall, the prevalence of cytosolic cathepsin B in human diseases emphasizes the critical importance of this study to gain an understanding of the unique neutral pH properties of cathepsin B compared to its normal acidic lysosomal features.

In summary, the novel pH-dependent cleavage properties of the major dipeptidyl carboxypeptidase activity of cathepsin B were revealed by MSP-MS substrate profiling that led to design of pH-selective substrates and novel peptidic AOMK inhibitors. Notably, Z-Arg-Lys–AOMK was demonstrated as a potent, neutral pH inhibitor of cathepsin B. These findings demonstrate that the distinct pH-dependent cleavage properties of cathepsin B can provide the basis for development of a neutral pH inhibitor with more than 100-fold greater potency at pH 7.2 compared to pH 4.6. The novel Z-Arg-Lys–AOMK inhibitor may allow future studies to probe the role of pathogenic neutral pH cathepsin B functions that participate in brain disorders and human diseases.

2.4 Methods and Materials

2.4.1 Enzymes, Peptides, and Reagents

Recombinant human cathepsin B and cathepsin proteases were obtained from R&D Systems (Minneapolis, MN) or Abcam (Cambridge, MA), consisting of cathepsin B (R&D no. 953-CY-010), cathepsin L (R&D no. 952-CY-010), cathepsin V (R&D no. 1080-CY-010), cathepsin S (R&D no. 1183-CY-010), cathepsin K (Abcam no. ab157067), cathepsin C (R&D no. 1071-CY-010), and cathepsin H (R&D no. 75116-CY-010). The design and synthesis of the 228 14-mer peptides used for MSP-MS assays have been described previously. (53,89) MSP-MS assays utilized low-bind 600 μL microtubes (Corning, Reynosa, MX), dithiothreitol (DTT; Promega no. V351, Madison, WI), urea (Teknova no. U2222, Hollister, CA), HPLC-grade water

(Fisher Chemical no. W6-4), citric acid monohydrate (Merck no. 1.00244.0500, Burlington, MA), sodium phosphate dibasic anhydrous (EMD no. SX-072305, Burlington, MA), sodium acetate (Fisher Scientific no. BP-333-500, Fair Lawn, NJ), EDTA (Calbiochem no. 324503, Burlington, MA), sodium chloride (Fisher Chemical no. S271-1, Pittsburgh, PA), acetonitrile (Fisher Chemical no. A955-4, Pittsburgh, PA), formic acid (FA; Fisher Chemical no. A117-50, Pittsburgh, PA), trifluoroacetic acid (TFA; Fisher Chemical no. A116-50, Pittsburgh, PA), C18 LTS Tips (Rainin no. PT-LC18-960, Oakland, CA), C18 for SPE stage-tips (3 M company no. 2215-C18, Maplewood, MN), and BEH C18 packing material (Waters Corporation no. 186004661, Milford, MA). Fluorogenic peptide substrates were obtained from Bachem, Torrance, CA, and consisted of Abz-Gly-Ile-Val-Arg-Ala-Lys(Dnp)-OH (no. 4049308), Z-Arg-Arg–AMC (no. 4004789), Arg–AMC (no. I-1050), and Gly-Arg–AMC (no. 4002196). Z-Phe-Arg–AMC was purchased from Anaspec, Fremont, CA (no. AS-24096). Z-Lys-Lys–AMC, Z-Lys-Arg–AMC, Z-Arg-Lys–AMC, Z-Glu-Lys–AMC, and Z-Glu-Arg–AMC were custom synthesized by Genscript (Piscataway, NJ). MCA-Arg-Pro-Pro-Gly-Phe-Ser-Ala-Phe-Lys(Dnp)-OH was from CPC Scientific, San Jose, CA (no. AMYD-111A). E64c was from Selleckchem (Houston, TX); CA-074 and CA-074Me were from SigmaMillipore (Burlington, MA). Cell culture media components MEMalpha, F-12K, and FBS were from ThermoFisher (Watham, MA), and F-12K was from ATCC (Manassas, VA). The DC protein kit was from Biorad (Hercules, CA).

2.4.2 Cathepsin B Activity and Stability

Recombinant human pro-cathepsin B was activated to mature cathepsin B by incubation at 37 °C for 30 min in activation buffer (20 mM Na-acetate (pH 5.5), 1 mM EDTA, 5 mM DTT, 100 mM NaCl). To examine enzyme activity and stability, cathepsin B was preincubated at pH 7.2 or pH 4.6 at room temperature (RT, 27 °C) and 37 °C for times of 0.5, 1, 2, 3, and 4 h. Cathepsin B

activity was then assayed in 50 mM citrate phosphate at pH 7.2 or pH 4.6, 40 mM Z-Phe-Arg–AMC substrate, 1 mM EDTA, 100 mM NaCl, 5 mM DTT, and 0.01% Tween20 with incubation at RT for 30 min. Cleavage of Z-Phe-Arg–AMC to generate fluorescent AMC was monitored at excitation 360 nm and emission 460 nm. Assays for each condition were conducted in triplicate, and the mean ± SD values were calculated.

2.4.3 Cathepsin B Cleavage Site Analysis by Multiplex Substrate Profiling by Mass Spectrometry (MSP-MS)

Cathepsin B activity (activated) was titrated with E64c to calculate the concentration of active cathepsin B. For MSP-MS assays, cathepsin B (0.1 ng/μL, activated) was incubated with a peptide library of 228 14-mer peptides, each at 0.5 μM peptide, in buffer consisting of 50 mM citrate phosphate at pH 7.2 or pH 4.6, 1 mM EDTA, 100 mM NaCl, and 4 mM DTT (total volume of 46 μL). After incubation for 15 and 60 min at 25 °C, 20 μL aliquots were removed and combined with 80 μL of 8 M urea. An inactivated cathepsin B control consisted of cathepsin B in assay buffer combined with 8 M urea for 60 min at 25 °C for denaturation, followed by addition of the peptide library. After incubation, samples were acidified by addition of 40 μL of 2% FA, desalted using C18 LTS Tips (Rainin), evaporated to dryness in a vacuum centrifuge, and stored at −70 °C. Samples were resuspended in 20 μL of 0.1% FA (solvent A), and 1 μL was used for LC-MS/MS analysis. All MSP-MS conditions were conducted in quadruplicate assays.

MSP-MS assay samples were then subjected to LC-MS/MS performed on a Q-Exactive mass spectrometer (Thermo) equipped with an Ultimate 3000 HPLC (Thermo Fisher). Peptides were separated by reverse phase chromatography on a C18 column (1.7 μm bead size, 75 μm × 20 cm, 65 °C) at a flow rate of 400 nL/min using solvent A (0.1% FA in water) and solvent B (0.1% FA in acetonitrile). LC separation was performed using a 50 min linear gradient of 5% to 30% solvent B followed by a 15 min linear gradient of 30% to 75% solvent B. Survey scans were

recorded over a 200–2000 *m*/*z* range (70000 resolutions at 200 *m*/*z*, AGC target 1×10^6, 75 ms maximum). MS/MS was performed in data-dependent acquisition mode with HCD fragmentation (30 normalized collision energy) on the 10 most intense precursor ions (17500 resolutions at 200 *m*/*z*, AGC target 5×10^4, 120 ms maximum, dynamic exclusion 15 s). A technical report of the LC-MS/MS method is provided in Methods S1.

Peak integration and peptide data analysis were performed using PEAKS (v 8.5) software (Bioinformatics Solutions Inc.). A summary of the PEAKS search parameters is provided in the Methods S2. MS^2 data were searched against the 228-member tetradecapeptide library sequences, and a decoy search was conducted with sequences in reverse order. A precursor tolerance of 20 ppm and 0.01 Da for MS^2 fragments was defined. No protease digestion was specified. Data were filtered to 1% peptide false discovery rates with the target-decoy strategy. Peptide intensities were quantified, and data was normalized by Loess-G algorithm (http://normalyzer.immunoprot.lth.se/) and filtered by 0.5 peptide quality. Outliers from replicates were removed by Dixon's Q testing (90) when there were at least 3 replicate values found out of the 4 replicates for each condition for every peptide. Missing and zero values are imputed with random normally distributed numbers in the range of the average of the smallest 5% of the data ± SD. An ANOVA test was performed for peptide data found in the three conditions of control, 15 min incubation, and 60 min incubation; those with $p < 0.05$ were considered for further analysis. Cleaved peptide products were defined as those with intensity scores of 8-fold or more above the quenched inactive cathepsin B, assessed using the ratio of $\log_2$(Cat.B/inactivated enzyme) for each peptide product. Ratios were evaluated for $p < 0.05$ by 2-tailed homoscedastic *t* test (Methods S3 for "Workbook of MSP-MS data").

2.4.4 Analyses of MSP-MS Data for Cleavage Preferences of Cathepsin B by iceLogo

Evaluation of the frequencies of amino acids adjacent to the cleavage sites was conducted using the iceLogo software. (91) IceLogo analyses utilized (a) the "positive data set" consisting of the P2 to P2′ amino acids that surround the cleavage sites between the 12th and 13th amino acid of the 14-mer peptides and (b) the "negative data set" consisting of the P2 to P2′ amino acids for the 228 cleavage sites of the peptide library between the 12th and 13th amino acid. All positive and negative data are listed in Methods S3. Analyses involved *Z*-scores calculated by the equation $X - \mu/\sigma$, where X is the frequency of the amino acid in the experimental data set, μ is the frequency of a particular amino acid at a specific position in the reference set (control "0" time), and σ is the standard deviation. *Z*-scores were utilized to generate iceLogo illustrations of the relative frequencies of amino acid residues at each of the P2 to P2′ positions of the cleaved peptides where heights of the single letter amino acids represent "percent difference", defined as the difference in frequency for an amino acid appearing in the positive data set relative to the negative data set. Positive differences are shown above the midline, and negative differences are represented below the midline. Residues below the line shown in gray are those that were absent in the positive data set.

2.4.5 Synthesis of Z-Arg-Lys–AOMK and Z-Glu-Lys–AOMK inhibitors

Inhibitor synthesis was achieved in three steps via production of Fmoc-Lys(Boc)–AOMK, semicarbazide aminomethyl polystyrene resin (**5**), and Z-Arg-Lys–AOMK and Z-Glu-Lys–AOMK (illustrated in Figure 2.S5).

For Fmoc-Lys(Boc)–AOMK synthesis, *N*-methylmorpholine (1.06 g, 10.5 mmol) and isobutyl chloroformate (1.434 g, 10.5 mmol) were added dropwise to a stirred solution of amino acid **1** (4.68 g, 10.0 mmol) in 100 mL of dry tetrahydrofuran (THF) in a 200 mL flame polished

round-bottom flask at −10 °C. After 15 min, ethereal diazomethane was generated and distilled from Diazald (6.43 g, 30.0 mmol) in accordance to procedures outlined in the Aldrich Technical Bulletin al180 into stirred solution over the course of 30 min (AL-180) (Sigma-Aldrich Technical Bulletin al180 for Diazald and Diazomethane Generators). After distillation, the reaction was warmed to 25 °C and stirring was continued for 1 h. Glacial acetic acid was added dropwise after being chilled to quench excess diazomethane, and 33% HBr in acetic acid was added dropwise until a red tint persisted for more than 5 min. The solvent was removed *in vacuo*, and the products was re-dissolved in ethyl acetate and subsequently washed with water, sat. aq. $NaHCO_3$ twice, and sat. aq. NaCl, and dried over $MgSO_4$. A flame-dried 20 mL scintillation vial charged with anhydrous potassium fluoride (5 g, 100 mmol) and 26-dimethylbenzoic acid (7.509 g. 50 mmol) in 10 mL of anhydrous dimethylformamide (DMF) was sonicated for 5 min. Compound **2** dissolved in a minimal amount of anhydrous DMF was added dropwise to stirred solution of carboxylic acid and base. After 30 min, the solution was diluted with 250 mL of ethyl acetate, washed twice with 200 mL of sat. aq. NaCl and briefly with 1 M NaOH, sat. aq. $NaHCO_3$, and sat. aq. NaCl, and dried over $MgSO_4$. The crude oil was purified by flash chromatography using 3:1 hexane/ethyl acetate to yield **3** in 81% yield.

For production of semicarbazide aminomethyl polystyrene resin (**5**), a flame-dried 500 mL round-bottom flask was charged with a magnetic stir bar, aminomethyl polystyrene resin (25 g, 28.75 mmol), and *N*,*N*′-carbonyldiimidazole (46.62 g, 287.5 mmol) in 250 mL of anhydrous dichloromethane (DCM), and the reaction was stirred under positive argon pressure for 3 h to generate **4** (Figure 2.S5). The resin was washed once with anhydrous DCM and once with anhydrous DMF, transferred into a new flame-dried vessel, and resuspended in 250 mL of anhydrous DMF. To this stirred solution, anhydrous hydrazine (55.29 g, 54.15 mL, 1725 mmol)

was added gradually over 5 min. The reaction was stirred at RT for 1 h. The resin was filtered, washed 5 times with DCM and 5 times with MeOH, dried thoroughly *in vacuo,* and stored at 4 °C.

A flame-dried 100 mL round-bottom flask was charged with amino acid **3** (1.09 g, 2.0 mmol) and **5** (1.00 g, 1.15 mmol/g), and the mixture was dried *in vacuo* for 6 h and suspended in 20 mL of anhydrous THF. This stirred solution was heated at 70 °C for 18 h to generate preloaded resin, Fmoc-Lys(Boc)–AOMK:SCR **6**. The excess amino acid derivative was recovered, and the resin washed twice each with DMF, DCM, and MeOH, dried thoroughly, and stored at −20 °C.

For synthesis of Z-Arg-Lys–AOMK and Z-Glu-Lys–AOMK, preloaded resin **6** was presolvated in DCM for 30 min before two 15 min treatments of 5% diethylamine in DMF (1 mL/100 mg). Fmoc-glycine, *O*-(1*H*-6-chlorobenzotriazole-1-yl)-1,1,3,3-tetramethyluronium hexafluorophosphate (HCTU), and *N*,*N*-diisopropylethylamine at a 3:3:10 ratio with respect to the loading of the resin were used to couple Z-Arg-OH or Z-Glu-OH. The resin was washed with DCM and MeOH 3 times before being dried *in vacuo*. Cleavage was performed using 1 mL of TFA/water/triisopropylsilane at a 95:2.5:2.5 ratio per 100 mg of resin for 1 h. The resin was washed with another aliquot of cleavage cocktail, and the combined cleavage solutions were concentrated before precipitation with cold diethyl ether. The pellet was dried under a stream of argon and dissolved in a minimal volume of DMSO before purification by preparatory reverse phase HPLC (19 mm × 150 mm XBridge C18, CH_3CN/H_2O/0.1% TFA, 25:75 to 70:30 over 13 min; 20 mL/min) and lyophilization.

2.4.6 Cathepsin B Activity Assayed by Fluorogenic Peptide Substrates

Proteolytic assays of cathepsin B were conducted with Z-Arg-Lys–AMC and Z-Gly-Lys–AMC substrates in 50 mM citrate phosphate at pH 7.2 or pH 4.6, 1 mM EDTA, 100 mM NaCl, and 5 mM DTT. Assays with Z-Phe-Arg–AMC substrate were conducted under identical

conditions and included 0.01% Tween20. Assays were performed in 384 well plates at 25 °C in a total volume of 30 μL. Fluorescence was quantified by a Biotek Synergy HTX microplate plate reader with excitation 360 nm, emission 460 nm, gain 50, top optics, and read height 1 mm. Proteolytic activity is reported as relative fluorescent units per second (RFU/s) and was calculated using the highest slope recorded for 10 consecutive readings. Fluorescent readings were taken in 46 s intervals, and therefore activity is calculated over a total of 460 s. To ensure that initial velocity is assessed, only readings within the first 30 min of the reaction were analyzed. RFU/s readings were converted to enzyme specific activity of pmol/(min/μg) using the conversion factor of 1227 RFU per micromolar AMC.

For Michaelis–Menten kinetic characterization, assays contained 20 μL of substrate (Z-Phe-Arg–AMC, at different concentrations) and 10 μL of 0.125 ng/μL cathepsin B for a final enzyme concentration of 0.0417 ng/μL. The final concentrations of substrates were 225 μM to 2.6 μM with DMSO concentration of 4.5% v/v.

For the substrates Z-Arg-Lys–AMC, Z-Glu-Lys–AMC, and Z-Phe-Arg–AMC, k_{cat}/K_m values were calculated using the equation $v_0 = V_{max}[S]/(K_m + [S])$ where v_0 is the activity at a corresponding substrate concentration [S] and V_{max} is the maximum enzyme velocity at saturated [S] concentration. $V_{max} = k_{cat}[E]_T$, where $[E]_T$ is the total enzyme concentration. K_m is the x-axis value where $y = V_{max}/2$ and V_{max} is the maximum rate at saturating substrate concentrations. At low [S], k_{cat}/K_m was calculated from the slope of the plot of $v_o/[E]$ vs [S] concentration (linear portion of plot). All data was plotted, calculated, and analyzed using GraphPad Prism9 software.

To generate the pH profile of cathepsin B activity with the substrates Z-Arg-Lys–AMC, Z-Glu-Lys–AMC, and Z-Phe-Arg–AMC, 60 μM of each substrate and 0.04 ng/μL cathepsin B were

assayed in citrate phosphate buffers ranging from pH 2.2 to 7.4 in increments of 0.4 pH units, including pH 7.2. For assay buffers ranging from pH 7.4 to 9.0, 50 mM Tris-HCl was used instead of 50 mM citrate phosphate, with inclusion of pH 7.2.

2.4.7 Inhibitor Kinetic Characterization Using Fluorogenic Assays for Cathepsin B Activity

Kinetic analyses of IC_{50}, K_I, k_{obs}, and k_{inact}/K_I values for Z-Arg-Lys–AOMK and Z-Glu-Lys–AOMK inhibition of cathepsin B were conducted by fluorogenic proteolytic assays consisting of 40 μM Z-Phe-Arg–AMC, 40 mM citrate phosphate at pH 7.2 or pH 4.6, 1 mM EDTA, 100 mM NaCl, 5 mM DTT, and 0.01% Tween 20; assays were performed at RT (22–27 °C) in quadruplicate. Inhibitor and substrate were combined in the reaction well, and the assay was started upon addition of cathepsin B (0.04 ng/μL). The inhibitor concentration ranged from 5.5 μM to 1.1 nM (1.5-fold serial dilution). A vehicle control assay contained 2% DMSO instead of inhibitor. Enzyme velocity (RFU/s) was measured during a 30 min incubation period as relative fluorescent units per second (RFU/s), calculated using the highest slope recorded for 10 consecutive readings taken at 46 s intervals (thus, activity is calculated over a total of 460 s). Prism software was used to analyze enzyme activity data in kinetic studies. IC_{50} values were calculated (without preincubation of inhibitor and enzyme) as the concentration of inhibitor that reduced cathepsin B activity by 50%.

For determination of K_I and k_{inact}/K_I kinetic inhibition constants, k_{obs} constants were determined by plots of cathepsin B activity in time courses with different inhibitor concentrations by curve fitting slope data of RFU versus time into $Y = Y_0\ e^{(-k_{obs}X)}$, where Y_0 is the activity for the control with no inhibitor condition, Y is the activity in the presence of inhibitor, and X is time. K_I and k_{inact} values were calculated from curve fitting the k_{obs} values into the equation $k_{obs} = k_{inact}[I]/(K_I + [I])$, where [I] is inhibitor concentration, K_I is the x-axis inhibitor

concentration at which $y = k_{inact}/2$, and k_{inact} is the maximum rate of inactivation at saturating inhibitor concentrations. (92,93) These kinetic analyses are for irreversible inhibitors, Z-Arg-Lys–AOMK and Z-Glu-Lys–AOMK of this study, that utilize K_I values, rather than K_i values used for reversible inhibitors. (92)

2.4.8 Irreversible Mechanism of Inhibitors

The irreversible or reversible mechanism of cathepsin B inhibition was assessed for Z-Arg-Lys–AOMK and Z-Glu-Lys–AOMK inhibitors. At pH 7.2, cathepsin B was incubated with 190 nM Z-Arg-Lys–AOMK and 4.99 μM Z-Glu-Lys–AOMK for 15 min in pH 7.2 assay buffer, and the assay was performed as described above for pH 4.6. Proteolytic activity was monitored for 2 h. At pH 4.6, cathepsin B (activated, 3.7 ng/μL) was incubated with 4.24 μM Z-Arg-Lys–AOMK and 3.48 μM Z-Glu-Lys–AOMK for 15 min in 40 mM citrate phosphate (pH 4.6), 1 mM EDTA, 100 mM NaCl, and 5 mM DTT; a vehicle control contained 2.5% DMSO. Each reaction was then diluted 100-fold in assay buffer such that the final assay composition was 0.04 ng/μL cathepsin B, 40 μM Z-Phe-Arg–AMC, and an inhibitor concentration of 1/10th the IC_{50} value.

2.4.9 Inhibitor Inhibition of Peptide Cleavages Characterized by MSP-MS

MSP-MS assays in the presence of inhibitors were performed as outlined above except cathepsin B (0.1 ng/μL) was preincubated with Z-Arg-Lys–AOMK (64 nM) or a vehicle control (0.5% DMSO) for 30 min at 25 °C prior to incubation with the peptide library for 60 min in 40 mM citrate phosphate at pH 7.2 or pH 4.6, 1 mM EDTA, 100 mM NaCl, and 5 mM DTT buffer. Assays were conducted in quadruplicate and immediately stored at −70 °C following quenching with 8 M urea.

2.4.10 Specificity of Inhibitors for Other Cysteine Cathepsin Proteases

The effects of Z-Arg-Lys–AOMK and Z-Glu-Lys–AOMK on cathepsin V, L, K, S, X, H, and C activities were assessed. IC_{50} values were calculated at pH 4.6 and pH 7.2 conditions, consisting of 40 mM citrate phosphate, 1 mM EDTA, 100 mM NaCl, and 5 mM DTT. The inhibitor concentrations ranged from 16.38 μM to 0.5 nM with 2-fold serial dilutions. When activity (RFU/s) in the presence of 16.38 μM inhibitor was reduced by <50% compared to DMSO control, the IC_{50} value was indicated as >16 μM. Cathepsin V (0.04 ng/μL), cathepsin L (0.03 ng/μL), cathepsin K (0.10 ng/μL), and cathepsin S (0.20 ng/μL) were assayed with 40 μM Z-Phe-Arg–AMC. Cathepsin X (0.20 ng/μL), cathepsin C (0.51 ng/μL), and cathepsin H (0.1 ng/μL) were assayed with 40 μM MCA-Arg-Pro-Pro-Gly-Phe-Ser-Ala-Phe-Lys(Dnp)-OH, Gly-Arg–AMC, and Arg–AMC, respectively. Activation of pro-cathepsin H to cathepsin H was conducted by incubation of cathepsin H (4.4 ng/μL) with cathepsin L (1.1 ng/μL) at RT for 2 h in activation buffer (20 mM citrate phosphate (pH 6.0), 100 mM NaCl, and 5 mM DTT). Cathepsin C (13.78 ng/μL) was activated by incubation with cathepsin L (3.4 ng/μL) at RT for 1 h in activation buffer (20 mM citrate phosphate (pH 6.0), 100 mM NaCl, 5 mM DTT). It was confirmed that cathepsin L did not cleave the cathepsin C and cathepsin H substrates Gly-Arg–AMC and Arg–AMC, respectively. For all assays containing peptide–AMC substrates, the fluorescent microplate reader settings were the same as outlined above for cathepsin B. For the cathepsin X assay, the plate reader was set to excitation 320 nm, emission 400 nm, gain 105, top optics, and read height 1 mm. To convert RFU/s to pmol/min, 10 μM to 0.005 μM (2-fold serial dilution) of MCA-Arg-Pro-Pro-Gly-Phe-Ser-Ala-Phe-Lys(Dnp)-OH was fully hydrolyzed with excess cathepsin X and a standard curve was generated using the total fluorescence values calculated at each concentration.

2.4.11 MOE Modeling of Z-Arg-Lys–AOMK Binding Interactions with Cathepsin B

The Molecular Operating Environment (MOE) modeling software (64,65) was used to model Z-Arg-Lys–AOMK binding to cathepsin B using the crystal structure of cathepsin B (PDB 1QDQ), (60) cocrystal template with the inhibitor CA-074 as default binding ligand. The builder function of MOE was used to examine binding poses that considered polar contacts and hydrogen bonds between ligand and the active site pocket of 1QDQ at pH 7.2. Docking simulations were performed with energy-minimized structures to assess ligand flexibility and poses using the MOE docking feature.

2.4.12 Cathepsin B in Human Neuroblastoma Cells Treated with Inhibitors

Neuroblastoma cells (human SHSY5Y) were grown in media consisting of 50% MEMalpha and 50% F12-K with 10% heat-inactivated FBS at 37 °C in an atmosphere of 95% air and 5% CO_2. First, cell homogenates were prepared by collection of cells in 0.32 M sucrose and freeze–thawing. Second, cells were incubated with Z-Arg-Lys–AOMK or CA-074Me for 6 h at 37 °C and washed 3 times in phosphate-buffered saline, and homogenates were prepared in 0.32 M sucrose with freeze–thawing. CA-074Me is a methyl ester form of the active CA-074 selective inhibitor of cathepsin B; (69) CA-074Me penetrates the cell and is converted by intracellular esterases to CA-074.

Cathepsin B activity in the homogenates was monitored with Z-Arg-Arg–AMC substrate (60 μM) with buffer conditions of 40 mM citrate-phosphate (pH 5.5), 5 mM DTT, 1 mM EDTA, 100 mM NaCl, and 1.2% DMSO, followed by incubation at 37 °C for 30 min and reading of AMC fluorescence. CA-074-senstive activity was monitored to indicate cathepsin B activity, since CA-074 is a selective inhibitor of this enzyme. (69) Protein content was measured in homogenates with

the DC protein assay kit. Cathepsin B specific activity was calculated as nmol AMC/(μg/min) and reported as the mean ± SD (with analyses for statistical significance, $p < 0.05$ by Student's t test).

2.4.13 Data availability

LC-MS/MS files for the MSP-MS experiments can be accessed at www.massive.ucsd.edu under the dataset identifier numbers MSV000086449 and MSV000086447.

2.5 Supporting Information

Table 2.S1 Cathepsin B cleavages at positions 1-13 of peptide library substrates at 15 min. and 60 min. in MSP-MS analyses Supplemental Figures[a]

Cleavage at peptide bond number	pH 7.2 # cleavages		pH 4.6 # cleavages	
	15 min.	60 min.	15 min.	60 min.
1	0	0	0	0
2	0	0	0	0
3	0	0	0	0
4	0	0	0	0
5	0	0	0	0
6	0	0	0	0
7	1	1	0	1
8	0	2	1	2
9	1	2	1	2
10	5	11	11	30
11	1	2	3	8
12	30	44	67	95
13	2	3	1	4

[a]Cathepsin B was subjected to MSP-MS (multiplex substrate profiling mass spectrometry) analysis at neutral pH 7.2 and acidic pH 4.6. The number of cleavages at each of the peptide bonds at positions 1- 13 are illustrated for 15 minutes and 60 incubation of cathepsin B with the 228 14-mer peptide library in MSP-MS analyses. MSP-MS data by nano-LC-MS/MS was analyzed as described in the methods.

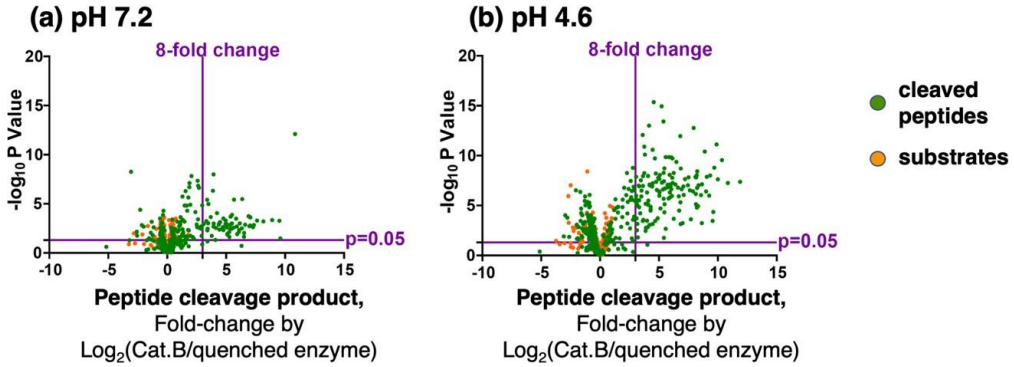

Figure 2.S1 Volcano plot of cathepsin B peptide cleavage products by MSP-MS at pH 7.2 and 4.6. Cathepsin B cleavage products generated were quantitated by log2(Cat.B/inactivated enzyme) as a measure of fold-change of peptide intensities above the quenched inactive enzyme, and assessed for p values ($p < 0.05$). (a) MSP-MS peptide products at pH 7.2. (b) MSP-MS peptide products at pH 4.6.

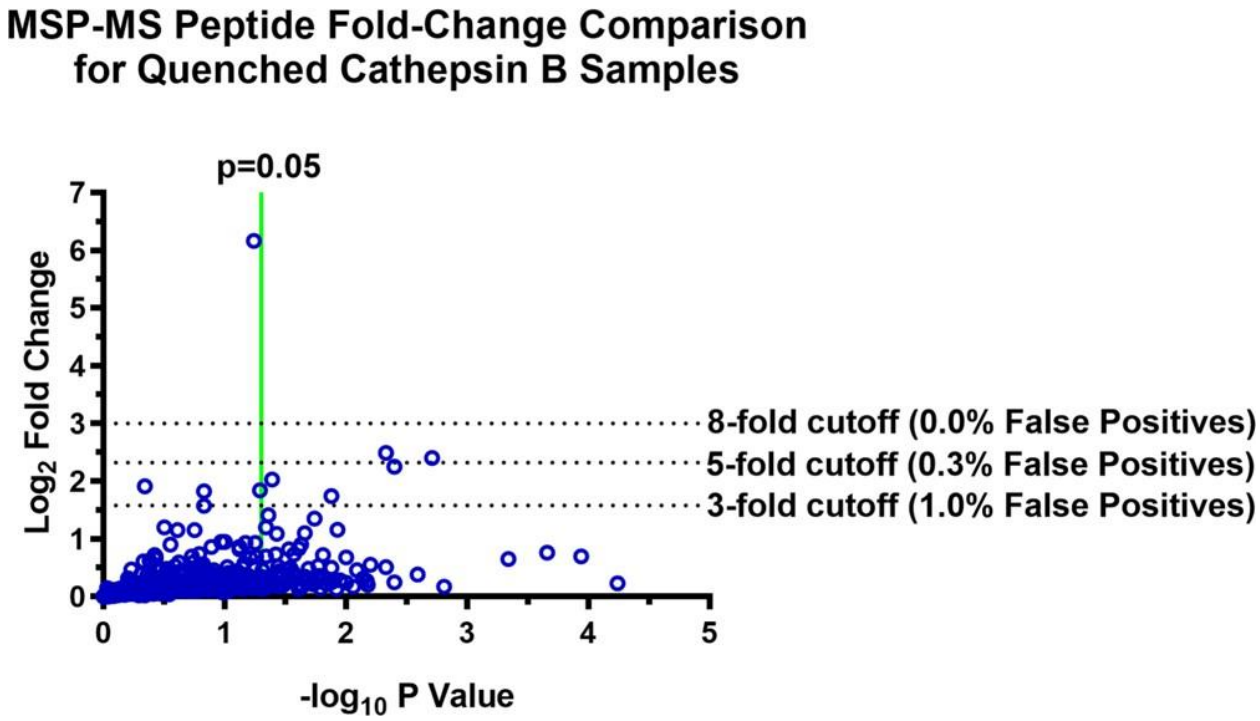

Figure 2.S2 MSP-MS assays: 0% False Positive Rate (FPR) for quenched cathepsin B control.

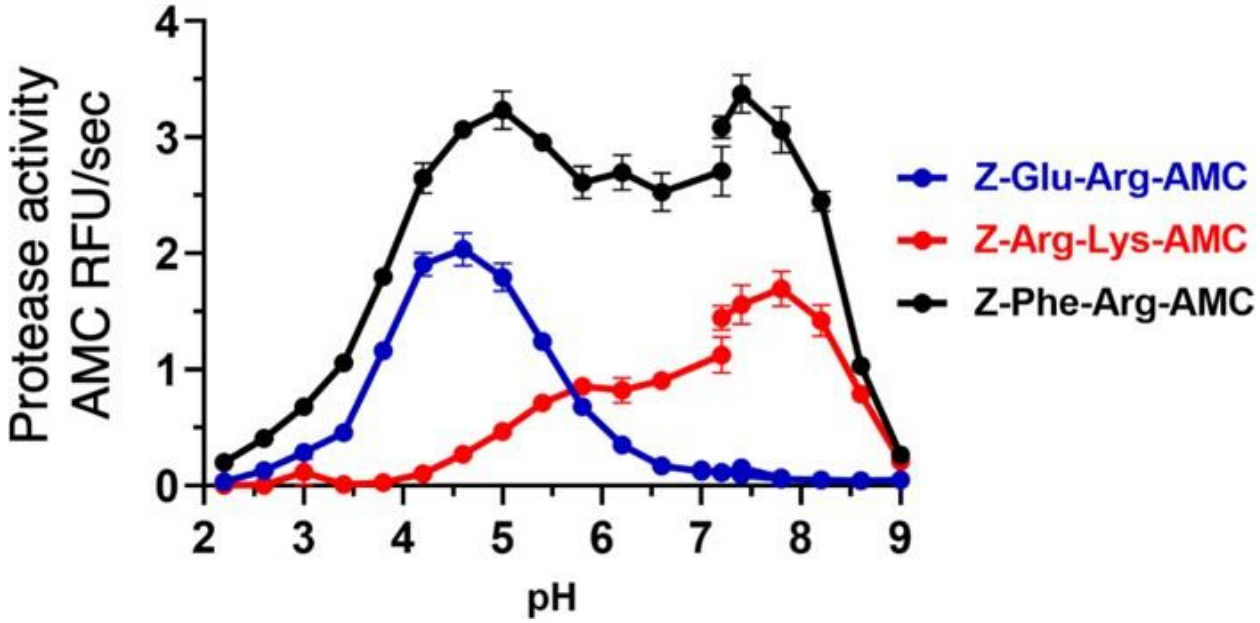

Figure 2.S3 pH curves for the substrates Z-Arg-Lys-AMC, Z-Glu-Lys-AMC, and Z-Phe-Arg-AMC with absolute relative fluorescence (RFU) values for cathepsin B activity.

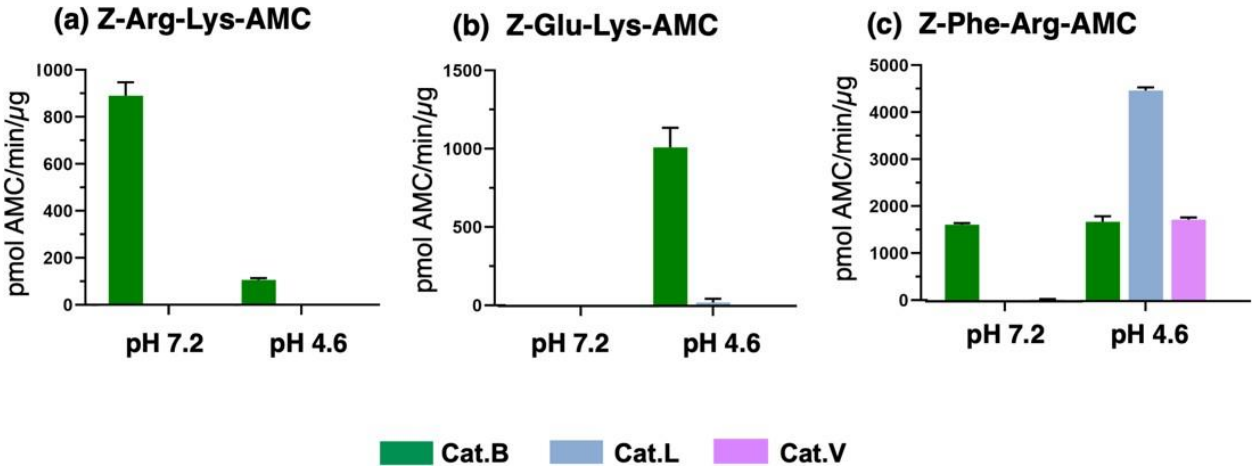

Figure 2.S4 Selectivity of Z-Arg-Lys-AMC and Z-Glu-Lys-AMC substrates for cathepsin B compared to cathepsins L and V, at pH 7.2 and pH 4.6, with comparison to Z-Phe-Arg-AMC. (a) Z-Arg-Lys-AMC substrate for cathepsin B compared to cathepsins L and V. (b) Z-Glu-Lys-AMC substrate for cathepsin B compared to cathepsins L and V. (c) Z-Phe-Arg-AMC substrate for cathepsin B compared to cathepsins L and V.

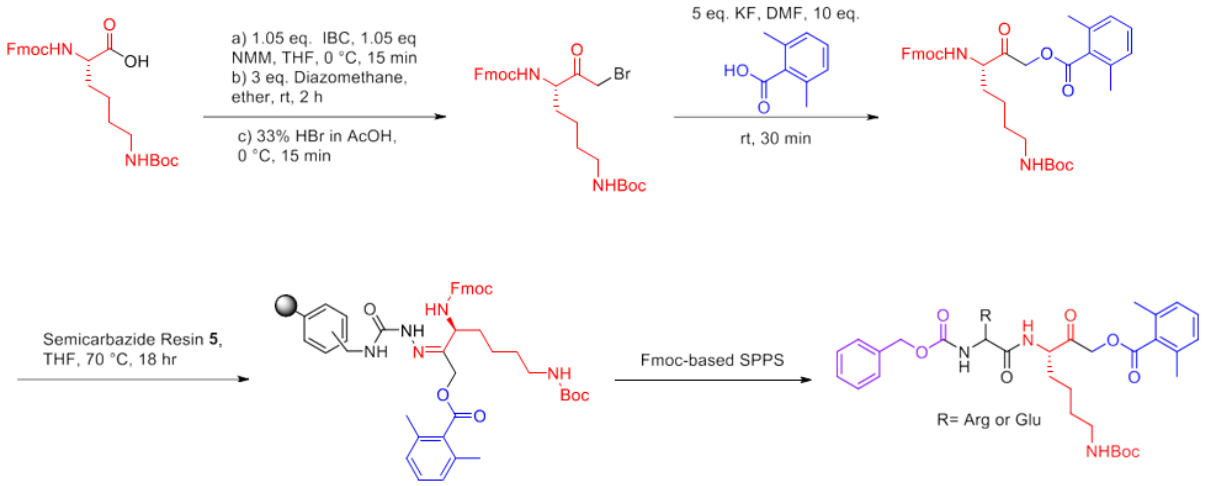

Figure 2.S5 Chemical synthesis of Z-Arg-Lys-AOMK and Z-Glu-Lys-AOMK inhibitors. The chemical synthetic steps for Z-Arg-Lys-AOMK and Z-Glu-Lys-AOMK inhibitors are illustrated. The AOMK warhead (blue), with the Lys residue (red), Arg or Glu at the P1 position (black), and the blocking group (purple) are shown. The chemical synthetic steps are described in the methods.

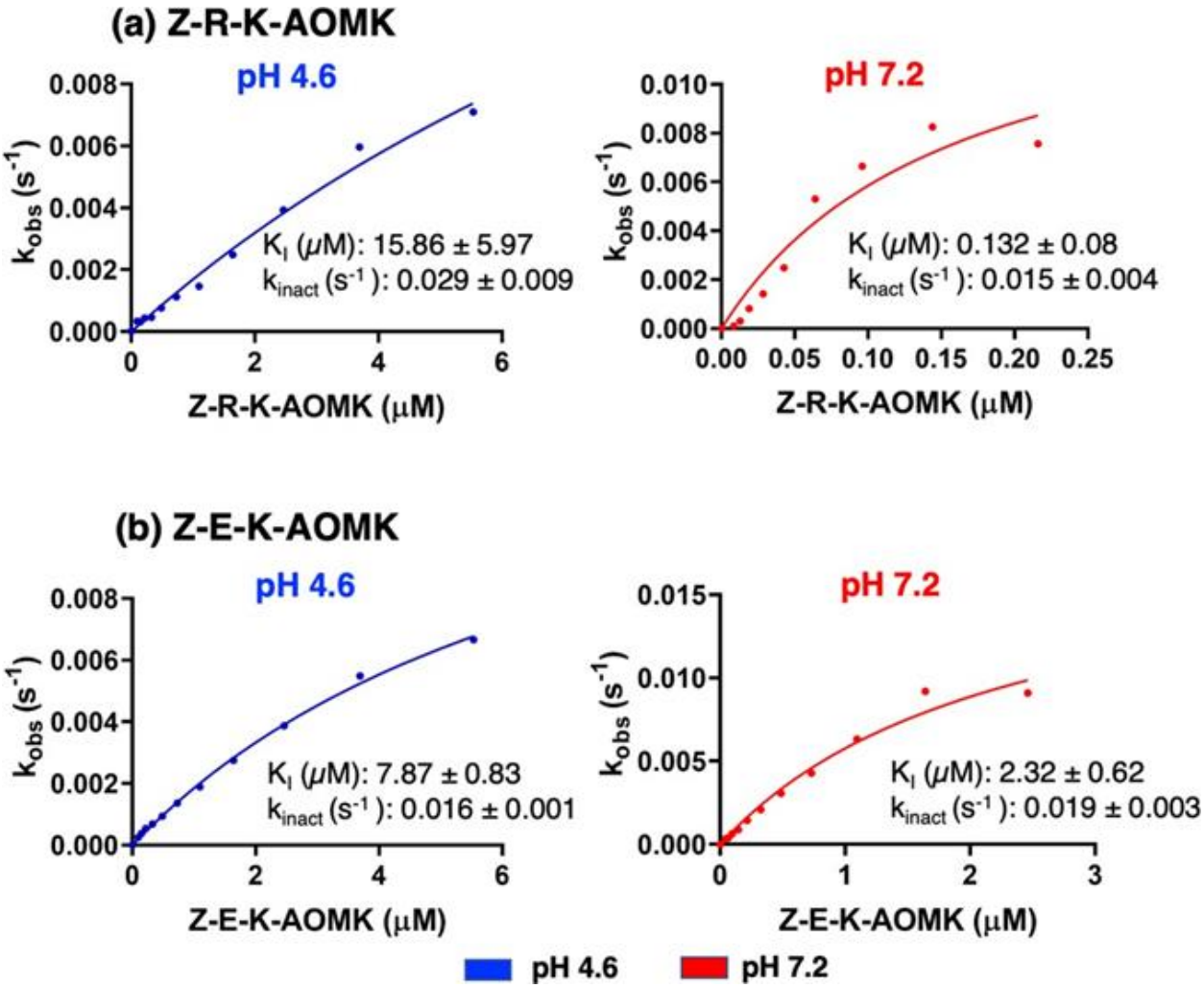

Figure 2.S6 KI determination of the cathepsin B inhibitors Z-Arg-Lys-AOMK and Z-Glu-Lys-AOMK. (a) Z-Arg-Lys-AOMK K_I determination at pH 7.2 and pH 4.6. (b) Z-Glu-Lys-AOMK K_I determination at pH 7.2 and pH 4.6.

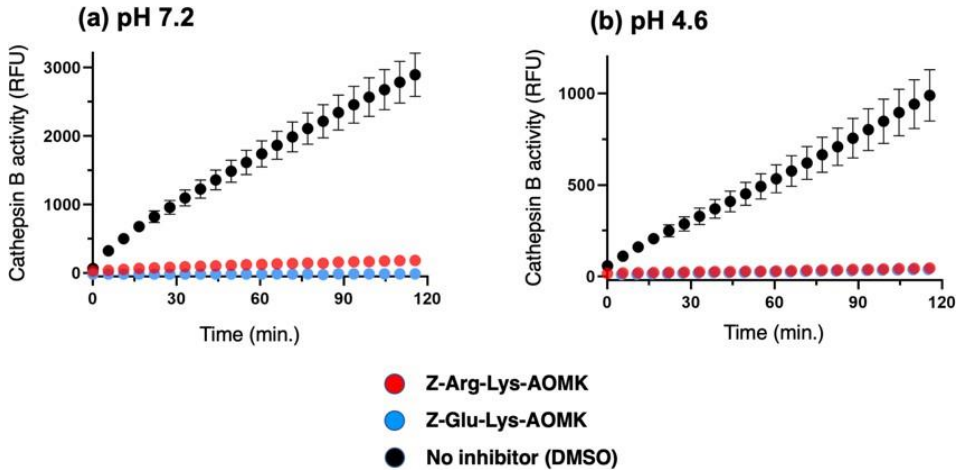

Figure 2.S7 Irreversible mechanism of Z-Arg-Lys-AOMK and Z-Glu-Lys-AOMK inhibition.

(a) Z-Arg-Lys-AOMK inhibition.

(b) Z-Glu-Lys-AOMK inhibition

Inhibitors were evaluated for irreversible or reversible inhibition of cathepsin B by dilution experiments. Cathepsin B was pre-incubated with inhibitor at 10 times the IC50 concentration, followed by dilution to 1/10 the IC50 concentration, addition of substrate (Z-F-R-AMC), and monitoring activity in time-course assays. Inhibition of cathepsin B following dilution indicates the irreversible inhibitory mechanism of Z-Arg-Lys- AOMK and Z-Glu-Lys-AOMK.

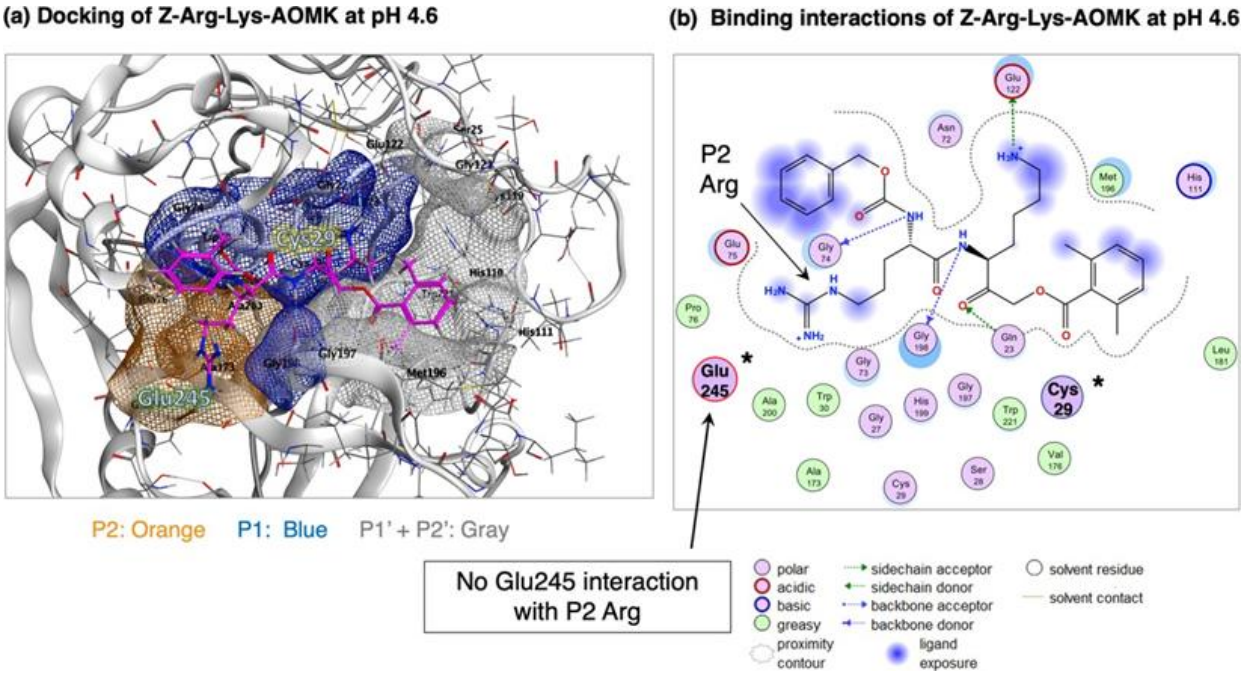

Figure 2.S8 Model of Z-Arg-Lys-AOMK inhibitor binding interactions to cathepsin B at pH 4.6.

(a) Model of the Z-Arg-Lys-AOMK inhibitor docking to cathepsin B at pH 4.6.

(b) Two-dimensional illustration of Z-Arg-Lys-AOMK and cathepsin B binding interactions at pH 4.6, showing lack of Glu245 interactions with the P2 Arg residue of the Z-Arg-Lys-AOMK inhibitor.

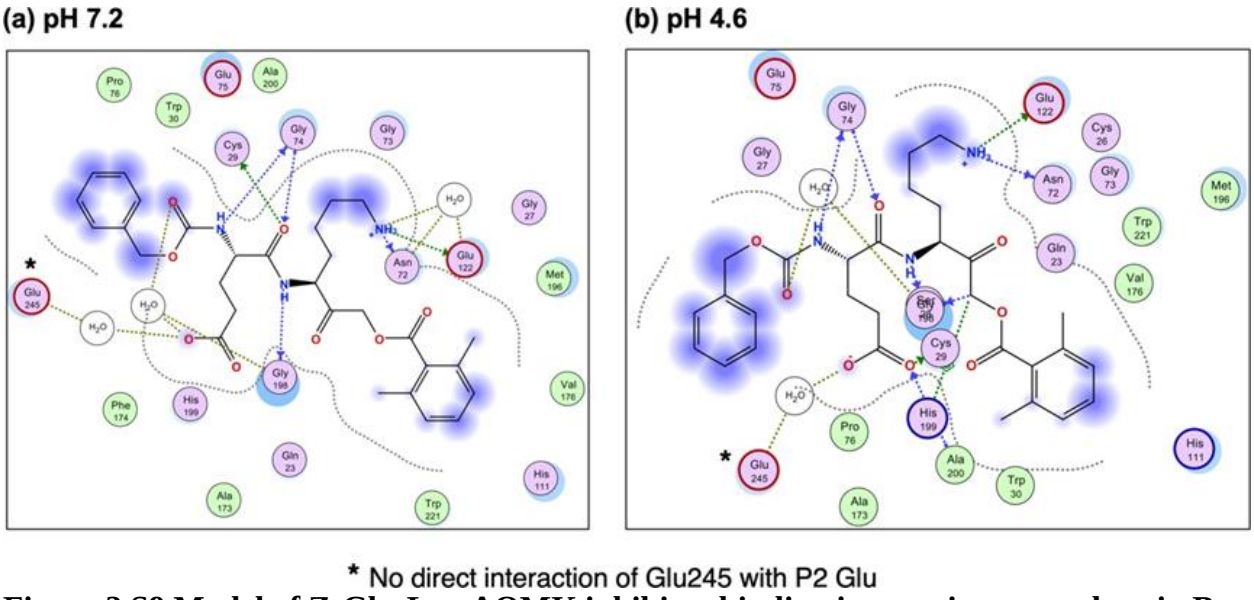

Figure 2.S9 Model of Z-Glu-Lys-AOMK inhibitor binding interactions to cathepsin B at pH 4.6 and pH 7.2. (a) pH 7.2 inhibitor docking. Two-dimensional illustration of Z-Glu-Lys-AMOK interactions with cathepsin B at pH 7.2. (b) pH 4.6 inhibitor docking. Two-dimensional illustration of Z-Glu-Lys-AMOK interactions with cathepsin B at pH 4.6.

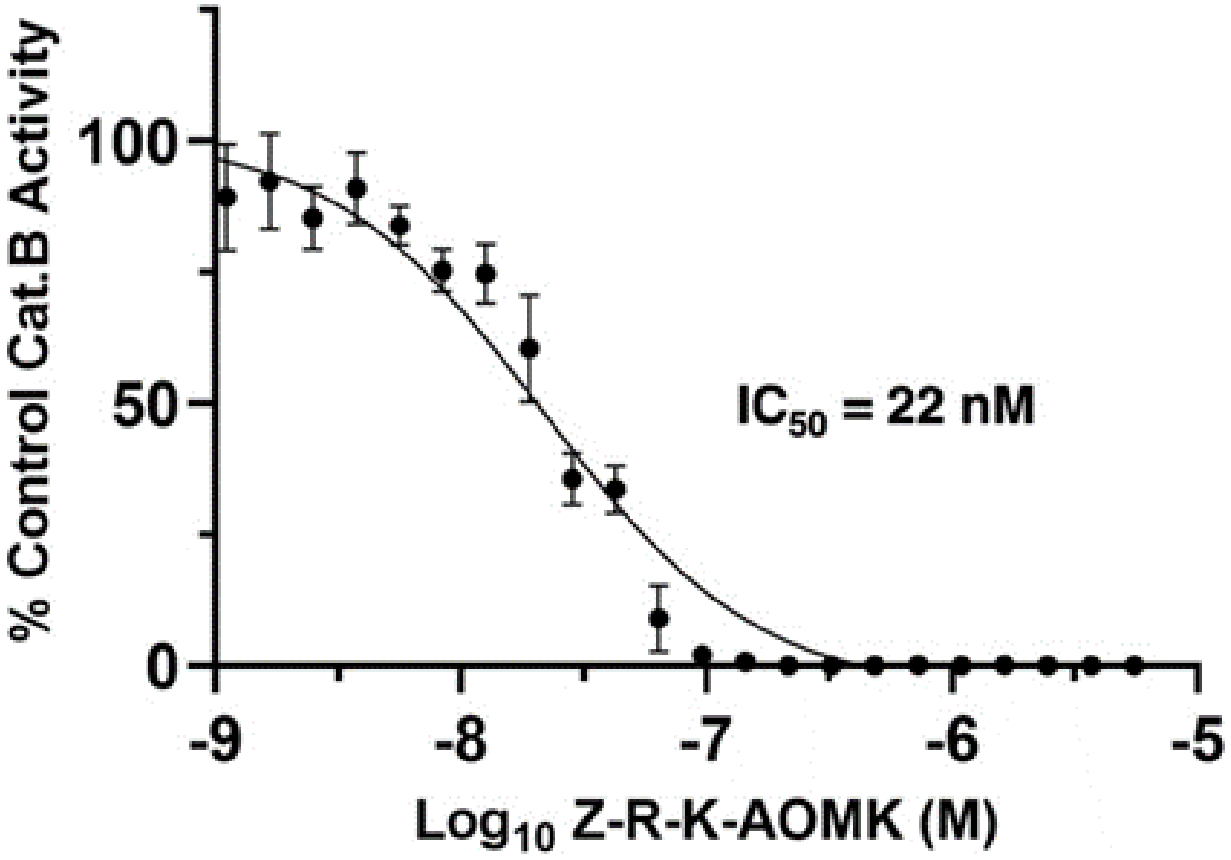

Figure 2.S10 Z-Arg-Lys-AOMK inhibition of cathepsin B at pH 6.8 and IC50 value.

2.6 References

1. De Duve, C.; Wattiaux, R. Functions of lysosomes. Annu. Rev. Physiol. 1966, 28, 435−92.

2. Lawrence, R. E.; Zoncu, R. The lysosome as a cellular centre for signaling, metabolism and quality control. Nat. Cell Biol. 2019, 21, 133−142.

3. Xu, H.; Ren, D. Lysosomal physiology. Annu. Rev. Physiol. 2015, 77, 57−80.

4. Barrett, A. J.; Rawlings, N. D.; Woessner, J. F. Handbook of Proteolytic Enzymes, 2nd ed.; Elsevier Academic Press: Amsterdam, 2004.

5. Turk, V.; Stoka, V.; Vasiljeva, O.; Renko, M.; Sun, T.; Turk, B.; Turk, D. Cysteine cathepsins: from structure, function and regulation to new frontiers. Biochim. Biophys. Acta, Proteins Proteomics 2012, 1824, 68−88.

6. Mindell, J. A. Lysosomal acidification mechanisms. Annu. Rev. Physiol. 2012, 74, 69−86.

7. Ishida, Y.; Nayak, S.; Mindell, J. A.; Grabe, M. A model of lysosomal pH regulation. J. Gen. Physiol. 2013, 141, 705−20.

8. Ohkuma, S.; Poole, B. Fluorescence probe measurement of the intralysosomal pH in living cells and the perturbation of pH by various agents. Proc. Natl. Acad. Sci. U. S. A. 1978, 75, 3327−31.

9. Bright, G. R.; Fisher, G. W.; Rogowska, J.; Taylor, D. L. Fluorescence ratio imaging microscopy: temporal and spatial measurements of cytoplasmic pH. J. Cell Biol. 1987, 104, 1019−33.

10. Madshus, I. H. Regulation of intracellular pH in eukaryotic cells. Biochem. J. 1988, 250, 1−8.

11. Swietach, P.; Tiffert, T.; Mauritz, J. M.; Seear, R.; Esposito, A.; Kaminski, C. F.; Lew, V. L.; Vaughan-Jones, R. D. Hydrogen ion dynamics in human red blood cells. J. Physiol. 2010, 588, 4995−5014.

12. Hook, V.; Yoon, M.; Mosier, C.; Ito, G.; Podvin, S.; Head, B. P.; Rissman, R.; O'Donoghue, A. J.; Hook, G. Cathepsin B in neurodegeneration of Alzheimer's disease, traumatic brain injury, and related brain disorders. Biochim. Biophys. Acta, Proteins Proteomics 2020, 1868, 140428.

13. Nakanishi, H. Microglial cathepsin B as a key driver of inflammatory brain diseases and brain aging. Neural Regener. Res. 2020, 15, 25−29.

14. Yang, A. J.; Chandswangbhuvana, D.; Margol, L.; Glabe, C. G. Loss of endosomal/lysosomal membrane impermeability is an early event in amyloid Abeta1−42 pathogenesis. J. Neurosci. Res. 1998, 52, 691−8.

15. Ditaranto, K.; Tekirian, T. L.; Yang, A. J. Lysosomal membrane damage in soluble Abeta-mediated cell death in Alzheimer's disease. Neurobiol. Dis. 2001, 8, 19−31.

16. De Kimpe, L.; van Haastert, E. S.; Kaminari, A.; Zwart, R.; Rutjes, H.; Hoozemans, J. J.; Scheper, W. Intracellular accumulation of aggregated pyroglutamate amyloid beta: convergence of aging and Aβ pathology at the lysosome. Age 2013, 35, 673−87.

17. Umeda, T.; Tomiyama, T.; Sakama, N.; Tanaka, S.; Lambert, M. P.; Klein, W. L.; Mori, H. Intraneuronal amyloid β oligomers cause cell death via endoplasmic reticulum stress, endosomal/lysosomal leakage, and mitochondrial dysfunction in vivo. J. Neurosci. Res. 2011, 89, 1031−42.

18. Lafrenaye, A. D.; McGinn, M. J.; Povlishock, J. T. Increased intracranial pressure after diffuse traumatic brain injury exacerbates neuronal somatic membrane poration but not axonal injury: evidence for primary intracranial pressure-induced neuronal perturbation. J. Cereb. Blood Flow Metab. 2012, 32, 1919−32.

19. Luo, C. L.; Chen, X. P.; Li, L. L.; Li, Q. Q.; Li, B. X.; Xue, A. M.; Xu, H. F.; Dai, D. K.; Shen, Y. W.; Tao, L. Y.; Zhao, Z. Q. Poloxamer 188 attenuates in vitro traumatic brain injury-induced mitochondrial and lysosomal membrane permeabilization damage in cultured primary neurons. J. Neurotrauma 2013, 30, 597−607.

20. Windelborn, J. A.; Lipton, P. Lysosomal release of cathepsins causes ischemic damage in the rat hippocampal slice and depends on NMDA-mediated calcium influx, arachidonic acid metabolism, and free radical production. J. Neurochem. 2008, 106, 56−69.

21. Kilinc, M.; Gürsoy-Ozdemir, Y.; Gürer, G.; Erdener, S. E.; Erdemli, E.; Can, A.; Dalkara, T. Lysosomal rupture, necroapoptotic interactions and potential crosstalk between cysteine proteases in neurons shortly after focal ischemia. Neurobiol. Dis. 2010, 40, 293− 302.

22. Dong, H.; Qin, Y.; Huang, Y.; Ji, D.; Wu, F. Poloxamer 188 rescues MPTP-induced lysosomal membrane integrity impairment in cellular and mouse models of Parkinson's disease. Neurochem. Int. 2019, 126, 178−186.

23. Freeman, D.; Cedillos, R.; Choyke, S.; Lukic, Z.; McGuire, K.; Marvin, S.; Burrage, A. M.; Sudholt, S.; Rana, A.; O'Connor, C.; Wiethoff, C. M.; Campbell, E. M. Alpha-synuclein induces lysosomal rupture and cathepsin dependent reactive oxygen species following endocytosis. PLoS One 2013, 8, e62143.

24. Amritraj, A.; Peake, K.; Kodam, A.; Salio, C.; Merighi, A.; Vance, J. E.; Kar, S. Increased activity and altered subcellular distribution of lysosomal enzymes determine neuronal vulnerability in Niemann-Pick type C1-deficient mice. Am. J. Pathol. 2009, 175, 2540−56.

25. Chung, C.; Puthanveetil, P.; Ory, D. S.; Lieberman, A. P. Genetic and pharmacological evidence implicates cathepsins in Niemann-Pick C cerebellar degeneration. Hum. Mol. Genet. 2016, 25, 1434−46.

26. Fujisawa, A.; Kambe, N.; Saito, M.; Nishikomori, R.; Tanizaki, H.; Kanazawa, N.; Adachi, S.; Heike, T.; Sagara, J.; Suda, T.; Nakahata, T.; Miyachi, Y. Disease-associated mutations in CIAS1 induce cathepsin B-dependent rapid cell death of human THP-1 monocytic cells. Blood 2007, 109, 2903−11.

27. Fujisawa, A.; Kambe, N.; Saito, M.; Nishikomori, R.; Tanizaki, H.; Kanazawa, N.; Adachi, S.; Heike, T.; Sagara, J.; Suda, T.; Nakahata, T.; Miyachi, Y. Disease-associated mutations in CIAS1 induce cathepsin B-dependent rapid cell death of human THP-1 monocytic cells. Blood 2007, 109, 2903−11.

28. Rajamäki, K.; Lappalainen, J.; Oörni, K.; Välimäki, E.; Matikainen, S.; Kovanen, P. T.; Eklund, K. K. Cholesterol crystals activate the NLRP3 inflammasome in human macrophages: a novel link between cholesterol metabolism and inflammation. PLoS One 2010, 5, e11765.

29. Gonzalez, E. A.; Martins, G. R.; Tavares, A. M. V.; Viegas, M.; Poletto, E.; Giugliani, R.; Matte, U.; Baldo, G. Cathepsin B inhibition attenuates cardiovascular pathology in mucopolysaccharidosis I mice. Life Sci. 2018, 196, 102−109.

30. Saluja, A.; Dudeja, V.; Dawra, R.; Sah, R. P. Early Intra-Acinar Events in Pathogenesis of Pancreatitis. Gastroenterology 2019, 156, 1979−1993.

31. Amaral, E. P.; Riteau, N.; Moayeri, M.; Maier, N.; MayerBarber, K. D.; Pereira, R. M.; Lage, S. L.; Kubler, A.; Bishai, W. R.; D'Império-Lima, M. R.; Sher, A.; Andrade, B. B. Lysosomal Cathepsin Release Is Required for NLRP3-Inflammasome Activation by Mycobacterium tuberculosis in Infected Macrophages. Front. Immunol. 2018, 9, 1427.

32. Morchang, A.; Panaampon, J.; Suttitheptumrong, A.; Yasamut, U.; Noisakran, S.; Yenchitsomanus, P. T.; Limjindaporn, T. Role of cathepsin B in dengue virus-mediated apoptosis. Biochem. Biophys. Res. Commun. 2013, 438, 20−5.

33. de Castro, M. A.; Bunt, G.; Wouters, F. S. Cathepsin B launches an apoptotic exit effort upon cell death-associated disruption of lysosomes. Cell Death Discov 2016, 2, 16012.

34. Droga-Mazovec, G.; Bojic, L.; Petelin, A.; Ivanova, S.; Romih, R.; Repnik, U.; Salvesen, G. S.; Stoka, V.; Turk, V.; Turk, B. Cysteine cathepsins trigger caspase-dependent cell death through cleavage of bid and antiapoptotic Bcl-2 homologues. J. Biol. Chem. 2008, 283, 19140−50.

35. Kavčič , N.; Pegan, K.; Turk, B. Lysosomes in programmed cell death pathways: from initiators to amplifiers. Biol. Chem. 2017, 398, 289−301.

36. Wei, M. C.; Lindsten, T.; Mootha, V. K.; Weiler, S.; Gross, A.; Ashiya, M.; Thompson, C. B.; Korsmeyer, S. J. tBID, a membrane targeted death ligand, oligomerizes BAK to release cytochrome c. Genes Dev. 2000, 14, 2060−71.

37. Campden, R. I.; Zhang, Y. The role of lysosomal cysteine cathepsins in NLRP3 inflammasome activation. Arch. Biochem. Biophys. 2019, 670, 32−42.

38. Bai, H.; Yang, B.; Yu, W.; Xiao, Y.; Yu, D.; Zhang, Q. Cathepsin B links oxidative stress to the activation of NLRP3 inflammasome. Exp. Cell Res. 2018, 362, 180−187.

39. Lian, D.; Lai, J.; Wu, Y.; Wang, L.; Chen, Y.; Zhang, Y.; Boini, K. M.; Huang, Y.; Chen, Y. Cathepsin B-mediated NLRP3 inflammasome formation and activation in angiotensin II -Induced hypertensive mice: role of macrophage digestion dysfunction. Cell. Physiol. Biochem. 2018, 50, 1585−1600.

40. Kindy, M. S.; Yu, J.; Zhu, H.; El-Amouri, S. S.; Hook, V.; Hook, G. R. Deletion of the cathepsin B gene improves memory deficits in a transgenic Alzheimer's disease mouse model expressing AβPP containing the wild-type β-secretase site sequence. J. Alzheimer's Dis. 2012, 29, 827−40.

41. Hook, G. R.; Yu, J.; Sipes, N.; Pierschbacher, M. D.; Hook, V.; Kindy, M. S. The cysteine protease cathepsin B is a key drug target and cysteine protease inhibitors are potential therapeutics for traumatic brain injury. J. Neurotrauma 2014, 31, 515−29.

42. Buck, M. R.; Karustis, D. G.; Day, N. A.; Honn, K. V.; Sloane, B. F. Degradation of extracellular-matrix proteins by human cathepsin B from normal and tumour tissues. Biochem. J. 1992, 282, 273−8.

43. Cavallo-Medved, D.; Dosescu, J.; Linebaugh, B. E.; Sameni, M.; Rudy, D.; Sloane, B. F. Mutant K-ras regulates cathepsin B localization on the surface of human colorectal carcinoma cells. Neoplasia 2003, 5, 507−19.

44. Victor, B. C.; Anbalagan, A.; Mohamed, M. M.; Sloane, B. F.; Cavallo-Medved, D. Inhibition of cathepsin B activity attenuates extracellular matrix degradation and inflammatory breast cancer invasion. Breast Cancer Res. 2011, 13, R115.

45. Aggarwal, N.; Sloane, B. F. Cathepsin B: multiple roles in cancer. Proteomics: Clin. Appl. 2014, 8, 427−37.

46. Bian, B.; Mongrain, S.; Cagnol, S.; Langlois, M. J.; Boulanger, J.; Bernatchez, G.; Carrier, J. C.; Boudreau, F.; Rivard, N. Cathepsin B promotes colorectal tumorigenesis, cell invasion, and metastasis. Mol. Carcinog. 2016, 55, 671−87.

47. Mort, J. S.; Recklies, A. D.; Poole, A. R. Extracellular presence of the lysosomal proteinase cathepsin B in rheumatoid synovium and its activity at neutral pH. Arthritis Rheum. 1984, 27, 509−15.

48. Jordans, S.; Jenko-Kokalj, S.; Kühl, N. M.; Tedelind, S.; Sendt, W.; Brömme, D.; Turk, D.; Brix, K. Monitoring compartment-specific substrate cleavage by cathepsins B, K, L, and S at physiological pH and redox conditions. BMC Biochem 2009, 10, 23.

49. Tedelind, S.; Poliakova, K.; Valeta, A.; Hunegnaw, R.; Yemanaberhan, E. L.; Heldin, N. E.; Kurebayashi, J.; Weber, E.; Kopitar-Jerala, N.; Turk, B.; Bogyo, M.; Brix, K. Nuclear cysteine cathepsin variants in thyroid carcinoma cells. Biol. Chem. 2010, 391, 923−35.

50. Hämälistö, S.; Stahl, J. L.; Favaro, E.; Yang, Q.; Liu, B.; Christoffersen, L.; Loos, B.; Guasch Boldú, C.; Joyce, J. A.; Reinheckel, T.; Barisic, M.; Jäättelä, M. Spatially and temporally defined lysosomal leakage facilitates mitotic chromosome segregation. Nat. Commun. 2020, 11, 229.

51. Almeida, P. C.; Nantes, I. L.; Chagas, J. R.; Rizzi, C. C.; FaljoniAlario, A.; Carmona, E.; Juliano, L.; Nader, H. B.; Tersariol, I. L. Cathepsin B activity regulation. Heparin-like glycosaminogylcans protect human cathepsin B from alkaline pH-induced inactivation. J. Biol. Chem. 2001, 276, 944−51.

52. Pratt, M. R.; Sekedat, M. D.; Chiang, K. P.; Muir, T. W. Direct measurement of cathepsin B activity in the cytosol of apoptotic cells by an activity-based probe. Chem. Biol. 2009, 16, 1001−12.

53. O'Donoghue, A. J.; Eroy-Reveles, A. A.; Knudsen, G. M.; Ingram, J.; Zhou, M.; Statnekov, J. B.; Greninger, A. L.; Hostetter, D. R.; Qu, G.; Maltby, D. A.; Anderson, M. O.; Derisi, J. L.; McKerrow, J. H.; Burlingame, A. L.; Craik, C. S. Global identification of peptidase specificity by multiplex substrate profiling. Nat. Methods 2012, 9, 1095−100.

54. Lapek, J. D., Jr; Jiang, Z.; Wozniak, J. M.; Arutyunova, E.; Wang, S. C.; Lemieux, M. J.; Gonzalez, D. J.; O'Donoghue, A. J. Quantitative Multiplex Substrate Profiling of Peptidases by Mass Spectrometry. Mol. Cell Proteomics 2019, 18, 968−981.

55. Ivry, S. L.; Knudsen, G. M.; Caiazza, F.; Sharib, J. M.; Jaradeh, K.; Ravalin, M.; O'Donoghue, A. J.; Kirkwood, K. S.; Craik, C. S. The lysosomal aminopeptidase tripeptidyl peptidase 1 displays increased activity in malignant pancreatic cysts. Biol. Chem. 2019, 400, 1629− 1638.

56. Xu, J. H.; Jiang, Z.; Solania, A.; Chatterjee, S.; Suzuki, B.; Lietz, C. B.; Hook, V. Y. H.; O'Donoghue, A. J.; Wolan, D. W. A Commensal Dipeptidyl Aminopeptidase with Specificity for N-Terminal Glycine Degrades Human-Produced Antimicrobial Peptides in Vitro. ACS Chem. Biol. 2018, 13, 2513−2521.

57. Leontovyc, A.; Ulrychová, L.; O˘'Donoghue, A. J.; Vondrásek, J.;˘Maresová, L.; Hubálek, M.; Fajtová, P.; Chanová, M.; Jiang, Z.; Craik,˘C. S.; Caffrey, C. R.; Mares, M.; Dvor˘ák, J.; Horn, M. SmSP2: A˘serine protease secreted by the blood fluke pathogen Schistosoma mansoni with anti-hemostatic properties. PLoS Neglected Trop. Dis. 2018, 12, e0006446.

58. Li, H.; Goh, B. N.; Teh, W. K.; Jiang, Z.; Goh, J. P. Z.; Goh, A.; Wu, G.; Hoon, S. S.; Raida, M.; Camattari, A.; Yang, L.; O'Donoghue, A. J.; Dawson, T. L., Jr. Skin Commensal Malassezia globosa Secreted Protease Attenuates Staphylococcus aureus Biofilm Formation. J. Invest. Dermatol. 2018, 138, 1137−1145.

59. Beekman, C.; Jiang, Z.; Suzuki, B. M.; Palmer, J. M.; Lindner, D. L.; O'Donoghue, A. J.; Knudsen, G. M.; Bennett, R. J. Characterization of PdCP1, a serine carboxypeptidase from Pseudogymnoascus destructans, the causal agent of White-nose Syndrome. Biol. Chem. 2018, 399, 1375−1388.

60. Yamamoto, A.; Tomoo, K.; Hara, T.; Murata, M.; Kitamura, K.; Ishida, T. Substrate specificity of bovine cathepsin B and its inhibition by CA074, based on crystal structure refinement of the complex. J. Biochem. 2000, 127, 635−43.

61. Thornberry, N. A.; Peterson, E. P.; Zhao, J. J.; Howard, A. D.; Griffin, P. R.; Chapman, K. T. Inactivation of interleukin-1 beta converting enzyme by peptide (acyloxy)methyl ketones. Biochemistry 1994, 33, 3934−40.

62. Albrow, V. E.; Ponder, E. L.; Fasci, D.; Békés, M.; Deu, E.; Salvesen, G. S.; Bogyo, M. Development of small molecule inhibitors and probes of human SUMO deconjugating proteases. Chem. Biol. 2011, 18, 722−32.

63. Shan, L. Carbobenzoxy-capped Phe-Lys(Cy5)-acyloxymethyl ketone. Molecular Imaging and Contrast Agent Database (MICAD) [Internet]. National Center for Biotechnology Information (US): Bethesda, MD, 2010 May 9 [updated 2010 May 25].

64. Vilar, S.; Cozza, G.; Moro, S. Medicinal chemistry and the molecular operating environment (MOE): application of QSAR and molecular docking to drug discovery. Curr. Top. Med. Chem. 2008, 8, 1555−72.

65. Roy, U.; Luck, L. A. Molecular modeling of estrogen receptor using molecular operating environment. Biochem. Mol. Biol. Educ. 2007, 35, 238−43.

66. Schechter, I. Mapping of the active site of proteases in the 1960s and rational design of inhibitors/drugs in the 1990s. Curr. Protein Pept. Sci. 2005, 6, 501−12.

67. Hasnain, S.; Hirama, T.; Huber, C. P.; Mason, P.; Mort, J. S. Characterization of cathepsin B specificity by site-directed mutagenesis. Importance of Glu245 in the S2-P2 specificity for arginine and its role in transition state stabilization. J. Biol. Chem. 1993, 268, 235−40.

68. Musil, D.; Zucic, D.; Turk, D.; Engh, R. A.; Mayr, I.; Huber, R.; Popovic, T.; Turk, V.; Towatari, T.; Katunuma, N. The refined 2.15 A X-ray crystal structure of human liver cathepsin B: the structural basis for its specificity. EMBO J. 1991, 10, 2321−30.

69. Murata, M.; Miyashita, S.; Yokoo, C.; Tamai, M.; Hanada, K.; Hatayama, K.; Towatari, T.; Nikawa, T.; Katunuma, N. Novel epoxysuccinyl peptides. Selective inhibitors of cathepsin B, in vitro. FEBS Lett. 1991, 280, 307−10.

70. Buttle, D. J.; Murata, M.; Knight, C. G.; Barrett, A. J. CA074 methyl ester: a proinhibitor for intracellular cathepsin B. Arch. Biochem. Biophys. 1992, 299, 377−80.

71. Choe, Y.; Leonetti, F.; Greenbaum, D. C.; Lecaille, F.; Bogyo, M.; Brömme, D.; Ellman, J. A.; Craik, C. S. Substrate profiling of cysteine proteases using a combinatorial peptide library identifies functionally unique specificities. J. Biol. Chem. 2006, 281, 12824−32.

72. Poreba, M.; Groborz, K.; Vizovisek, M.; Maruggi, M.; Turk, D.; Turk, B.; Powis, G.; Drag, M.; Salvesen, G. S. Fluorescent probes towards selective cathepsin B detection and visualization in cancer cells and patient samples. Chem. Sci. 2019, 10, 8461−8477.

73. Turk, B.; Dolenc, I.; Zerovnik, E.; Turk, D.; Gubensek, F.; Turk, V. Human cathepsin B is a metastable enzyme stabilized by specific ionic interactions associated with the active site. Biochemistry 1994, 33, 14800−6.

74. Song, J.; Xu, P.; Xiang, H.; Su, Z.; Storer, A. C.; Ni, F. The active-site residue Cys-29 is responsible for the neutral-pH inactivation and the refolding barrier of human cathepsin B. FEBS Lett. 2000, 475, 157−62.

75. Vidak, E.; Javorsek, U.; Vizovis˘ ek, M.; Turk, B. Cysteine˘ Cathepsins and their Extracellular Roles: Shaping the Microenvironment. Cells 2019, 8, 264.

76. Spizz, G.; Blackshear, P. J. Identification and characterization of cathepsin B as the cellular MARCKS cleaving enzyme. J. Biol. Chem. 1997, 272, 23833−42.

77. Maciewicz, R. A.; Wotton, S. F.; Etherington, D. J.; Duance, V. C. Susceptibility of the cartilage collagens types II, IX and XI to degradation by the cysteine proteinases, cathepsins B and L. FEBS Lett. 1990, 269, 189−93.

78. Taha, T. A.; Kitatani, K.; Bielawski, J.; Cho, W.; Hannun, Y. A.; Obeid, L. M. Tumor necrosis factor induces the loss of sphingosine kinase-1 by a cathepsin B-dependent mechanism. J. Biol. Chem. 2005, 280, 17196−202.

79. Illy, C.; Quraishi, O.; Wang, J.; Purisima, E.; Vernet, T.; Mort, J. S. Role of the occluding loop in cathepsin B activity. J. Biol. Chem. 1997, 272, 1197−202.

80. Nägler, D. K.; Storer, A. C.; Portaro, F. C.; Carmona, E.; Juliano, L.; Ménard, R. Major increase in endopeptidase activity of human cathepsin B upon removal of occluding loop contacts. Biochemistry 1997, 36, 12608−15.

81. Melo, R. L.; Barbosa Pozzo, R. C.; Alves, L. C.; Perissutti, E.; Caliendo, G.; Santagada, V.; Juliano, L.; Juliano, M. A. Synthesis and hydrolysis by cathepsin B of fluorogenic substrates with the general structure benzoyl-X-ARG-MCA containing non-natural basic amino acids at position X. Biochim. Biophys. Acta, Protein Struct. Mol. Enzymol. 2001, 1547, 82−94.

82. Linebaugh, B. E.; Sameni, M.; Day, N. A.; Sloane, B. F.; Keppler, D. Exocytosis of active cathepsin B enzyme activity at pH 7.0, inhibition and molecular mass. Eur. J. Biochem. 1999, 264, 100−9.

83. Boutté, A. M.; Hook, V.; Thangavelu, B.; Sarkis, G. A.; Abbatiello, B. N.; Hook, G.; Jacobsen, J. S.; Robertson, C. S.; Gilsdorf, J.; Yang, Z.; Wang, K. K. W.; Shear, D. A. Penetrating Traumatic Brain Injury Triggers Dysregulation of Cathepsin B Protein Levels Independent of Cysteine Protease Activity in Brain and Cerebral Spinal Fluid. J. Neurotrauma 2020, 37, 1574−1586.

84. Hoegen, T.; Tremel, N.; Klein, M.; Angele, B.; Wagner, H.; Kirschning, C.; Pfister, H. W.; Fontana, A.; Hammerschmidt, S.; Koedel, U. The NLRP3 inflammasome contributes to brain injury in pneumococcal meningitis and is activated through ATP-dependent lysosomal cathepsin B release. J. Immunol. 2011, 187, 5440−51.

85. Yamashima, T. Can 'calpain-cathepsin hypothesis' explain Alzheimer neuronal death? Ageing Res. Rev. 2016, 32, 169−179.

86. Yamashima, T. Hsp70.1 and related lysosomal factors for necrotic neuronal death. J. Neurochem. 2012, 120, 477−94.

87. Zhang, X.; Lin, Y.; Gillies, R. J. Tumor pH and its measurement. J. Nucl. Med. 2010, 51, 1167−70.

88. Chen, L. Q.; Pagel, M. D. Evaluating pH in the Extracellular Tumor Microenvironment Using CEST MRI and Other Imaging Methods. Adv. Radiol 2015, 2015, 206405.

89. O'Donoghue, A. J.; Knudsen, G. M.; Beekman, C.; Perry, J. A.; Johnson, A. D.; DeRisi, J. L.; Craik, C. S.; Bennett, R. J. Destructin-1 is a collagen-degrading endopeptidase secreted by Pseudogymnoascus destructans, the causative agent of white-nose syndrome. Proc. Natl. Acad. Sci. U. S. A. 2015, 112, 7478−83.

90. Rorabacher, D. B. Statistical treatment for rejection of deviant values: critical values of Dixon's Q parameter and related subrange ratios at the 95% confidence level. Anal. Chem. 1991, 63, 139−146.

91. Colaert, N.; Helsens, K.; Martens, L.; Vandekerckhove, J.; Gevaert, K. Improved visualization of protein consensus sequences by iceLogo. Nat. Methods 2009, 6, 786−787.

92. Strelow, J. M. A Perspective on the Kinetics of Covalent and Irreversible Inhibition. SLAS Discov 2017, 22, 3−20.

93. Tonge, P. J. Quantifying the Interactions between Biomolecules: Guidelines for Assay Design and Data Analysis. ACS Infect. Dis. 2019, 5, 796−808.

2.7 Copyright Permission

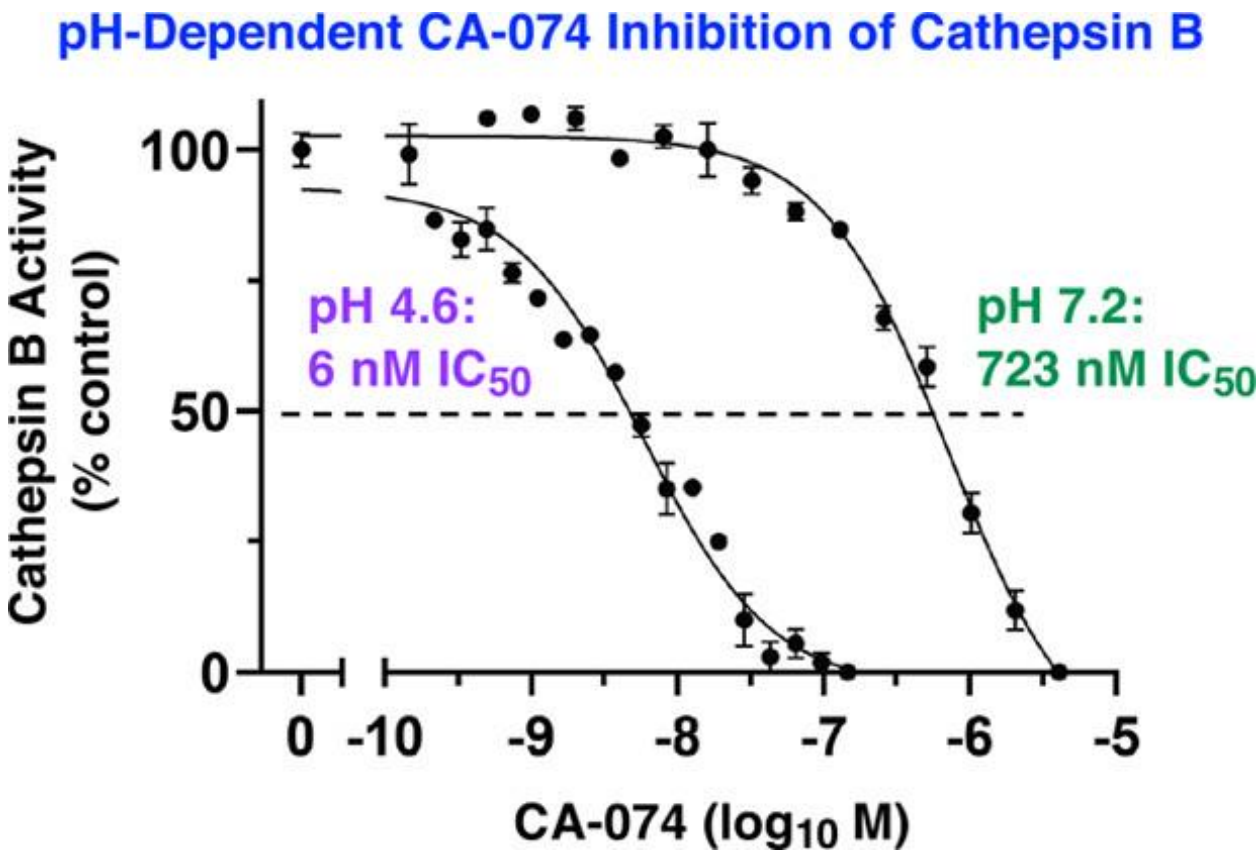

Chapter 3 Graphical Abstract. CA-074 is a selective inhibitor of cathepsin B, a lysosomal cysteine protease. CA-074 has been utilized in numerous studies to demonstrate the role of this protease in cellular and physiological functions. Cathepsin B in numerous human disease mechanisms involves its translocation from acidic lysosomes of pH 4.6 to neutral pH 7.2 of cellular locations, including the cytosol and extracellular environment. To gain in-depth knowledge of CA-074 inhibition under these different pH conditions, this study evaluated the molecular features, potency, and selectivity of CA-074 for cathepsin B inhibition under acidic and neutral pH conditions. This study demonstrated that CA-074 is most effective at inhibiting cathepsin B at an acidic pH of 4.6 with nM potency, which was more than 100-fold more potent than its inhibition at a neutral pH of 7.2. The pH-dependent inhibition of CA-074 was abolished by methylation of its C-terminal proline, indicating the requirement for the free C-terminal carboxyl group for pH-dependent inhibition. Under these acidic and neutral pH conditions, CA-074 maintained its specificity for cathepsin B over other cysteine cathepsins, displayed irreversible inhibition, and inhibited diverse cleavages of peptide substrates of cathepsin B assessed by profiling mass spectrometry. Molecular docking suggested that pH-dependent ionic interactions of the C-terminal carboxylate of CA-074 occur with His110 and His111 residues in the S2′ subsite of the enzyme at pH 4.6, but these interactions differ at pH 7.2. While high levels of CA-074 or CA-074Me (converted by cellular esterases to CA-074) are used in biological studies to inhibit cathepsin B at both acidic and neutral pH locations, it is possible that adjusted levels of CA-074 or CA-074Me may be explored to differentially affect cathepsin B activity at these different pH values. Overall, the results of this study demonstrate the molecular, kinetic, and protease specificity features of CA-074 pH-dependent inhibition of cathepsin B.

3.1 Introduction

Cathepsin B is a lysosomal cysteine protease that participates in protein degradation for cellular protein homeostasis. (1−3) Significantly, cathepsin B generates biologically active protein fragments that regulate functions in numerous human diseases, including neurological disorders such as Alzheimer's disease (AD) and traumatic brain injury (TBI) , (3−8) ischemia, (9) cancer, (10−12) autoinflammatory disease conditions, such as rheumatoid arthritis, (13−15) atherosclerosis, (16,17) and others. (18,19) The use of the selective cathepsin B inhibitor, CA-074, has facilitated studies of cathepsin B inhibition that ameliorates dysfunctional phenotypes in cell and animal models of human disease conditions. (3) For example, CA-074 improves memory deficits and neuropathology in an AD mouse model, (6) and CA-074 reduces the severity of ischemia and provides neuroprotection. (9) These animal studies administered the proinhibitor CA-074Me that is converted by esterases in vivo to the potent CA-074 inhibitor. (6,9)

CA-074 is an epoxysuccinyl peptide known as *N*-(L-3-trans-propylcarbamoyloxirane-2-carbonyl)-L-isoleucyl-L-proline that was designed as a derivative of E-64 (L-trans-epoxysuccinyl-leucylamido(4-guanidino)butane, (20,21) a natural product molecule originally isolated from *Aspergillus japonicus*. (22) CA-074 has been reported to potently inhibit cathepsin B with nanomolar potency (20,21) and selectivity for inhibition of cathepsin B compared to the related cysteine cathepsins L, H, and S. (20−22) These inhibitory properties of CA-074 used purified rat cathepsin B activity monitored at pH 5.5 with the fluorogenic substrate Z-Arg-Arg-AMC. (21)

While cathepsin B normally functions at a lysosomal pH of 4.6, (23,24) evidence shows that in numerous human disease conditions, lysosomal leakage results in movement of cathepsin B to the cytosol of neutral pH 7.2. (25,26) Cathepsin B in the cytosol is proteolytically active and initiates inflammation and cell death in numerous neurological disorders. (3) Cell death lysis

results in extracellular cathepsin B that causes damage through proteolysis at neutral pH. (27,28) Cathepsin B also translocates to the nucleus of neutral pH (29) where it results in telomere-related chromosome segregation defects (30) and degradation of sirtuins that promote aging. (31) Furthermore, cathepsin B functions in secretory vesicles at a moderately acidic pH of 5.5 for production of peptide neurotransmitters. (32) These results indicate that cathepsin B functions under neutral pH conditions which differs from its function in acidic lysosomes.

To gain more in-depth knowledge of CA-074 inhibition of cathepsin B under neutral pH conditions compared to acidic pH conditions, this study examined the potency, molecular properties, and protease specificity of CA-074 inhibition at pH 4.6, 5.5, and 7.2. At pH 4.6, CA-074 was 7-fold and 120-fold more potent than that at pH 5.5 and pH 7.2, respectively, for inhibiting cathepsin B. CA-074 retained specificity for inhibition of cathepsin B compared to other cysteine cathepsin family members under the acidic and neutral pH conditions. Notably, the methylated form of CA-074, CA-074Me, (33) did not display pH-dependent inhibition and was much less potent than CA-074. These findings reveal the pH-dependent inhibitory properties of CA-074 for specific inhibition of cathepsin B.

3.2 Results

3.2.1 CA-074 Displays Activity under Acidic to Neutral pH Conditions That Correspond to Subcellular Locations of Cathepsin B Functions

We assessed cathepsin B activity under acidic to neutral pH conditions using the fluorogenic substrate, Z-Phe-Arg-7-amino-4-methylcoumarin (Z-Phe-Arg-AMC). Z-Phe-Arg-AMC monitors cathepsin B activity from acidic to neutral pH conditions (Figure 3.1). Data show that robust cathepsin B activity occurs between pH 4.6 and pH 7.2 (Figure 3.1). These results showed that cathepsin B is active at pH 4.6 of acidic lysosomes, (23,24) pH 5.5 of mildly acidic secretory vesicles, (29) and neutral pH 7.2 of cytosol, (25,26) nuclei, (29) and extracellular

locations. (29) Thus, cathepsin B is active over a wide pH range that correlated with the environment of multiple subcellular and extracellular locations.

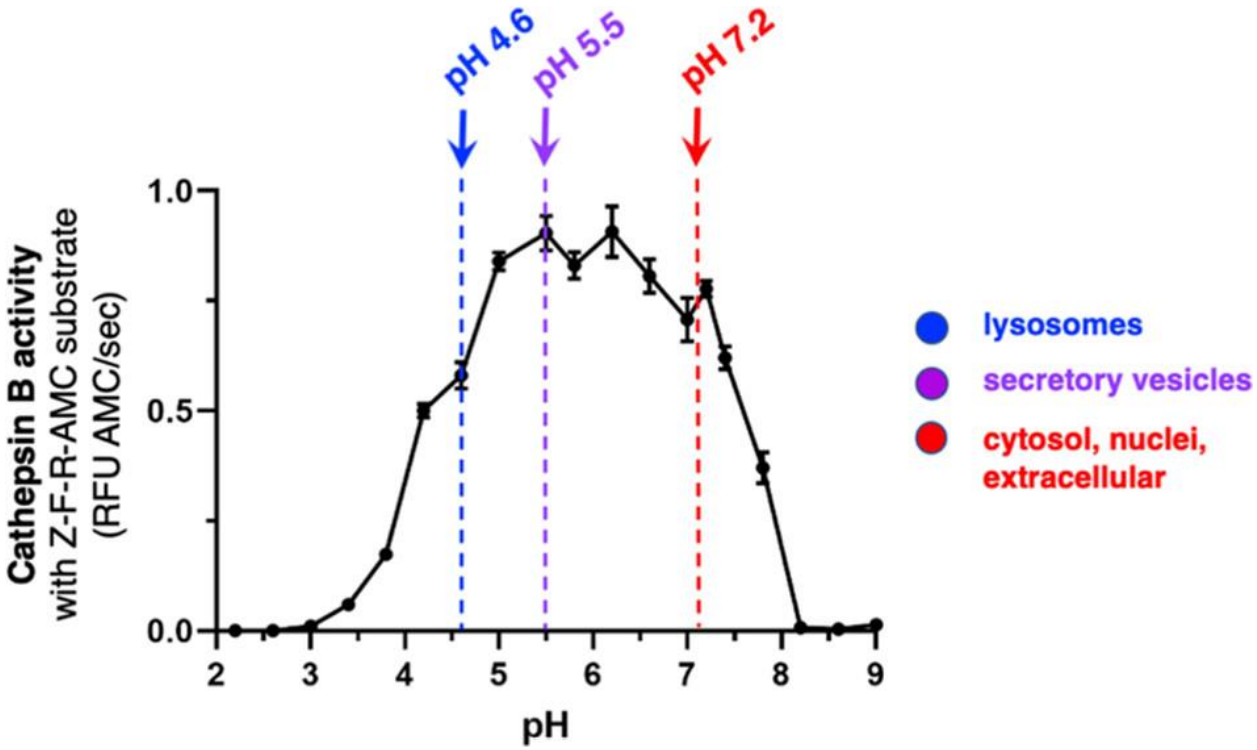

Figure 3.1 Cathepsin B activity under acidic to neutral pH conditions representing the varying pH environments of cellular organelles from lysosomes to cytosol and extracellular locations. Cathepsin B activity was monitored at pH 2.2 to pH 9.0 in increments of 0.4 pH units with addition of pH 7.2. The substrate Z-Phe-Arg-AMC (Z-F-R-AMC) was utilized in the cathepsin B assays. The biological pH conditions of lysosomes at pH 4.6, (23,24) secretory vesicles at pH 5.5, (29,32) and neutral cellular compartments of the cytosol, nuclei, and extracellular locations (28−30) are indicated.

3.2.2 Differential Potencies of CA-074 Inhibition of Cathepsin B at Acidic to Neutral pH Values

The potency of CA-074 inhibition of cathepsin B was assessed at pH 4.6, 5.5, and 7.2 (Figure 3.2a). At a lysosomal pH of 4.6, CA-074 was an effective inhibitor with an IC_{50} value of 6 nM (IC_{50}, concentration of inhibitor for 50% inhibition), but at neutral pH 7.2 it was 120-fold less potent with an IC_{50} value of 723 nM (Figure 3.2a.ii). Inhibition at pH 5.5 was also assessed because cathepsin B is present in secretory vesicles. (32) The pH of 5.5 was used in the original

studies of CA-074 (21) and is also the pH condition that is routinely used in the field. (34,35) At pH 5.5, CA-074 inhibited cathepsin B with an IC_{50} value of 44 nM (Figure 3.2a.ii). These data show that CA-074 at pH 4.6 is 7-fold and 120-fold more potent than that at pH 5.5 and pH 7.2, respectively, demonstrating the pH-dependent properties of CA-074 for cathepsin B inhibition.

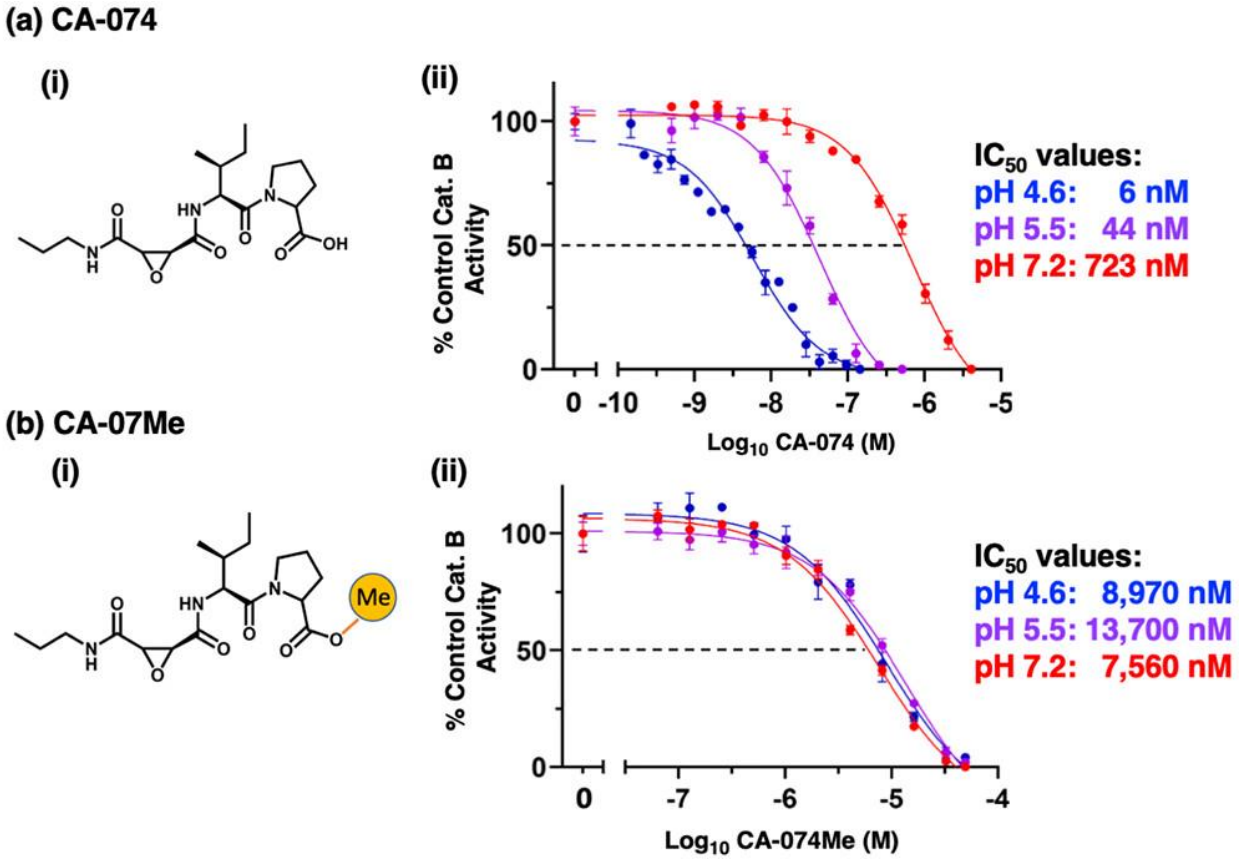

Figure 3.2 CA-074 pH-dependent inhibition of cathepsin B under acidic to neutral pH conditions requires unmodified C-terminal proline. (a) Effective pH-dependent CA-074 inhibition of cathepsin B at pH 4.6, 5.5, and 7.2. (i) CA-074 structure. The chemical structure of CA-074 [*N*-3-trans-propylcarbamoyl-exirane-2-carbonyl)-L-isoleucyl-L-proline] is illustrated. CA-074 is an epoxysuccinyl inhibitor of cathepsin B. (20,21) (ii) Potent, pH-dependent CA-074 inhibition of cathepsin B under acidic to neutral pH conditions. Potencies of CA-074 inhibition of cathepsin B were assessed at pH 4.6, pH 5.5, and pH 7.2 over a range of concentrations of CA-074. Inhibitory potencies were assessed by IC_{50} values, representing inhibitor concentrations that reduced cathepsin B activity by 50%. (b) Poor CA-074Me inhibition of cathepsin B at pH 4.6, 5.5, and 7.2. (i) CA-074Me structure. The chemical structure of CA-074Me is illustrated, showing methylation of the carboxylate group of the C-terminal proline of CA-074. (33) (ii) Poor CA-074Me inhibition of cathepsin B under acidic to neutral pH conditions. Potencies of CA-074 inhibition of cathepsin B were assessed at pH 4.6, pH 5.5, and pH 7.2 over a range of concentrations of CA-074Me. Inhibitory potencies were evaluated by IC_{50} values, representing inhibitor concentrations that reduced cathepsin B by 50%.

3.2.3 Methylation of CA-074 Abolishes Its pH-dependent Inhibition and Reduces Potency

Importantly, methylation of the C-terminal proline of CA-074, generating CA-074Me, resulted in no pH-dependent inhibition of cathepsin B (Figure 3.2b). These data indicate that the nonmethylated C-terminal carboxylate of the proline residue of CA-074 is necessary for its potency and pH-dependent inhibition. Compared to CA-074, CA-074Me was a weak inhibitor of cathepsin B under acidic and neutral pH conditions, shown by its high IC_{50} values of 8.9, 13.7, and 7.6 μM at pH 4.6, 5.5, and 7.2, respectively (Figure 3.2b.ii). Thus, CA-074Me was less potent than CA-074 by 1495-fold, 311-fold, and 10-fold at pH 4.6, pH 5.5, and pH 7.2, respectively.

3.2.4 Irreversible Mechanism of CA-074 Inhibition under Acidic and Neutral pH Conditions

CA-074 has been proposed as an irreversible inhibitor based on structural binding analyses of the inhibitor to the cathepsin B protein structure. (36,37) However, direct evaluation of the irreversible nature of CA-074 inhibition has not yet been assessed. Therefore, the irreversible or reversible nature of protease inhibitors was assessed for CA-074. CA-074 was incubated with cathepsin B for 30 min at pH 4.6, pH 5.5, and pH 7.2 at 10 times the IC_{50} concentrations and then diluted 100-fold followed by addition of the Z-F-R-AMC substrate (Figure 3.3). The lack of cathepsin B activity after dilution demonstrates the irreversible inhibitory mechanism of CA-074 under all three pH conditions. As a control, cathepsin B was preincubated without an inhibitor and displayed a linear formation of products in the assay (Figure 3.3). These data show that inhibition of cathepsin B with CA-074 is irreversible under acidic and neutral pH conditions.

In addition, CA-074Me also displays irreversible inhibition of cathepsin B at pH 4.6, 5.5, and 7.2 (Figure 3.S1). These results illustrate the irreversible mechanism of the weak inhibitor CA-074Me.

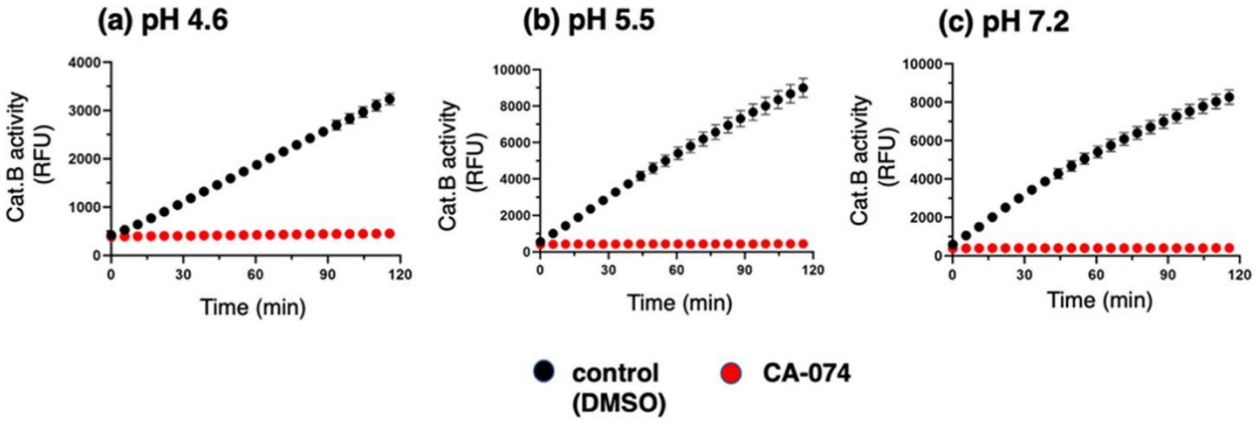

Figure 3.3 Irreversible CA-074 inhibition of cathepsin B at pH 4.6, pH 5.5, and pH 7.2. CA-074 at pH 4.6 (panel a), pH 5.5 (panel b), and pH 7.2 (panel c) was evaluated for irreversible or reversible inhibition of cathepsin B by dilution experiments. Cathepsin B was preincubated with inhibitor at 10 times the IC_{50} concentration (corresponding to 58 nM at pH 4.6, 440 nM at pH 5.5, and 7230 nM at pH 7.2) followed by dilution to 1/10 the IC_{50} concentration, addition of substrate (Z-F-R-AMC), and measurement of activity in time-course assays. Inhibition of cathepsin B following dilution indicates the irreversible inhibitory mechanism of CA-074 under acidic and neutral pH conditions.

3.2.5 Kinetic Evaluation of CA-074 K_I and k_{inact} Values for Inhibition of Cathepsin B at Acidic and Neutral pH Values

Kinetic characterization of CA-074 irreversible inhibition was conducted to assess K_I and k_{inact} values based on plots of inhibitor concentration and k_{obs} values. The k_{obs} values were assessed from plots of cathepsin B activity at different inhibitor concentrations (Figure 3.S2). Data showed that CA-074 was most potent at pH 4.6 with a K_I of 22 nM (Figure 3.4) and was a less effective inhibitor at pH 7.2 with a K_I of 1.98 μM (Figure 3.4). Inhibition at pH 5.5 was observed with a moderate K_I value of 211 nM. These K_I values showed that the potency of inhibition at pH 4.6 was about 10-fold and 90-fold greater compared to that at pH 5.5 and pH 7.2, respectively (Table 3.1). Thus, K_I and IC_{50} values both indicated the greater potency of CA-074 under acidic compared to neutral pH conditions (Table 3.1). Evaluation of k_{inact}/K_I values showed more effective inhibition kinetics at pH 4.6 than that at pH 5.5 or pH 7.2. At pH 4.6, the k_{inact}/K_I value of 4.5×10^5 M^{-1} s^{-1} was 4-fold and 52-fold greater than such values at pH 5.5 or

pH 7.2 with values of 1.1×10^5 and 8.6×10^3 M^{-1} s^{-1}, respectively (Table 3.1). These data illustrate the kinetic properties of pH-dependent inhibition by CA-074.

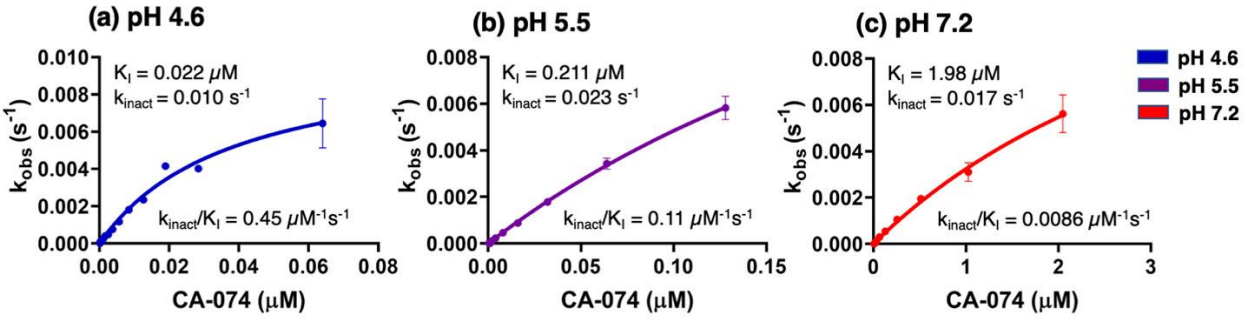

Figure 3.4 Kinetics of CA-074 inhibition of cathepsin B under acidic and neutral pH conditions. Kinetic analyses of CA-074 inhibition of cathepsin B were conducted at pH 4.6 (panel a), pH 5.5 (panel b), and pH 7.2 (panel c) to determine the kinetic values of K_I, k_{inact}, and k_{inact}/K_I, conducted as described in the methods.

Table 3.1 Kinetic Values for CA-074 and CA-074Me Inhibition of Cathepsin B at pH 4.6, pH 5.5, and pH 7.2[a]

kinetic constant	cathepsin B CA-074			cathepsin B CA-074Me		
	pH 4.6	pH 5.5	pH 7.2	pH 4.6	pH 5.5	pH 7.2
IC_{50} (nM)	6	44	723	8970	13,700	7560
K_I (nM)	22	211	1980	52,000	56,000	29,000
k_{inact} (s^{-1})	0.010	0.023	0.017	0.016	0.014	0.014
k_{inact}/K_I (M^{-1} s^{-1})	4.5×10^5	1.1×10^5	8.6×10^3	3.1×10^2	2.5×10^2	4.8×10^2

[a]IC_{50} values were calculated for cathepsin B based on assays with the Z-Phe-Arg-AMC substrate in the presence of a range of inhibitor concentrations (from Figure 3.2). The K_I, k_{inact}, and k_{inact}/K_I values were calculated as described in the methods to measure k_{obs} values at different inhibitor concentrations (Figures 3.S2 and 3.S3) for determination of K_I, k_{inact}, and k_{inact}/K_I values shown in this table. K_I calculation utilized K_m values for the Z-Phe-Arg-AMC substrate at pH 4.6, 5.5, and 7.2 (Figure 3.S6).

The kinetic properties of CA-074Me were assessed, indicating its poor inhibition of cathepsin B (Table 3.1 and Figure 3.S3). CA-074Me inhibition of cathepsin B at pH 4.6, pH 5.5, and pH 7.2 occurred with K_I values of 52, 56, and 29 μM, respectively, which represented lower potencies by 1/2363, 1/265, and 1/15 at these respective pH values compared to CA-074.

The k_{inact}/K_I values of CA-074Me also indicated substantially weaker inhibition compared to CA-074 (Table 3.1).

3.2.6 Specificity of CA-074 Inhibition of Cathepsin B Compared to Other Cysteine Cathepsins at Acidic and Neutral pH Values

Cathepsin B is one among 11 lysosomal cysteine cathepsin proteases consisting of cathepsins B, C, F, H, K, L, O, S, V, W, and X (also known as cathepsin Z). (1,38) While previous studies of CA-074 assessed its selectivity for cathepsin B compared to cathepsins L and H at pH 5.5, (20,21) selectivity for the full spectrum of cysteine cathepsins was not assessed under both acidic and neutral pH conditions. Therefore, we evaluated the selectivity of CA-074 among the cysteine cathepsins at pH 4.6, pH 5.5, and pH 7.2 (Table 3.2). At pH 4.6, 16 μM CA-074 had no effect on cathepsins C, H, and L; CA-074 at 16 μM displayed minor effects on cathepsins K, S, V, and X of 5–20% inhibition. At pH 5.5, 16 μM CA-074 μM had no effect on these cysteine cathepsins C, H, L, K, V, and X; but cathepsin S was inhibited with an IC_{50} value of 4.8 μM, showing 109-fold less potency than inhibition of cathepsin B. At pH 7.2, CA-074 at 16 μM had no effect on cathepsin C, H, K, and V, and partial inhibition of cathepsin S by 29%; cathepsins L and X were inactive at pH 7.2. These findings illustrate the high specificity of CA-074 for cathepsin B over other cysteine cathepsin enzymes under acidic and neutral pH conditions.

Table 3.2 Specificity of CA-074 and CA-074Me for Inhibition of Cathepsin B Compared to Other Cysteine Cathepsins[a]

protease	CA-074 IC_{50} (nM) (% inhibition)			CA-074Me IC_{50} (nM) (% inhibition)		
	pH 4.6	pH 5.5	pH 7.2	pH 4.6	pH 5.5	pH 7.2
cathepsin B	6	44	723	8970	13,700	7560
cathepsin C	>16,000	>16,000	>16,000	>16,000	>16,000	>16,000
	0%	0%	0%	5%	0%	4%
cathepsin H	>16,000	>16,000	>16,000	>16,000	>16,000	>16,000
	0%	0%	0%	0%	0%	19%
cathepsin L	>16,000	>16,000	NA	>16,000	>16,000	NA
	0%	0%		0%	0%	
cathepsin K	>16,000	>16,000	>16,000	>16,000	>16,000	>16,000
	8%	0%	0%	0%	0%	16%
cathepsin S	>16,000	4800	>16,000	>16,000	5500	3800
	20%		29%	22%		
cathepsin V	>16,000	>16,000	>16,000	12,000	>16,000	>16,000
	10%	0%	0%	33%	22%	0%
cathepsin X	>16,000	>16,000	NA	>16,000	>16,000	NA
	5%	0%		0%	0%	

[a]Inhibitors were evaluated for protease selectivity among members of the cysteine cathepsin family. The activity of each cathepsin was assessed in the presence of CA-074 or CA-074Me at 0.5 nM to 16 μM (with the exception of 50 μM CA-074Me for cathepsin B). IC_{50} values were determined for CA-074 and CA-074Me for each protease. IC_{50} values are indicated as >16,000 nM when partial inhibition or no inhibition was observed. NA indicates that the enzyme had no activity at the indicated pH.

With respect to CA-074Me, it displayed nearly no inhibition of the cysteine cathepsins assessed at up to 16 μM CA-074Me (Table 3.2). Cathepsin S, however, was inhibited by high concentrations illustrated by the micromolar IC_{50} values of 5.5 μM and 3.8 μM CA-074Me at pH 5.5 and pH 7.2, respectively.

3.2.7 CA-074 Inhibition of Peptide Cleavages of Cathepsin B Assessed by Multiplex Substrate Profiling by Mass Spectrometry (MSP-MS)

The inhibitory properties of CA-074 have largely been evaluated with dipeptide-AMC fluorogenic substrates such as Z-Phe-Arg-AMC and Z-Arg-Arg-AMC, (20,21) but the information about CA-074 inhibition of diverse cathepsin B cleavages is needed to characterize the inhibitor effects. To gain knowledge of cathepsin B peptide cleavages that can be inhibited by CA-074 at pH 4.6 and pH 7.2 for broader substrates, we evaluated the ability of CA-074 to inhibit cathepsin B cleavages by a global, unbiased cleavage profiling approach known as MSP-MS. (39,40) The MSP-MS approach uses a substrate library consisting of 228 peptides (14 residues in length) containing 2964 distinct cleavage sites. In the absence and presence of CA-074, cathepsin B cleavage products of the library were identified and quantified by nano-liquid chromatography tandem mass spectrometry (nano-LC–MS/MS). In the presence of 10 nM CA-074, cleavages of peptide substrates of the library were blocked by CA-074 (Figure 3.5). At pH 7.2, 10 nM CA-074 had no effect on cathepsin B cleavage of the Z-Phe-Arg-AMC substrate (Figure 3.2) and, similarly, had no effect on cleaving peptide substrates in the MSP-MS assay (Figure 3.5). These findings confirm that CA-074 has selectivity for inhibiting cathepsin B peptide cleavages at pH 4.6 over pH 7.2 for broader substrates.

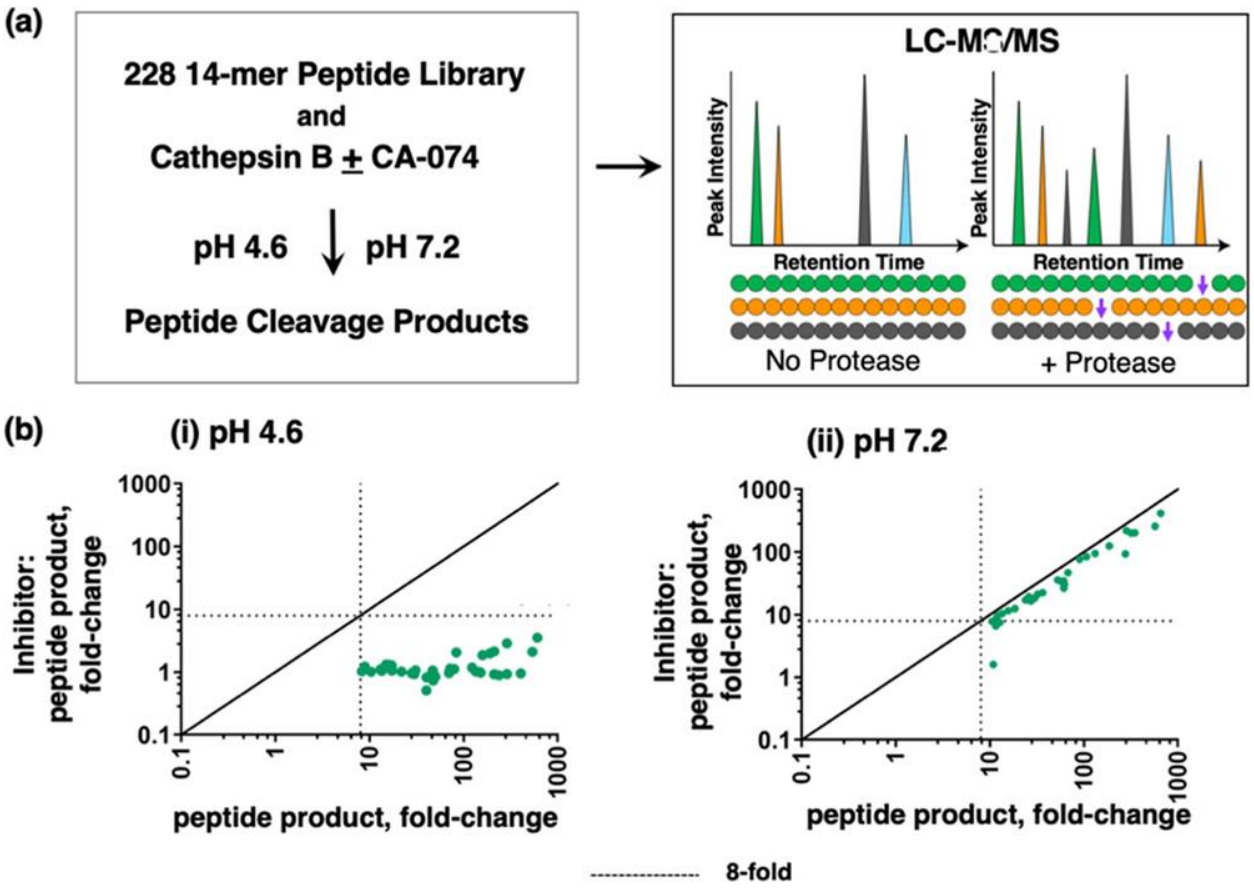

Figure 3.5 CA-074 inhibition of peptide cleavages by cathepsin B analyzed by MSP-MS. (a) MSP-MS approach for cleavage profiling of cathepsin B in the presence or absence of CA-074. Cathepsin B was preincubated with CA-074 (10 nM) at pH 4.6 and pH 7.2 for 30 min at room temperature (RT) and without an inhibitor as the control. These cathepsin B conditions were then subjected to MSP-MS assays by addition of the peptide library and incubation (at RT) for 60 min followed by LC–MS/MS identification and quantification of peptide cleavage products. (b) Cleaved peptide products of cathepsin B in MSP-MS at pH 4.6 (panel i) and pH 7.2 (panel ii). The quantities of each cleaved peptide product generated in the absence of an inhibitor or in the presence of an inhibitor were plotted as the fold-change of each cleaved peptide product relative to no enzyme activity control. Cleaved peptides were defined as those with intensity scores of 8-fold or more (----) above the quenched inactive cathepsin B, evaluated using the ratio of $\log_2$(Cat.B/inactivated enzyme) for each peptide product, with $p < 0.05$ by the two-tailed homoscedastic t-test.

3.2.8 Molecular Docking of CA-074 Interactions with Cathepsin B at Acidic pH 4.6 and Neutral pH 7.2

Modeling of CA-074 binding interactions to cathepsin B at acidic pH 4.6 and neutral pH 7.2 was evaluated using the molecular operating environment (MOE) docking software. (41,42) The MOE modeled CA-074 binding to bovine cathepsin B (PDB: 1QDQ) (36) at

pH 4.6 and pH 7.2, showing similar orientation at the active site (Figure 3.6a). Mature human and bovine cathepsin B share 88.3% protein sequence identity and 100% sequence identity for the amino acids (His 110 and His111) that directly interact with CA-074. (37) The docking assessment shows that CA-074 interacts with the S2, S1, S1′, and S2′ subsites of the enzyme according to the Schechter–Berger nomenclature, (43) where the subsites interact with the corresponding amino acids adjacent to the cleavage site indicated as P2-P1-↓P1′-P2′. At pH 4.6, the P2′ residue of CA-074 at the C-terminus (proline residue) shows a strong ionic interaction His110 and His111 in the S2′ subsite of the enzyme (Figure 3.6b), reflected by a total binding energy of −58.3 kcal/mol (Table 3.3 and Figure 3.S4). However, at pH 7.2, the P2′ residue of CA-074 at the C-terminus partially loses ionic interaction with His111 in the S2′ subsite of the enzyme (Figure 3.6c), reflected by the altered binding energy of −43 kcal/mol (Table 3.3 and Figure 3.S5), when compared to the binding energy at pH 4.6. These MOE docking analyses show that CA-074 binds more favorably to cathepsin B at pH 4.6 than at pH 7.2, which supports our experimental data illustrating the greater inhibition by CA-074 under acidic compared to neutral pH conditions.

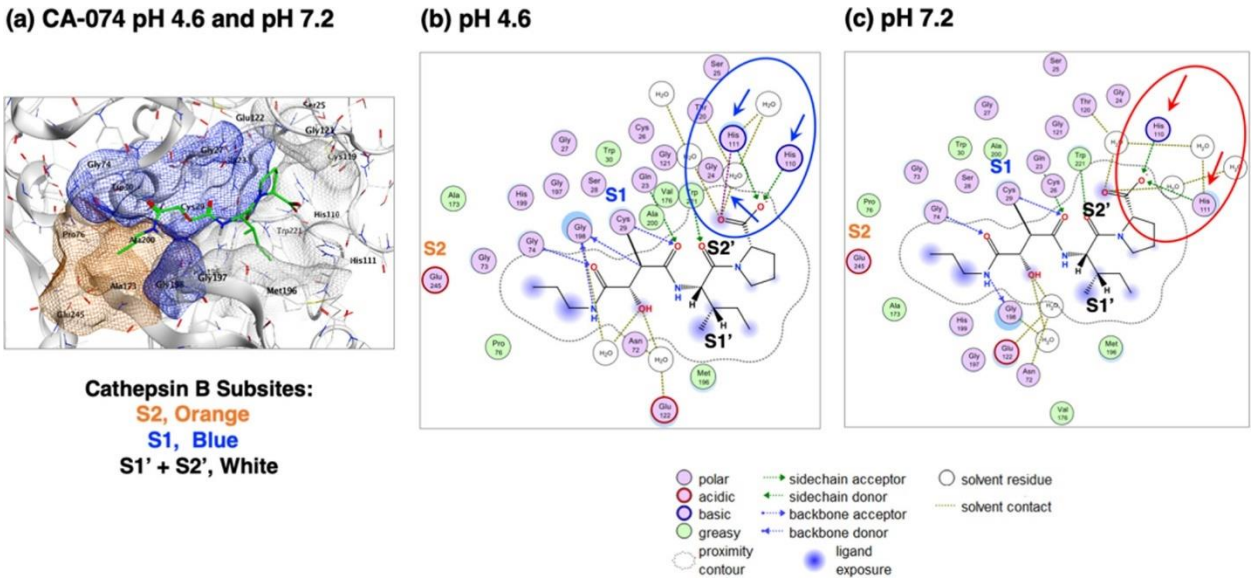

Figure 3.6 Molecular docking of CA-074 to cathepsin B at pH 4.6 and pH 7.2 (a) Model of CA-074 docking to cathepsin B at pH 4.6 and pH 7.2. Analysis of CA-074 inhibitor binding to enzyme was conducted by MOE at pH 4.6 and pH 7.2 to illustrate the predicted docking orientation of the inhibitor to the cathepsin B structure of PDB 1QDQ as the template for analyses. (36,37) CA-074 interacts with S2 to S2′ subsites of the enzyme substrate binding region (Schechter–Berger nomenclature (43)), containing the active site Cys29 residue. Cathepsin B enzyme subsites are shown as the S2 subsite in orange, the S1 subsite in blue, and the S1′ and S2′ subsites in gray-white. (b) Two-dimensional illustration of CA-074 and cathepsin B binding interactions at pH 4.6. At pH 4.6, the P2′ proline residue of CA-074 at its C-terminus shows strong ionic interactions with His110 and His111 in the S2′ subsite of the occluding loop region of the enzyme (panel b, indicated by blue arrows), indicated by the total binding energy of −58.3 kcal/mol (Table 3.3 and Figure 3.S4). (c) Two-dimensional illustration of CA-074 and cathepsin B binding interactions at pH 7.2. At pH 7.2, the P2′ proline residue of CA-074 at the C-terminus partially loses ionic interaction with His111 in the S2′ subsite of the enzyme (panel c, indicated by red arrows), reflected by the altered binding energy of −43 kcal/mol (Table 3.3 and Figure 3.S5), when compared to the binding energy at pH 4.6. These MOE docking analyses predict the differential binding features of CA-074 to the occluding loop domain of cathepsin B at pH 4.6 compared to pH 7.2.

Table 3.3 Binding Energies of CA-074 to Cathepsin B at pH 4.6 and pH 7.2[a]

pH condition	binding energy
pH 4.6	−58.3 kcal/mol
pH 7.2	−43.0 kcal/mol

[a]The more negative binding energy calculated for pH 4.6 compared to pH 7.2 predicts the more favorable interaction of CA-074 to cathepsin B at pH 4.6.

3.3 Discussion

This study demonstrates the potency, molecular features, and protease specificity of CA-074 inhibition of cathepsin B, showing that CA-074 displays preference for inhibition at the acidic lysosomal pH of 4.6 compared to the mildly acidic pH 5.5 of secretory vesicles and the neutral pH of 7.2 of cytosol and extracellular locations. K_I values indicate that CA-074 is 90-fold more potent for inhibition of cathepsin B at acidic pH 4.6 compared to neutral pH 7.2. CA-074 at pH 5.5 was about 10-fold less effective than that at pH 4.6 (based on K_I) and was 9-fold more potent than that at pH 7.2. These results demonstrate that the potency of CA-074 increases as the pH decreases from pH 7.2 to 4.6. Under these acidic and neutral pH conditions, CA-074 maintains its specificity for cathepsin B over other cysteine cathepsins, displays irreversible inhibition, and inhibits diverse peptide cleavages of cathepsin B assessed by MSP-MS profiling. Molecular docking suggested pH-dependent ionic interactions of the carboxylate group of the C-terminal proline of CA-074 with His110 and His111 residues at the S2 subsite of the enzyme. Notably, CA-074Me showed no pH-dependent inhibition, indicating that methylation of the C-terminal proline of CA-074 abolishes its pH-dependent inhibition of cathepsin B. These results demonstrate the pH-dependent structural and kinetic properties of CA-074 for specific inhibition of cathepsin B.

The distinct features of cathepsin B that result in its preferential inhibition by CA-074 at acidic pH suggest that this enzyme possesses different properties at acidic compared to neutral pH environments. Indeed, cathepsin B has been shown to possess different cleavage specificities at pH 4.6 compared to pH 7.2, (44) observed during unbiased cleavage profiling analyses by MSP-MS. (44) Based on the peptide substrate preferences of cathepsin B under the two different pH conditions, a neutral pH-selective substrate was modified with the AOMK warhead to generate Z-Arg-Lys-AOMK that displayed neutral pH-selective inhibition of cathepsin B with high

potency. (44) These new findings distinguish cathepsin B properties in its normal acidic environment of lysosomes, versus its abnormal location in the cytosol and extracellularly in numerous human diseases. Together, these data support the hypothesis that neutral pH cathepsin B may represent a pathogenic form of the enzyme involved in disease mechanisms.

Our molecular docking studies by MOE demonstrated the more favorable interaction of the C-terminal region of CA-074 with the occluding loop of cathepsin B at pH 4.6 rather than at pH 7.2. Our molecular docking assessment by the MOE at pH 4.6 and pH 7.2 using X-ray crystallography data for cathepsin B (36) shows the importance of the enzyme occluding loop interaction with the C-terminal carboxylate of CA-074. Binding energies of docking at pH 4.6 compared to pH 7.2 support the hypothesis that CA-074 at pH 4.6 displays preferable interaction with the occluding loop through its C-terminal proline carboxylate interaction with His110 and His111 of the enzyme. His110 and His111 have been shown to be key residues for cathepsin B exopeptidase activity. Mutagenesis of His110 to Gln, or His111 to Ala, results in reduction of cathepsin B activity to less than 1% of the wild-type cathepsin B activity when using substrates containing P2′ residues with a C-terminal carboxylic acid group. (45) Notably, methylation at the carboxylate residue of CA-074, forming CA-074Me, abolished the pH-dependent property of CA-074 with substantially decreased potency at acidic and neutral pH values. These findings indicate that the C-terminus of CA-074 participates in its pH-dependent inhibition and potency. These findings advance previous knowledge (20,21,36,46,47) concerning the importance of His110 and His111 of the occluding loop for interacting with the C-terminus of CA-074 in a pH-dependent manner.

In cellular and animal studies, the prodrug CA-074Me is widely used for CA-074 inhibition of cathepsin B. (3) Treatment of cells with CA-074Me has been shown to more effectively inhibit

intracellular cathepsin B compared to incubating cells with CA-074. (33) It has been hypothesized that CA-074Me is more cell permeable and is converted by intracellular esterases to CA-074. (33) In numerous cellular studies, the concentration of CA-074Me used to inhibit intracellular cathepsin B generally ranges from 10 to 50 μM. (4,48−50) With the assumption that most of the proinhibitors are converted to CA-074, the high concentration of CA-074 would be sufficient to inhibit cathepsin B located in different subcellular pH conditions of acidic lysosomes and neutral pH locations including cytosol. In animal studies, CA-074Me concentrations in the approximate range of 4–10 mg/kg and higher have been administered, (6,51−54) which may correspond to micromolar and greater levels of the inhibitor that would inhibit cathepsin B at acidic to neutral pH cellular locations. Measurements of CA-074 and CA-074Me in vivo levels and clearance in animal studies will be important in future studies to assess in vivo inhibitor concentrations.

The new findings of this study suggest that adjustment of CA-074 concentrations may allow assessment of cathepsin B functions in acidic lysosomes compared to neutral pH locations such as the cytosol, nuclei, and extracellular environment. (3,11,27,30,55−57) We previously discovered that Z-Arg-Lys-AOMK is >100-fold selective at inhibiting cathepsin B at pH 7.2 over pH 4.6, (44) while in this study CA-074 has the opposite property for preferring inhibition at acidic pH 4.6. Use of these two inhibitors in cellular studies, at concentrations where they maintain pH selectivity, may allow evaluation of the functional roles of lysosomal compared to nonlysosomal cathepsin B.

In summary, this study has demonstrated the pH-dependent inhibitory properties of CA-074 inhibition of cathepsin B with respect to its potency, molecular features, and specificity. At appropriate concentrations, CA-074 may potentially serve as a selective acidic pH inhibitor of cathepsin B, with specificity for cathepsin B over other cysteine cathepsins. The proof-of concept

of these findings shows that it may be possible to develop other pH-selective inhibitors. Novel pH-selective inhibitors may allow studies in the future to specifically probe the role of cathepsin B in distinct pH cellular compartments such as the cytosol that have implicated to be involved in brain disorders and other human diseases.

3.4 Methods and Materials

3.4.1 Inhibitors, Enzymes, Peptides, and Reagents

CA-074 inhibitor was purchased from Calbiochem (Millipore Sigma #205530, St. Louis, MO). CA-074Me was purchased from Sigma (#205531). Recombinant human cathepsin B (accession NP_001899.1) and cysteine cathepsin proteases were from R & D Systems (Minneapolis, MN) or Abcam (Cambridge, MA) consisting of cathepsin B (R & D #953-CY-010), cathepsin L (R & D #952-CY-010), cathepsin V (R & D #1080-CY-010), cathepsin S (R & D #1183-CY-010), cathepsin K (Abcam #ab157067), cathepsin C (R & D #1071-CY-010), cathepsin H (R & D #75116-CY-010), and cathepsin X (R & D #934-CY)-010). Fluorogenic substrates consisted of Z-Phe-Arg-AMC ((#AS-24096, Anaspec, Fremont, CA), Gly-Arg-AMC and Arg-AMC from Bachem ((#4002196 and (#I-1050, respectively, Torrance, CA), and MCA-Arg-Pro-Pro-Gly-Phe-Ser-Ala-Phe-Lys(Dnp)-OH ((#AMYD-111A, CPC Scientific, San Jose, CA). MSP-MS assays utilized a library of 228 peptides of 14 amino acids in length, designed, and synthesized to contain all neighbor and near-neighbor diversity in residues, as described previously. (39,40) These assays utilized buffer components of citric acid monohydrate (Merck #1.00244.0500, Burlington, MA), sodium phosphate dibasic anhydrous (EMD #SX-072305, Burlington, MA), sodium acetate (Fisher Scientific #BP-333-500, Fair Lawn, NJ), EDTA (Calbiochem #324503, Burlington, MA), sodium chloride (Fisher Chemical #S271-1, Pittsburgh, PA), dithiothreitol (DTT) (Promega #V351, Madison, WI), and urea (Teknova #U2222, Hollister,

CA). Peptide extraction reagents consisted of C18 LTS tips (Rainin #PT-LC18-960, Oakland, CA) and C18 for SPE stage-tips (3 M company #2215-C18, Maplewood, MN), and (3) nano-LC–MS/MS reagents consisting of the BEH C18 packing material (Waters Corporation #186004661, Milford, MA), acetonitrile (Fisher Chemical #A955-4, Pittsburgh, PA), formic acid (FA) (Fisher Chemical #A117-50, Pittsburgh, PA), trifluoroacetic acid (TFA) (Fisher Chemical #A116-50, Pittsburgh, PA), and HPLC-grade water (Fisher Chemical #W6-4).

3.4.2 Cathepsin B Activity Assay

Procathepsin B (recombinant) was activated to mature cathepsin B by incubation at 37 °C for 30 min in 20 mM Na-acetate pH 5.5, 1 mM EDTA, 5 mM DTT, and 100 mM NaCl. Assay of cathepsin B activity utilized final buffer conditions of 0.04 ng/μL cathepsin B, 40 μM Z-Phe-Arg-AMC, 40 mM citrate phosphate (pH 4.6, pH 5.5, or pH 7.2), 1 mM EDTA, 100 mM NaCl, 5 mM DTT, and 0.01% Tween-20. Assays were conducted at RT (25 °C) in quadruplicate, and relative fluorescence readings (RFUs) (excitation 360 nm, emission 460 nm) were recorded every 46 s over a period of 30 min (for inhibitor assays) in a Biotek HTX microplate plate reader. For other assays, RFUs were recorded every 101, 30, and 70 s for studies of pH dependence (Figure 3.1), irreversibility (Figure 3.3), and K_m values (SI Figure 3.S6), respectively. Enzyme velocity (RFU/sec) calculations used the highest slope recorded for 10 consecutive fluorescent readings. RFU/s were converted to specific activity of pmol/min/μg using AMC standards. Specific activity was defined as pmol/min/μg enzyme. Data analysis was conducted using Prism GraphPad software.

For the pH curve experiment (Figure 3.1), cathepsin B activity was also monitored over the entire pH range of 2.2 to 9.0 in 40 mM citrate phosphate (pH 2.2 to pH 7.4) or 40 mM Tris–HCl (pH 7.8 to 9.0), 1 mM EDTA, 5 mM DTT, 100 mM NaCl, and 0.01% Tween-20, with

preincubation in each pH buffer for 10 min prior to initiating the assay by adding a substrate. We noted that preincubation at pH values of 3.0 or 8.0 resulted in reduced activity when compared with our previous studies (44) that had no preincubation step.

3.4.3 Inhibition of Cathepsin B by CA-074 and CA-074Me in Kinetic Studies

Kinetic analyses of CA-074 and CA-074Me inhibition of cathepsin B were conducted at pH 4.6, pH 5.5, and pH 7.2 to determine IC_{50}, K_I, k_{obs}, and k_{inact}/K_I. The CA-074 inhibitor concentrations ranged from 4096 to 0.5 nM (2-fold serial dilution) or 144 to 0.5 nM (1.5-fold serial dilution). CA-074Me inhibitor concentrations ranged from 65,536 to 64 nM (2-fold serial dilution) or 50,000 to 64 nM (1.5-fold dilution). Inhibitors were added to the enzyme at the start of the incubation period (at RT); thus, there was no preincubation. A vehicle control assay without inhibitor contained enzyme, substrate, and 2% (v/v) DMSO. Cathepsin B proteolytic assays with CA-074 were conducted as described above. IC_{50} values were calculated as the inhibitor concentration that reduced cathepsin B activity by 50%.

For determination of K_I and k_{inact}/K_I kinetic inhibition constants, k_{obs} constants were determined for each inhibitor concentration by plots of cathepsin B activity in time courses with various inhibitor concentrations by curve fitting slope data of RFU versus time into $Y = Y_0 \times e^{(-k_{obs} \times X)}$, where Y_0 is the activity for the control with no inhibitor, Y is the activity in the presence of the inhibitor, and X is time. K_I and k_{inact} values were determined by plots of k_{obs} and inhibitor concentration, combined with curve fitting the k_{obs} values with the equation $k_{obs} = k_{inact} \times [I]/(K_I + [I])$, where $[I]$ is inhibitor concentration, k_{inact} is the maximum rate of inactivation at saturating inhibitor concentrations, and $K_{I,app}$ is the x-axis inhibitor concentration where $y = k_{inact}/2$. (58,59)K_I, values were determined from $K_{I,app}$ and K_m values by the

equation $K_{I,app} = K_I \times (1 + [S]_0/K_m)$. Determination of K_m values is described in the next paragraph. These analyses are for irreversible inhibitor kinetic characterization.

K_m values were determined for Cathepsin B (Z-Phe-Arg-AMC substrate), Cathepsin C (Gly-Arg-AMC), Cathepsin H (Arg-AMC), Cathepsin L (Z-Phe-Arg-AMC), Cathepsin K (Z-Phe-Arg-AMC), Cathepsin S (Z-Phe-Arg-AMC), Cathepsin V (Z-Phe-Arg-AMC), and Cathepsin X (MCA-Arg-Pro-Pro-Gly-Phe-Ser-Ala-Phe-Lys(Dnp)-OH) at pH 4.6, pH 5.5, and pH 7.2 (Figure 3.S6). Enzymes were assayed at different substrate concentrations ranging from 225 to 4 μM (1.5-fold serial dilution), and the slope of RFU per unit time was determined for each substrate concentration; plots of substrate concentration and velocity were assessed by Prism 9 by curve fitting using the equation $v_0 = V_{max} \times [S]/(K_m + [S])$ to determine K_m values. These kinetic methods are for irreversible inhibitor kinetic characterization.

3.4.4 Irreversible Inhibition Mechanism

The irreversible mechanisms of CA-074 and CA-074Me inhibition of cathepsin B were conducted at pH 4.6, pH 5.5, and pH 7.2. Cathepsin B was preincubated with each inhibitor at 10 times the IC_{50} concentration followed by dilution to 1/10 the IC_{50} concentration, addition of substrate (Z-F-R-AMC), and monitoring activity in time-course assays. Inhibition of cathepsin B following dilution indicates the irreversible inhibitory mechanism of CA-074 and CA-074Me under acidic and neutral pH conditions.

3.4.5 Selectivity of CA-074 for Cathepsin B and Cysteine Cathepsin Proteases

The selectivity of CA-074 and CA-074Me was assessed by comparing its inhibitory potencies for cathepsin B compared to other cysteine cathepsin proteases consisting of cathepsin V, L, K, S, X, H, and C. IC_{50} values were determined for pH 4.6, pH 5.5, and pH 7.2 conditions (with no preincubation of inhibitor and enzyme), consisting of 40 mM citrate phosphate, 1 mM

EDTA, 5 mM DTT, and 100 mM NaCl. The inhibitor concentrations ranged from 16.38 μM to 256 nM in 2-fold serial dilutions. When activity (RFU/s) in the presence of 16.38 μM inhibitor was reduced by <50%, the IC_{50} value was indicated as >16 μM. Cathepsin L (0.03 ng/μL), cathepsin K (0.10 ng/μL), cathepsin S (0.20 ng/uL), and cathepsin V (0.04 ng/μL) were assayed with 40 μM Z-Phe-Arg-AMC. Cathepsin C (0.51 ng/uL), cathepsin H (0.1 ng/μL), and cathepsin X (0.20 ng/uL) were assayed with 40 μM of MCA-Arg-Pro-Pro-Gly-Phe-Ser-Ala-Phe-Lys(Dnp)-OH, Gly-Arg-AMC, and Arg-AMC, respectively. Activation of procathepsin H to cathepsin H was achieved by incubation of cathepsin H (4.4 ng/μL) with cathepsin L (1.1 ng/μL) at RT for 2 h in 20 mM citrate phosphate pH 6.0, 5 mM DTT, and 100 mM NaCl. Cathepsin C (13.78 ng/μL) was activated by incubation with cathepsin L (3.4 ng/μL) at RT for 1 h in 20 mM citrate phosphate, pH 6.0, 100 mM NaCl, and 5 mM DTT. Cathepsin L did not cleave the cathepsin C and cathepsin H substrates Gly-Arg-AMC and Arg-AMC, respectively. These fluorogenic assays used a fluorescent microplate reader as described for cathepsin B. For assay of cathepsin X, the reader was set to excitation 320 nm and emission 400 nm. To convert RFU/s to picomol/min, 10 μM to 0.005 μM (in 2-fold dilutions) of MCA-Arg-Pro-Pro-Gly-Phe-Ser-Ala-Phe-Lys(Dnp)-OH was fully hydrolyzed with excess Cathepsin X, and a standard curve was generated using the fluorescence values measured at each concentration.

3.4.6 CA-074 Inhibition of Cathepsin B Peptide Cleavages Assessed by MSP-MS

CA-074 inhibition of peptide cleavages was evaluated by MSP-MS assays of cathepsin B. Cathepsin B was preincubated at 25 °C for 30 min with 10 nM of CA-074 in pH 4.6 buffer or pH 7.2 buffer. As a control, cathepsin B was preincubated with 2.5% DMSO in each assay buffer. In a total volume of 10 μL, cathepsin B (0.1 ng/μL) preincubated with CA-074 was incubated with a mixture of 228 14-mer peptides (0.5 μM for each peptide) in assay buffer composed of 40 mM

citrate phosphate at pH 4.6 or pH 7.2, 1 mM EDTA, 100 mM NaCl, and 5 mM DTT for 60 min at 25 °C. After 60 min incubation, the 10 μL aliquot was combined with 60 μL of 8 M urea. A control assay used activated cathepsin B in each assay buffer mixed with 8 M urea for 60 min at 25 °C for inactivation, prior to addition of the peptide library. Assays were conducted in quadruplicate. Samples were acidified by addition of 40 μL of 2% TFA, enriched, and desalted using C18 LTS Tips (Rainin), evaporated to dryness in a vacuum centrifuge, and placed at −70 °C. Samples were resuspended in 40 μL of 0.1% FA (solvent A), and 4 μL was used for LC–MS/MS.

LC–MS/MS was performed on a Q-Exactive Mass Spectrometer (Thermo) equipped with an Ultimate 3000 HPLC (Thermo Fisher). Peptides were separated by reverse-phase chromatography on a C18 column (1.7 μm bead size, 75 μm × 20 cm, 65 °C) heated to 65 °C at a flow rate of 400 nL/min using solvent A and 0.1% FA in acetonitrile (solvent B). LC separation used a 50-minute linear gradient of 5–30% solvent B with a subsequent 15-minute linear gradient of 30–75% solvent B. Survey scans were recorded over a 200–2000 *m*/*z* range (70,000 resolutions at 200 *m*/*z*, AGC target 1×10^6, 75 ms maximum). MS/MS was performed in data-dependent acquisition mode with HCD fragmentation (30 normalized collision energy) on the 10 most intense precursor ions (17,500 resolutions at 200 *m*/*z*, AGC target 5×10^4, 120 ms maximum, dynamic exclusion 15 s).

MS/MS data analysis was performed using PEAKS (v 8.5) software (Bioinformatics Solutions Inc.). MS^2 data were searched against the 228-member tetradecapeptide library sequences, and a decoy search was conducted with sequences in reverse order. A precursor tolerance of 20 ppm and 0.01 Da for MS^2 fragments was defined. No protease digestion was specified. Data were filtered to 1% peptide and protein level false discovery rates with the target-decoy strategy. Peptides were quantified with label-free quantification, and data were normalized

by the Loess-G algorithm and filtered by 0.5 peptide quality. Using R scripts, outliers from replicates were removed by Dixon's Q testing. Missing and zero values are imputed with random normally distributed numbers in the range of the average of smallest 5% of the data ± SD. Analysis of variance testing was performed for peptide data of control and 60 min incubation conditions; those with $p < 0.05$ were considered for further analysis. Criteria for cleaved peptide products were those with intensity scores of 8-fold or more above the quenched inactive cathepsin B, evaluated by $\log_2$(active/inactivated enzyme) ratios for each peptide product; with $p < 0.05$ by the two-tailed homoscedastic t-test.

3.4.7 MOE Modeling of CA-074 Interactions with Cathepsin B under Acidic and Neutral pH Conditions

The MOE molecular modeling tool was used to model CA-074 binding to cathepsin B using the crystal structure of bovine cathepsin B (PDB 1QDQ) and a co-crystal template with the inhibitor CA-074 as the default binding ligand. The builder function of the MOE was used to examine binding poses that considered polar contacts and hydrogen bonds between the ligand and the active site pocket of 1QDQ at pH 4.6 and pH 7.2. Docking simulations used energy-minimized structures to assess ligand flexibility and poses.

3.4.8 Data availability

LC-MS/MS files for the MSP-MS experiments can be accessed at www.massive.ucsd.edu under the dataset identifier numbers MSV000086449 and MSV000086447.

3.5 Supporting Information

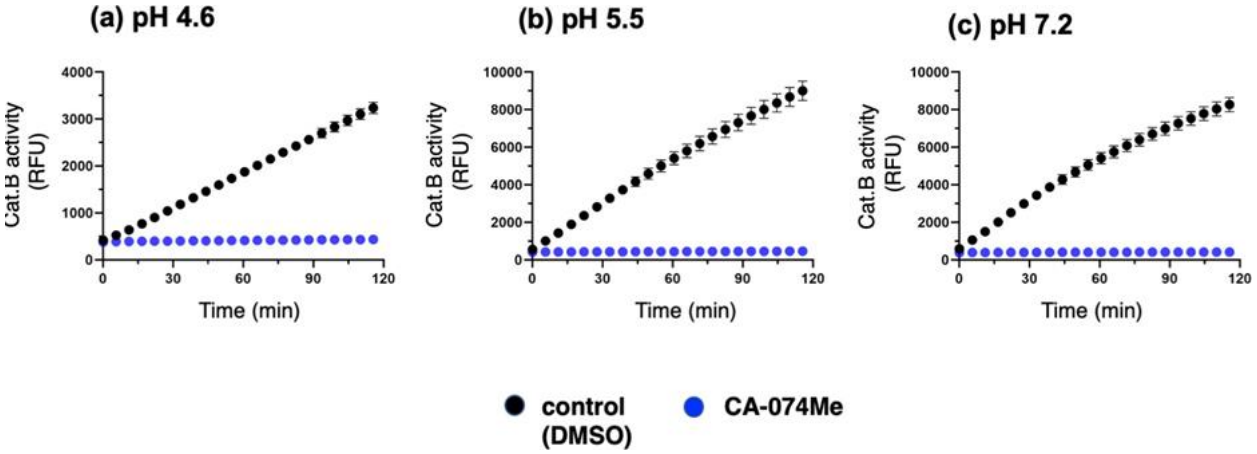

Figure 3.S1 Irreversible mechanism of CA-074Me inhibition of cathepsin B at pH 4.6, pH 5.5, and pH 7.2. CA-074Me at pH 4.6 (panel a), pH 5.5 (panel b), and pH 7.2 (panel c) was evaluated for irreversible or reversible inhibition of cathepsin B. Cathepsin B was pre-incubated with inhibitor at 10 times the IC50 concentration (consisting of CA-074Me at 90 µM at pH 4.6, 137 µM at pH 5.5, and 75 µM at pH 7.2), followed by dilution to 1/10 the IC50 concentration, addition of substrate (Z-F-R-AMC), and measurement of activity in time-course assays. Inhibition of cathepsin B following dilution indicates the irreversible inhibitory mechanism of CA-074Me.

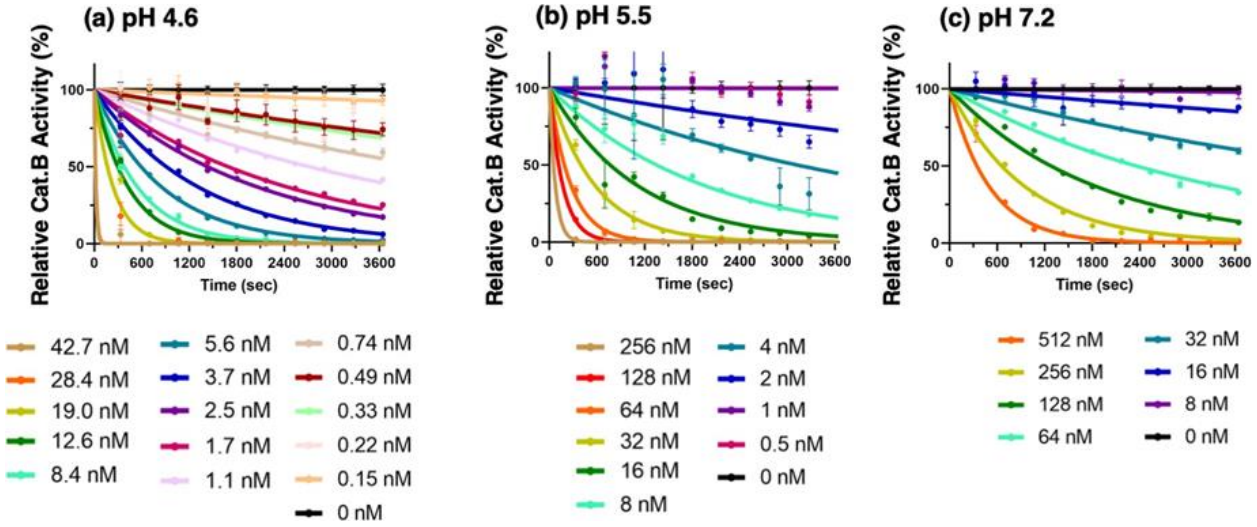

Figure 3.S2 Kinetic analysis of CA-074 inhibition of cathepsin B at acidic to neutral pH conditions. Cathepsin B activity was monitored in time-course assays at different concentrations of CA-074, conducted at pH 4.6 (panel a), pH 5.5 (panel b), and pH 7.2 (panel c). Values for kobs were calculated by Prism using the equation $Y=Y0*e^{(-kobs*X)}$ where X is time and Y/Y_0 is activity (measured as slope of RFU vs time) with inhibitor relative to activity with no inhibitor. The kobs values were used to calculate kinact and KI values by plotting kobs vs inhibitor concentration (shown in Figure 3.3).

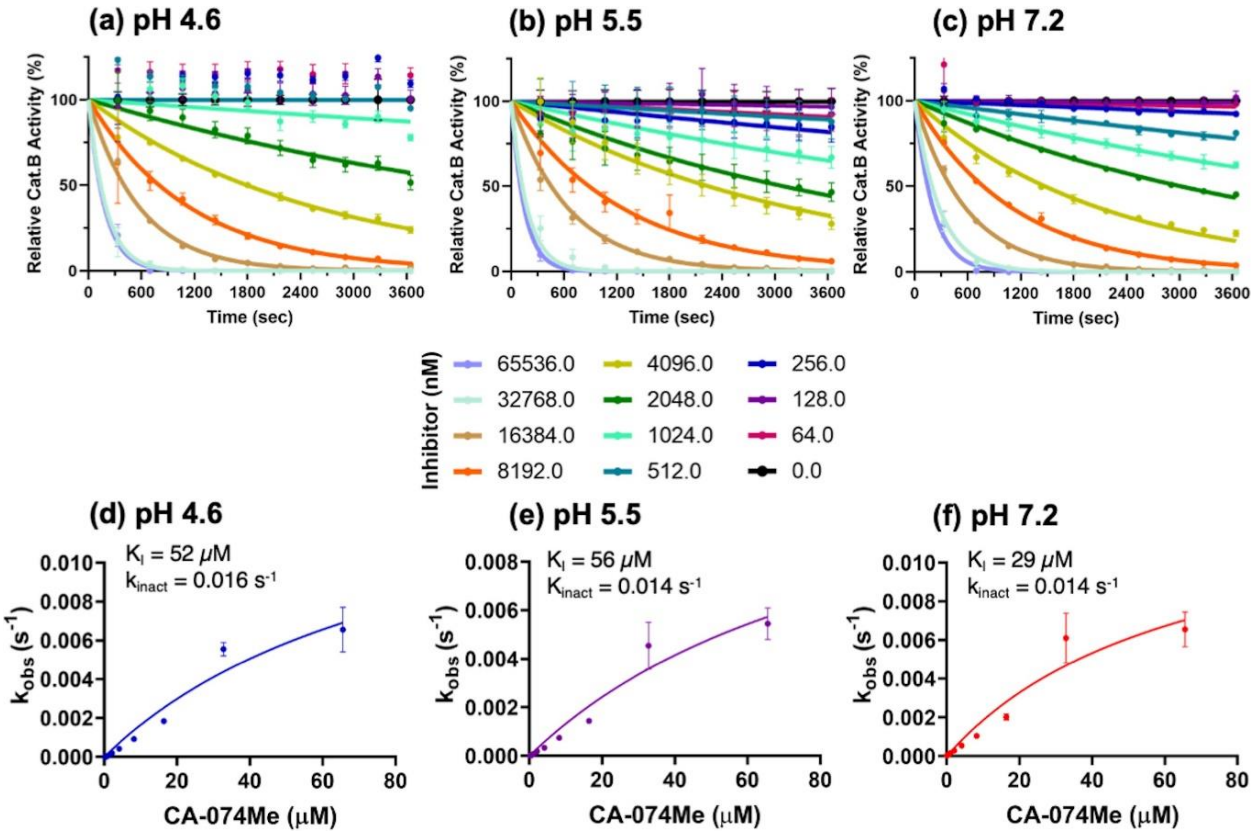

Figure 3.S3 Kinetic analysis of CA-074Me inhibition of cathepsin B at acidic to neutral pH conditions.

(a) to (c). CA-074Me and cathepsin B in kinetic studies for kobs values. Cathepsin B activity was monitored in time-course assays at different concentrations of CA-074, conducted at pH 4.6 (panel a), pH 5.5 (panel b), and pH 7.2 (panel c). Values for kobs were calculated by the equation $Y=Y_0*e^{(-kobs*X)}$ where X is time and Y/Y_0 is activity with inhibitor relative to activity with no inhibitor. The kobs values were used to calculate kinact and K_I values by plotting kobs vs inhibitor concentration (shown in d-f).

(d) to (f). CA-074Me inhibition of cathepsin B kinetics for K_I, k_{inact}, and k_{inact}/K_I values. Kinetic analyses of CA-074Me inhibition of cathepsin B was conducted at pH 4.6 (panel d), pH 5.5 (panel e), and pH 7.2 (panel f) to determine K_I, k_{inact}, and k_{inact}/K_I values, conducted as described in the methods.

Ligand Interactions Report

Mon Oct 12 12:58:04 2020 (MOE 2019.01)

1QDQ: HYDROLASE / 1QDQ: HYDROLASE

Inhibitor		Enzyme				Interaction	Distance	E (kcal/mol)
N1	11	O	GLY	198	(A)	H-donor	2.84	-2.0
O2	17	O	HOH	399	(A)	H-donor	2.61	-1.6
C6	19	O	GLY	198	(A)	H-donor	3.37	-0.5
O1	14	N	GLY	74	(A)	H-acceptor	3.04	-2.3
O2	17	O	HOH	282	(A)	H-acceptor	2.86	-1.2
O3	22	NE2	GLN	23	(A)	H-acceptor	2.90	-1.4
O3	22	N	CYS	29	(A)	H-acceptor	3.26	-1.9
O4	28	NE1	TRP	221	(A)	H-acceptor	2.89	-4.2
O	46	O	HOH	388	(A)	H-acceptor	2.62	-1.1
O	46	O	HOH	395	(A)	H-acceptor	2.65	-3.3
OT	56	ND1	HIS	110	(A)	H-acceptor	2.70	-11.2
OT	56	NE2	HIS	111	(A)	H-acceptor	2.73	-10.9
O	46	NE2	HIS	111	(A)	Ionic	3.19	-3.3
OT	56	ND1	HIS	110	(A)	Ionic	2.70	-6.8
OT	56	NE2	HIS	111	(A)	Ionic	2.73	-6.6

CA074:
Bound @ pH4.6

Total Interactions:

-58.3 kcal/mol

Nuc-E Distance: N/Å

Figure 3.S4 Binding energy of CA-074 bound to cathepsin B at pH 4.6.
Components comprising the binding energy of CA-074 binding to cathepsin B at pH 4.6 were assessed by the MOE docking software. Energies of the binding interactions of the inhibitor with the enzyme (specific residues are indicated) are shown, combined with the total binding energy indicated as -58.3 kcal/mol.

Ligand Interactions Report

Mon Oct 12 13:33:09 2020 (MOE 2019.01)

1QDQ: HYDROLASE / 1QDQ: HYDROLASE

Inhibitor		Enzyme				Interaction	Distance	E (kcal/mol)
N1	11	O	GLY	198	(A)	H-donor	2.84	-2.0
O2	17	O	HOH	399	(A)	H-donor	2.61	-1.6
O1	14	N	GLY	74	(A)	H-acceptor	3.04	-2.3
O2	17	O	HOH	282	(A)	H-acceptor	2.87	-1.2
O3	22	NE2	GLN	23	(A)	H-acceptor	2.90	-1.3
O3	22	N	CYS	29	(A)	H-acceptor	3.26	-1.9
O4	28	NE1	TRP	221	(A)	H-acceptor	2.90	-4.4
O	46	O	HOH	388	(A)	H-acceptor	2.61	-1.1
O	46	O	HOH	395	(A)	H-acceptor	2.62	-3.1
OT	56	ND1	HIS	110	(A)	H-acceptor	2.69	-11.1
OT	56	NE2	HIS	111	(A)	H-acceptor	2.83	-6.1
OT	56	ND1	HIS	110	(A)	Ionic	2.69	-6.9

CA074:
Bound @ pH7.2

Total Interactions:

-43.0 kcal/mol

Nuc-E Distance: N/Å

Figure 3.S5 Binding energy of CA-074 bound to cathepsin B at pH 7.2.
Components comprising the binding energy of CA-074 binding to cathepsin B at pH 7.2 were assessed by the MOE docking software. Energies of the binding interactions of the inhibitor with the enzyme (residues are indicated) are shown, combined with the total binding energy indicated as -43.0 kcal/mol.

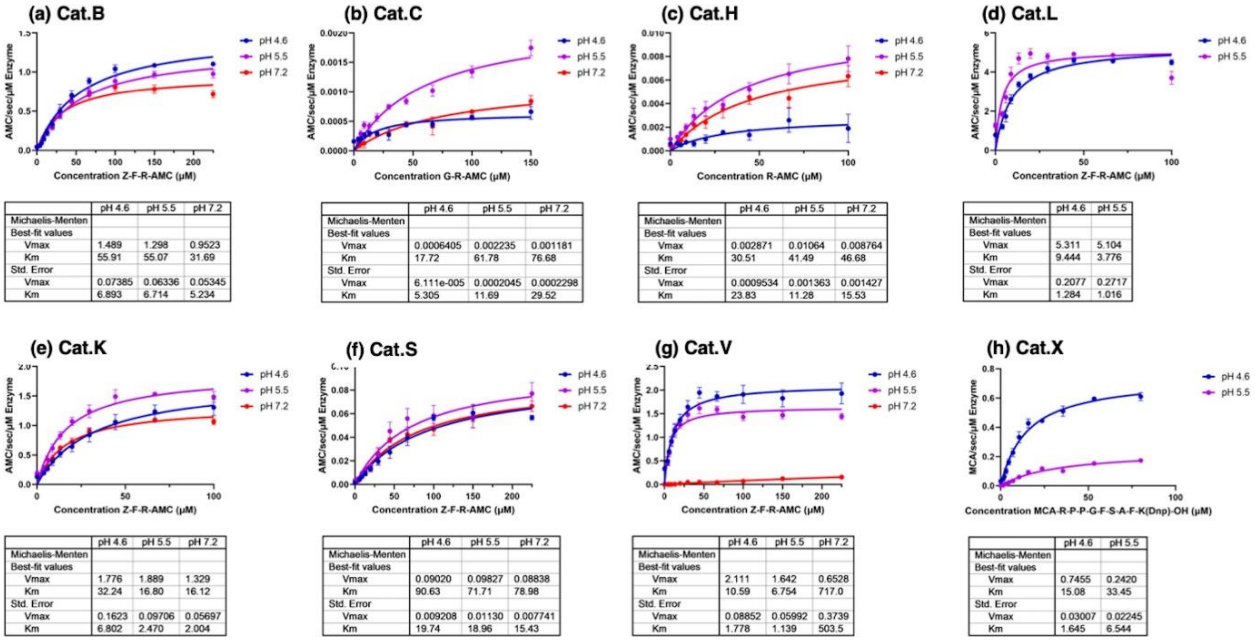

	pH 4.6	pH 5.5	pH 7.2
Michaelis-Menten Best-fit values			
Vmax	1.489	1.298	0.9523
Km	55.91	55.07	31.69
Std. Error			
Vmax	0.07385	0.06336	0.05345
Km	6.893	6.714	5.234

	pH 4.6	pH 5.5	pH 7.2
Michaelis-Menten Best-fit values			
Vmax	0.0006405	0.002235	0.001181
Km	17.72	61.78	76.68
Std. Error			
Vmax	6.111e-005	0.0002045	0.0002298
Km	5.305	11.69	29.52

	pH 4.6	pH 5.5	pH 7.2
Michaelis-Menten Best-fit values			
Vmax	0.002871	0.01064	0.008764
Km	30.51	41.49	46.68
Std. Error			
Vmax	0.0009534	0.001363	0.001427
Km	23.83	11.28	15.53

	pH 4.6	pH 5.5
Michaelis-Menten Best-fit values		
Vmax	5.311	5.104
Km	9.444	3.776
Std. Error		
Vmax	0.2077	0.2717
Km	1.284	1.016

	pH 4.6	pH 5.5	pH 7.2
Michaelis-Menten Best-fit values			
Vmax	1.776	1.889	1.329
Km	32.24	16.80	16.12
Std. Error			
Vmax	0.1623	0.09706	0.05697
Km	6.802	2.470	2.004

	pH 4.6	pH 5.5	pH 7.2
Michaelis-Menten Best-fit values			
Vmax	0.09020	0.09827	0.08838
Km	90.63	71.71	78.98
Std. Error			
Vmax	0.009208	0.01130	0.007741
Km	19.74	18.96	15.43

	pH 4.6	pH 5.5	pH 7.2
Michaelis-Menten Best-fit values			
Vmax	2.111	1.642	0.6528
Km	10.59	6.754	717.0
Std. Error			
Vmax	0.08852	0.05992	0.3739
Km	1.778	1.139	503.5

	pH 4.6	pH 5.5
Michaelis-Menten Best-fit values		
Vmax	0.7455	0.2420
Km	15.08	33.45
Std. Error		
Vmax	0.03007	0.02245
Km	1.645	6.544

Figure 3.S6 Km plots for cathepsin B and cysteine cathepsins at pH 4.6, 5.5, and 7.2. Km values were determined for cathepsin B (panel a) and the cysteine cathepsins (cathepsins C, H, L K, S, V, and X with each of their indicated substrates, shown in panels b, c, d, e, f, g, and h, respectively. Michaelis-Menten kinetics was used for Km data analysis (conducted as described in the methods) using the equation $V_0=V_{max}*[S]/(K_m+[S])$ with curve-fitting using Prism 9.Cathepsin L and cathepsin X had no activity at pH 7.2 and, therefore, Km was determined for pH 4.6 and 5.5.

3.6 References

1. Turk, V.; Stoka, V.; Vasiljeva, O.; Renko, M.; Sun, T.; Turk, B.; Turk, D. Cysteine cathepsins: from structure, function and regulation to new frontiers. Biochim. Biophys. Acta 2012, 1824, 68−88.

2. Reiser, J.; Adair, B.; Reinheckel, T. Specialized roles for cysteine cathepsins in health and disease. J. Clin. Invest. 2010, 120, 3421− 3431.

3. Hook, V.; Yoon, M.; Mosier, C.; Ito, G.; Podvin, S.; Head, B. P.; Rissman, R.; O'Donoghue, A. J.; Hook, G. Cathepsin B in neurodegeneration of Alzheimer's disease, traumatic brain injury, and related brain disorders. Biochim. Biophys. Acta, Proteins Proteomics 1868, 1868, No. 140428.

4. Wu, Z.; Ni, J.; Liu, Y.; Teeling, J. L.; Takayama, F.; Collcutt, A.; Ibbett, P.; Nakanishi, H. Cathepsin B plays a critical role in inducing Alzheimer's disease-like phenotypes following chronic systemic exposure to lipopolysaccharide from Porphyromonas gingivalis in mice. Brain, Behav., Immun. 2017, 65, 350−361.

5. Kindy, M. S.; Yu, J.; Zhu, H.; El-Amouri, S. S.; Hook, V.; Hook, G. R. Deletion of the cathepsin B gene improves memory deficits in a transgenic Alzheimer's disease mouse model expressing AβPP containing the wild-type β-secretase site sequence. J. Alzheimers Dis. 2012, 29, 827−840.

6. Hook, V. Y.; Kindy, M.; Hook, G. Inhibitors of cathepsin B improve memory and reduce beta-amyloid in transgenic Alzheimer disease mice expressing the wild-type, but not the Swedish mutant, beta-secretase site of the amyloid precursor protein. J. Biol. Chem. 2008, 283, 7745−7753.

7. Hook, G. R.; Yu, J.; Sipes, N.; Pierschbacher, M. D.; Hook, V.; Kindy, M. S. The cysteine protease cathepsin B is a key drug target and cysteine protease inhibitors are potential therapeutics for traumatic brain injury. J. Neurotrauma. 2014, 31, 515−529.

8. Boutté, A. M.; Hook, V.; Thangavelu, B.; Sarkis, G. A.; Abbatiello, B. N.; Hook, G.; Jacobsen, J. S.; Robertson, C. S.; Gilsdorf, J.; Yang, Z.; Wang, K. K. W.; Shear, D. A. Penetrating Traumatic Brain Injury Triggers Dysregulation of Cathepsin B Protein Levels Independent of Cysteine Protease Activity in Brain and Cerebral Spinal Fluid. J. Neurotrauma. 2020, 37, 1574−1586.

9. Zuo, X.; Hou, Q.; Jin, J.; Chen, X.; Zhan, L.; Tang, Y.; Shi, Z.; Sun, W.; Xu, E. Inhibition of Cathepsins B Induces Neuroprotection Against Secondary Degeneration in Ipsilateral Substantia Nigra After Focal Cortical Infarction in Adult Male Rats. Front Aging Neurosci. 2018, 10, 125.

10. Aggarwal, N.; Sloane, B. F. Cathepsin B: multiple roles in cancer. Proteomics Clin. Appl. 2014, 8, 427−437.

11. Victor, B. C.; Anbalagan, A.; Mohamed, M. M.; Sloane, B. F.; Cavallo-Medved, D. Inhibition of cathepsin B activity attenuates extracellular matrix degradation and inflammatory breast cancer invasion. Breast Cancer Res. 2011, 13, R115.

12. Bian, B.; Mongrain, S.; Cagnol, S.; Langlois, M. J.; Boulanger, J.; Bernatchez, G.; Carrier, J. C.; Boudreau, F.; Rivard, N. Cathepsin B promotes colorectal tumorigenesis, cell invasion, and metastasis. Mol. Carcinog. 2016, 55, 671−687.

13. Mort, J. S.; Recklies, A. D.; Poole, A. R. Extracellular presence of the lysosomal proteinase cathepsin B in rheumatoid synovium and its activity at neutral pH. Arthritis Rheum. 1984, 27, 509−515.

14. Fujisawa, A.; Kambe, N.; Saito, M.; Nishikomori, R.; Tanizaki, H.; Kanazawa, N.; Adachi, S.; Heike, T.; Sagara, J.; Suda, T.; Nakahata, T.; Miyachi, Y. Disease-associated mutations in CIAS1 induce cathepsin B-dependent rapid cell death of human THP-1 monocytic cells. Blood 2007, 109, 2903−2911.

15. Toomey, C. B.; Cauvi, D. M.; Hamel, J. C.; Ramirez, A. E.; Pollard, K. M. Cathepsin B regulates the appearance and severity of mercury-induced inflammation and autoimmunity. Toxicol. Sci. 2014, 142, 339−349.

16. Rajamäki, K.; Lappalainen, J.; Oörni, K.; Välimäki, E.; Matikainen, S.; Kovanen, P. T.; Eklund, K. K. Cholesterol crystals activate the NLRP3 inflammasome in human macrophages: a novel link between cholesterol metabolism and inflammation. PLoS One 2010, 5, e11765.

17. Gonzalez, E. A.; Martins, G. R.; Tavares, A. M. V.; Viegas, M.; Poletto, E.; Giugliani, R.; Matte, U.; Baldo, G. Cathepsin B inhibition attenuates cardiovascular pathology in mucopolysaccharidosis I mice. Life Sci. 2018, 196, 102−109.

18. Van Acker, G. J.; Saluja, A. K.; Bhagat, L.; Singh, V. P.; Song, A. M.; Steer, M. L. Cathepsin B inhibition prevents trypsinogen activation and reduces pancreatitis severity. Am. J. Physiol.: Gastro- intest. Liver Physiol. 2002, 283, G794−G800.

19. Cantres-Rosario, Y. M.; Ortiz-Rodríguez, S. C.; Santos- Figueroa, A. G.; Plaud, M.; Negron, K.; Cotto, B.; Langford, D.; Melendez, L. M. HIV Infection Induces Extracellular Cathepsin B Uptake and Damage to Neurons. Sci. Rep. 2019, 9, 8006.

20. Towatari, T.; Nikawa, T.; Murata, M.; Yokoo, C.; Tamai, M.; Hanada, K.; Katunuma, N. Novel epoxysuccinyl peptides A selective inhibitor of cathepsin B, in vivo. FEBS Lett. 1991, 280, 311−315.

21. Murata, M.; Miyashita, S.; Yokoo, C.; Tamai, M.; Hanada, K.; Hatayama, K.; Towatari, T.; Nikawa, T.; Katunuma, N. Novel epoxysuccinyl peptides Selective inhibitors of cathepsin B, in vitro. FEBS Lett. 1991, 280, 307−310.

22. Barrett, A. J.; Kembhavi, A. A.; Brown, M. A.; Kirschke, H.; Knight, C. G.; Tamai, M.; Hanada, K. L-trans-Epoxysuccinyl- leucylamido(4-guanidino)butane (E-64) and its analogues as inhibitors of cysteine proteinases including cathepsins B, H and L. Biochem. J. 1982, 201, 189−198.

23. Mindell, J. A. Lysosomal acidification mechanisms. Annu. Rev. Physiol. 2012, 74, 69−86.

24. Ishida, Y.; Nayak, S.; Mindell, J. A.; Grabe, M. A model of lysosomal pH regulation. J. Gen. Physiol. 2013, 141, 705−720.

25. Bright, G. R.; Fisher, G. W.; Rogowska, J.; Taylor, D. L. Fluorescence ratio imaging microscopy: temporal and spatial measurements of cytoplasmic pH. J. Cell Biol. 1987, 104, 1019−1033.

26. Madshus, I. H. Regulation of intracellular pH in eukaryotic cells. Biochem. J. 1988, 250, 1−8.

27. Wang, F.; Gómez-Sintes, R.; Boya, P. Lysosomal membrane permeabilization and cell death. Traffic 2018, 19, 918−931.

28. Porter, K.; Lin, Y.; Liton, P. B. Cathepsin B is up-regulated and mediates extracellular matrix degradation in trabecular meshwork cells following phagocytic challenge. PLoS One 2013, 8, e68668.

29. Casey, J. R.; Grinstein, S.; Orlowski, J. Sensors and regulators of intracellular pH. Nat. Rev. Mol. Cell Biol. 2010, 11, 50−61.

30. Hämälistö, S.; Stahl, J. L.; Favaro, E.; Yang, Q.; Liu, B.; Christoffersen, L.; Loos, B.; Guasch Boldú, C.; Joyce, J. A.; Reinheckel, T.; Barisic, M.; Jättelä, M. Spatially and temporally defined lysosomal leakage facilitates mitotic chromosome segregation. Nat. Commun. 2020, 11, 229.

31. Meng, J.; Liu, Y. C.; Xie, Z.; Qing, H.; Lei, P.; Ni, J. Nucleus distribution of cathepsin B in senescent microglia promotes brain aging through degradation of sirtuins. Neurobiol. Aging 2020, 96, 255−266.

32. Jiang, Z.; Lietz, C. B.; Podvin, S.; Yoon, M. C.; Toneff, T.; Hook, V.; O'Donoghue, A. J. Differential Neuropeptidomes of Dense Core Secretory Vesicles (DCSV) Produced at Intravesicular and Extracellular pH Conditions by Proteolytic Processing. ACS Chem. Neurosci. 2021, 12, 2385−2398.

33. Buttle, D. J.; Murata, M.; Knight, C. G.; Barrett, A. J. CA074 methyl ester: a proinhibitor for intracellular cathepsin B. Arch. Biochem. Biophys. 1992, 299, 377−380.

34. Choe, Y.; Leonetti, F.; Greenbaum, D. C.; Lecaille, F.; Bogyo, M.; Brömme, D.; Ellman, J. A.; Craik, C. S. Substrate profiling of cysteine proteases using a combinatorial peptide library identifies functionally unique specificities. J. Biol. Chem. 2006, 281, 12824−12832.

35. Poreba, M.; Groborz, K.; Vizovisek, M.; Maruggi, M.; Turk, D.; Turk, B.; Powis, G.; Drag, M.; Salvesen, G. S. Fluorescent probes towards selective cathepsin B detection and visualization in cancer cells and patient samples. Chem. Sci. 2019, 10, 8461−8477.

36. Yamamoto, A.; Tomoo, K.; Hara, T.; Murata, M.; Kitamura, K.; Ishida, T. Substrate specificity of bovine cathepsin B and its inhibition by CA074, based on crystal structure refinement of the complex. J. Biochem. 2000, 127, 635−643.

37. Yamamoto, A.; Hara, T.; Tomoo, K.; Ishida, T.; Fuji, T.; Hata, Y.; Murata, M.; Kitamura, K. Binding mode of CA074, a specific irreversible inhibitor, to bovine cathepsin B as determined by X-ray crystal analysis of the complex. J. Biochem. 1997, 121, 974−977.

38. Hsu, A.; Podvin, S.; Hook, V. Lysosomal Cathepsin Protease Gene Expression Profiles in the Human Brain During Normal Development. J. Mol. Neurosci. 2018, 65, 420−431.

39. O'Donoghue, A. J.; Eroy-Reveles, A. A.; Knudsen, G. M.;Ingram, J.; Zhou, M.; Statnekov, J. B.; Greninger, A. L.; Hostetter, D. R.; Qu, G.; Maltby, D. A.; Anderson, M. O.; Derisi, J. L.; McKerrow, J. H.; Burlingame, A. L.; Craik, C. S. Global identification of peptidase specificity by multiplex substrate profiling. Nat. Methods 2012, 9, 1095−1100.

40. Lapek, J. D., Jr.; Jiang, Z.; Wozniak, J. M.; Arutyunova, E.; Wang, S. C.; Lemieux, M. J.; Gonzalez, D. J.; O'Donoghue, A. J. Quantitative Multiplex Substrate Profiling of Peptidases by Mass Spectrometry. Mol. Cell. Proteomics 2019, 18, 968−981.

41. Vilar, S.; Cozza, G.; Moro, S. Medicinal chemistry and the molecular operating environment (MOE): application of QSAR and molecular docking to drug discovery. Curr. Top. Med. Chem. 2008, 8, 1555−1572.

42. Roy, U.; Luck, L. A. Molecular modeling of estrogen receptor using molecular operating environment. Biochem. Mol. Biol. Educ. 2007, 35, 238−243.

43. Schechter, I. Mapping of the active site of proteases in the 1960s and rational design of inhibitors/drugs in the 1990s. Curr. Protein Pept. Sci. 2005, 6, 501−512.

44. Yoon, M. C.; Solania, A.; Jiang, Z.; Christy, M. P.; Podvin, S.; Mosier, C.; Lietz, C. B.; Ito, G.; Gerwick, W. H.; Wolan, D. W.; Hook, G.; O'Donoghue, A. J.; Hook, V. Selective Neutral pH Inhibitor of Cathepsin B Designed Based on Cleavage Preferences at Cytosolic and Lysosomal pH Conditions. ACS Chem. Biol. 2021, 16, 1626− 1643.

45. Krupa, J. C.; Hasnain, S.; Nägler, D. K.; Ménard, R.; Mort, J. S. S2' substrate specificity and the role of His110 and His111 in the exopeptidase activity of human cathepsin B. Biochem. J. 2002, 361, 613−619.

46. Turk, D.; Podobnik, M.; Popovic, T.; Katunuma, N.; Bode, W.; Huber, R.; Turk, V. Crystal structure of cathepsin B inhibited with CA030 at 20-A resolution: A basis for the design of specific epoxysuccinyl inhibitors. Biochemistry 1995, 34, 4791−4797.

47. Katunuma, N. Structure-based development of specific inhibitors for individual cathepsins and their medical applications. Proc. Jpn. Acad., Ser. B 2011, 87, 29−39.

48. Jiang, M.; Meng, J.; Zeng, F.; Qing, H.; Hook, G.; Hook, V.; Wu, Z.; Ni, J. Cathepsin B inhibition blocks neurite outgrowth in cultured neurons by regulating lysosomal trafficking and remodeling. J. Neurochem. 2020, 155, 300−312.

49. Matarrese, P.; Ascione, B.; Ciarlo, L.; Vona, R.; Leonetti, C.; Scarsella, M.; Mileo, A. M.; Catricalà, C.; Paggi, M. G.; Malorni, W. Cathepsin B inhibition interferes with metastatic potential of human melanoma: an in vitro and in vivo study. Mol. Cancer 2010, 9, 207.

50. Asai, M.; Yagishita, S.; Iwata, N.; Saido, T. C.; Ishiura, S.; Maruyama, K. An alternative metabolic pathway of amyloid precursor protein C-terminal fragments via cathepsin B in a human neuroglioma model. FASEB J. 2011, 25, 3720−3730.

51. Yamashima, T.; Kohda, Y.; Tsuchiya, K.; Ueno, T.; Yamashita, J.; Yoshioka, T.; Kominami, E. Inhibition of ischaemic hippocampal neuronal death in primates with cathepsin B inhibitor CA-074: a novel strategy for neuroprotection based on 'calpain-cathepsin hypothesis'. Eur. J. Neurosci. 1998, 10, 1723−1733.

52. Yoshida, M.; Yamashima, T.; Zhao, L.; Tsuchiya, K.; Kohda, Y.; Tonchev, A. B.; Matsuda, M.; Kominami, E. Primate neurons show different vulnerability to transient ischemia and response to cathepsin inhibition. Acta. Neuropathol. 2002, 104, 267−272.

53. Zhang, L.; Fu, X. H.; Yu, Y.; Shui, R. H.; Li, C.; Zeng, H. Y.; Qiao, Y. L.; Ni, L. Y.; Wang, Q. Treatment with CA-074Me, a Cathepsin B inhibitor, reduces lung interstitial inflammation and fibrosis in a rat model of polymyositis. Lab. Invest. 2015, 95, 65−77.

54. Van Acker, G. J.; Weiss, E.; Steer, M. L.; Perides, G. Cause- effect relationships between zymogen activation and other early events in secretagogue-induced acute pancreatitis. Am. J. Physiol.: Gastrointest. Liver Physiol. 2007, 292, G1738−G1746.

55. Stoka, V.; Turk, V.; Turk, B. Lysosomal cathepsins and their regulation in aging and neurodegeneration. Ageing Res. Rev. 2016, 32, 22−37.

56. Tedelind, S.; Poliakova, K.; Valeta, A.; Hunegnaw, R.; Yemanaberhan, E. L.; Heldin, N. E.; Kurebayashi, J.; Weber, E.; Kopitar-Jerala, N.; Turk, B.; Bogyo, M.; Brix, K. Nuclear cysteine cathepsin variants in thyroid carcinoma cells. Biol. Chem. 2010, 391, 923−935.

57. Sloane, B. F.; Yan, S.; Podgorski, I.; Linebaugh, B. E.; Cher, M. L.; Mai, J.; Cavallo-Medved, D.; Sameni, M.; Dosescu, J.; Moin, K. Cathepsin B and tumor proteolysis: contribution of the tumor microenvironment. Semin. Cancer Biol. 2005, 15, 149−157.

58. Strelow, J. M. A Perspective on the Kinetics of Covalent and Irreversible Inhibition. SLAS Discov. 2017, 22, 3−20.

59. Tonge, P. J. Quantifying the Interactions between Biomole- cules: Guidelines for Assay Design and Data Analysis. ACS Infect. Dis. 2019, 5, 796−808.

3.7 Copyright Permission

CHAPTER 4 – Cathepsin B Dipeptidyl Carboxypeptidase and Endopeptidase Activities Demonstrated across a Broad pH Range

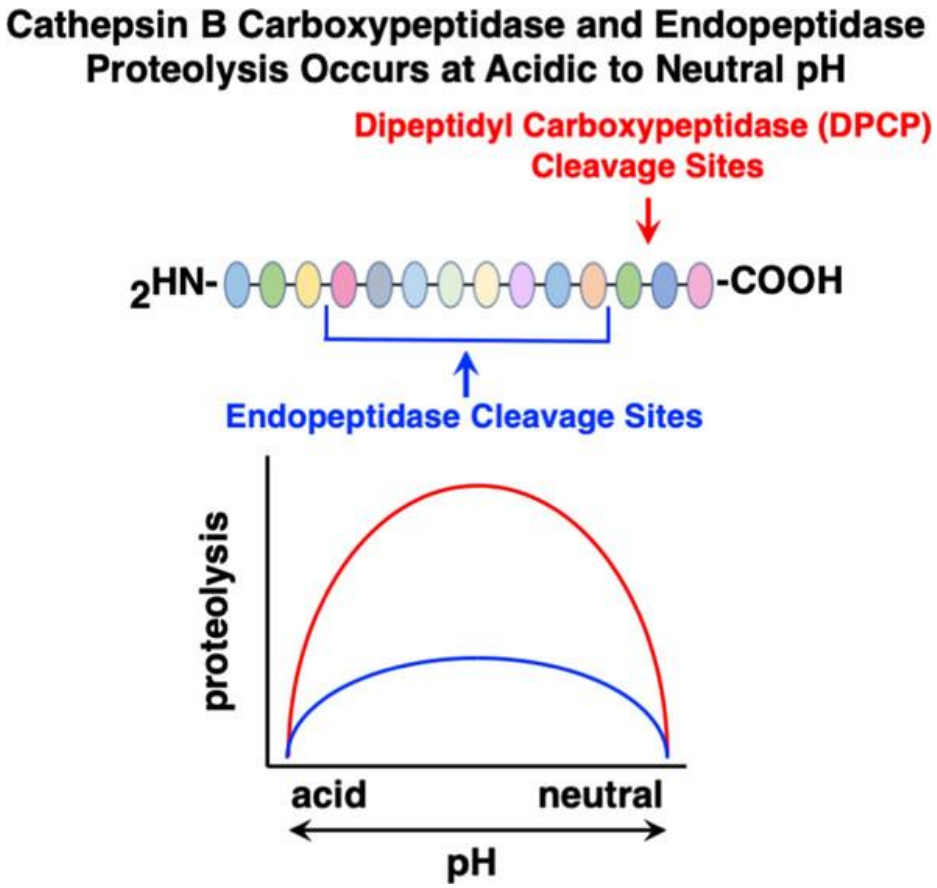

Chapter 4 Graphical Abstract. Cathepsin B is a lysosomal protease that participates in protein degradation. However, cathepsin B is also active under neutral pH conditions of the cytosol, nuclei, and extracellular locations. The dipeptidyl carboxypeptidase (DPCP) activity of cathepsin B, assayed with the Abz-GIVR↓AK(Dnp)-OH substrate, has been reported to display an acidic pH optimum. In contrast, the endopeptidase activity, monitored with Z-RR-↓AMC, has a neutral pH optimum. These observations raise the question of whether other substrates can demonstrate cathepsin B DPCP activity at neutral pH and endopeptidase activity at acidic pH. To address this question, global cleavage profiling of cathepsin B with a diverse peptide library was conducted under acidic and neutral pH conditions. Results revealed that cathepsin B has (1) major DPCP activity and modest endopeptidase activity under both acidic and neutral pH conditions and (2) distinct pH-dependent amino acid preferences adjacent to cleavage sites for both DPCP and endopeptidase activities. The pH-dependent cleavage preferences were utilized to design a new Abz-GnVR↓AK(Dnp)-OH DPCP substrate, with norleucine (n) at the P3 position, having improved DPCP activity of cathepsin B at neutral pH compared to the original Abz-GIVR↓AK(Dnp)-OH substrate. The new Z-VR-AMC and Z-ER-AMC substrates displayed improved endopeptidase activity at acidic pH compared to the original Z-RR-AMC. These findings illustrate the new concept that cathepsin B possesses DPCP and endopeptidase activities at both acidic and neutral pH values. These results advance understanding of the pH-dependent cleavage properties of the dual DPCP and endopeptidase activities of cathepsin B that function under different cellular pH conditions.

4.1 Introduction

Cathepsin B is a member of the cysteine cathepsin family of lysosomal proteases (1) participating in protein degradation and homeostasis. (2,3) Recent studies indicate that the lysosome functions as a signaling complex for regulation of cellular functions in health and in disease. (4,5) Cathepsin B is also located outside of acidic lysosomes under neutral pH conditions of the cytosol, nuclei, and extracellular locations in numerous human diseases including neurodegenerative diseases, (6−8) cancer, (9−12) autoinflammation, (13−15) viral infection, (16) and pathogen-induced pyroptosis. (17) The translocation of lysosomal cathepsin B to the cytosol participates in lysosomal signaling regulation of cellular functions including inflammation and cell death in disease. (8)

Cathepsin B is active at the neutral pH 7.2 (18,19) of the cytosol and other neutral pH compartments of biological systems, (20,21) as well as at the acidic pH 4.6 of lysosomes. (22,23) Importantly, cathepsin B is primarily a dipeptidyl carboxypeptidase (DPCP) type of exopeptidase (18) and also functions as an endopeptidase shown by cleavage of peptide and protein substrates at sites distal from the C-terminus of peptide substrates. (18,24,25)

Examination of DPCP activity of cathepsin B with internally quenched fluorogenic peptide substrates containing a free carboxy termini led to identification of 2-aminobenzoyl-Gly-Ile-Val-Arg-Ala-Lys(2,4-dinitrophenyl)-OH (Abz-GIVRAK(Dnp)-OH) as an excellent substrate for DPCP activity where cleavage occurs between R↓A to result in the dipeptide AK(Dnp)-OH product. (26) This substrate is routinely used in the field for monitoring DPCP activity of cathepsin B. (1,27−29) Evaluation of this substrate over a pH range of pH 2.5–8 showed optimal DPCP activity at acidic pH 4.5. (26) In contrast, cathepsin B activity with Z-Arg-Arg-7-amino-4-methylcoumarin (Z-RR-AMC), an endopeptidase substrate, displayed highest cleaving activity at neutral pH. (30−32) Peptide-AMC substrates with a blocked N-terminus (e.g., Z-group) have been

extensively used to quantify endopeptidase activity (33,34) and, therefore, it has been assumed that Z-RR-AMC is also detecting endopeptidase activity of cathepsin B. From this interpretation, it has been widely thought that the DPCP activity of cathepsin B decreases as pH increases, (31,35,36) while endopeptidase activity increases as pH increases. (29,37−40)

Previous studies by our group have shown that peptide cleavage efficiencies by cathepsin B under different pH conditions are dependent on the sequences of the peptide substrates. (18) We, therefore, questioned whether the pH-dependent differences that have been observed for Abz-GIVRAK(Dnp)-OH and Z-RR-AMC cleavages by cathepsin B may be due to differences in substrate sequences rather than a pH-dependent transition between DPCP and endopeptidase activities. To address this question, we evaluated the DPCP and endopeptidase cleavage profiles of cathepsin B under acidic and neutral pH conditions with a peptide library using the approach of multiplex substrate profiling by mass spectrometry (MSP-MS). (18,41,42) The library consists of 228 14-mer peptides, and cleavage at any one of the 2964 peptide bonds can be determined by LC–MS/MS. (43) The cleavage profiling of cathepsin B was performed in parallel with the endopeptidase cathepsin K to demonstrate the difference between DPCP and endopeptidase activities. Cathepsin K was selected for these control studies because it is a cysteine protease homologous to cathepsin B, both enzymes are active at pH 4.6 and pH 7.2, both cleave the substrate Z-FR-AMC, (18,44) yet cathepsin B has dual DPCP and endopeptidase activity while cathepsin K has only endopeptidase activity. (45,46)

Data from this study illustrate the new concept that cathepsin B displays both DPCP and endopeptidase activities under acidic to neutral pH conditions, illustrated by novel substrates designed based on cleavage properties under different pH conditions. These results change the widely held view that cathepsin B transitions from having exopeptidase to endopeptidase activity

as the pH increases (31,35−39) to the new finding that both types of activities occur under acidic to neutral pH conditions. To illustrate this new concept of cathepsin B cleavage properties, novel peptide substrates were designed based on pH-dependent cleavage profiling features of this enzyme. We showed that the new DPCP substrate Abz-GnVRAK(Dnp)-OH is cleaved efficiently across a broad pH range, while the endopeptidase substrate Z-ER-AMC was cleaved more efficiently at acidic pH compared to Z-RR-AMC. This study demonstrates the new concept that the major DPCP and minor endopeptidase activities of cathepsin B both occur under acidic and neutral pH conditions.

4.2 Results

4.2.1 pH Profile of Cathepsin B Activity with Abz-GIVRAK(Dnp)-OH DPCP and Z-RR-AMC Endopeptidase Substrates

Human cathepsin B activity is commonly measured with the Abz-GIVRAK(Dnp)-OH substrate for DPCP activity and the Z-RR-AMC substrate for endopeptidase activity. The pH profiles of these two substrates were directly compared, and data showed that cathepsin B cleaved Abz-GIVR↓AK(Dnp)-OH with highest efficiency at pH 5.4, with ≥50% of maximal activity observed at pH 4.6 to pH 5.8 (Figure 4.1a). We confirmed by nano-LC–MS/MS tandem mass spectrometry that cleavage of Abz-GIVR↓AK(Dnp)-OH occurred between R↓A to yield the product AK(Dnp)-OH (Figure 4.S1). In contrast, cleavage of Z-RR-AMC was highest at pH 6.2 and displayed ≥50% of maximal activity at pH 5.0 to pH 7.4 (Figure 4.1a). Illustration of Abz-GIVR↓AK(Dnp)-OH cleavage occurring between R↓A indicates the P1↓P1′ cleavage site with adjacent residues which separate the fluorescent reporter group (Abz) and the quencher group (Dnp) (Figure 4.1b). Cleavage of Z-RR-AMC occurs between R-↓AMC with P1 as the Arg residue to release the free fluorescent AMC reporter (Figure 4.1c).

These pH profiles show that cathepsin B cleavage of the DPCP substrate Abz-GIVR↓AK(Dnp)-OH occurred preferentially in the acidic range of pH 4.6–5.8, whereas cleavage of Z-RR-AMC, an endopeptidase substrate, occurred in a more neutral pH range of pH 5.0–7.4. Cathepsin B cleaves numerous diverse substrates and, thus, it is not known whether other diverse peptide substrates show the same pH profiles as the Abz-GIVR↓AK(Dnp)-OH DPCP substrate and the Z-RR-AMC endopeptidase substrate. Therefore, the pH profiles of a diverse set of peptide substrates were assessed for DPCP and endopeptidase activities of cathepsin B under acidic and neutral pH conditions using the approach of MSP-MS.

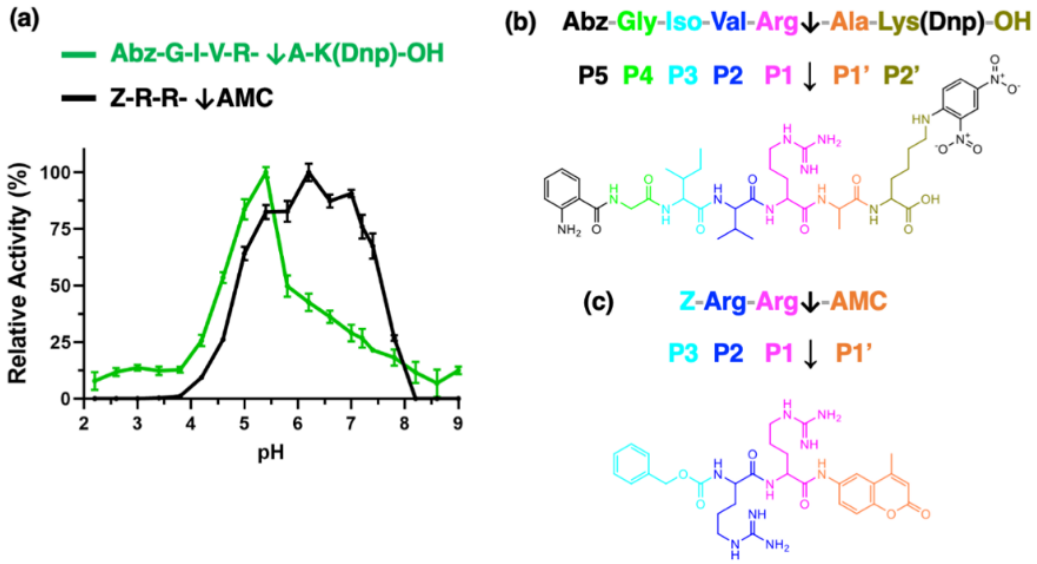

Figure 4.1 Cathepsin B activity monitored with Abz-GIVRAK(Dnp)-OH and Z-RR-AMC substrates under acidic to neutral pH conditions.
(a) Acidic and neutral pH properties of cathepsin B monitored with Abz-GIVRAK(Dnp)-OH and Z-RR-AMC substrates. The pH-dependent cleavage activity of cathepsin B for the substrates Abz-GIVRAK(Dnp)-OH and Z-RR-AMC was assessed at pH 2.2–9.0, with substrate concentrations of 40 µM. Cathepsin B specific activity for each substrate has been normalized to its maximum activity detected across all pH conditions. Data are shown as the mean ± SD (standard deviation) of technical triplicates (n = 3) and this experiment was conducted three times. Cathepsin B activities at the pH values tested were significantly different from that of the enzyme's optimum pH of 5.4 ($p < 0.05$, Student's t-test).
(b) Abz-GIVR↓AK(Dnp)-OH residues adjacent to the P1-P1' cleavage site. The structure of the Abz-GIVR↓AK(Dnp)-OH substrate showing the amino acid residues at the P5 to P2′ positions of the P1↓P1′ cleavage site is illustrated.
(c) Z-RR-↓AMC residues at the P1-P1' cleavage site. The structure Z-RR-↓AMC illustrates the amino acid residues at the P3 to P1′ positions of the P1↓P1′ cleavage site.

4.2.2 Cleavage Profiling of Cathepsin B by MSP-MS Reveals That the Major DPCP and Minor Endopeptidase Activities Both Occur at Acidic and Neutral pH Conditions, with pH-dependent Cleavage Properties

MSP-MS protease cleavage profiling utilized a library of 228 14-mer peptides that can be cleaved by endopeptidases and exopeptidases. Each peptide has a free carboxyl terminus that can be cleaved by carboxypeptidases (42,47) and a free amino terminus that is cleavable by aminopeptidases. (42,48,49) Furthermore, the peptides can be cleaved by endopeptidases at sites that are distal from the N- and C-termini. (41,43) Cathepsin B was incubated with the peptide library at pH 4.6 and pH 7.2, and cleavage products were identified and quantitated by LC–MS/MS tandem mass spectrometry. In parallel, the same peptide library was incubated with human cathepsin K at pH 4.6 and pH 7.2; cathepsin K was chosen for this comparative study because it is (1) a homologous cysteine cathepsin protease of cathepsin B and (2) active across a broad pH range and (3) has been validated as a strict endopeptidase. (45)

In the pH 4.6 MSP-MS assay, cathepsin B cleaved the peptide library at 179 sites with the majority occurring at peptide bond #12 (Figure 4.2a). At pH 7.2, cathepsin B (at the same concentration as pH 4.6) cleaved at 109 sites with the majority also occurring at peptide bond #12 (Figure 4.2a). Cleavage at peptide bond #12 releases dipeptides from the C-terminus and thereby validates the strong DPCP activity of this enzyme. Cleavage at other sites is due to either sequential release of a dipeptide (e.g., positions #10, #8 and #6) or endopeptidase activity (e.g., position #5, #7, #9 and #11). To contrast these properties of cathepsin B with the cleavage site profile of an endopeptidase, we show that cathepsin K displays solely endopeptidase activity by cleavage at positions 3–10 (Figure 4.2b). Significantly, MSP-MS analysis of cathepsin B showed that major DPCP and minor endopeptidase cleavages occur under both acidic pH 4.6 and neutral pH 7.2 conditions of the 14-mer peptide substrates. The MSP-MS assay advantageously distinguishes between endopeptidase and DPCP activities (Figure 4.2).

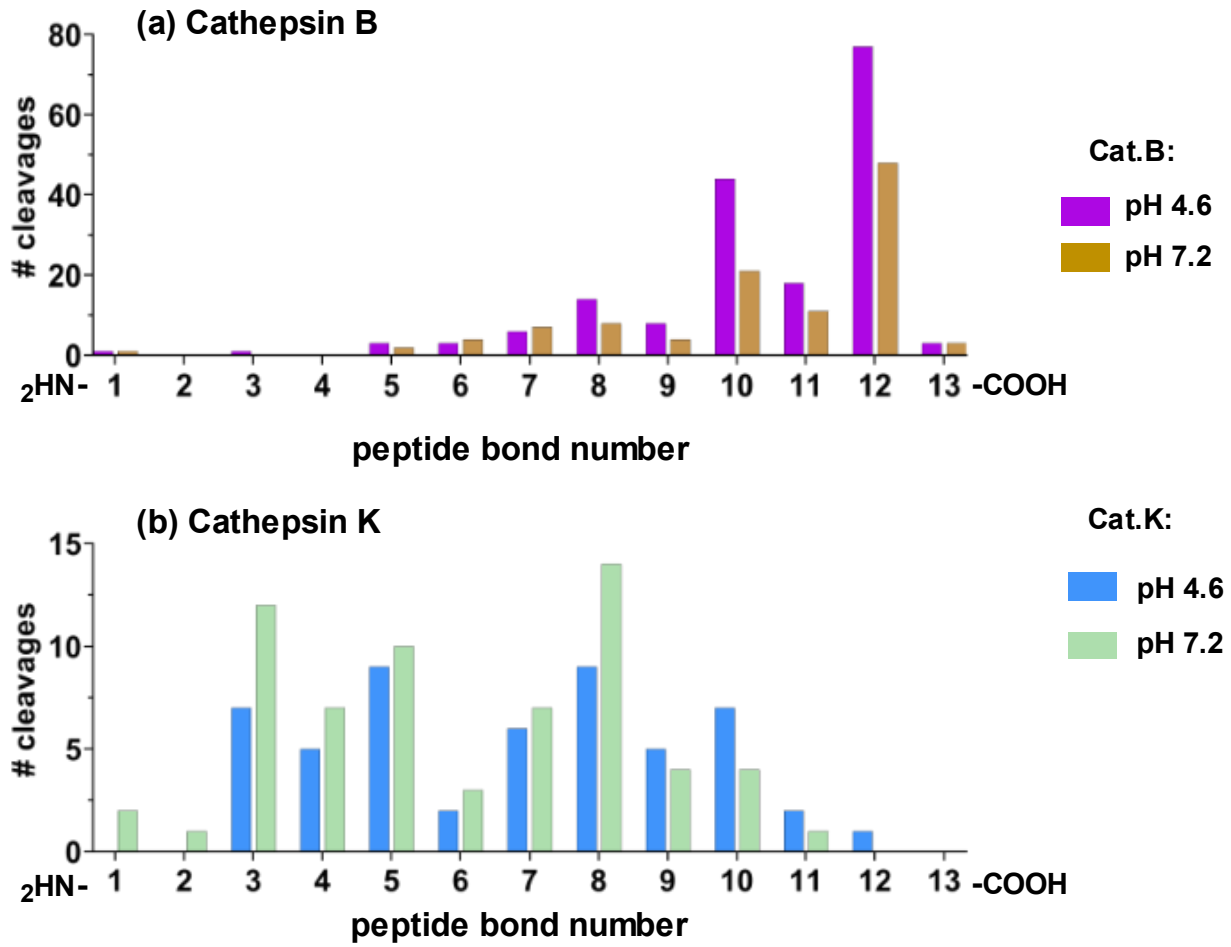

Figure 4.2 Cleavage profiling of cathepsin B DPCP and endopeptidase activities by MSP-MS conducted at acidic pH 4.6 and neutral pH 7.2.
(a) Cathepsin B MSP-MS under acidic and neutral pH conditions demonstrates major DPCP activity. Cathepsin B was subjected to MSP-MS analysis of exopeptidase and endopeptidase cleavage sites at pH 4.6 and pH 7.2 (using four technical replicates). The number of cleavages at peptide bonds #1–13 of the diverse library of 228 peptides after incubation for 15 min was determined as described in the methods. At pH 4.6, 179 cleavages were assessed in the plotted graph for the number of cleavages at each peptide bond location. At pH 7.2, 109 cleavages of the peptide library are graphed similarly. This MSP-MS experiment was conducted two times.
(b) Cathepsin K MSP-MS under acidic and neutral pH conditions demonstrates major endopeptidase activity. Cathepsin K was subjected to MSP-MS analysis at pH 4.6 and pH 7.2. The number of cleavages at each of the peptide bonds #1–13 of the peptide library generated after 15 min incubation was determined as described in the methods using four technical replicates.

Cathepsin B DPCP cleavages at peptide bonds #12 and #10 may occur sequentially, as shown, for example, by conversion of the QAVRPNGnYWHYLn 14-mer peptide substrate to its 12-mer QAVRPNGnYWHY and 10-mer QAVRPNGnYW products in a time-dependent manner

(Figure 4.3). Sequential DPCP cleavages of the peptide library substrates at peptide bond #12 followed by sequential DPCP cleavages would be indicated by products with cleavages occurring at peptide bonds #10 and #8 (Figure 4.2a).

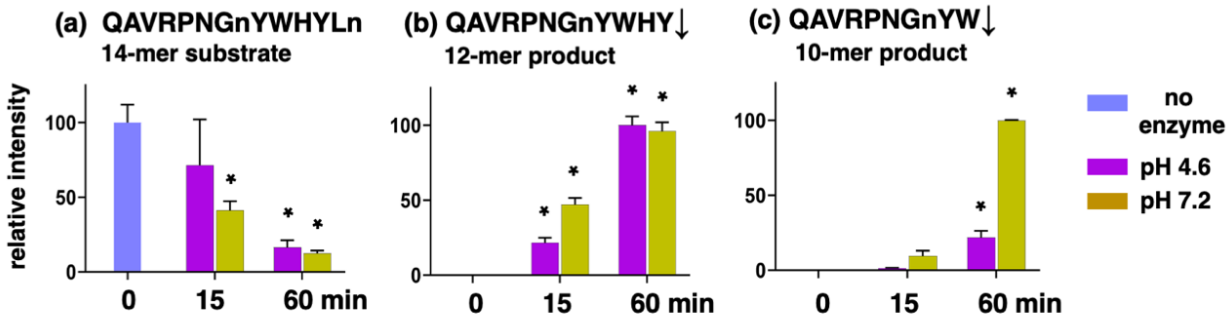

Figure 4.3 Sequential DPCP activity demonstrated by the time-dependent conversion of a 14-mer peptide substrate to 12-mer and 10-mer peptide products. The 14-mer substrate QVRPNGnYWYLn (panel a), 12-mer product QAVRPNGnYWHY (panel b), and the 10-mer product QAVRPNGnYW (panel c) were quantitated at time points of 15- and 60-min incubation times (using four technical replicates). This experiment was conducted two times. Norleucine is represented by "n". Data are shown as the mean ± SEM (standard error of the mean) of four technical replicates (n = 4). Values at 15 min or 60 min that are significantly different from the "0" time at each pH are indicated by asterisks (*) ($p < 0.05$ by Student's t-test).

4.2.3 MSP-MS Analysis of Cleavage Site Preferences by Cathepsin B Leads to Design of pH-Dependent Substrates for DPCP Activity

MPS-MS data characterized the preferred amino acid residues at the P4 to P4′ positions adjacent to the P1↓P1′ cleavage sites at acidic pH 4.6 compared to neutral pH 7.2. z-scores provided quantitative comparison of preferred and nonpreferred residues at the P4 to P4′ positions illustrated by heatmaps (Figure 4.4a). The heatmaps were used to assess differences in preferred residues under the two pH conditions for the goal of designing pH-selective substrates for DPCP activity of cathepsin B. More specifically, we focused on pH differences at the P2 position because several preferred residues at this position differed at pH 4.6 compared to pH 7.2 (Figure 4.4a).

At pH 4.6, Glu at the P2 position was preferred with a z-score of 1.0, but Glu was not preferred at pH 7.2 shown by the z-score of −1.5 (Figure 4.4a). These z-scores had a difference of 2.5 which was the largest among preferred residues at the P2 position for pH 4.6. These data

predicted that incorporation of Glu into the substrate Abz-GIER↓AK(Dnp)-OH may generate an acid pH-selective substrate of DPCP activity.

At pH 7.2, Arg at the P2 position was preferred with a *z*-score of 2.7, but at pH 4.6, Arg at P2 had a smaller *z*-score of 0.6 (Figure 4.4a). The difference in the *z*-score of 2.1 for Arg at pH 7.2 and pH 4.6 suggested that Arg at P2 may provide a neutral pH-selective substrate. This finding suggested that inclusion of Arg in the substrate Abz-GIRR↓AK(Dnp)-OH may provide a neutral pH-selective substrate.

The standard DPCP substrate of Abz-GIVR↓AK(Dnp)-OH contains isoleucine at P3, valine at P2, and arginine at the P1 position. With respect to the P2 and P1 residues, there are strong preferences by cathepsin B for Val at the P2 residue at both pH 4.6 (*z*-score of 3.8) and pH 7.2 (*z*-score of 3.6) and stronger preference for Arg by cathepsin B at the P1 residue at pH 4.6 (*z*-score of 4.2) compared to pH 7.2 (*z*-score of 3.8). However, for the P3 residue, there is a weak preference for isoleucine at pH 7.2 (*z*-score of 0.2). However, norleucine at P3 is highly preferred at pH 4.6 (*z*-score of 2.4) and pH 7.2 (*z*-score of 3.2) (Figure 4.4a), which is also depicted by iceLogo (Figure 4.4b). It was, therefore, predicted that Abz-GnVR↓AK(Dnp)-OH would display DPCP activity of cathepsin B under neutral pH as well as under acidic pH conditions, as shown by data described in the next section.

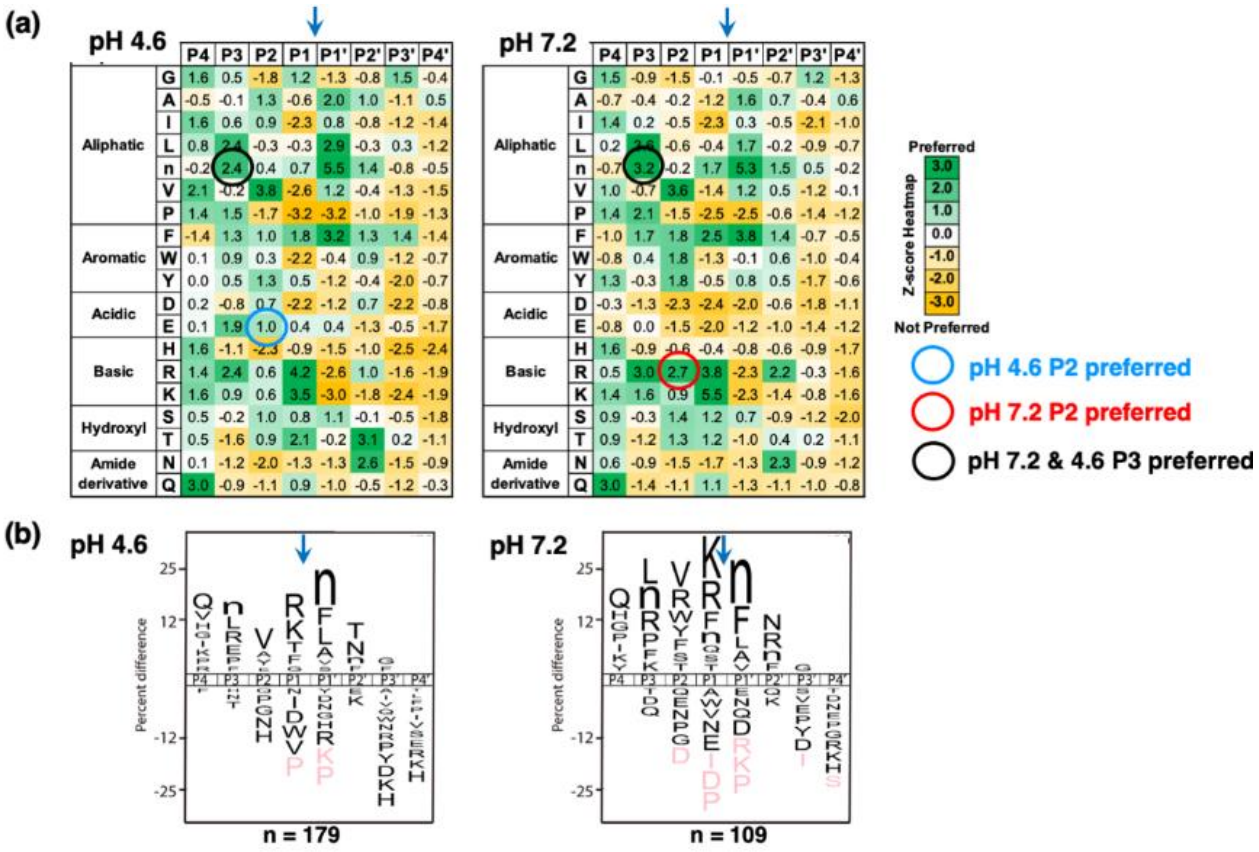

Figure 4.4 Preferred residues of cathepsin B peptide cleavages at pH 4.6 and pH 7.2 assessed by MSP-MS data.

(a) Heatmap of *z*-scores for preferred amino acids adjacent to the cleavage sites at pH 4.6 and pH 7.2. Preferred amino acid residues at P4 to P4′ positions of the cleavage sites are shown for pH 4.6 and pH 7.2 as *z*-score analysis of MSP-MS cleavage profiling data as described in the methods. The experiment was conducted with four technical replicates, and the experiment was repeated two times. The heatmap of *z*-scores shows norleucine as "n."

(b) IceLogo illustration of the primary residues adjacent to cleavage sites. MSP-MS data were analyzed by iceLogo (based on *z*-scores) to show the relative frequency of residues at the P4 to P4′ positions of peptide cleavage sites. Relative to the cleavage site, amino acids shown above the mid-line are preferred amino acids by cathepsin B and those below the mid-line are amino acids not preferred by cathepsin B, based on comparison of experimental cleavage data and all possible products within the MSP-MS peptide library with $p < 0.3$ as described in the methods.

4.2.4 pH-Dependent Substrates for DPCP Activity of Cathepsin B

Novel substrates for DPCP activity of cathepsin B predicted to be selective for acidic pH or neutral pH conditions, based on MSP-MS *z*-score data, were demonstrated (Figure 4.5a). Cleavage of the substrate Abz-GIER↓AK(Dnp)-OH occurred at acidic pH 4.0–5.0 and demonstrated no detectable DPCP activity above pH 6.2. In contrast, cleavage of the substrate

Abz-GIRR↓AK(Dnp)-OH occurred in a higher pH range of pH 5–7 and demonstrated no detectable DPCP activity by cathepsin B under acidic pH conditions below pH 4.6. Furthermore, the substrate Abz-GnVR↓AK(Dnp)-OH detected enhanced DPCP activity of cathepsin B under both acidic and neutral pH conditions compared to the original substrate Abz-GIVR↓AK(Dnp)-OH (Figure 4.5a), especially toward neutral pH. Thus, the cleavage profiling data obtained by MSP-MS (Figure 4.4) provided design and demonstration of pH-dependent DPCP substrates as well as Abz-GnVR↓AK(Dnp)-OH displaying a broad pH range for detecting DPCP activity of cathepsin B (Figure 4.5a). Cleavage of all these DPCP substrates was verified to occur between R↓A to generate AK(Dnp)-OH demonstrated by mass spectrometry (Figures 4.S2–4.S4).

4.2.5 Comparison of Cathepsin B DPCP and Endopeptidase Activities Monitored with Abz-GIVRAK(Dnp)-OH and Abz-GIVRAK(Dnp)-NH_2 Substrates, Respectively

To evaluate the effect of the substrate C-terminal carboxylate on cathepsin B's pH-dependent DPCP activity, the Abz-GIVR↓AK(Dnp)-OH substrate for DPCP activity was modified with a C-terminal amide to generate the endopeptidase substrate Abz-GIVR↓AK(Dnp)-NH_2. Assessment of cathepsin B activity with these two substrates at pH 2–9 showed that the DPCP activity monitored by Abz-GIVR↓AK(Dnp)-OH was greater than the endopeptidase activity monitored by Abz-GIVR↓AK(Dnp)-NH_2, with a 12-fold difference at the optimal pH of 5.4 (Figure 4.5b). The endopeptidase activity was lower than the DPCP activity across the entire pH range of 2–9. Cathepsin B cleavages of Abz-GIVRAK(Dnp)-OH and Abz-GIVRAK(Dnp)-NH_2 substrates between R↓A was confirmed by mass spectrometry of peptide products (Figures 4.S1 and 4.S5).

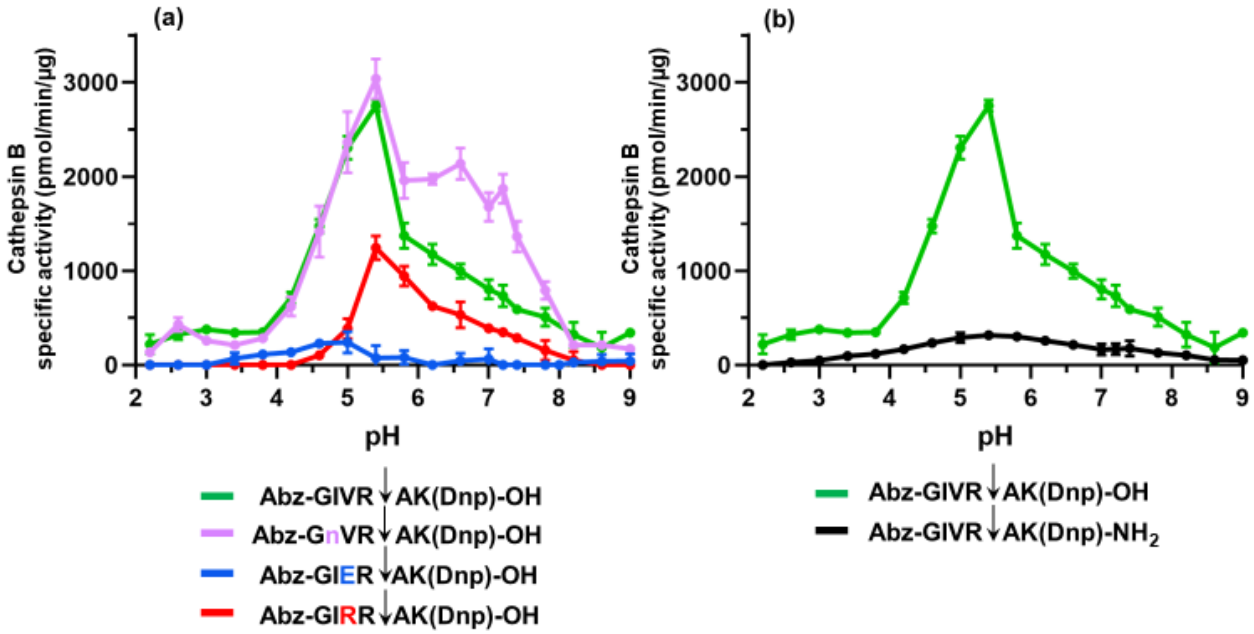

Figure 4.5 Cathepsin B displays DPCP activity under acidic to neutral pH conditions, illustrated by pH-dependent peptide substrates.

(a) Analysis of the pH-dependence of cathepsin B with DPCP substrates containing variant P2 residues, and pH-independence of a substrate with a variant P3 residue.

The Abz-GIVR↓AK(Dnp)-OH typically used in the field (24) to monitor cathepsin B DPCP activity was modified at the P2 position to generate Abz-GIRR↓AK(Dnp)-OH and Abz-GIER↓AK(Dnp)-OH substrates and then was assessed at pH 2–9 for DPCP activity. The substrate Abz-GnVRAK(Dnp)-OH with variant residue at the P3 position was also assessed at pH 2–9 for DPCP activity. Data are shown as the mean ± SD (standard deviation) of three technical replicates (n = 3), and this experiment was repeated three times. Cleavage of these substrates between R↓A occurred to generate AK(Dnp)-OH was confirmed by mass spectrometry (Figures 4.S1–4.S4).

(b) Comparison of cathepsin B activity with the DPCP substrate Abz-GIVRAK(Dnp)-OH and the endopeptidase substrate Abz-GIVRAK(Dnp)-NH_2 at pH 2–9.

Cathepsin B activity was monitored with the Abz-GIVRAK(Dnp)-OH and Abz-GIVRAK(Dnp)-NH_2 substrates for DPCP and endopeptidase activity was assessed at pH 2–9. Data points are the averages from 3 replicate assays. Data are shown as the mean ± SD (standard deviation) of three technical replicates (n = 3), and this experiment was repeated three times. Cleavage at R↓A to generate AK(Dnp)-NH_2 was confirmed by mass spectrometry (Figure 4.S5). For Abz-GIVRAK(Dnp)-OH (panel a and b), Abz-GnVRAK(Dnp)-OH (panel a), and Abz-GIRRAK(Dnp)-OH (panel a) substrates, cathepsin B activity with these substrates was optimal at pH 5.4 and the other pH values were significantly different from that of pH 5.4 ($p < 0.05$, Student's t-test). For the Abz-GIERAK(Dnp)-OH substrate (panel a), optimal activity was observed at pH 5.0 with >50% reduction at pH 3.8 and pH 5.4. For Abz-GIVRAK(Dnp)-NH_2 substrate (panel b), optimal activity was observed at pH 5.4 with a plateau of similar activity at pH 4.6–6.2, and significantly lower activity at pH 4.2 or below and at pH 6.6 or above (with the exception of pH 7.4) ($p < 0.05$, Student's t-test).

Kinetic constants of the DPCP activity monitored with the Abz-GIVRAK(Dnp)-OH substrate and the endopeptidase activity monitored with the Abz-GIVRAK(Dnp)-NH_2 substrate were compared under the pH conditions of pH 4.6 representing lysosomes, (22,23) pH 5.5 representing secretory vesicles, (42) and pH 7.2 representing cytosol, nuclei, and extracellular locations of cathepsin B (20,21) (Table 4.1). The DPCP specific activity was 7 times greater than the endopeptidase activity at pH 5.5. DPCP activity was also substantially greater than the endopeptidase activity at each pH condition.

The kinetic constants k_{cat}/K_M and k_{cat} were higher for DPCP compared to endopeptidase activity at pH 4.6 and pH 5.5, but at pH 7.2. With respect to K_M values, the DPCP activity showed values of 15 and 51 μM at pH 4.6 and pH 5.5, respectively, but DPCP activity showed a higher K_M value of 156 μM at pH 7.2. The endopeptidase activity at pH 4.6, pH 5.5, and pH 7.2 displayed K_M values of 25, 40, and 53 μM, respectively.

These data show the importance of the C-terminal carboxylate of Abz-GIVRAK(Dnp)-OH for DPCP activity of cathepsin B because replacement with the amide group of Abz-GIVRAK(Dnp)-NH_2 resulted in endopeptidase activity that was substantially lower than the DPCP activity.

Table 4.1 Kinetic Evaluation of Cathepsin B Activity with Abz-GIVRAK(Dnp)-OH and Abz-GIVRAK(Dnp)-NH_2 Substrates for DPCP and Endopeptidase Activities, Respectively[a]

substrate	pH	K_m (μM)	k_{cat} (s^{-1})	k_{cat}/K_m (s^{-1} mM^{-1})	specific activity (pmol/min/μg)
Abz-GIVRAK(Dnp)-OH (DPCP)	4.6	15 ± 2.3	4.2 ± 0.2	280	1500
	5.5	51 ± 8.6	7.4 ± 0.7	150	2800
	7.2	156 ± 64	2.3 ± 0.7	15	730
Abz-GIVRAK(Dnp)-NH_2 (endopeptidase)	4.6	25 ± 3.7	0.4 ± 0.02	16	290
	5.5	40 ± 5.6	0.4 ± 0.03	10	390
	7.2	53 ± 14	0.2 ± 0.04	3.8	200

[a]Abz-GIVRAK(Dnp)-OH and Abz-GIVRAK(Dnp)-NH_2 substrates for cathepsin B DPCP activity were characterized for kinetic values at pH 4.6, 5.5, and 7.2 as described in the methods.

4.2.5 pH Profiles of Endopeptidase Activities of Cathepsin B Monitored with Peptide-AMC Substrates.

Endopeptidase activity was evaluated with the peptide-AMC substrates Z-RR-AMC, Z-ER-AMC, and Z-VR-AMC with alterations of the P2 residues at acid to neutral pH conditions (Figure 4.6). Also, these peptide-AMC substrates were compared to the parallel Abz-GIRRAK(Dnp)-OH, Abz-GIERAK(Dnp)-OH, and Abz-GIVRAK(Dnp)-OH substrates (Figure 4.5a). Z-RR-AMC with Arg as the P2 residue displayed cathepsin B activity over the range of pH 5.0 to neutral pH 7.5, similar to that of Abz-GIRRAK(Dnp)-OH. Z-ER-AMC with Glu as the P2 residue displayed acidic pH cathepsin B activity at pH 4.5–5.5, similar to Abz-GIERAK(Dnp)-OH. Z-VR-AMC with Val as the P2 residue displayed optimal activity at pH 5.0, with activity occurring at pH 4–7, which had a broad pH profile more similar to Abz-GIVRAK(Dnp)-NH_2 than Abz-GIVRAK(Dnp)-OH (Figure 4.S6).

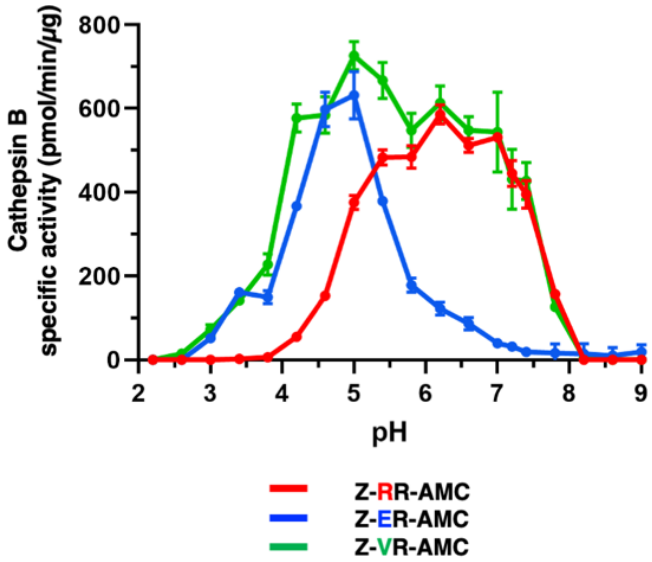

Figure 4.6 pH-dependent cathepsin B endopeptidase substrates illustrated by Z-RR-AMC, Z-ER-AMC, and Z-VR-AMC at pH 2-9. Cathepsin B activity was evaluated at pH 2–9 with peptide-AMC substrates having variant P2 residues consisting of Z-RR-AMC, Z-ER-AMC, and Z-VR-AMC. Data are shown as the mean ± SD (standard deviation) of triplicates (n = 3). For Z-RR-AMC, cathepsin B activity was optimal at pH 6.2 and activity at other pHs were significantly lower ($p < 0.05$, student's t-test). For Z-ER-AMC, cathepsin B activity was optimal at pH 6.2 and activity at other pHs were significantly lower ($p < 0.05$, student's t-test). For Z-VR-AMC, cathepsin B activity was optimal at pH 5.0 and activity was significantly lower at pH 4.6 and below, at pH 5.8 to pH 6.6, and at pH 7.2 and above ($p < 0.05$, student's t-test).

Despite similar pH profiles between the parallel DPCP and endopeptidase substrates, all the endopeptidase substrates had lower specific activity than each of their DPCP substrate counterparts. These differences may be explained by the lack of a C-terminal carboxylate group on these Z-peptide-AMC substrates that would otherwise promote favorable interactions with cathepsin B (Figure 4.5b and 4.S6). These data support the MSP-MS findings that cathepsin B displays prominent DPCP activity over endopeptidase activity under both acidic and neutral pH conditions. However, endopeptidase activity can still be demonstrated across all pH conditions with activity being defined by amino acids in the P2 position. Taken together, these studies provide insight for Z-RR-AMC with Arg as the P2 residue as being poorly cleaved by cathepsin B at acidic pH, but activity is greatly improved by substituting either Glu or Val for Arg at P2.

4.2.6 Cathepsin B's DPCP activity at neutral pH can be readily detected with the novel Abz-GnVRAK(Dnp)-OH substrate, and cathepsin B's endopeptidase activity at acidic pH can be readily detected with the Z-ER-AMC substrate

New data from this study support adjustment of the prior view in the field that cathepsin B's DPCP activity is higher at acidic pH and decreases at neutral pH (Figure 4.1), (26) because here we showed that the DPCP activity monitored with Abz-GnVR↓AK(Dnp)-OH displayed activity across a broad pH range (Figure 4.7). These data illustrate the new concept that DPCP activity of cathepsin B occurs under acidic and neutral pH conditions.

While Z-RR-AMC cleaving activity of cathepsin B has been reported to occur optimally at neutral pH and poorly at acidic pH (Figure 4.1), (28,30−32) this study shows that Z-ER-AMC has the converse properties to monitor high endopeptidase activity of cathepsin B at acidic pH (Figure 4.7). These findings illustrate the new concept that the endopeptidase activity of cathepsin B occurs under acidic to neutral pH conditions.

Significantly, these data demonstrate that the pH-dependent cleavage of peptide substrates by cathepsin B under acidic to neutral pH conditions is based on the sequence of the substrate for both DPCP and endopeptidase activities of the enzyme.

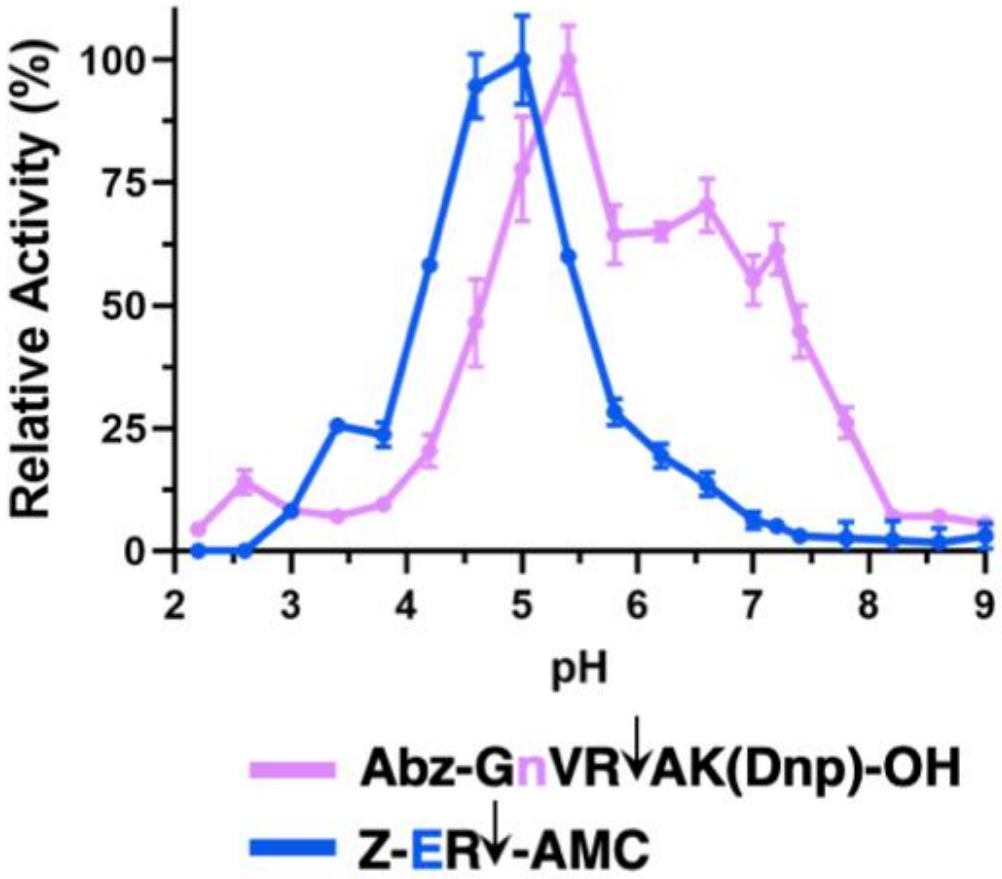

Figure 4.7 Cathepsin B DPCP activity at neutral pH monitored with the Abz-GnVRAK(Dnp)-OH substrate possessing a broad pH range for activity, and endopeptidase activity at acidic pH monitored with the pH-dependent substrate Z-ER-AMC. We developed novel substrates illustrating the concept that the Abz-GnVRAK(Dnp)-OH substrate monitors cathepsin DPCP activity at neutral pH with a broad pH profile for activity, and the acid pH-dependent substrate Z-ER-AMC monitors cathepsin B at acidic pH. Assays were conducted in triplicate; the mean ± SD are shown. These data are shown from Figures 4.5 and 4.6 in a normalized manner by maximum activity observed with each substrate.

4.3 Discussion

Cathepsin B is a unique protease because it possesses dual DPCP and endopeptidase activities. While prior studies showed that this enzyme displays DPCP activity at acidic pH using the Abz-GIVRAK(Dnp)-OH substrate and endopeptidase activity a neutral pH using the Z-RR-

AMC substrate, (31,35−39) our recent finding that cathepsin B cleaves peptide substrates in a pH-dependent manner (18) raises the question of whether the DPCP and endopeptidase activities may occur over a broad pH range represented by pH-dependent substrates rather than under restricted pH conditions. The answer was achieved in this study by global MSP-MS cleavage profiling of cathepsin B using a diverse library of 228 14-mer peptides. Importantly, MSP-MS cleavage results showed that the major DPCP and minor endopeptidase cleavages both occur under acidic and neutral pH conditions for cathepsin B. The proteolytic activities occurred from acidic to neutral pH conditions with pH-dependent substrates as well as substrates with broad pH activity profiles. These findings modify the prior view in the field of DPCP activity at acidic pH and endopeptidase activity at neutral pH (31,35−39) to the new concept that the dual DPCP exopeptidase and endopeptidase activities of cathepsin B both occur under acidic to neutral pH conditions using pH-dependent peptide substrates.

The MSP-MS cleavage profiling data advantageously monitor DPCP and endopeptidase cleavages. DPCP cleavages remove C-terminal dipeptides from the 14-mer peptide substrates. These data demonstrated DPCP as the major type of proteolytic activity of cathepsin B, whereas the endoproteolytic cleavages occurred less frequently. These DPCP and endopeptidase cleavage properties of cathepsin B contrast with cathepsin K as a protease with only endopeptidase activity as shown by the MSP-MS assays. These MSP-MS data demonstrate the prominent DPCP and minor endopeptidase cleavages by cathepsin B.

Cleavage profiling data by MSP-MS provided design and demonstration of substrates with different pH profiles for the DPCP activity of cathepsin B. The novel DPCP substrate Abz-GnVR↓AK(Dnp)-OH utilized the preferred norleucine (n) residue at the P3 position and was found to effectively monitor DPCP activity of cathepsin B over a broad pH range, from acidic to neutral

pH values, with high specific activity. The broad pH profile of the Abz-GnVRAK(Dnp)-OH substrate contrasts with the restricted acidic pH profile of the original Abz-GIVR↓AK(Dnp)-OH substrate. These findings demonstrate Abz-GnVR↓AK(Dnp)-OH as a useful substrate to monitor DPCP of cathepsin B over a broad pH range. Preferences for different P2 residues under acidic and neutral pH conditions led to development of Abz-GIRR↓AK(Dnp)-OH as a substrate that was cleaved by cathepsin B at pH 5–7. Abz-GIER↓AK(Dnp)-OH was designed and displayed activity at pH 4–5 representing acidic conditions. Thus, pH-dependent substrates for DPCP activity exist as illustrated by Abz-GIRR↓AK(Dnp)-OH and Abz-GIER↓AK(Dnp)-OH that display pH profiles in the neutral and acidic pH ranges, respectively. These findings demonstrate that modification of P3 and P2 residues of Abz-GIVR↓AK(Dnp)-OH leads to altered pH profiles of cathepsin B's DPCP activity.

Cleavage profiling data facilitated the design and assessment of Z-peptide-AMC endopeptidase substrates with pH-selective preferences for P2 residues. The known Z-RR-AMC substrate, with Arg as the preferred P2 residue at neutral pH 7.2, is cleaved by cathepsin B activity in a more neutral pH range compared to acid pH conditions, consistent with MSP-MS data indicating Arg as a preferred P2 residue at neutral pH 7.2 compared to acidic pH 4.6. In contrast, the Z-ER-AMC substrate, with Glu as the preferred P2 residue at pH 4.6, preferentially monitored cathepsin B activity in the acid pH condition compared to neutral pH. Furthermore, Val as P2 residue is preferred at both acidic and neutral pH and, thus, the Z-VR-AMC substrate monitors cathepsin B activity over a broad pH range at acidic and neutral pH. These peptide-AMC substrates demonstrate pH-dependent as well as broad pH activity profiles for the endopeptidase activity of cathepsin B.

Comparison of the DPCP activity of cathepsin B monitored with the Abz-GIVRAK(Dnp)-OH substrate with C-terminal carboxylate compared to the endopeptidase substrate Abz-GIVRAK(Dnp)-NH_2 with C-terminal amide further demonstrated the major DPCP activity with greater specific activity than the endopeptidase activity under acidic to neutral pH conditions. Like Abz-GIVRAK(Dnp)-NH_2, the Z-VR-AMC endopeptidase substrate also displayed a broad pH profile for activity of lower specific activity than the DPCP substrate Abz-GIVRAK(Dnp)-OH. These data support the concept that the major DPCP activity and lesser endopeptidase activity of cathepsin B occur over a broad pH range.

Prior evaluation of the structural features of cathepsin B, conducted at pH 5.5, suggested that the unique occluding loop may participate in mediating the DPCP activity under acidic pH conditions, and alteration of the occluding loop at neutral pH may allow the active site to become accessible to endopeptidase substrates. (37,38) The occluding loop corresponding to residues 102–128 contains two His residues (His110 and His111) that directly interact with the C-terminal carboxylic acid group. (50,51) It has been viewed that the occluding loop accommodates DPCP substrates at acidic pH and may acquire a pose at neutral pH that allows accessibility to endopeptidase substrates. However, the ongoing view of the occluding loop should now be modified based on the findings that DPCP and endopeptidase cleavages of cathepsin B occur under both acidic and neutral pH conditions. The current data of this study suggest that the occluding loop allows both DPCP and endopeptidase substrates to bind cathepsin B at the active site for proteolysis. Changes in the configuration of the occluding loop may be predicted to participate in utilization of pH-dependent DPCP and endopeptidase substrates across acidic to neutral pH conditions. Several studies have shown that mutagenesis of the occluding loop domain alters the relative DPCP and endopeptidase activities of cathepsin B. (36,38) It will be of interest in future

studies to compare cathepsin B crystal structures under acidic and neutral pH conditions to gain understanding of the molecular features for substrate docking to achieve dual DPCP and endopeptidase activities of the enzyme.

In summary, global cleavage profiling of cathepsin B with a diverse library of peptide substrates provided evidence that the primary DPCP and modest endopeptidase activities of cathepsin B both occur under acidic and neutral pH conditions. Significantly, MSP-MS data indicated norleucine (n) as a preferred residue at the P3 position at acidic and neutral pH conditions which led to design of the novel substrate Abz-GnVRAK(Dnp)-OH that efficiently monitors DPCP activity of cathepsin B over a broad pH range. The broad pH profile of Abz-GnVRAK(Dnp)-OH contrasts with the more restricted acidic pH profile of the original Abz-GIVRAK(Dnp)-OH substrate. Furthermore, modification of the P2 residue of the original Z-RR-AMC substrate demonstrated that the endopeptidase activity of cathepsin B can be readily detected at acidic pH with the Z-ER-AMC substrate, as well as with the Z-VR-AMC substrate that has a broader pH activity profile. These peptide-AMC substrates demonstrate that pH-dependent and broad pH activity profile substrates of cathepsin B exist for both its DPCP and endopeptidase activities. This study highlights the unique properties of cathepsin B having dual DPCP and endopeptidase activities covering biological pH conditions from lysosomal acidic pH to cytosolic and other neutral pH cellular conditions.

Cathepsin B cleavage of biological substrates in prior studies have illustrated the enzyme's endopeptidase and exopeptidase activities under acidic to neutral pH conditions, consistent with findings of this study for the broad pH ranges of endopeptidase and DPCP cleavages by this protease. Cathepsin B endopeptidase activity cleaves biological substrates that include the propeptide region within pro-cathepsin for autoactivation to mature cathepsin

B, (52) thyroglobulin, (53,54) MARCKS, (25) invariant chain, (55) secretory leucoprotease inhibitor, (56) sphingosine kinase-1, (57) collagen, (58) amyloid precursor protein (APP) as a candidate β-secretase, (59,60) and proneuropeptide substrates (42) under pH conditions ranging from acidic lysosomal pH to mildly acidic secretory vesicles and neutral extracellular pH conditions. In addition, exopeptidase activity has also been detected using thyroglobulin and glucagon as substrates. (53,61) Interestingly, different products were generated from collagen by cathepsin B cleavage that varied with pH conditions. (58) We postulate that these observed differences in cleavage sites of biological substrates are due to pH-dependent amino acid preferences as demonstrated by the MSP-MS cleavage profiling data of this study. It will, therefore, be of interest in future studies to gain knowledge of *in vivo* substrates of cathepsin B at cellular locations of distinct pH conditions in health and disease.

4.4 Methods and Materials

4.4.1 Cathepsin B Fluorogenic Activity Assays

Recombinant human cathepsin B was purchased from R&D Systems (Minneapolis, MN) and was activated to mature cathepsin B by incubation at 37 °C for 30 min in activation buffer (20 mM Na-acetate pH 5.5, 1 mM EDTA, 5 mM DTT, 100 mM NaCl). For the pH profiling, cathepsin B activity was monitored over the pH range of pH 2.2–9.0 in 40 mM citrate phosphate (pH 2.2 to pH 7.4) or 40 mM Tris–HCl (pH 7.8–9.0), 1 mM EDTA, 100 mM NaCl, and 5 mM DTT, with preincubation in each pH buffer for 10 min prior to initiating the assay by adding 40 μM substrate. The substrates Z-VR-AMC, Z-ER-AMC, Abz-GIRRAK(Dnp)-OH, Abz-GnVRAK(Dnp)-OH ("n" represents norleucine), and Abz-GIVRAK(Dnp)-NH_2 were custom synthesized by GenScript (Piscataway, NJ). Z-RR-AMC was purchased from Bachem (#4004789) (Torrance, CA), and Abz-GIVRAK(Dnp)-OH was purchased from Bachem (#4049308) (Torrance, CA). Z-FR-AMC was purchased from Anaspec (#AS-24096) (Fremont, CA). Abz-GIERAK(Dnp)-OH was custom

synthesized by the Wolan Lab at TSRI (La Jolla, CA). Assays were conducted at room temperature in triplicate, and relative fluorescence readings (RFUs) (excitation 320 nm, emission 400 nm for internally quenched substrates and excitation 360 nm, emission 460 nm for peptide-AMC substrates) were recorded over a period of 30 min by a Biotek HTX microplate plate reader. Enzyme velocity (RFU/sec) was calculated using the highest slope recorded for 10 consecutive fluorescent readings within the initial 30 min, and the mean and standard deviation (SD) were determined from the three technical replicates. RFU/s were converted to specific activity pmol/min/μg using AMC standards. For peptide-AMC substrates, specific activity was defined as AMC pmol/min/μg enzyme. To convert RFU/s to pmol/min for the internally quenched substrates Abz-GIVRAK(Dnp)-OH, Abz-GnVRAK(Dnp)-OH, Abz-GIERAK(Dnp)-OH, Abz-GIRRAK(Dnp)-OH, and Abz-GIVRAK(Dnp)-NH_2, these substrates of 40–0.02 μM were serially diluted and incubated with excess cathepsin B (160 ng/μL) to generate a standard curve using the total fluorescence values detected at each concentration.

The kinetic parameters of k_{cat} and K_m for Abz-GIVRAK(Dnp)-OH and Abz-GIVRAK(Dnp)-NH_2 substrates were determined at pH 4.6, pH 5.5, and pH 7.2, using substrate concentrations of 80–0.9 μM with 0.04 ng/μL cathepsin B for Abz-GIVRAK(Dnp)-OH and 0.40 ng/μL of cathepsin B for Abz-GIVRAK(Dnp)-NH_2. RFU values were converted to s^{-1} using standard curves obtained from full digestion of Abz-GIVRAK(Dnp)-OH and Abz-GIVRAK(Dnp)-NH_2 by using excess cathepsin B (160 ng/μL). The k_{cat} and K_m values were obtained from curve fitting the converted RFU data to the equation $v_0 = V_{max}[S]/(K_m + [S])$ where v_0 is the activity at its corresponding substrate concentration $[S]$ and V_{max} is the maximum enzyme velocity at saturated $[S]$ concentration. $V_{max} = k_{cat}[E]_T$, where $[E]_T$ is the total cathepsin B concentration. K_m is the x-axis value (substrate concentration) where $y = V_{max}/2$. SD values

for k_{cat} and K_m were determined from curving fitting the v_0 and [S] data from three technical replicates. All data were plotted, calculated, and analyzed using GraphPad Prism9 software.

4.4.2 Protease Cleavage Profiling by MSP-MS

MSP-MS was performed for cathepsin B, as well as cathepsin K, at pH 4.6 and pH 7.2. In a total volume of 22 μL, cathepsin B (0.1 ng/μL) or cathepsin K (0.07 ng/μL) were incubated with a mixture of 228 14-mer peptides (0.5 μM for each peptide) in assay buffer composed of 50 mM citrate phosphate at pH 4.6 or pH 7.2, 1 mM EDTA, 100 mM NaCl, and 4 mM DTT for 15 and 60 min at 25 °C. 10 μL was removed at 15 and 60 min and was combined with 60 μL of 8 M urea. A control assay used cathepsin B and cathepsin K in each assay buffer mixed with 8 M urea for 60 min at 25 °C for inactivation, prior to addition of the peptide library. Assays were conducted in quadruplicate technical replicates. Samples were acidified by addition of 40 μL of 2% TFA, enriched, and desalted using custom-made C18 spin tips, evaporated to dryness in a vacuum centrifuge, and placed at −70 °C. Samples were resuspended in 40 μL of 0.1% TFA (solvent A), and 4 μL was used for LC–MS/MS using the method described previously. (18)

MS/MS data analysis was performed using PEAKS (v 8.5) software (Bioinformatics Solutions Inc.). MS2 data were searched with the 228-member 14-mer library sequence as the database, and a decoy search was conducted with peptide amino acid sequences in reverse order. A precursor tolerance of 20 ppm and 0.01 Da for MS2 fragments was defined. No protease digestion was specified. Data were filtered to 1% peptide and protein level false discovery rates with the target-decoy strategy. Peptides were quantified with label-free quantification and data normalized by TIC. Outliers from replicates were removed by Dixon's Q testing. Missing and zero values were imputed with random normally distributed numbers in the range of the average of smallest 5% of the data ± SD. The control 0 min values in MSP-MS obtained for cathepsin B at

pH 4.6 and pH 7.2 and cathepsin K at pH 4.6 were also analyzed by PEAKS (for $n = 12$). ANOVA testing was performed for peptide data of control 0, 15, and 60 min incubation conditions; those with $p < 0.05$ were considered for further analysis. Criteria for identification of cleaved peptide products included those with intensity scores of 8-fold or more above the quenched inactive cathepsins, evaluated by $\log_2$(active/inactivated enzyme) ratios for each peptide product with $p < 0.05$ by the two-tailed homoscedastic *t*-test.

Evaluation of the frequencies of the P4 to P4′ amino acids adjacent to the cleavage sites was conducted using the iceLogo software 1.3.8 where the "experimental data set" consisted of the detected cleavage sites and the "reference data set" consisted of all 2965 possible cleavages within the 228 MSP-MS library. Analyses involved *z*-scores calculated by the equation $(X - \mu)/\sigma$, where X is the frequency of the amino acid in the "experimental data set", μ is the frequency of a particular amino acid at a specific position in the "reference data set", and σ is the SD. *z*-scores were utilized to generate iceLogo illustrations of the relative frequencies of amino acid residues at each of the P4 to P4′ positions of the cleaved peptides where heights of the single letter amino acids represent "percent difference", defined as the difference in frequency for an amino acid appearing in the "experimental data set" relative to the "reference data set". Ranked preferred amino acids are shown above the midline, and unpreferred amino acid differences are represented below the midline using $p < 0.30$ cutoff criteria in the iceLogo software.

4.4.3 Cathepsin B Cleavage of DPCP Peptide Substrates Determined by Mass Spectrometry

Cathepsin B (0.148 ng/μL) was incubated in a total volume of 30 μL with 40 μM substrate (Abz-GIVRAK(Dnp)-OH, Abz-GIERAK(Dnp)-OH, and Abz-GIRRAK(Dnp)-OH, Abz-GnVRAK(Dnp)-OH or Abz-GIVRAK(Dnp)-NH_2) in assay buffer consisting of 40 mM citrate phosphate at pH 4.6 or pH 7.2, 1 mM EDTA, 100 mM NaCl, and 5 mM DTT for 15 and 240 min

at 25 °C. After incubation at the indicated time, 10 μL aliquots were removed and combined with 60 μL of 8 M urea. A control inactive cathepsin B assay consisted of cathepsin B in assay buffer combined with 8 M urea for 60 min at 25 °C, prior to addition of substrate. After incubation, collected samples were acidified by addition of 40 μL of 2% TFA, desalted using C18 spin tips, evaporated to dryness in a vacuum centrifuge, and stored at −70 °C. Samples were resuspended in 400 μL of 0.1% TFA (solvent A) and 1 μL was used for LC–MS/MS analysis. Determination of peptide products for cleavage site analysis was performed by searching MS1 data for predicted *m/z* values of peptide cleavage products (Table 4.S1).

4.4.4 Data availability

LC-MS/MS files for the MSP-MS experiments can be accessed at www.massive.ucsd.edu under the dataset identifier numbers MSV000088932.

4.5 Supporting Information

Table 4.S1 DPCP peptide substrates and cleavage products generated by cathepsin B[a]

peptide substrate	DPCP cleavage products	Exact mass	m/z (+1)
Abz-GIVR↓AK(Dnp)-OH	Abz-GIVR	562.32	563.327
	AK(Dnp)-OH	383.14	384.147
Abz-GnVR↓AK(Dnp)-OH	Abz-GnVR	562.32	563.327
	AK(Dnp)-OH	383.14	384.147
Abz-GIER↓AK(Dnp)-OH	Abz-GIER	592.30	593.307
	AK(Dnp)-OH	383.14	384.147
Abz-GIRR↓AK(Dnp)-OH	Abz-GIRR	619.36	620.367
	AK(Dnp)-OH	383.14	384.147
Abz-GIVR↓AK(Dnp)-NH_2	Abz-GIVR	562.32	563.327
	AK(Dnp)- NH_2	382.16	383.167

[a]Masses of predicted DPCP cleavage products generated by cathepsin B from the indicated substrates are shown. Nano-LC-MS/MS tandem mass spectrometry identified the dipeptide product AK(Dnp)-OH and AK(Dnp)-NH_2. The Abz-tetrapeptide products were not well observed in the LC-MS/MS method. However, the dipeptide products demonstrate DPCP type of proteolytic activity of cathepsin B.

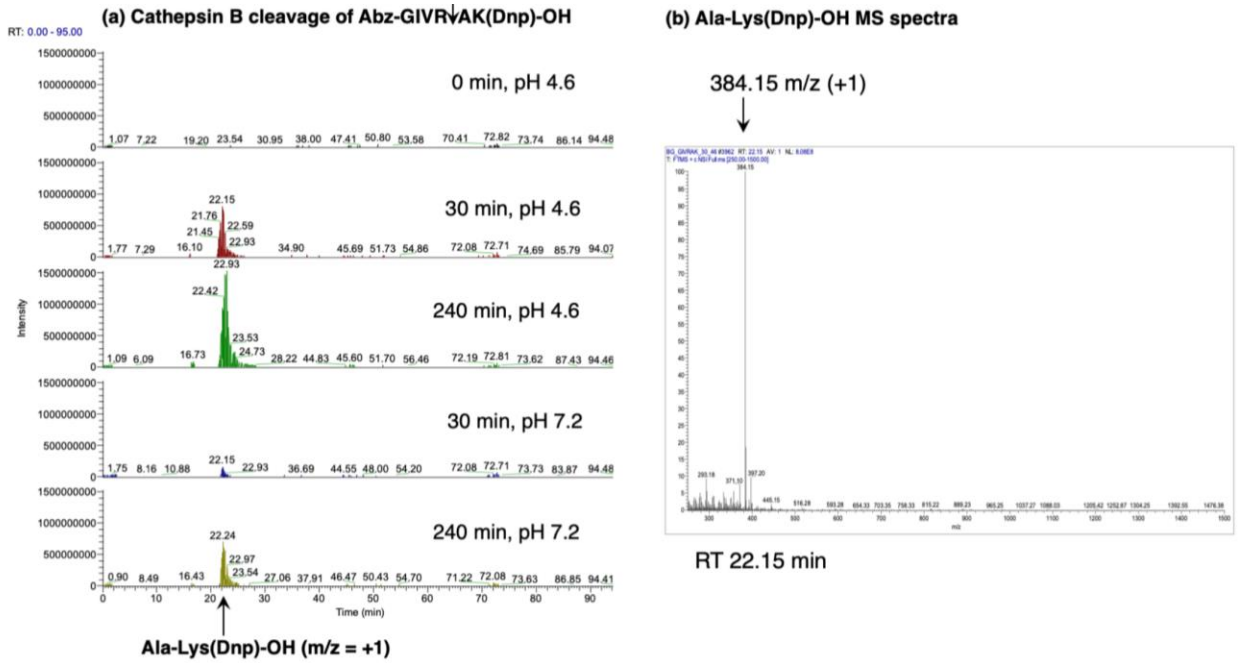

Figure 4.S1 Abz-GIVR↓AK(Dnp)-OH cleavage by cathepsin B generates AK(Dnp)-OH illustrated by mass spectrometry. A time-course of cathepsin B incubation with Abz-GIVRAK(Dnp)-OH for 30 min and 240 min at pH 4.6 and pH 7.2 was analyzed by nano-LC-MS mass spectrometry. The TIC (total ion chromatogram) illustrates the retention time (RT) of the AK(Dnp)-OH cleavage product, panel a. Mass spectra for the DPCP cleavage product of AK(Dnp)-OH m/z (+1) of 384.15 is shown in panel b.

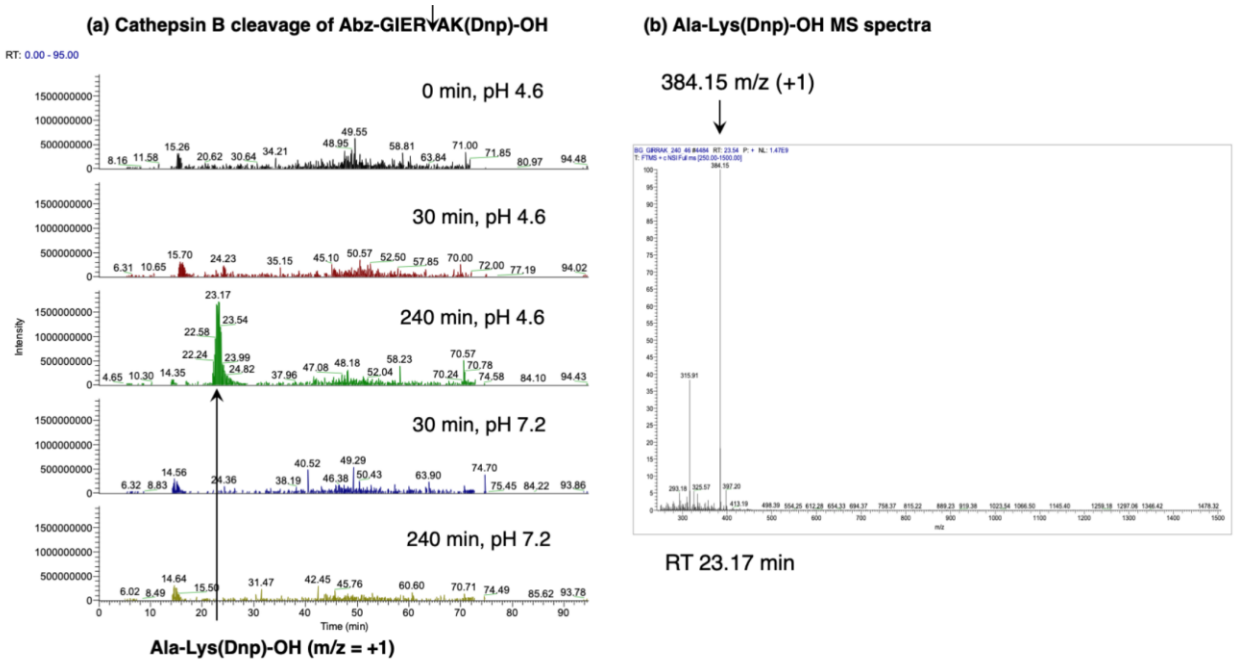

Figure 4.S2 Abz-GIER↓AK(Dnp)-OH cleavage by cathepsin B generates AK(Dnp)-OH illustrated by mass spectrometry. Cathepsin B was incubated with this substrate at pH 4.6 and pH 7.2 at time-course points of 30 min and 240 min, and the TIC illustrates production of the AK(Dnp)-OH cleavage product in panel a. Mass spectra for the DPCP cleavage product of AK(Dnp)-OH m/z (+1) of 384.15 is shown in panel b.

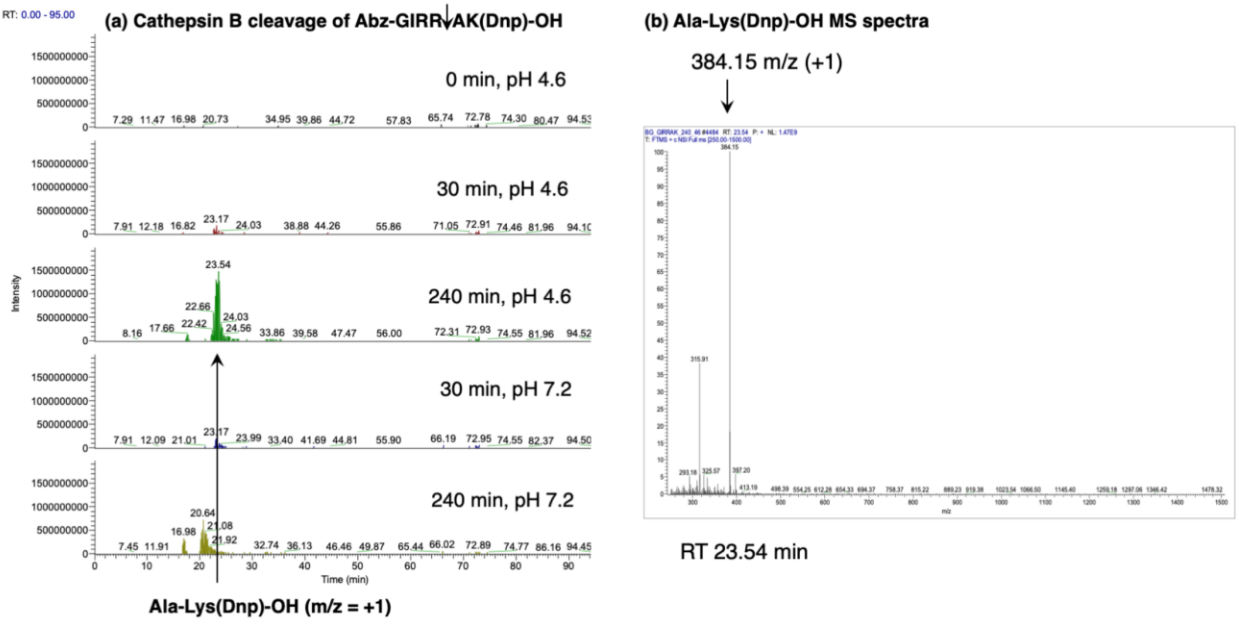

Figure 4.S3 Abz-GIRR↓AK(Dnp)-OH cleavage by cathepsin B generates AK(Dnp)-OH illustrated by mass spectrometry. Cathepsin B was incubated with this substrate at pH 4.6 and pH 7.2 at time-course points of 30 min and 240 min, and the TIC illustrates production of the AK(Dnp)-OH cleavage product in panel a. Mass spectra for the DPCP cleavage product of AK(Dnp)-OH m/z (+1) of 384.15 is shown in panel b.

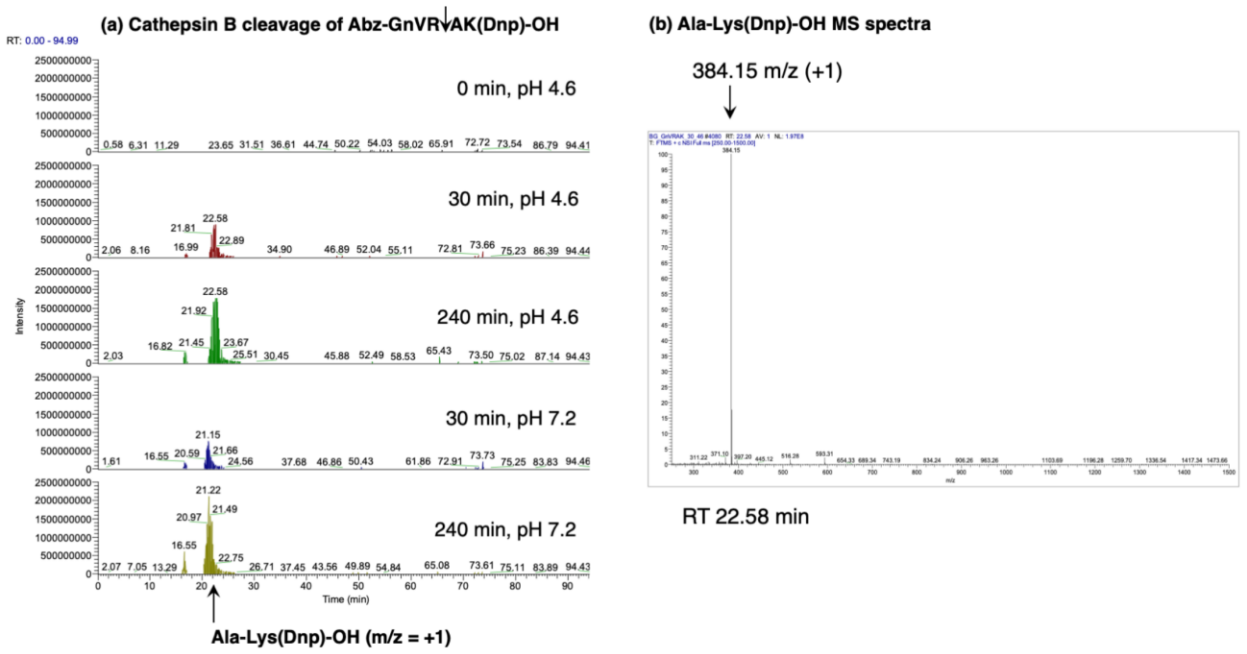

Figure 4.S4 Abz-GnVR↓AK(Dnp)-OH cleavage by cathepsin B generates AK(Dnp)-OH illustrated by mass spectrometry. Cathepsin B was incubated with this substrate at pH 4.6 and pH 7.2 at time-course points of 30 min and 240 min, and the TIC illustrates production of the AK(Dnp)-OH cleavage product in panel a. Mass spectra for the DPCP cleavage product of AK(Dnp)-OH m/z (+1) of 384.15 is shown in panel b.

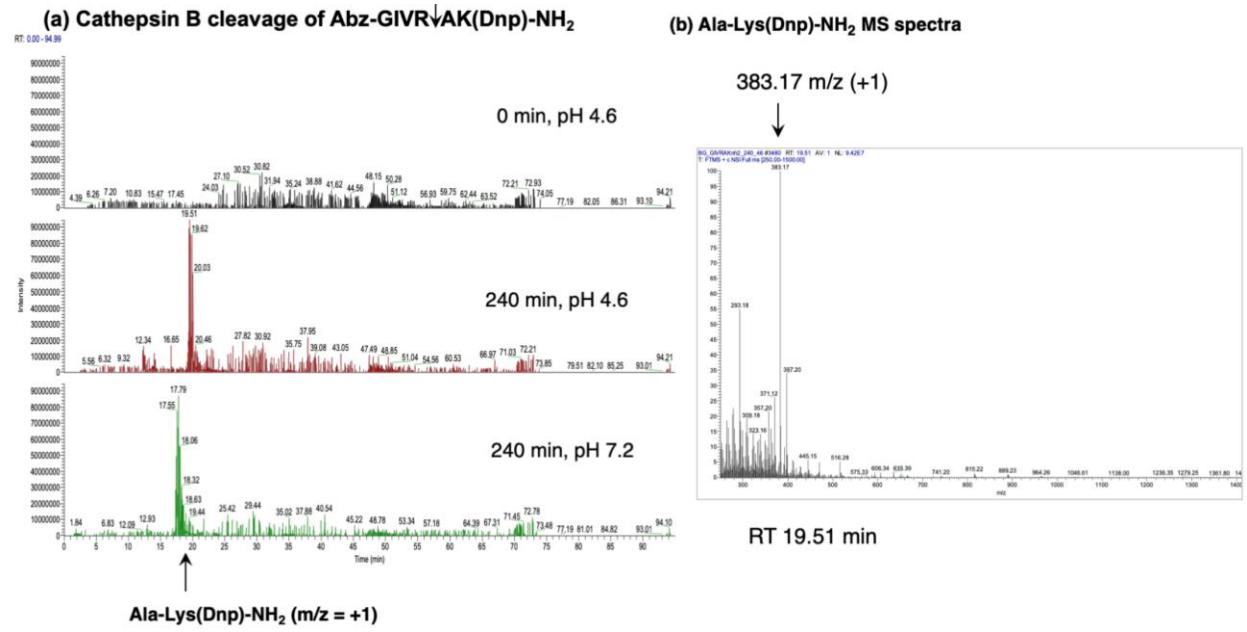

Figure 4.S5 Abz-GIVR↓AK(Dnp)-NH2 cleavage by cathepsin B generates AK(Dnp)-NH2 illustrated by mass spectrometry. Cathepsin B was incubated with this substrate at pH 4.6 and pH 7.2 at time-course points of 30 min and 240 min, and TIC shows the retention time (RT) of the AD(Dnp)-NH_2 cleavage product, panel a. Mass spectra for the DPCP cleavage product of AK(Dnp)-NH_2 m/z (+1) of 383.17 is shown in panel b.

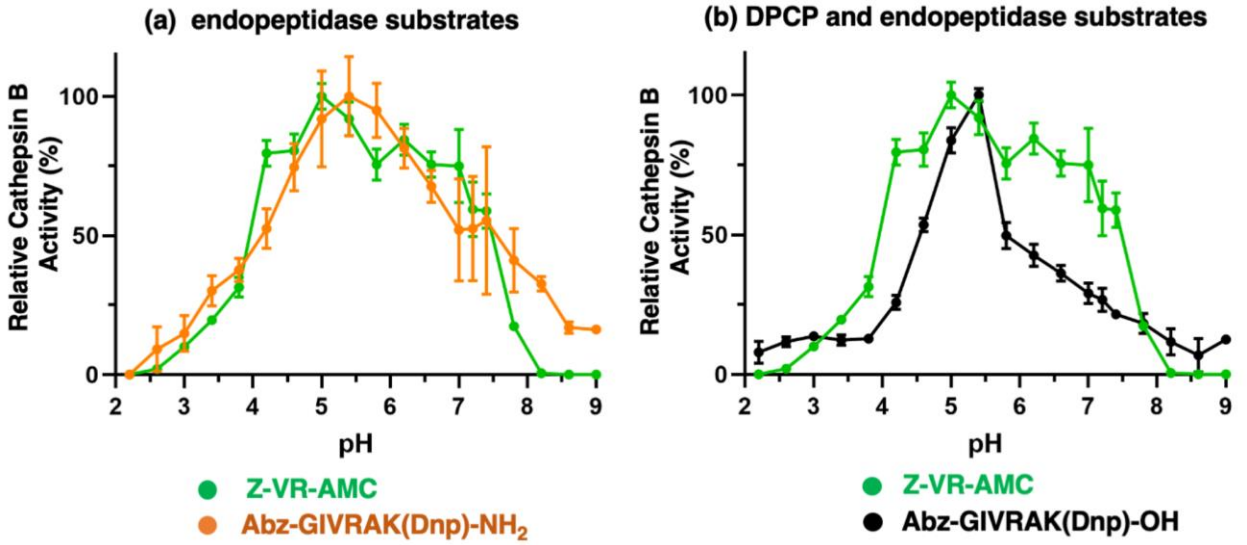

Figure 4.S6 Cathepsin B cleavage of the endopeptidase substrates Abz-GIVRAK(Dnp)-NH_2 and Z-VR-AMC compared to the DPCP substrate Abz-GIVRAK(Dnp)-OH.
(a) pH profile of cathepsin B endopeptidase activity monitored with Abz-GIVRAK(Dnp)-NH_2 and Z-VR-AMC substrates. The full pH profile assessed the pH properties of the DPCP activity of cathepsin B assayed with the Abz-GIVRAK(Dnp)-NH_2 and Z-VR-AMC substrates. Cathepsin B specific activity is illustrated as the percent of its highest activity observed at the pH optimum with each substrate; data are shown as mean + SD (n = 3).
(b) pH profile of cathepsin B's Z-VR-AMC endopeptidase activity compared to the enzyme's DPCP activity monitored with Abz-GIVRAK(Dnp)-OH substrate. The pH profile of the Z-VR-AMC endopeptidase activity of cathepsin B and the Abz-GIVRAK(Dnp)-OH DPCP activity were assessed. Cathepsin B specific activity is indicated as percent of its highest activity observed at the pH optimum of the substrate; data are shown as mean + SD (n = 3).

4.6 References

1. Turk, V.; Stoka, V.; Vasiljeva, O.; Renko, M.; Sun, T.; Turk, B.; Turk, D. Cysteine cathepsins: from structure, function and regulation to new frontiers. Biochim. Biophys. Acta 2012, 1824, 68−88.

2. De Duve, C.; Wattiaux, R. Functions of lysosomes. Annu. Rev. Physiol. 1966, 28, 435−492.

3. Lawrence, R. E.; Zoncu, R. The lysosome as a cellular centre for signalling, metabolism and quality control. Nat. Cell Biol. 2019, 21, 133−142.

4. Inpanathan, S.; Botelho, R. J. The Lysosome Signaling Platform: Adapting With the Times. Front. Cell Dev. Biol. 2019, 7, 113.

5. Savini, M.; Zhao, Q.; Wang, M. C. Lysosomes: Signaling Hubs for Metabolic Sensing and Longevity. Trends Cell Biol. 2019, 29, 876− 887.

6. Amritraj, A.; Peake, K.; Kodam, A.; Salio, C.; Merighi, A.; Vance, J. E.; Kar, S. Increased activity and altered subcellular distribution of lysosomal enzymes determine neuronal vulnerability in Niemann-Pick type C1-deficient mice. Am. J. Pathol. 2009, 175, 2540−2556.

7. Dong, H.; Qin, Y.; Huang, Y.; Ji, D.; Wu, F. Poloxamer 188 rescues MPTP-induced lysosomal membrane integrity impairment in cellular and mouse models of Parkinson's disease. Neurochem. Int. 2019, 126, 178−186.

8. Hook, V.; Yoon, M.; Mosier, C.; Ito, G.; Podvin, S.; Head, B. P.; Rissman, R.; O'Donoghue, A. J.; Hook, G. Cathepsin B in neurodegeneration of Alzheimer's disease, traumatic brain injury, and related brain disorders. Biochim. Biophys. Acta Proteins Proteom. 2020, 1868, No. 140428.

9. Buck, M. R.; Karustis, D. G.; Day, N. A.; Honn, K. V.; Sloane, B. F. Degradation of extracellular-matrix proteins by human cathepsin B from normal and tumour tissues. Biochem. J. 1992, 282, 273−278.

10. Cavallo-Medved, D.; Dosescu, J.; Linebaugh, B. E.; Sameni, M.; Rudy, D.; Sloane, B. F. Mutant K-ras regulates cathepsin B localization on the surface of human colorectal carcinoma cells. Neoplasia 2003, 5, 507−519.

11. Jane, D. T.; Morvay, L.; Dasilva, L.; Cavallo-Medved, D.; Sloane, B. F.; Dufresne, M. J. Cathepsin B localizes to plasma membrane caveolae of differentiating myoblasts and is secreted in an active form at physiological pH. Biol. Chem. 2006, 387, 223−234.

12. Giusti, I.; D'Ascenzo, S.; Millimaggi, D.; Taraboletti, G.; Carta, G.; Franceschini, N.; Pavan, A.; Dolo, V. Cathepsin B mediates the pH-dependent proinvasive activity of tumor-shed microvesicles. Neoplasia 2008, 10, 481−488.

13. Fujisawa, A.; Kambe, N.; Saito, M.; Nishikomori, R.; Tanizaki, H.; Kanazawa, N.; Adachi, S.; Heike, T.; Sagara, J.; Suda, T.; Nakahata, T.; Miyachi, Y. Disease-associated mutations in CIAS1 induce cathepsin B-dependent rapid cell death of human THP-1 monocytic cells. Blood 2007, 109, 2903−2911.

14. Rajamäki, K.; Lappalainen, J.; Oörni, K.; Välimäki, E.; Matikainen, S.; Kovanen, P. T.; Eklund, K. K. Cholesterol crystals activate the NLRP3 inflammasome in human macrophages: a novel link between cholesterol metabolism and inflammation. PLoS One 2010, 5, No. e11765.

15. Gonzalez, E. A.; Martins, G. R.; Tavares, A. M. V.; Viegas, M.; Poletto, E.; Giugliani, R.; Matte, U.; Baldo, G. Cathepsin B inhibition attenuates cardiovascular pathology in mucopolysaccharidosis I mice. Life Sci. 2018, 196, 102−109.

16. Morchang, A.; Panaampon, J.; Suttitheptumrong, A.; Yasamut, U.; Noisakran, S.; Yenchitsomanus, P. T.; Limjindaporn, T. Role of cathepsin B in dengue virus-mediated apoptosis. Biochem. Biophys. Res. Commun. 2013, 438, 20−25.

17. Hu, Y.; Shi, Y.; Chen, H.; Tao, M.; Zhou, X.; Li, J.; Ma, X.; Wang, Y.; Liu, N. Blockade of Autophagy Prevents the Progression of Hyperuricemic Nephropathy Through Inhibiting NLRP3 Inflammasome-Mediated Pyroptosis. Front. Immunol. 2022, 13, No. 858494.

18. Yoon, M. C.; Solania, A.; Jiang, Z.; Christy, M. P.; Podvin, S.; Mosier, C.; Lietz, C. B.; Ito, G.; Gerwick, W. H.; Wolan, D. W.; Hook, G.; O'Donoghue, A. J.; Hook, V. Selective Neutral pH Inhibitor of Cathepsin B Designed Based on Cleavage Preferences at Cytosolic and Lysosomal pH Conditions. ACS Chem. Biol. 2021, 16, 1628− 1643.

19. Song, Y.; Wright, J. G.; Anderson, M. J.; Rajendran, S.; Ren, Z.; Hua, D. H.; Koehne, J. E.; Meyyappan, M.; Li, J. Quantitative Detection of Cathepsin B Activity in Neutral pH Buffers Using Gold Microelectrode Arrays: Toward Direct Multiplex Analyses of Extracellular Proteases in Human Serum. ACS Sensors 2021, 6, 3621−3631.

20. Bright, G. R.; Fisher, G. W.; Rogowska, J.; Taylor, D. L. Fluorescence ratio imaging microscopy: temporal and spatial measurements of cytoplasmic pH. J. Cell Biol. 1987, 104, 1019−1033.

21. Madshus, I. H. Regulation of intracellular pH in eukaryotic cells. Biochem. J. 1988, 250, 1−8.

22. Mindell, J. A. Lysosomal acidification mechanisms. Annu. Rev. Physiol. 2012, 74, 69−86.

23. Ohkuma, S.; Poole, B. Fluorescence probe measurement of the intralysosomal pH in living cells and the perturbation of pH by various agents. Proc. Natl. Acad. Sci. U. S. A. 1978, 75, 3327−3331.

24. Maciewicz, R. A.; Etherington, D. J. A comparison of four cathepsins (B, L, N and S) with collagenolytic activity from rabbit spleen. Biochem. J. 1988, 256, 433−440.

25. Spizz, G.; Blackshear, P. J. Identification and characterization of cathepsin B as the cellular MARCKS cleaving enzyme. J. Biol. Chem. 1997, 272, 23833−23842.

26. Cotrin, S. S.; Puzer, L.; de Souza Judice, W. A.; Juliano, L.; Carmona, A. K.; Juliano, M. A. Positional-scanning combinatorial libraries of fluorescence resonance energy transfer peptides to define substrate specificity of carboxydipeptidases: Assays with human cathepsin B. Anal. Biochem. 2004, 335, 244−252.

27. Sosic,ˇ I.; Mirkovic,́ B.; Arenz, K.; Š tefane, B.; Kos, J.; Gobec, S. Development of new cathepsin B inhibitors: Combining bioisosteric replacements and structure-based design to explore the structureactivity relationships of nitroxoline derivatives. J. Med. Chem. 2013, 56, 521−533.

28. Sosic,ˇ I.; Mitrovic,́ A.; Ć uric,́ H.; Knez, D.; Brodnik Ž ugelj, H.; Š tefane, B.; Kos, J.; Gobec, S. Cathepsin B inhibitors: Further exploration of the nitroxoline core. Bioorg. Med. Chem. Lett. 2018, 28, 1239−1247.

29. Zeng, G. Z.; Pan, X. L.; Tan, N. H.; Xiong, J.; Zhang, Y. M. Natural biflavones as novel inhibitors of cathepsin B and K. Eur. J. Med. Chem. 2006, 41, 1247−1252.

30. Mitrovic,́ A.; Mirkovic,́ B.; Sosic,ˇ I.; Gobec, S.; Kos, J. Inhibition of endopeptidase and exopeptidase activity of cathepsin B impairs extracellular matrix degradation and tumour invasion. Biol. Chem. 2016, 397, 164−174.

31. Almeida, P. C.; Nantes, I. L.; Chagas, J. R.; Rizzi, C. C.; FaljoniAlario, A.; Carmona, E.; Juliano, L.; Nader, H. B.; Tersariol, I. L. Cathepsin B activity regulation. Heparin-like glycosaminogylcans protect human cathepsin B from alkaline pH-induced inactivation. J. Biol. Chem. 2001, 276, 944−951.

32. Linebaugh, B. E.; Sameni, M.; Day, N. A.; Sloane, B. F.; Keppler, D. Exocytosis of active cathepsin B enzyme activity at pH 7.0, inhibition and molecular mass. Eur. J. Biochem. 1999, 264, 100− 109.

33. Corvo, I.; Ferraro, F.; Merlino, A.; Zuberbühler, K.; O'Donoghue, A. J.; Pastro, L.; Pi-Denis, N.; Basika, T.; Roche, L.; McKerrow, J. H.; Craik, C. S.; Caffrey, C. R.; Tort, J. F. Substrate Specificity of Cysteine Proteases Beyond the S2 Pocket: Mutagenesis and Molecular Dynamics Investigation of Fasciola hepatica Cathepsins L. Front. Mol. Biosci. 2018, 5, 40.

34. Strauss, A. W.; Zimmerman, M.; Boime, I.; Ashe, B.; Mumford, R. A.; Alberts, A. W. Characterization of an endopeptidase involved in pre-protein processing. Proc. Natl. Acad. Sci. U. S. A. 1979, 76, 4225− 4229.

35. Vidak, E.; Javorsek,ˇ U.; Vizovisek,ˇ M.; Turk, B. Cysteine Cathepsins and their Extracellular Roles: Shaping the Microenvironment. Cell 2019, 8, 264.

36. Illy, C.; Quraishi, O.; Wang, J.; Purisima, E.; Vernet, T.; Mort, J. S. Role of the occluding loop in cathepsin B activity. J. Biol. Chem. 1997, 272, 1197−1202.

37. Cavallo-Medved, D.; Moin, K.; Sloane, B. Cathepsin B: Basis Sequence: Mouse. AFCS Nat. Mol. Pages 2011, 2011, A000508.

38. Nägler, D. K.; Storer, A. C.; Portaro, F. C.; Carmona, E.; Juliano, L.; Ménard, R. Major increase in endopeptidase activity of human cathepsin B upon removal of occluding loop contacts. Biochemistry 1997, 36, 12608−12615.

39. Krupa, J. C.; Hasnain, S.; Nägler, D. K.; Ménard, R.; Mort, J. S. S2' substrate specificity and the role of His110 and His111 in the exopeptidase activity of human cathepsin B. Biochem. J. 2002, 361, 613−619.

40. Polgár, L.; Csoma, C. Dissociation of ionizing groups in the binding cleft inversely controls the endo- and exopeptidase activities of cathepsin B. J. Biol. Chem. 1987, 262, 14448−14453.

41. O'Donoghue, A. J.; Eroy-Reveles, A. A.; Knudsen, G. M.; Ingram, J.; Zhou, M.; Statnekov, J. B.; Greninger, A. L.; Hostetter, D. R.; Qu, G.; Maltby, D. A.; Anderson, M. O.; Derisi, J. L.; McKerrow, J. H.; Burlingame, A. L.; Craik, C. S. Global identification of peptidase specificity by multiplex substrate profiling. Nat. Methods 2012, 9, 1095−1100.

42. Jiang, Z.; Lietz, C. B.; Podvin, S.; Yoon, M. C.; Toneff, T.; Hook, V.; O'Donoghue, A. J. Differential Neuropeptidomes of Dense Core Secretory Vesicles (DCSV) Produced at Intravesicular and Extracellular pH Conditions by Proteolytic Processing. ACS Chem. Neurosci. 2021, 12, 2385−2398.

43. Lapek, J. D., Jr.; Jiang, Z.; Wozniak, J. M.; Arutyunova, E.; Wang, S. C.; Lemieux, M. J.; Gonzalez, D. J.; O'Donoghue, A. J. Quantitative Multiplex Substrate Profiling of Peptidases by Mass Spectrometry. Mol. Cell. Proteomics 2019, 18, 968−981.

44. Choe, Y.; Leonetti, F.; Greenbaum, D. C.; Lecaille, F.; Bogyo, M.; Brömme, D.; Ellman, J. A.; Craik, C. S. Substrate profiling of cysteine proteases using a combinatorial peptide library identifies functionally unique specificities. J. Biol. Chem. 2006, 281, 12824−12832.

45. Konttinen, Y. T.; Mandelin, J.; Li, T. F.; Salo, J.; Lassus, J.; Liljeström, M.; Hukkanen, M.; Takagi, M.; Virtanen, I.; Santavirta, S. Acidic cysteine endoproteinase cathepsin K in the degeneration of the superficial articular hyaline cartilage in osteoarthritis. Arthritis Rheum. 2002, 46, 953−960.

46. Bromme, D. Cathepsin K. In Handbook of proteolytic enzymes; Barrett, A., Rawlings, R., Woessner, J.; Elsevier: San Diego, 2012; Vol. 2, pp. 108−1817.

47. Beekman, C.; Jiang, Z.; Suzuki, B. M.; Palmer, J. M.; Lindner, D. L.; O'Donoghue, A. J.; Knudsen, G. M.; Bennett, R. J. Characterization of PdCP1, a serine carboxypeptidase from Pseudogymnoascus destructans, the causal agent of White-nose Syndrome. Biol. Chem. 2018, 399, 1375−1388.

48. Xu, J. H.; Jiang, Z.; Solania, A.; Chatterjee, S.; Suzuki, B.; Lietz, C. B.; Hook, V. Y. H.; O'Donoghue, A. J.; Wolan, D. W. A Commensal Dipeptidyl Aminopeptidase with Specificity for NTerminal Glycine Degrades Human-Produced Antimicrobial Peptides in Vitro. ACS Chem. Biol. 2018, 13, 2513−2521.

49. Ivry, S. L.; Knudsen, G. M.; Caiazza, F.; Sharib, J. M.; Jaradeh, K.; Ravalin, M.; O'Donoghue, A. J.; Kirkwood, K. S.; Craik, C. S. The lysosomal aminopeptidase tripeptidyl peptidase 1 displays increased activity in malignant pancreatic cysts. Biol. Chem. 2019, 400, 1629− 1638.

50. Yamamoto, A.; Tomoo, K.; Hara, T.; Murata, M.; Kitamura, K.; Ishida, T. Substrate specificity of bovine cathepsin B and its inhibition by CA074, based on crystal structure refinement of the complex. J. Biochem. 2000, 127, 635−643.

51. Yamamoto, A.; Hara, T.; Tomoo, K.; Ishida, T.; Fujii, T.; Hata, Y.; Murata, M.; Kitamura, K. Binding mode of CA074, a specific irreversible inhibitor, to bovine cathepsin B as determined by X-ray crystal analysis of the complex. J. Biochem. 1997, 121, 974−977.

52. Rozman, J.; Stojan, J.; Kuhelj, R.; Turk, V.; Turk, B. Autocatalytic processing of recombinant human procathepsin B is a bimolecular process. FEBS Lett. 1999, 459, 358−362.

53. Dunn, A. D.; Crutchfield, H. E.; Dunn, J. T. Thyroglobulin processing by thyroidal proteases. Major sites of cleavage by cathepsins B, D, and L. J. Biol. Chem. 1991, 266, 20198−20204.

54. Jordans, S.; Jenko-Kokalj, S.; Kühl, N. M.; Tedelind, S.; Sendt, W.; Brömme, D.; Turk, D.; Brix, K. Monitoring compartment-specific substrate cleavage by cathepsins B, K, L, and S at physiological pH and redox conditions. BMC Biochem. 2009, 10, 23.

55. Reyes, V. E.; Lu, S.; Humphreys, R. E. Cathepsin B cleavage of Ii from class II MHC alpha- and beta-chains. J. Immunol. 1991, 146, 3877−3880.

56. Taggart, C. C.; Lowe, G. J.; Greene, C. M.; Mulgrew, A. T.; O'Neill, S. J.; Levine, R. L.; McElvaney, N. G. Cathepsin B, L, and S cleave and inactivate secretory leucoprotease inhibitor. J. Biol. Chem. 2001, 276, 33345−33352.

57. Taha, T. A.; El-Alwani, M.; Hannun, Y. A.; Obeid, L. M. Sphingosine kinase-1 is cleaved by cathepsin B in vitro: identification of the initial cleavage sites for the protease. FEBS Lett. 2006, 580, 6047−6054.

58. Maciewicz, R. A.; Wotton, S. F.; Etherington, D. J.; Duance, V. C. Susceptibility of the cartilage collagens types II, IX and XI to degradation by the cysteine proteinases, cathepsins B and L. FEBS Lett. 1990, 269, 189−193.

59. Hook, V.; Toneff, T.; Bogyo, M.; Greenbaum, D.; Medzihradszky, K. F.; Neveu, J.; Lane, W.; Hook, G.; Reisine, T. Inhibition of cathepsin B reduces beta-amyloid production in regulated secretory vesicles of neuronal chromaffin cells: evidence for cathepsin B as a candidate beta-secretase of Alzheimer's disease. Biol. Chem. 2005, 386, 931−940.

60. Kindy, M. S.; Yu, J.; Zhu, H.; El-Amouri, S. S.; Hook, V.; Hook, G. R. Deletion of the cathepsin B gene improves memory deficits in a transgenic ALZHeimer's disease mouse model expressing AβPP containing the wild-type β-secretase site sequence. J. Alzheimers Dis. 2012, 29, 827−840.

61. Kirschke, H.; Langner, J.; Riemann, S.; Wiederanders, B.; Ansorge, S.; Bohley, P. Lysosomal cysteine proteinases. In Ciba Foundation Symposium; Excerpta Medica/Elsevier: North Holland, Amsterdam, 1979; Vol. 75, pp. 15−35.

4.7 Copyright Permission

CHAPTER 5 – Differential Neuropeptidomes of Dense Core Secretory Vesicles (DCSV) Produced at Intravesicular and Extracellular pH Conditions by Proteolytic Processing

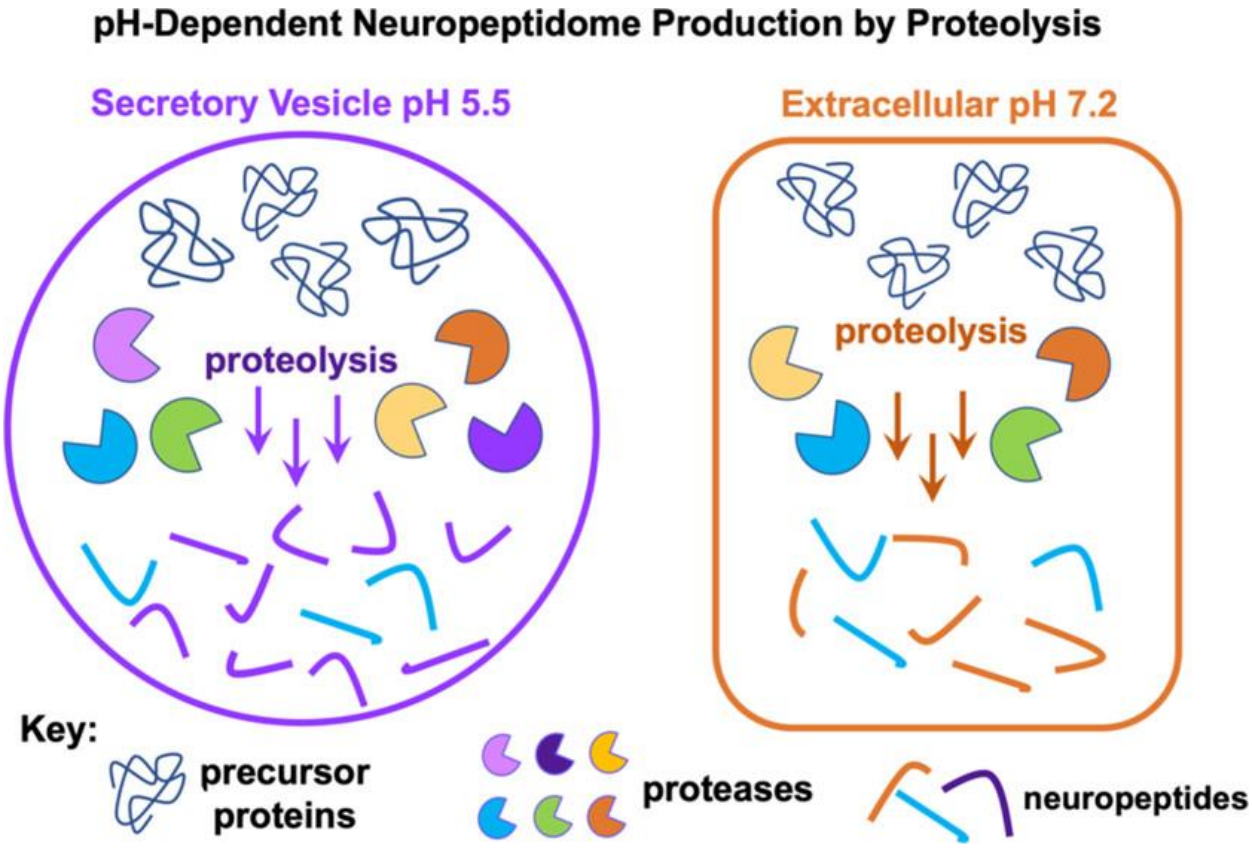

Chapter 5 Graphical Abstract. Neuropeptides mediate cell–cell signaling in the nervous and endocrine systems. The neuropeptidome is the spectrum of peptides generated from precursors by proteolysis within dense core secretory vesicles (DCSV). DCSV neuropeptides and contents are released to the extracellular environment where further processing for neuropeptide formation may occur. To assess the DCSV proteolytic capacity for production of neuropeptidomes at intravesicular pH 5.5 and extracellular pH 7.2, neuropeptidomics, proteomics, and protease assays were conducted using chromaffin granules (CG) purified from adrenal medulla. CG are an established model of DCSV. The CG neuropeptidome consisted of 1239 unique peptides derived from 15 proneuropeptides that were colocalized with 64 proteases. Distinct CG neuropeptidomes were generated at the internal DCSV pH of 5.5 compared to the extracellular pH of 7.2. Class-specific protease inhibitors differentially regulated neuropeptidome production involving aspartic, cysteine, serine, and metallo proteases. The substrate cleavage properties of CG proteases were assessed by multiplex substrate profiling by mass spectrometry (MSP-MS) that uses a synthetic peptide library containing diverse cleavage sites for endopeptidases and exopeptidases. Parallel inhibitor-sensitive cleavages for neuropeptidome production and peptide library proteolysis led to elucidation of six CG proteases involved in neuropeptidome production, represented by cathepsins A, B, C, D, and L and carboxypeptidase E (CPE). The MSP-MS profiles of these six enzymes represented the majority of CG proteolytic cleavages utilized for neuropeptidome production. These findings provide new insight into the DCSV proteolytic system for production of distinct neuropeptidomes at the internal CG pH of 5.5 and at the extracellular pH of 7.2.

5.1 Introduction

The neuropeptidome within dense core secretory vesicles (DCSV) of adrenal medulla, known as chromaffin granules (CG), provides a diverse and rich source of neuropeptides that mediate cell–cell communication in response to stress. (1−5) The CG provide a model of the DCSV organelle system for the production and release of neuropeptides in the nervous and endocrine systems. (6−9) Neuropeptides comprise hundreds to thousands of unique peptides whose primary amino acid sequences designate their biological activities as peptide neurotransmitters and peptide hormones. (10−16) Within CG, diverse neuropeptides are generated from their proneuropeptide precursors by proteolytic processing. (12,15,17) The coordinate biosynthesis of CG neuropeptides by proteases is necessary for adrenal medullary chromaffin cells to respond to stress through release of cell signaling neuropeptides.

Neuropeptidomes are generated by the endogenous DCSV protease system to convert proneuropeptides into peptide products. (12,15,16) Several types of proteases are utilized in DCSV for neuropeptide formation consisting of endopeptidases cleaving within protein sequences of precursors at dibasic as well as at nonbasic residues, followed by exopeptidases that further process peptide intermediates into mature neuropeptides. Elucidation of the complex repertoire of endopeptidase and exopeptidase activities involved in proneuropeptide processing can facilitate the challenge of understanding systems of proteases for neuropeptidome production, as prior studies have largely studied individual proteases in processing proneuropeptides. (12,15,17) The complexity of neuropeptide production by the simultaneous actions of multiple DCSV proteases has not been revealed. Therefore, this study investigated proteolytic mechanisms of neuropeptidome production in DCSV modeled by CG using proteomics, peptidomics, and peptide cleavage profiling by mass spectrometry.

The CG neuropeptidome is produced within the intravesicular acidic pH of 5.5 for DCSV (18−20) for subsequent release to the extracellular environment of pH 7.2. (21−23) It is likely that neuropeptidome production may also occur at the extracellular neutral pH condition, since soluble CG proteases would be cosecreted with precursors of the neuropeptidome. Therefore, the goal of this study was to gain understanding of neuropeptidome production at intravesicular pH 5.5 compared to extracellular pH 7.2 by aspartic, cysteine, serine, and metallo protease classes of highly purified CG. Results of these peptidomics and proteomics studies demonstrated that distinct CG neuropeptidomes are generated at pH 5.5 compared to pH 7.2 for numerous peptides including the chromogranins, secretogranins, enkephalins, neuropeptide Y, VIP, and galanin. Furthermore, CG proteolytic cleavages for neuropeptidome production used differential profiles of protease classes at each of the pH 5.5 and 7.2 conditions.

To define the CG proteolytic properties utilized for neuropeptidome production, CG cleavage profiles were characterized by multiplex substrate profiling by mass spectrometry (MSP-MS) which uses a peptide substrate library consisting of 228 synthetic tetradecapeptides designed to contain diverse protease cleavage sites. (24−26) The MSP-MS assays distinguish endopeptidases and exopeptidases in complex biological samples such as plasma, pancreatic cyst fluid, and gastric juice. (25−28) Inhibitor-sensitive cleavage profiles of CG proteolysis in MSP-MS assays matched endogenous cleavages utilized for neuropeptidome production and led to identification of CG proteases that matched the cleavage properties of cathepsins A, B, C, D, and L, combined with carboxypeptidase E (CPE). Recombinant purified forms of these six proteases in MSP-MS assays confirmed their CG-like cleavage properties. Support for the roles of these six proteases in the production of selected neuropeptides has also been provided in the literature. These results demonstrate the differential CG proteolytic activities utilized for neuropeptidome

production at the intravesicular pH of 5.5 compared to the extracellular pH of 7.2. These findings indicate that neuropeptidome diversity is generated by proteolysis within DCSV as well as by extracellular postrelease processing mechanisms.

5.2 Results

5.2.1 Strategy for Analyzing Neuropeptidome Production by the DCSV Chromaffin Granule Proteolytic System

To gain understanding of the protease systems involved in production of the CG neuropeptidome, highly purified CG from bovine adrenal medulla were analyzed by proteomics, peptidomics, and proteolytic cleavage profiling assays by MSP-MS (Figure 5.1). The endogenous CG proneuropeptide precursors and proteases were identified by proteomics (Figure 5.1A). Neuropeptidomics defined the spectrum of peptides derived from processing of proneuropeptides utilizing the proteolytic capacity of the CG at the intravesicular pH of 5.5 and at the extracellular pH of 7.2 (Figure 5.1B). Furthermore, class-specific protease inhibitors indicated roles for aspartic, cysteine, serine, and metallo protease classes in neuropeptidome production. Deconvolution of the complexity of the CG protease activities was achieved by MSP-MS analysis of the peptide substrate cleavage profiles in the presence of class-specific protease inhibitors (Figure 5.1C), combined with evaluation of recombinant proteases that represented the major CG cleavage profiles involved in neuropeptidome production at pH 5.5 and pH 7.2.

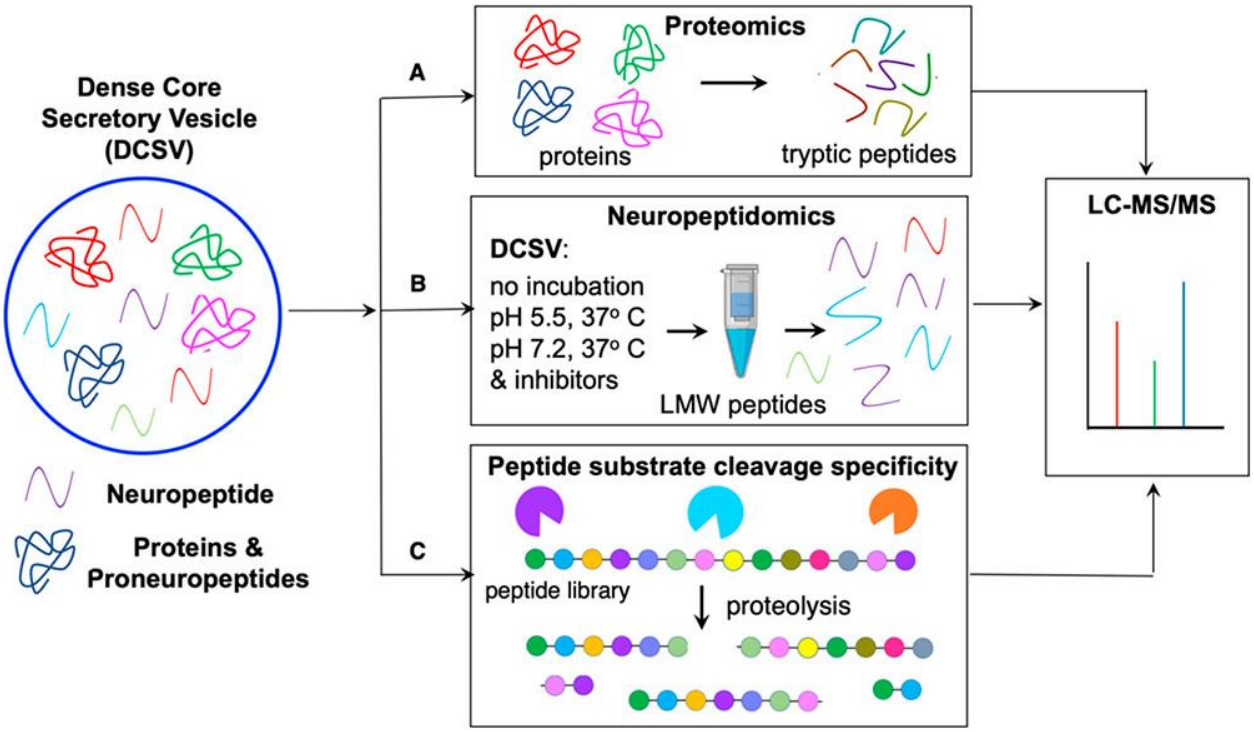

Figure 5.1 Neuropeptidome production by proteolysis by chromaffin granules (CG) at pH 5.5 within DCSV and at pH 7.2 of the extracellular environment. The production of the spectrum of diverse neuropeptides, the neuropeptidome, was analyzed in DCSV modeled by purified CG from adrenal medulla (bovine) by (A) proteomics identification of proneuropeptides and proteases, (B) neuropeptidomics analyses of neuropeptides generated during incubation of CG at the intravesicular pH 5.5 within DCSV and at the extracellular pH of 7.2, conducted in the absence and presence of class-specific protease inhibitors, and (C) proteolytic cleavage specificity analyses of CG proteases using a synthetic peptide substrate library by multiplex substrate profiling by mass spectrometry (MSP-MS) assays.

5.2.2 Proteomics Reveals Proteases, Proneuropeptides, and Neuropeptides in Chromaffin Granules of Adrenal Medulla

We isolated chromaffin granules from bovine adrenal medulla and identified 2110 unique proteins by proteomics (supplementary data 1). Proteins were grouped into 24 categories by gene ontology analysis. As expected, numerous proteins were categorized as proteases, enzyme modulators, and neuropeptide signaling molecules since the nervous system utilizes DCSV for regulated secretion of neuropeptides whose maturation requires proteolytic processing (Figure 5.S1A). Structural proteins as well as proteins that regulate calcium binding, vesicular trafficking, and exocytosis are also abundant components of CG and provide components of the internal

vesicle environment for biosynthesis, storage, and stimulated secretion of neurotransmitters and hormones.

With respect to proteolytic enzymes, the CG contain 64 distinct proteases, corresponding to 2.53% of the total protein abundance in the CG proteome as calculated by normalized spectral abundance factor (NSAF) (29) (Figure 5.S1B). These enzymes were further categorized by catalytic protease classes, revealing the presence of 2 aspartic proteases, 17 cysteine proteases, 21 serine proteases, and 24 metallo proteases (Figure 5.2A). Metallo proteases were the most abundant class of proteases by NSAF, followed by serine, cysteine, and aspartic proteases (Figure 5.2B). With respect to neuropeptide precursors, 15 well-characterized proneuropeptides were identified including chromogranins A and B (CHGA and CHGB), proenkephalin (PENK), neuropeptide Y (NPY), and secretogranins (Figure 5.2C). The proneuropeptides accounted for 8.79% of the total protein abundance in the chromaffin granules (Figure 5.S1B), with hromogranin A being the most abundant proneuropeptide (Figure 5.2C).

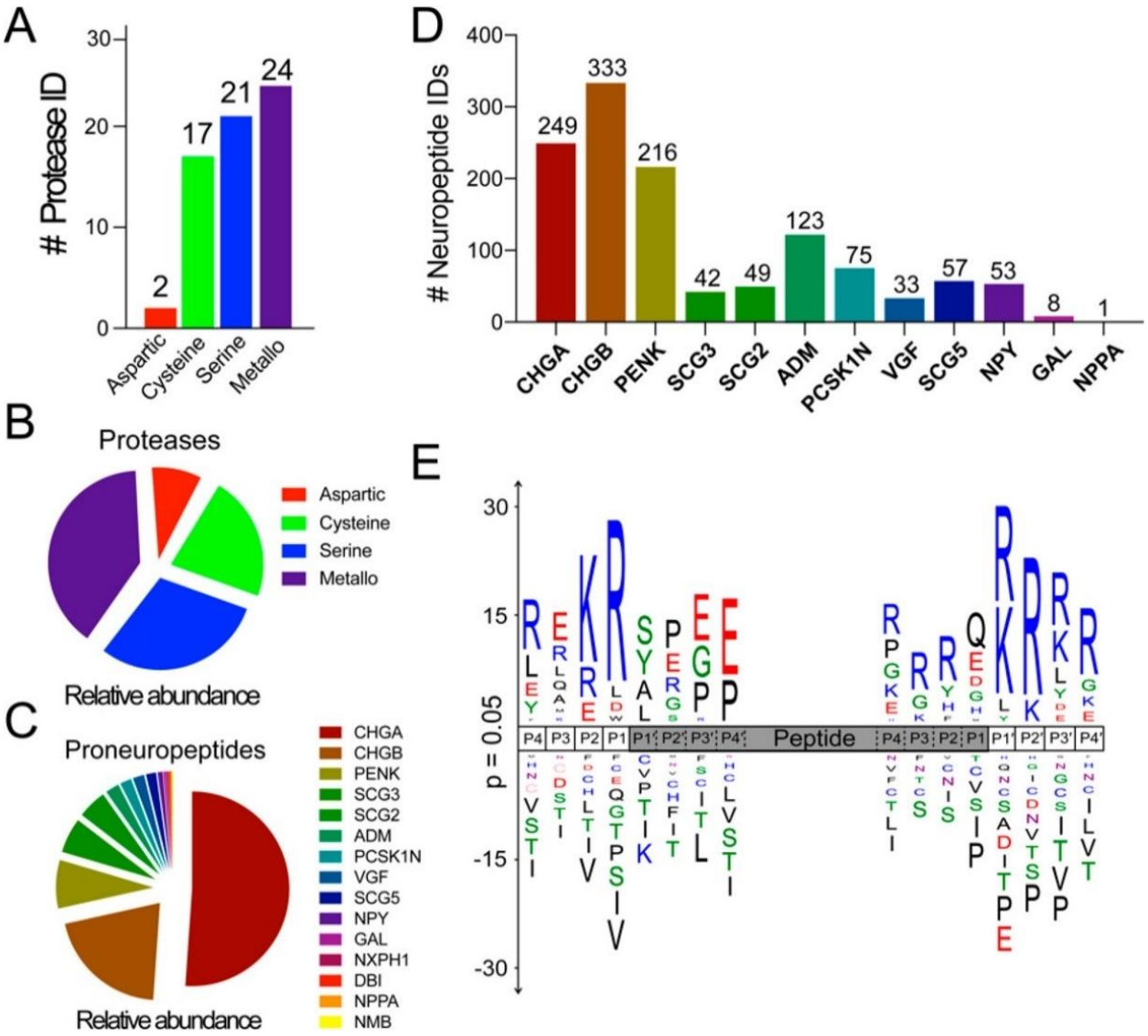

Figure 5.2 Diverse proteases and neuropeptides identified in CG by proteomics and peptidomics. (A) CG proteases numbering 64 were identified by proteomics and were categorized into four different classes. (B) Proteases were quantified by NSAF (normalized spectral abundance factor), and abundances are illustrated by the pie chart. (C) Proneuropeptides were identified by proteomics and quantified by NSAF. (D) Peptidomics identified 1981 unique peptides of which 1239 were derived from 12 different proneuropeptides. (E) Sequence logo shows the frequency of amino acids at the amino and carboxyl termini of proneuropeptide-derived peptides (shown by the gray area) identified by peptidomics.

5.2.3 Peptidomics Reveals Processing of Proneuropeptides in Chromaffin Granules

To gain an understanding of the diverse proneuropeptide-derived peptides generated by CG proteases, we performed peptidomics analysis to define the neuropeptidome in CG. The endogenous peptides in CG were separated from high molecular weight (MW) proteins using a 10

kDa molecular weight cutoff filter and analyzed by LC–MS/MS tandem mass spectrometry. A total of 1981 unique peptides that ranged from 5 to 50 amino acids in length were identified and quantified (supplementary data 1). Of these, 1239 peptides were identified to be the proteolytic fragments of 15 proneuropeptides and most of them were derived from the chromogranins, PENK, adrenomedullin (ADM), and secretogranin precursors (Figure 5.2D).

The proteolytic cleavage specificity profile of peptides derived from proneuropeptides was generated by aligning the proteolytic fragments to the precursor and calculating the frequency of amino acids occurring at both N- and C-termini of the peptides (Figure 5.2E). On the basis of protease nomenclature by Schechter-Berger, (30) cleavage occurs between the P1 and P1′ amino acids and the adjacent residues are defined as P2, P3, P4, etc. on the amino terminal side of the cleaved bond and as P2′, P3′, P4′, etc. on the carboxy terminal side of cleavages. We evaluated the frequency of amino acids at the P4 to P4′ positions at the N-terminal and C-terminal ends of the peptide products and discovered that the cleavage specificities were remarkably different.

At the N-terminus, Pro and Glu were frequently found at the P2′ to P4′ positions. Arg was abundant at the P1 to P4 positions, and Lys was most frequently found at the P2 position. Ser, Tyr, Ala, and Leu were common at P1′. At the C-terminal sides of the peptides, Arg was often the most abundant residue at P4 to P4′ with the notable exception being P1 where Gln, Glu, and Asp were frequently found. Lys was also abundant at P1′ to P4′. The frequent occurrence of basic amino acids near the peptide termini is consistent with previous studies showing that removal of dibasic amino acids is involved in proneuropeptide processing. (12,15) As there is little similarity in amino acid preferences at each terminus (e.g., P1 on the N-terminus compared to P1 on the C-terminus), it is clear that a distinct set of proteases may cleave at each of the N- and C-terminal ends of the peptides.

5.2.4 Neuropeptidome Production at Intravesicular and Extracellular pH Conditions

To evaluate the dynamic protease-mediated biosynthesis of the CG neuropeptidome components, the purified CG were incubated for 30 and 90 min at 37 °C at pH 5.5 to mimic the acidic environment within the DCSV. In parallel, the same CG samples were incubated at pH 7.2 to mimic the neutral extracellular pH environment.

At pH 5.5, 646 neuropeptides increased in abundance, of which 486 were not previously found in the nonincubated peptidomics data set. In addition, 225 neuropeptides found in the initial peptidome were significantly reduced following incubation at pH 5.5 (Figure 5.3A). During incubation at pH 7.2, 281 neuropeptides increased in abundance while 139 were decreased. These data indicated that proteolytic activities at pH 5.5 were more prevalent than at pH 7.2.

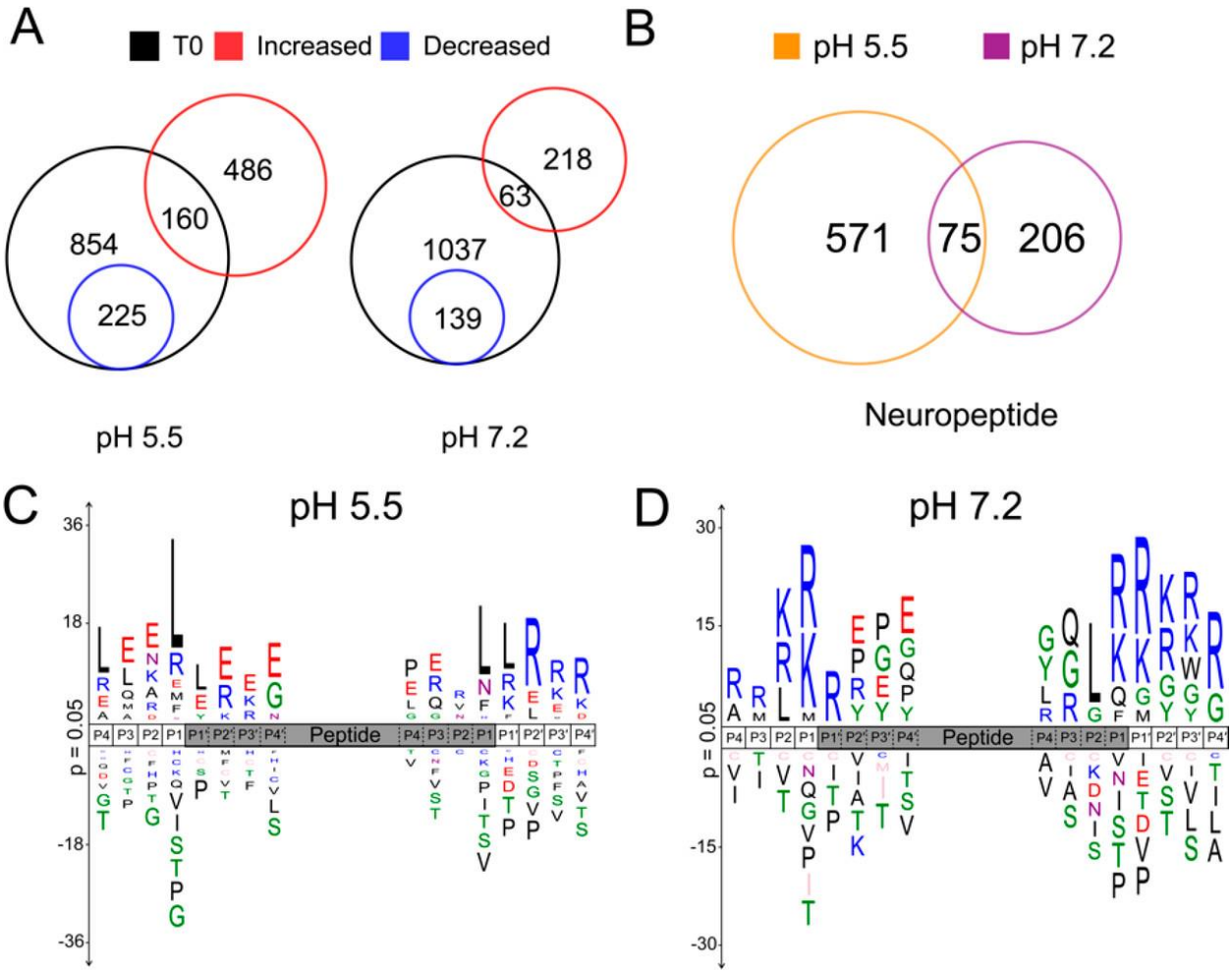

Figure 5.3 Neuropeptidome production after incubation of CG at pH 5.5 and pH 7.2 analyzed by peptidomics. (A) The Venn diagram shows the number of neuropeptides that were significantly increased or decreased after 90 min of incubation (37 °C) at pH 5.5 and pH 7.2, compared to nonincubated control CG samples. (B) Comparison of neuropeptide abundances that were significantly increased ($p < 0.05$) after 90 min of incubation at pH 5.5 and pH 7.2 conditions. (C, D) Sequence logos show the relative frequencies of amino acid residues flanking the amino and carboxy termini of the peptide cleavage products derived from proneuropeptides after 90 min incubation at pH 5.5 (C) and at pH 7.2 (D).

Many of the peptides identified before incubation remained unchanged following incubation at either pH condition. One possible reason for this observation is that these peptide sequences were resistant to further proteolytic processing or reached an equilibrium whereby the proteolytic formation of the peptide was equal to the rate of degradation. Another possible reason is that the change of reaction environment from intact CG to *in vitro* buffer conditions altered the concentrations and localization of enzymes, substrates, inhibitors, and cofactors, thereby

preventing proteolysis of certain neuropeptide precursors. Either scenario maintains a stable concentration for these peptides.

Next, we compared the cleavage products formed at the two different pH conditions. Of the 852 peptides that increased in abundance at the pH 5.5 and pH 7.2 conditions, only 75 were common to both data sets (Figure 5.3B). The high number of distinct peptides generated at each pH condition suggested differences in proteolytic activities at the acidic pH 5.5 intravesicular condition compared to the neutral pH 7.2 extracellular environment. The relative frequencies of amino acid residues flanking the termini of the peptide cleavage products at the two pH conditions were also distinct (Figure 5.3C,D). At pH 5.5, Leu, Glu, Arg, or Lys was frequently found at numerous positions (P4 to P4′), with Leu being the most frequent amino acid at P1. At pH 7.2, Arg and Lys were the most frequently identified amino acids at P1 and were also found to be the most common residues at other sites (P4 to P4′). Interestingly, Leu is frequently present at P2 in the pH 7.2 assays while frequently present at P1 in the pH 5.5 assays. Taken together, these data suggest that the proteases that are active at the acidic intravesicular conditions display different substrate specificity preferences compared to the proteases that function at the neutral extracellular environment.

5.2.5 Differential Neuropeptidome Production Regulated by Class-Specific Protease Inhibitors at Intravesicular and Extracellular pH Conditions

Proneuropeptide processing can utilize multiple proteases within DCSV. To deconvolute the complexity of proteolytic activities, neuropeptidome production was analyzed in the presence of four class-specific protease inhibitors consisting of pepstatin, E64c, AEBSF, and EDTA that inhibit aspartic, cysteine, serine, and metallo proteases, respectively. By comparing inhibitor treated samples to control (DMSO vehicle), we were able to determine the classes of proteases that were responsible for the formation of neuropeptides. The quantification of CG peptidomics results

was analyzed to show the abundance of each newly formed peptide before and after incubation at 37 °C, at pH 5.5 and pH 7.2 conditions, and in the presence or absence of the protease inhibitors (Figure 5.4). The neuropeptides shown in Figure 5.4 can be classified into six groups based on hierarchical clustering, with each group demonstrating differential neuropeptidomes regulated by the four inhibitors.

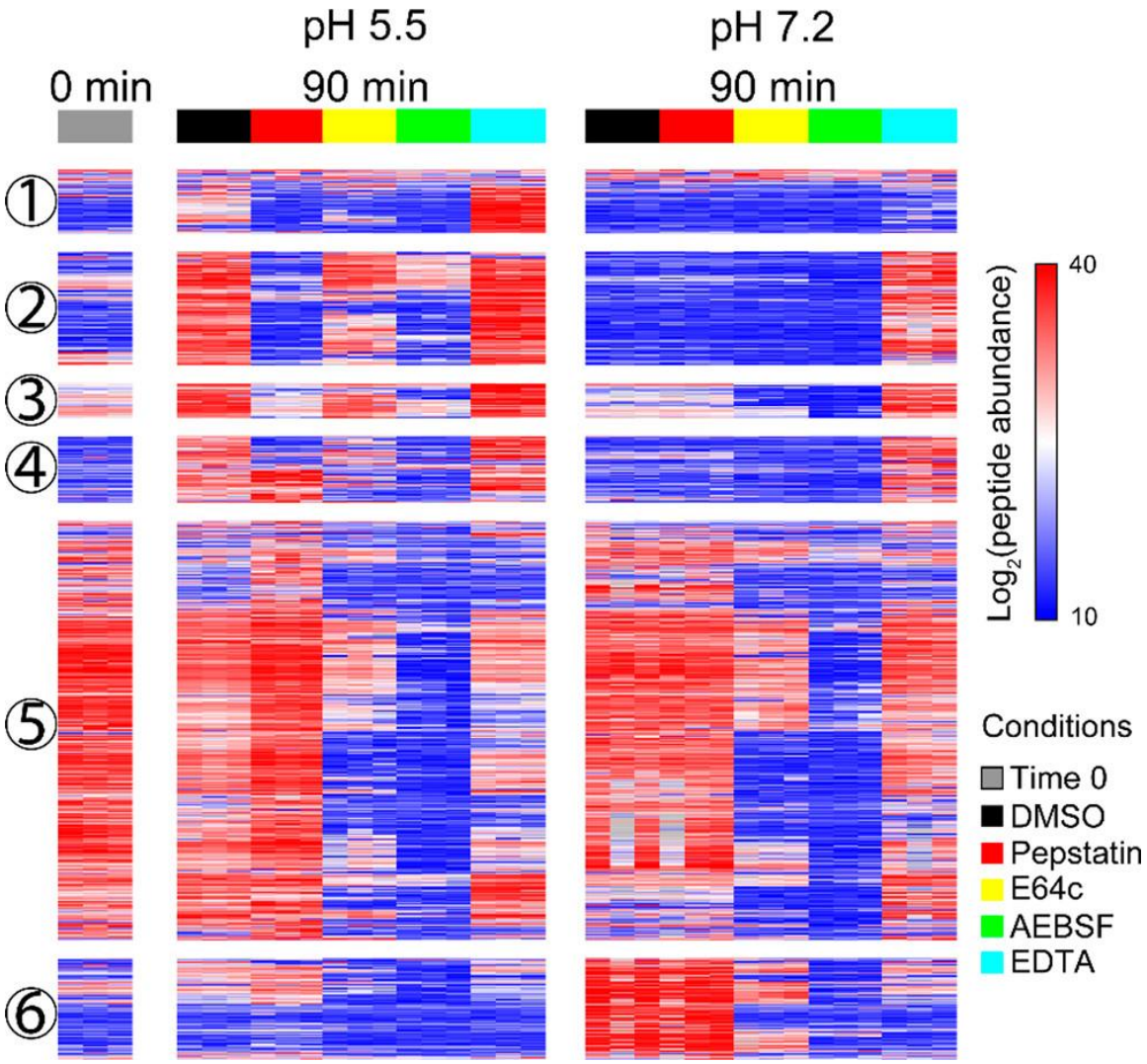

Figure 5.4 Effect of protease inhibitors on CG neuropeptidome production. The heatmap shows the abundance of newly formed CG neuropeptides after 90 min of incubation with and without class-specific inhibitors (DMSO vehicle, pepstatin, E64c, AEBSF, and EDTA) and time 0 min control. Each row represents a neuropeptide. Peptide abundance was $\log_2$ transformed and normalized within each peptide across all conditions. Neuropeptides colored in red are at higher abundance, and the ones colored in blue are at lower abundance. Hierarchical clustering was performed to group neuropeptides based on similar protease inhibition profiles. Data were shown as the average of three biological replicates.

Comparison of neuropeptidomics profiles generated by CG (no inhibitors) showed (1) neuropeptides that were increased at pH 5.5 but not at pH 7.2 (groups 1–4), (2) neuropeptides that were increased at pH 7.2 but not at pH 5.5 (group 6), and (3) peptides that displayed similar relative abundances after incubation at both pH conditions (group 5). These findings showed that selected groups of neuropeptides were formed at pH 5.5 but not pH 7.2, while other neuropeptides were formed at pH 7.2 but not at pH 5.5.

The formation of neuropeptides was sensitive to multiple class-specific inhibitors suggesting that aspartic, cysteine, serine, and metallo proteases were all involved in their production. Different inhibitor sensitivities were observed for pH 5.5 compared to pH 7.2 for neuropeptides of groups 1–4 and 6. At pH 5.5, peptide production was sensitive to inhibition by all four class selective inhibitors (pepstatin, E64, AEBSF, and EDTA), but at pH 7.2, little effect of pepstatin was observed compared to inhibition by E64, AEBSF, and EDTA. However, similar inhibitor sensitivities for production of neuropeptides of group 5 were observed for pH 5.5 and pH 7.2, suggesting that some proteases may be active at both pH conditions.

To evaluate proneuropeptide-derived peptides generated from each precursor, we generated heatmaps of protease inhibition profiles of peptides generated at pH 5.5 and pH 7.2. The heatmaps (Figure 5.5 and Figures 5.S2–5.S13) highlight the processed regions of proneuropeptides and illustrate the classes of proteases involved in the cleavages at these regions. It is notable that *in vitro* incubation of CG resulted in production of neuropeptidome components that were found in the static, nonincubated CG neuropeptidome. These data indicate that the *in vitro* CG processing assays reflect production of endogenous peptides (Figure 5.5 and Figures 5.S2–5.S13).

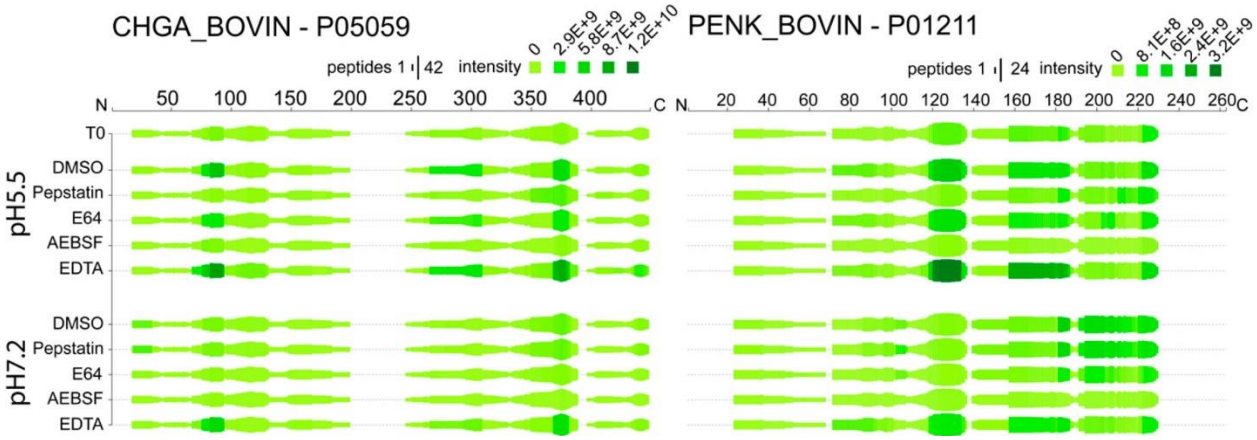

Figure 5.5 Neuropeptidomes generated from chromogranin A (CHGA) and proenkephalin (PENK) proneuropeptides in the presence of class-specific protease inhibitors. For each amino acid of proneuropeptides, the height of the green bars is proportional to the number of peptide amino acids overlapping the indicated region. The darkness of the color is proportional to the sum of the quantified peptide intensities. These heat maps illustrate peptides generated from CHGA and PENK that were sensitive to each of the indicated protease inhibitors of pepstatin, E64c, AEBSF, or EDTA.

Analysis of peptides derived from two of the most abundant proneuropeptides, chromogranin A (CHGA) and proenkephalin (PENK), indicated that multiple types of proteases were utilized for production of peptides derived from each of these precursors (Figure 5.5). During incubation of CG at pH of 5.5, formation of peptide fragments derived from CHGA and PENK precursors was reduced by pepstatin, E64c, and AEBSF which indicated roles for aspartic, cysteine, and serine proteases (Figure 5.5). EDTA increased production of peptides derived from several domains of CHGA and PENK. At pH 7.2, peptides derived from PENK were generated, but CHGA derived peptides were not produced at pH 7.2. Production of PENK-derived peptides at pH 7.2 was inhibited by E64c and AEBSF, indicating involvement of cysteine and serine proteases. EDTA increased production of several PENK-derived peptides but also decreased production of other PENK-derived peptides.

In addition to peptides derived from CHGA and PENK, heatmaps were also assessed for peptides generated from CHGB (chromogranin B), SCG3, SCG2, ADM, PCSK1N, VGF, SCG5, NPY (neuropeptide Y), GAL (galanin), and NPPA (shown in Figures 5.S2–5.S13). Analyses of

peptides generated from these 12 proneuropeptides show that (1) multiple protease classes of aspartic, cysteine, serine, and metallo types are all involved in peptide formation, (2) differential profiles of protease classes participate in peptide production from each distinct proneuropeptide, (3) the rate and diversity of proneuropeptide processing were higher at pH 5.5 compared to pH 7.2, (4) some peptides were generated at both pH 5.5 and 7.2, and (5) peptides from NPY and GAL proneuropeptides were generated at pH 7.2 with little production at pH 5.5. Importantly, these findings demonstrate differential utilization of the four protease classes at pH 5.5 compared to pH 7.2 for peptide production.

5.2.6 pH-Dependent CG Proteolytic Cleavage Profiles Defined by MSP-MS

MSP-MS characterizes proteolytic cleavage profiles using a defined peptide library consisting of 228 tetradecapeptides designed to contain all amino acid combinations surrounding protease cleavage sites. The peptide library was incubated with the CG, and cleavage products were identified and quantified by nano-LC–MS/MS. Although a substrate library of this size has fewer cleavable peptide bonds compared to the endogenous proteins and peptide substrates in CG, it offers several advantages for characterizing protease activities consisting of the following: (1) the substrates are sufficiently long to be able to quantify both the substrate and the cleaved products in parallel, which contrasts to the endogenous substrates that are often proteins or polypeptides that are too large for peptidomics analysis; (2) every cleavage product greater than five amino acids can be directly linked to a single precursor; (3) the synthetic peptide substrates have a defined length and sequence and have unmodified amino and carboxy termini that allow us to clearly distinguish aminopeptidase, endopeptidase, and carboxypeptidase activities; (4) the peptide library substrates are present at equal molar concentrations to rule out cleavage site bias due to substrate concentration, as is the case for endogenous substrates that differ greatly in concentration.

At pH 5.5, incubation of the peptide library with the purified CG resulted in cleavage of 600 out of the 2964 peptide bonds of the library substrates, while incubation at pH 7.2 resulted in 204 cleavage sites identified. When comparing these assays, 148 sites were cleaved by proteases at both pH conditions (Figure 5.6A). The pH 5.5 cleavage profiles showed preference for Arg at the P1 position as well as hydrophobic residues such as norleucine (n), Phe, Leu, and Tyr. At the P2, P1′, and P2′ positions many of the same hydrophobic residues were preferred with the addition of Ala at P2 and Ile at P1′ (Figure 5.6B). Under these conditions, the most frequently cleaved sites within the 14-mer peptides occurred between residues 13–14 and 12–13 that are common sites for mono- and dicarboxypeptidases, respectively, and also between residues 2–3 and 3–4 that are preferred sites for diaminopeptidases and triaminopeptidases, respectively (Figure 5.6D). Cleavage at sites distal from the amino and carboxy termini are likely to be cleaved by endopeptidases.

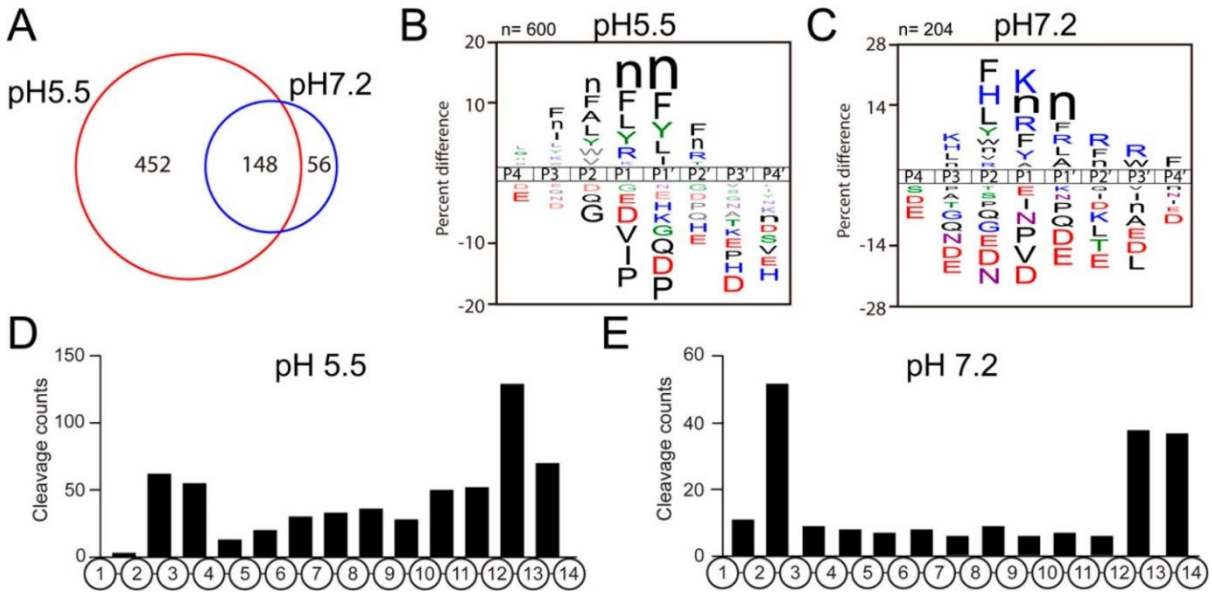

Figure 5.6 MSP-MS reveals distinct substrate cleavage properties of CG proteases at pH 5.5 compared to pH 7.2. (A) MSP-MS (multiplex substrate profiling mass spectrometry) was performed at pH 5.5 and pH 7.2 to characterize CG protease activities at the internal DCSV pH of 5.5 and at the extracellular pH of 7.2 into which CG contents are released. (B, C) Substrate leavage specificity profiles of CG proteases at pH 5.5 (B) and pH 7.2 (C). (D, E) The bar graphs summarize the cleavage frequency at each peptide bond within the 14-mer peptide substrates of the library at pH 5.5 (D) and pH 7.2 (E).

At pH 7.2, the cleavage profile was distinct from that at pH 5.5. Notable differences were an increase in the frequency of Lys and His at P3, His at P2, Lys at P1, Arg and Ala at P1′, Arg and Trp at P2′, and Phe at P4′ (Figure 5.6C). The most frequently cleaved sites occurred between residues 2–3 indicating the presence of diaminopeptidases; in addition, the peptides were also frequently cleaved by mono- and dicarboxypeptidases as cleavage occurred between residues 12–13 and 13–14 (Figure 5.6E).

5.2.7 Inhibitor-Sensitive CG Cleavage Profiles at pH 5.5 and pH 7.2 by MSP-MS

The protease classes that represent CG proteolysis were evaluated by MSP-MS cleavage profiling assays in the presence of protease class-specific protease inhibitors. These inhibitors consisted of pepstatin, E64c, AEBSF, and EDTA which inhibit aspartic, cysteine, serine, and metallo protease classes, respectively.

Pepstatin reduced the number of CG cleavage products in the MSP-MS analyses at pH 5.5 (Figure 5.S14). A total of 124 cleavage sites were sensitive to pepstatin compared to the vehicle control (DMSO). The pepstatin-sensitive cleavage sites were generally located in the central regions of the 14-mer peptide substrates between residues 4 and 12, indicating that the aspartic proteases have endopeptidase activity. Analysis of the substrate profile of the pepstatin-sensitive cleavage sites revealed a preference for cleaving hydrophobic residues such as Phe, Leu, Nle, and Tyr at P1 and Nle, Phe, Tyr, and Ile at P1′ (Figure 5.7A). Only two aspartic proteases are identified in the CG proteomics analysis, with cathepsin D present at 33.9-fold higher levels than presenilin-1 based on NSAF. These data indicate that under acidic pH 5.5 conditions, cathepsin D may likely be responsible for endopeptidase cleavage between hydrophobic amino acids. It is of interest that at pH 7.2, there were almost no pepstatin-sensitive cleavages (Figure 5.S14) revealing that aspartic proteases are unlikely to play a role in peptide hydrolysis at neutral pH 7.2.

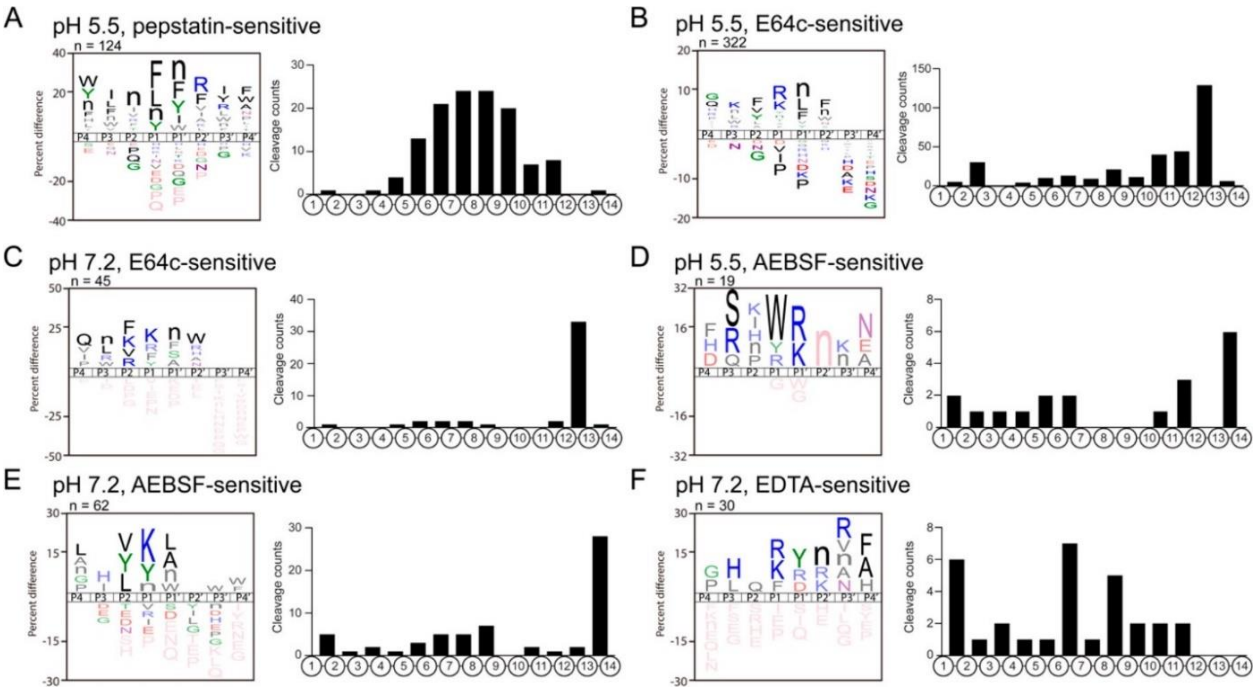

Figure 5.7 Inhibitor-sensitive protease cleavage profiles of CG neuropeptidome production at H 5.5 and pH 7.2. (A) Substrate cleavage profile of pepstatin-sensitive aspartic proteolytic activity at pH 5.5. (B, C) Substrate cleavage profile of E64c-sensitive cysteine proteolytic activity at pH 5.5 (B) and pH 7.2 (C). (D, E) Substrate cleavage profile of AEBSF-sensitive serine proteolytic activity at pH 5.5 (D) and pH 7.2 (E). (F) Substrate cleavage profile of EDTA-sensitive proteolytic activity at pH 7.2.

In the E64c-treated MSP-MS assays, three types of cysteine protease activities were revealed. Cysteine proteases with dicarboxypeptidase activity were active at both pH 5.5 and 7.2 represented by peptides being hydrolyzed between residues 12–13 (Figure 5.7B,C). In addition, diaminopeptidase activity was evident at pH 5.5 but not at pH 7.2, with several peptides cleaved between residues 2–3. Finally, cysteine endopeptidases that cleaved at sites distal from the termini were active at both pH conditions, but the number of cleaved peptides were higher at pH 5.5. The cysteine proteases that are active at pH 5.5 frequently displayed Arg and Lys at the P1 position, with Phe, Val, and Tyr at P2 and with Nle, Leu, and Phe at P1′. The substrate specificity at pH 7.2, which is likely to be dominated by the dicarboxypeptidase, has preferences for Phe, Lys, Val, and Arg at P1 and for Lys at P1′. The CG proteomics data identified 17 cysteine proteases with cathepsin B as the most abundant in this group. Among them, cathepsin B has dicarboxypeptidase

activity and is active at pH 5.5 and 7.2 and therefore may represent a candidate protease cleaving between residues 12–13. Also, cathepsin C and cathepsin L represent candidate proteases for the diaminopeptidase and endopeptidase activities, respectively, based on their known substrate specificities in the MEROPS protease database (as described in Methods) and relatively high abundance in the CG proteomics data.

When AEBSF was incubated with the chromaffin granules, the majority of AEBSF-sensitive serine protease activity occurred between residues 13 and 14 which indicates a monocarboxypeptidase at pH 5.5 and pH 7.2 (Figure 5.7D,E). Lower levels of aminopeptidase and endopeptidase activities were observed at pH 5.5 and pH 7.2 (Figure 5.7D,E). This monocarboxypeptidase may be represented by cathepsin A, the most abundant serine monocarboxypeptidase in the CG proteome.

EDTA treatment of CG in MSP-MS assays resulted in reduced cleavages of a few peptides at both pH 5.5 and pH 7.2 (Figure 5.S14). However, many peptide products increased after EDTA incubation (Figure 5.S14), which displayed endopeptidase and aminopeptidase activities (Figure 5.7F).

5.2.8 Cleavage Profiles of Recombinant Proteases Assessed by MSP-MS Represent the Majority of CG Cleavages at pH 5.5 and pH 7.2

We followed three criteria, (1) protease abundance in CG, (2) protease class, and (3) cleavage locations, to identify key CG proteases that were responsible for the different substrate specificity profiles. On the basis of our proteomics (supplementary data 2, tab “Fig. 5.2A-C and Fig. 5.S1B”), protease classes (Figures 5.4 and 5.7), and MSP-MS data (Figure 5.7), we identified cathepsins A, B, C, D, and L as key candidate proteases for further study. These recombinant enzymes were evaluated by MSP-MS, and the results (Figure 5.8A–H) confirmed that the specificity profiles of these five enzymes were found to closely match the CG inhibitor-sensitive

cleavage profiles observed by MSP-MS (Figure 5.7). These findings suggest that the identified cathepsins A, B, C, D, and L represent the majority of CG peptide cleavages at pH 5.5 and 7.2. In addition, carboxypeptidase E (CPE) was also investigated as it was the single most abundant protease in CG (Figure 5.8I,J).

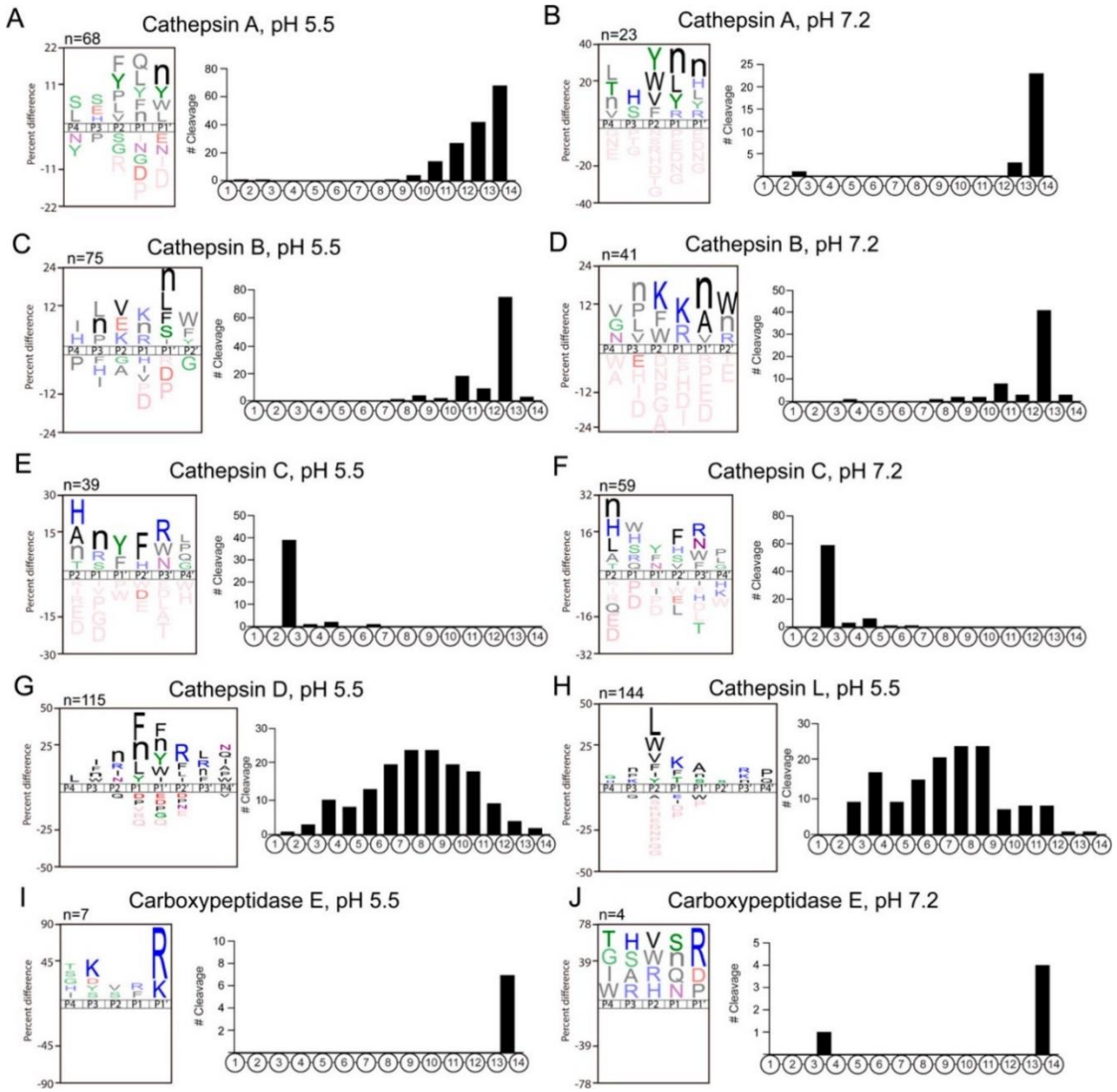

Figure 5.8 MSP-MS cleavage profiles of recombinant cathepsins A, B, C, D, as well as CPE. Recombinant, purified enzymes were subjected to substrate cleavage profiling analysis by MSP-MS. Sequence logos show the preferred amino acid adjacent to the cleavage site (P1–P1′), and the frequency of cleavages at each of the peptide bonds within the 14-mer peptides of the 228 peptide library is shown for (A) cathepsin A at pH 5.5, (B) cathepsin A at pH 7.2, (C) cathepsin B at pH 5.5, (D) cathepsin B at pH 7.2, (E) cathepsin C at pH 5.5, (F) cathepsin C at pH 7.2, (G) cathepsin D at pH 5.5, (H) cathepsin L at pH 5.5, (I) carboxypeptidase E (CPE) at pH 5.5, and (J) CPE at pH 7.2.

Cathepsin A displayed monocarboxypeptidase activity that removes single amino acids from the C-terminus at pH 5.5 and pH 7.2. Peptide hydrolysis was more efficient at the acidic pH condition. In general, Phe, Val, and Tyr were preferred at P2, Nle, with Tyr, Leu at P1 and Nle and Tyr at P1′ for both pH conditions (Figure 5.8A,B). These data show that cathepsin A is a serine protease that corresponds to AEBSF-sensitive proteolytic activity in CG.

Cathepsin B displays dicarboxypeptidase activity at pH 5.5 and 7.2 with a preference for Nle at P1′, for Arg and Lys at P1, and for Leu, Nle, and Pro at P3 in both specificity profiles (Figure 5.8C,D). The specificity profile of cathepsin B strongly correlates with the E64c-sensitive activity observed in the CG for neuropeptidome production.

For cathepsin C, peptide cleavage occurred between residues 2–3 at both pH conditions (Figure 5.8E,F). This diaminopeptidase preferentially cleaves substrates with His, Ala, Nle, or Thr at the amino terminus (P2 position) and also with Tyr and Phe at P1′, with Phe and His at P2′, with Arg, Trp, and Asn at P3′, and with Leu, Pro, and Gly at P4′. Cathepsin C is a cysteine protease inhibited by E64c.

Cathepsins D and L are clearly endopeptidases since the cleavage sites were located mainly in the mid-region for the 14-mer peptides of the library (Figure 5.8G,H) and have stronger activity at pH 5.5. Cathepsin D cleaves between hydrophobic residues such as Phe, Leu, and Tyr which has been reported previously. (31,32) Cathepsin L cleavage specificity is dominated by a P2 preference for hydrophobic residues such as Leu, Trp, Val, Phe, Ile, and Tyr, which correlates with specificity data generated by Choe and colleagues. (33) A strong correlation in peptide cleavage specificity occurs for the cathepsin D cleavage profile and the pepstatin-sensitive activities of CG. Finally, CPE generally cleaved peptides containing a C-terminal Arg residue at both pH conditions (Figure 5.8I,J), and this specificity has been reported previously. (34)

The combined cleavage sites of the MSP-MS assays achieved by the recombinant enzymes matched those of the CG MSP-MS cleavage profiles utilized for neuropeptidome production (Figure 5.9). CG cleavage of peptide bonds 1–13 of the 14-mer peptide library was mapped at pH 5.5 and pH 7.2 (colored in red, Figure 5.9). For each recombinant enzyme, cleavage at peptide bonds that match those of the CG cleavage site was also colored red. These data show that at pH 5.5, 67.3% of the CG proteolytic cleavage sites can be hydrolyzed by the recombinant enzymes (Figure 5.9A). Likewise, at pH 7.2, 88.5% of the CG-derived cleavage sites can be hydrolyzed by the recombinant proteases (Figure 5.9B). These findings indicate that the CG proteases of cathepsins A, B, C, D, and L possess cleavage specificities that match those utilized for endogenous CG neuropeptidome production at intravesicular and extracellular pH conditions.

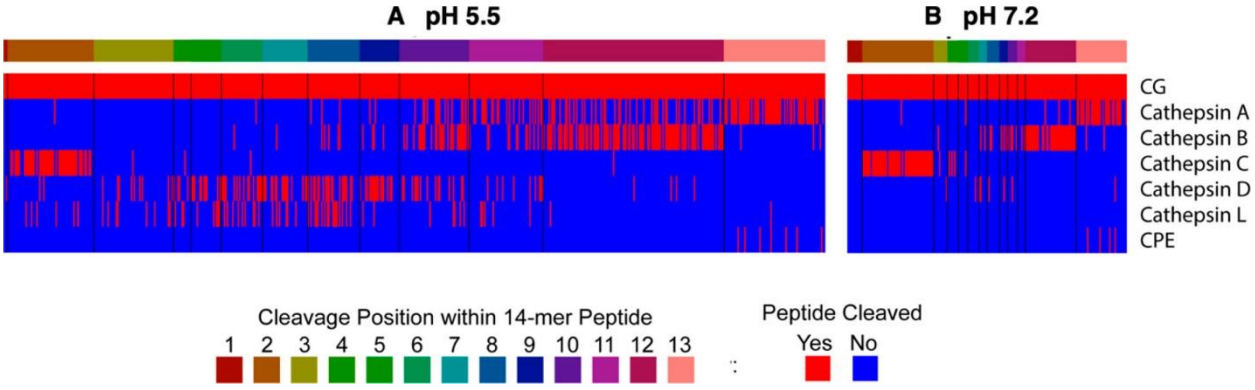

Figure 5.9 Parallel cleavage profiles of CG proteolytic activity utilized for neuropeptidome production with that of selected recombinant proteases analyzed by MSP-MS. Comparison of CG protease cleavage profiles with that of selected recombinant proteases identified in CG (by proteomics), conducted by MSP-MS analysis, was assessed at pH 5.5 (A) and pH 7.2 (B). Data show the matching cleavage profiles of endogenous CG proteolytic activity with that of purified recombinant enzymes consisting of cathepsins A, B, C, D, L, and CPE, assessed for each of the 13 cleavage sites of 14-mer peptides (228 total) of the substrate peptide library.

5.3 Discussion

Findings from this study show that distinct neuropeptidomes were generated by multiple classes of CG proteolytic activities at the intravesicular pH of 5.5 compared to the extracellular pH of 7.2. These pH differences were observed for peptides generated from each of the

proneuropeptides consisting of CHGA, CHGB, PENK, SCG3, SCG2, ADM, PCSK1N, VGF, SCG5, NPY, GAL, and NPPA. The 64 distinct proteases present in the CG proteome were evaluated with class-specific protease inhibitors to assess their roles in neuropeptidome biosynthesis. Results indicated differential utilization of aspartic, cysteine, serine, and metallo protease classes for neuropeptidome production at pH 5.5 compared to pH 7.2. Characterization of the CG proteases with a synthetic peptide library by MSP-MS analyses with class-specific inhibitors demonstrated aspartic, cysteine, serine, and metallo proteolytic activities of endopeptidase, carboxypeptidase, and aminopeptidase activities. The CG MSP-MS proteolytic cleavage profiles represented those of cathepsins A, B, C, D, L, and CPE that are present in CG. Purified recombinant forms of these six proteases cleaved the peptide library in a manner that represented the majority of cleavages displayed by the CG proteome. Our MSP-MS cleavage data for cathepsins B, D, and L, and CPE correlate well with other studies using different substrate specificity profiling methods. (32−37) However, little cleavage data are available for cathepsin C (38) and cathepsin A, (39,40) and therefore, the MSP-MS cleavage data for these enzymes are new in the field. The six proteases (cathepsins A, B, C, D, L, and CPE) identified for biosynthesis of the CG neuropeptidome in this study have been reported to process proneuropeptides or peptide intermediates for production of neuropeptides. (12,15,41−53) Notably, results demonstrate that distinct neuropeptidomes are generated by CG proteases at the internal DCSV pH of 5.5 compared to the extracellular pH of 7.2.

The approach of assessing neuropeptidome biosynthesis from both proneuropeptides and proneuropeptide-derived intermediates by the entire proteolytic capacity of CG, a model DCSV organelle, is unique in the field. Proteases involved in neuropeptide production have largely been investigated in focused studies of specific proteases in genetic enzyme knockout mice and cells,

gene expression, and inhibition studies. (12,15,17) The advantage of DCSV organelle-based neuropeptidome studies is the simultaneous assessment of the full spectrum of DCSV proteases for production of proneuropeptide-derived peptides.

Distinct CG neuropeptidomes were generated at the intravesicular pH of 5.5 and at the extracellular pH of 7.2. The differential neuropeptidomes produced at the two pH conditions were generated from the proneuropeptides CHGA, CHGB, PENK, SCG3, SCG2, ADM, PCSK1N, VGF, SCG5, NPY, GAL, and NPPA. Notably, production of CG neuropeptidomes in the presence of four class-specific protease inhibitors (pepstatin, E64c, AEBSF, and EDTA) indicated that aspartic, cysteine, serine, and metallo proteases participated in peptide production. For processing of individual proneuropeptides, different peptide products were sensitive to inhibition of the four protease classes. Production of peptide products from the proneuropeptide PENK (proenkephalin), as an example, at pH 5.5 was reduced by pepstatin, E64c, and AEBSF, whereas production of PENK-derived peptides at pH 7.2 were inhibited by E64c, AEBSF, and EDTA. These data show that different and similar protease classes participated in generating PENK-derived peptides at pH 5.5 compared to pH 7.2 conditions.

The matching CG cleavage profile results observed with the peptide library in MSP-MS assays and by neuropeptidomics elucidated the CG proteases involved in neuropeptide production. The endopeptidase activity was inhibited by pepstatin A which is consistent with the activity of the aspartic protease cathepsin D present in CG. E64c inhibition of the endopeptidase activity represented that of the cysteine protease cathepsin L. The E64c-sensitive dicarboxypeptidase activity matches that of the cysteine protease cathepsin B. The AEBSF-sensitive monocarboxypeptidase activity matches that of cathepsin A. The diaminopeptidase activity, inhibited by E64c, represents the cysteine protease cathepsin C. Carboxypeptidase E (CPE) is an

abundant CG metallo protease that was investigated since CPE removal of C-terminal Arg and Lys residues is known to be necessary for neuropeptide maturation. (12,15,53)

The identification and characterization of these 6 active proteases in CG also explained why we observed higher proteolytic activity at pH 5.5 compared to pH 7.2 (Figures 5.3B, 5.6A, 5.8, and 5.9). In this study, we observed that 4 out of 6 of the most active CG proteases in CG, cathepsins A, B, D and L, are more active at acidic pH than neutral pH. On the one hand, this observation aligns with the biological fundamental knowledge that the majority of the proteolytic processing of proneuropeptides occurs during the axonal transportation within the DCSVs, which has a pH of 5.5, so that mature neuropeptides at the nerve terminal can be released to the periphery, allowing such neuropeptides to function instantly for cell–cell communication. On the other hand, many cathepsins with optimal activities in an acidic environment have also been reported to be able to retain their activities at neutral pH. (54−56) Here, we observed distinct proteolytic activities at neutral pH in our CG peptidomics and MSP-MS assays, suggesting that proneuropeptides can also be processed by certain proteases at the postsecretion stage. The change of pH from acidic to neutral upon exocytosis may serve to regulate protease activities, particularly cathepsins A, B, C, D, and L, and subsequently regulate the biosynthesis of neuropeptides.

Involvement of these six CG proteases in neuropeptide production is supported by reported data showing that each of these proteases cleaves proneuropeptides or neuropeptide intermediate substrates. Cathepsin L, a cysteine endopeptidase, has been shown to process the proneuropeptides PENK, POMC, NPY, pro-CCK, and PDYN at dibasic residue cleavage sites. (41−45) Cathepsin D, an aspartic endopeptidase, cleaves protachykinin at basic residues as well as hydrophobic residues to generate substance P. (46,47) Cathepsin B, a cysteine protease, cleaves the PENK-derived intermediate BAM-12P to generate the (Met)-enkephalin-Arg (ME-Arg), demonstrating

its endopeptidase activity. (48) Cathepsin B also displays dicarboxypeptidase activity shown by removal of C-terminal dipeptides from ME-Arg-Phe, ME-Arg-Gly-Leu, and dynorphin (1–8). (49,50) The monocarboxypeptidase activity of cathepsin A cleaves ME-Arg-Phe by sequential removal C-terminal Phe and Arg to generate the ME neuropeptide. (51) The diaminopeptidase cathepsin C removes the N-terminal dipeptide from the neuropeptide ME. (52) The CPE exopeptidase has been shown to remove C-terminal Arg and Lys residues to generate numerous neuropeptides including ME. (12,15,53)

The findings of this study and those in the field demonstrate that different experimental approaches of gene homology, biochemical, and global neuropeptidomics result in identification of distinct proteases for neuropeptide production. A genetic approach of searching for mammalian gene homologues of the yeast Kex2 gene for pro-α-mating factor processing led to identification of mammalian proprotein convertases 1 and 2 (PC1 and PC2) (57−60) involved in processing prohormones, including POMC (proopmelanocortin), (61, 62) proinsulin, (63,64) proenkephalin, (65−67) and others. (12,17,68,69) The PC1 and PC2 proteases are members of the subtilisin-like serine protease family of mammalian processing proteases. The biochemical approach of identifying proenkephalin cleaving activity led to identification of cathepsin L for processing proenkephalin, POMC, prodynorphin, and several other proneuropeptides. (41-45) The approach of this study using peptidomics, proteomics, and MSP-MS led to identification of multiple proteases identified consisting of cathepsins A, B, C, D, L, and CPE that are present in CG. Clearly, the global neuropeptidomics combined with MSP-MS protease profiling provides a novel unbiased approach for elucidation of proteases involved in generating diverse neuropeptidomes.

Here, we presented our initial effort to develop a mass spectrometry platform to study proteases and substrates in a complex biological system. We utilized CG as our model system which are among the most homogeneous of cellular DCSVs. (12) However, a missing aspect in this study and the field is to investigate the nature of DCSV heterogeneity in proneuropeptide processing. Whether prohormones and proteases coexist within the same cell and CG will affect the proteolytic outcomes. One way to address this question is to perform studies at the single cell level. Even though current mass spectrometry technology is facing the challenge of low sensitivity in quantifying proteins from single cells, the advances in this field will ultimately contribute to deeper understanding of biological systems at single-cell resolution. Alternatively, cell sorting flow cytometry can also be performed to obtain more homogeneous samples.

Moving forward, it will be beneficial to gain understanding of neuropeptide biosynthesis by integration of peptidomics, proteomics, and protease cleavage profiling of the DCSV organelle from neuropeptide-rich cell types of multiple organisms. Investigations of neuropeptidomes under different conditions will advance understanding of the complexity of neuropeptidomes for cell–cell communication in disease and health.

5.4 Methods

5.4.1 Purification of Chromaffin Granules (CG) from Bovine Adrenal Medulla

Dense core secretory vesicles (DCSV), represented by CG present in adrenal medullary chromaffin cells, were isolated from fresh bovine adrenal medulla by differential sucrose density centrifugation as we have described previously. (70,71) In total, we obtained three biological replicate CG samples. Each replicate CG sample was obtained from 20 adrenal glands of fresh adrenal medulla (bovine) tissue (Sierra for Medical Science, Whittier, CA). Adrenal glands were gently homogenized in 0.32 M sucrose using a Polytron and centrifuged at 365*g* (20 min at 4 °C)

to remove nuclei (pellet). The CG-containing supernatant was centrifuged at 12 000*g* (20 min at 4 °C) to result in the CG pellet. The CG pellet was washed three times in 0.32 M sucrose (12 000*g*, 20 min, 4 °C). The washed CG pellet was resuspended in 0.32 M sucrose, layered on a 1.6 M sucrose step gradient with a cushion of 2.2 M sucrose, and centrifuged at 120 000*g* (120 min, 4 °C) in a Beckman SW28 rotor to result in purified CG at the interface of the 1.6/2.2 M sucrose. The CG were removed, resuspended in 0.32 M sucrose, layered on 1.6 M sucrose, and subjected to a second ultracentrifugation step (SW28 rotor, 120 000*g*, 120 min). The resultant purified CG was resuspended in 15 mM KCl and stored at −70 °C for analysis.

We have documented the high purity of this preparation of isolated CG by electron microscopy and biochemical markers. (70,71) The purified CG lack markers for the subcellular organelles of lysosomes (acid phosphatase marker), (70) cytoplasm (lactate dehydrogenase marker), (72) mitochondria (fumarase and glutamate dehydrogenase markers), (70) and endoplasmic reticulum (glucose-6-phosphatase marker). (72) Thus, the high purity of the isolated CG has been established. (70−73)

5.4.2 Proteomics Analysis for Identification of Proteins and Proteases in Chromaffin Granules

Proteins and proteases in CG were identified by proteomics analysis. Proteins of the purified CG (200 μg, in triplicate) were precipitated by incubation in ice-cold 90% MeOH (Thermo) for 15 min, centrifuged for 30 min (14 000*g*, 4 °C) to collect the protein pellet. The protein precipitate was resuspended in reduction buffer consisting of 8 M urea (MP Biomedicals), 50 mM Tris-HCl (MP Biomedicals), pH 8.0, 5 mM DTT (Sigma), and incubated at 55 °C for 45 min for protein denaturation and reduction. For alkylation of cysteine residues, samples were incubated in 15 mM iodoacetamide (Sigma) in the dark at RT for 30 min, followed by quenching by addition of DTT to a final concentration of 5 mM. Samples were diluted with 50 mM Tris-HCl,

pH 8.0, to reduce urea to 1.0 M or less. Samples were then digested by incubation with trypsin/LysC (Promega V5113) at a ratio of 50:1 protein/trypsin, at RT for 20 h at 37 °C. Reactions were quenched by addition of 10% TFA (Thermo) to 0.5% TFA to adjust the pH below 2.

Samples were subjected to peptide purification and desalting by C18 stage tip SPE using Empore C18 wafers (from 3M), using a protocol described by Rappsilber et al., 2007. (74) The C18 stage tip was washed with ACN (acetonitrile) and equilibrated with 0.1% TFA. Samples were loaded, washed with 0.1% TFA, eluted with 50% ACN/0.1% TFA, dried in a SpeedVac, resuspended in water, and peptide concentrations were measured by a total peptide assay kit (Pierce quantitative colorimetric peptide assay, Thermo Fisher). Samples were dried in a SpeedVac centrifuge, stored at −70 °C, and resuspended in H_2O for nano-LC–MS/MS.

Nano-LC–MS/MS utilized 2 μg of peptides from each sample for analysis on a Q-Exactive mass spectrometer (Thermo) equipped with an Ultimate 3000 HPLC (Thermo). Each triplicate sample was injected 3 times into the LC–MS/MS as technical replicates. Peptides were separated by reverse phase chromatography on a C18 column (1.7 μm bead size, 75 μm × 25 cm, heated to 65 °C) at a flow rate of 300 nL/min using a 145 min linear gradient from 5% B to 25% B, with solvent A consisting of 0.1% formic acid (H_2O) (Thermo) and solvent B consisting of 0.1% formic acid/acetonitrile (Thermo). Survey scans were recorded over a 310–1250 *m*/*z* range (35 000 resolutions at 200 *m*/*z*, AGC target 3×10^6, 100 ms maximum IT). MS/MS was performed in data-dependent acquisition mode with HCD fragmentation (28 normalized collision energy) on the 20 most intense precursor ions (175 000 resolutions at 200 *m*/*z*, AGC target 1×10^5, 50 ms maximum IT, dynamic exclusion 20 s).

MS/MS data were processed by PEAKS 8.5 (Bioinformatics Solutions Inc.). MS^2 data were searched against *Bos taurus* proteome (Aug 28, 2018) with decoy sequences in reverse order.

Fixed modifications of carbamidomethylation of cysteine (+57.021 46 Da), variable modification of acetylation of protein N-termini (+42.0106), and oxidation of methionine (+15.994 92 Da) were specified. A maximum of two missed cleavages of trypsin was allowed. A precursor tolerance of 20 ppm and 0.01 Da for MS^2 fragments was defined. Data were filtered to 1% peptide sequence and protein false discovery rates with the target decoy strategy. Proteins that were identified in at least 2 out of 3 technical injections were considered as identified in each replicate sample, and proteins identified in at least 2 out of 3 replicate samples were considered as identified in CG. Proteases in the CG proteome were compiled according to the MEROPS database of protease enzymes. (75)

5.4.3 Peptidomics Analysis of Chromaffin Granules

Purified CG samples (1.25 mg per replicate sample, triplicate samples prepared) were incubated at 37 °C for 0, 30, and 90 min at pH 5.5 (20 mM citrate–phosphate, pH 5.5, 100 mM NaCl, 1 mM $CaCl_2$, 1 mM $MgCl_2$, 2 mM DTT) and at pH 7.2 (phosphate buffered saline, pH 7.2, 1 mM $CaCl_2$, 1 mM $MgCl_2$, 2 mM DTT). Incubations were conducted in the absence of protease inhibitor and in the presence of each of the protease inhibitors pepstatin A (4 μM, MP Biomedicals), E64c (40 μM, Sigma), AEBSF (4 mM, Tocris), and EDTA (10 mM, MP Biomedicals). Endogenous peptides were then extracted by addition of ice cold HCl to 20 mM HCl (pH < 3), incubation on ice for 15 min, centrifugation for 30 min (14 000*g*, 4 °C), and the supernatant peptide fraction was collected. The acid extract was then brought up to 20% ACN and 10 mM HCl, filtered through a 10 kDa MW cutoff filter (Millipore MRCPRT010) (centrifugation for 45–60 min at 14,000*g*, 4 °C), followed by addition of 100 μL of 0.5 M NaCl and 10 mM HCl to the filter and centrifugation. The low molecular weight filtrate was neutralized by addition of 1 M ammonium bicarbonate to 30 mM, dried in a vacuum centrifuge, and stored at −70 °C for the

next step. Samples were then resuspended in 100 μL of urea buffer (6 M urea, 60 mM Tris-HCl, pH 8), and DTT (100 mM DTT stock) was added to a final concentration of 5 mM DTT and incubated at room temperature for 1 h. Iodoacetamide (IAA) stock solution (200 mM IAA in urea buffer) was added to each sample to obtain 15 mM IAA, and samples were incubated for 3 min at RT in the dark. The alkylation was quenched by addition of DTT to a final concentration of 10 mM, and samples were acidified by addition of TFA. Peptides were then collected by C18 stage-tip SPE as explained for CG proteomics (this Methods section); eluted samples were dried in a vacuum centrifuge and stored at −70 °C. Samples were resuspended in water and were briefly vortexed and sonicated, and total peptide content was measured as described for CG proteomics. Samples were dried in a SpeedVac and resuspended in 2% ACN/0.1% TFA to a peptide concentration of 0.11 μg/μL.

For nano-LC–MS/MS, 4.6 μL (∼500 ng) of each was injected into the LC–MS system. Peptides were separated by reverse phase chromatography on a C18 column (1.7 μm bead size, 75 μm × 25 cm, heated to 65 °C) at a flow rate of 300 nL/min using a gradient of solvent B (0.1% formic acid ACN) at 5–25% gradient over 75 min with solvent A (0.1% formic acid/H_2O). Survey scans were recorded over a 310–1250 *m*/*z* range (70 000 resolutions at 200 *m*/*z*, AGC target 3×10^6, 100 ms maximum IT). MS/MS was performed in data-dependent acquisition mode with HCD fragmentation (27 normalized collision energy) on the 15 most intense precursor ions (17 500 resolutions at 200 *m*/*z*, AGC target 1×10^5, 70 ms maximum IT, dynamic exclusion 30 s).

Bioinformatics of MS/MS data was analyzed using PEAKS 8.5 (Bioinformatics Solutions Inc.). MS^2 data were searched against the *Bos taurus* proteome (Apr 22, 2018) with decoy sequences in reverse order. Fixed modifications of carbamidomethylation of cysteines (+57.02146 Da), variable modification of acetylation of protein N-termini (+42.0106), oxidation of methionine

(+15.99492 Da), pyro-Glu from A (−17.03), and phosphorylation (STY) (+79.97) were specified. A precursor tolerance of 20 ppm and 0.01 Da for MS^2 fragments was defined. No protease digestion was specified. Data were filtered to 1% peptide and protein level false discovery rates with the target-decoy strategy. Peptides were quantified with label free quantification, and data were normalized by calculating the median of intensities for each sample and then scaling the data to their medians, and filtered by 0.3 peptide quality. Missing and zero values were imputed with random normally distributed numbers in the range of the average of the smallest 5% of the data ± SD.

5.4.4 Multiplex Substrate Profiling by Mass Spectrometry (MSP-MS) of Proteolytic Activities in Chromaffin Granules

CG proteolysis was subjected to peptide cleavage profiling analysis by MSP-MS. Proteolytic activity of CG was analyzed with a library of exogenous synthetic peptides, consisting of 228 tetradecapeptides that were designed to contain all known protease cleavage sites. (24,25,76) Cleavage products were identified and quantitated by nano-LC–MS/MS mass spectrometry for bioinformatics analysis of cleavage site properties.

All MSP-MS assays (conducted in quadruplicate) were conducted by incubating purified CG with the 228-peptide library at a final concentration of 0.5 μM for each peptide at pH 5.5 or pH 7.2 (using the same buffers as those used in the peptidomics methods). The MSP-MS assays utilized 200 μg/mL CG (purified). For MSP-MS assays using recombinant human proteases, all enzymes were purchased from R & D Systems. MSP-MS assays used 18.4 nM cathepsin A, 2.64 nM cathepsin B, 19.6 nM cathepsin C, 100 nM cathepsin D, 3.84 nM cathepsin L, and 18.8 nM carboxypeptidase E that were preincubated (30 min at 37 °C) without and with protease inhibitors consisting of 4 μM pepstatin (MP Biomedicals), 40 μM E64c (Sigma), 4 mM AEBSF (Tocris), or 10 mM EDTA (MP Biomedicals). MSP-MS assays were conducted at 37 °C for 30 and 90 min.

At each time point, 20 μL of the reaction mixture was removed and quenched by addition of GuHCl (MP Biomedicals) to 6.4 M and samples were immediately stored at −80 °C. Control reactions consisted of CG or recombinant protease samples preincubated with 6.4 M GuHCl to inactivate the enzyme prior to addition of the peptide library. All samples were desalted with C18 and dried in a vacuum centrifuge.

For each MSP-MS assay sample, ∼0.4 μg of peptides was injected into a Q-Exactive mass spectrometer (Thermo) equipped with an Ultimate 3000 HPLC. Peptides were separated by reverse phase chromatography on a C18 column (1.7 μm bead size, 75 μm × 25 cm, 65 °C) at a flow rate of 300 nL/min using a 60 min linear gradient from 5% to 30% B, with solvent A of 0.1% formic acid in water and solvent B of 0.1% formic acid in acetonitrile. Survey scans were recorded over a 150–2000 *m*/*z* range (70 000 resolution at 200 *m*/*z*, AGC target 3×10^6, 100 ms maximum). MS/MS was performed in data-dependent acquisition mode with HCD fragmentation (28 normalized collision energy) on the 12 most intense precursor ions (17 500 resolutions at 200 *m*/*z*, AGC target 1×10^5, 50 ms maximum, dynamic exclusion 20 s).

Data were processed using PEAKS 8.5 (Bioinformatics Solutions Inc.). MS^2 data were searched against the tetradecapeptide library sequences with decoy sequences in reverse order. A precursor tolerance of 20 ppm and 0.01 Da for MS^2 fragments was defined. No protease digestion was specified. Data were filtered to 1% peptide level false discovery rates with the target-decoy strategy. Peptides were quantified with label free quantification, and data were normalized by median and filtered by 0.3 peptide quality. Missing and zero values are imputed with random normally distributed numbers in the range of the average of smallest 5% of the data ± SD.

5.4.5 Data Analysis and Bioinformatics

Gene ontology analysis and protein classification (Figure 5.S1) were performed using the analysis tools from the PANTHER classification system. (77) Proneuropeptides were annotated

based on NeuroPedia, (78) and proteases were annotated based on MEROPS. (75) For peptidomics, peptides whose abundance increased by 2-fold with q value of <0.05 comparing the assays of 30 or 90 min incubation to controls were considered to be significantly increased, and those whose abundance decreased by 2-fold with q value of <0.05 were considered to be significantly decreased. For MSP-MS assays, peptides whose abundance π value of >2.6138 (79) (significance level of <0.005) comparing 90 min incubation to controls were considered to be increased (cleavage products). Those cleavage products whose π values were <−2.6138 comparing the assays of 90 min incubation with the inhibitor treated CG to DMSO controls were considered to be inhibited.

Proteolytic specificity profiles were generated using iceLogo software to visualize amino acid frequency surrounding the cleavage sites. (80) Amino acids that were most frequently observed (above axis) and least frequently observed (below axis) from P4 to P4′ positions were illustrated ($p < 0.3$). Norleucine (Nle) was represented as "n" in the reported profiles. Amino acids in opaque text were statistically significant ($p < 0.05$). Heatmaps were generated using peptides that were cleaved after 90 min of incubation without inhibitor at either pHs. Hierarchical clustering was performed using Euclidean distance and complete linkage. Peptidomics profiles of each proneuropeptide and peptide alignment maps were generated using Peptigram. (81)

5.4.6 Data Availability

All mass spectrometry data have been deposited in MassIVE and proteomeXchange with accession numbers. MassIVE: MSV000085957 (proteomics), MSV000085956 (peptidomics), MSV00008595 (MSP-MS). ProteomeXchange: PXD020926 (proteomics), PXD020925 (peptidomics).

5.5 Supporting Information

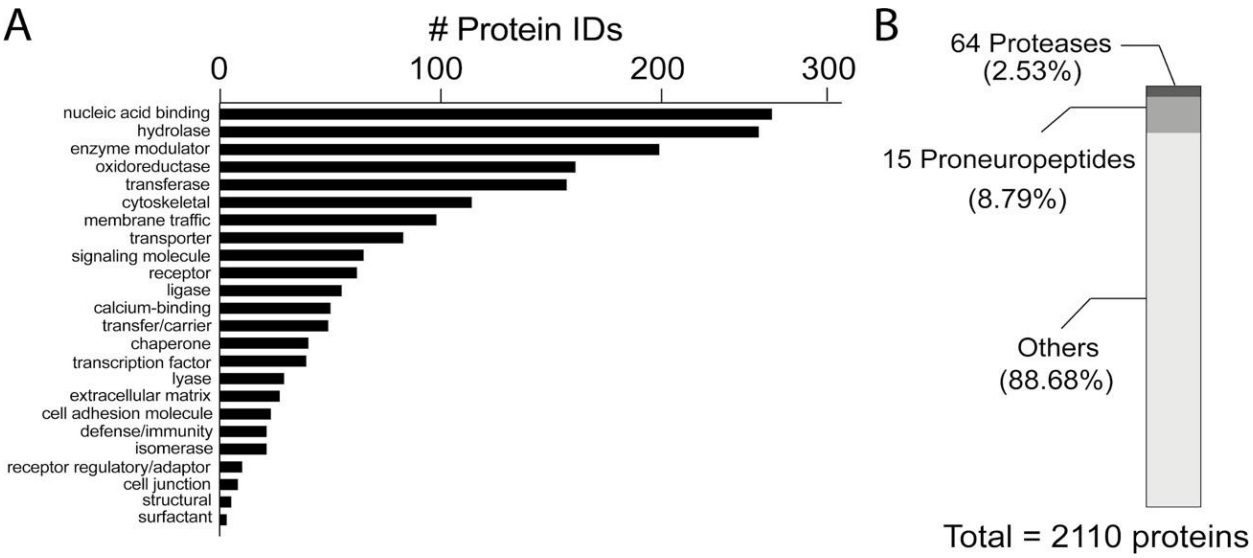

Figure 5.S1 Proteomics data assessed by GO (gene ontology) function (A) and relative abundance (calculated by normalized spectral abundance factor (NSAF)) of identified proteins as protease and proneuropeptide components (B).

Figures 5.S2-5.S13. Heatmaps of 12 proneuropeptide peptidome profiles, compiled from peptidomics data after 90 min incubation with addition of different inhibitors. For each amino acid of proneuropeptides, the height of the green bars is proportional to the number of amino acids overlapping this region. The darkness of the color is proportional to the sum of the peptide intensities.

Fig. S2

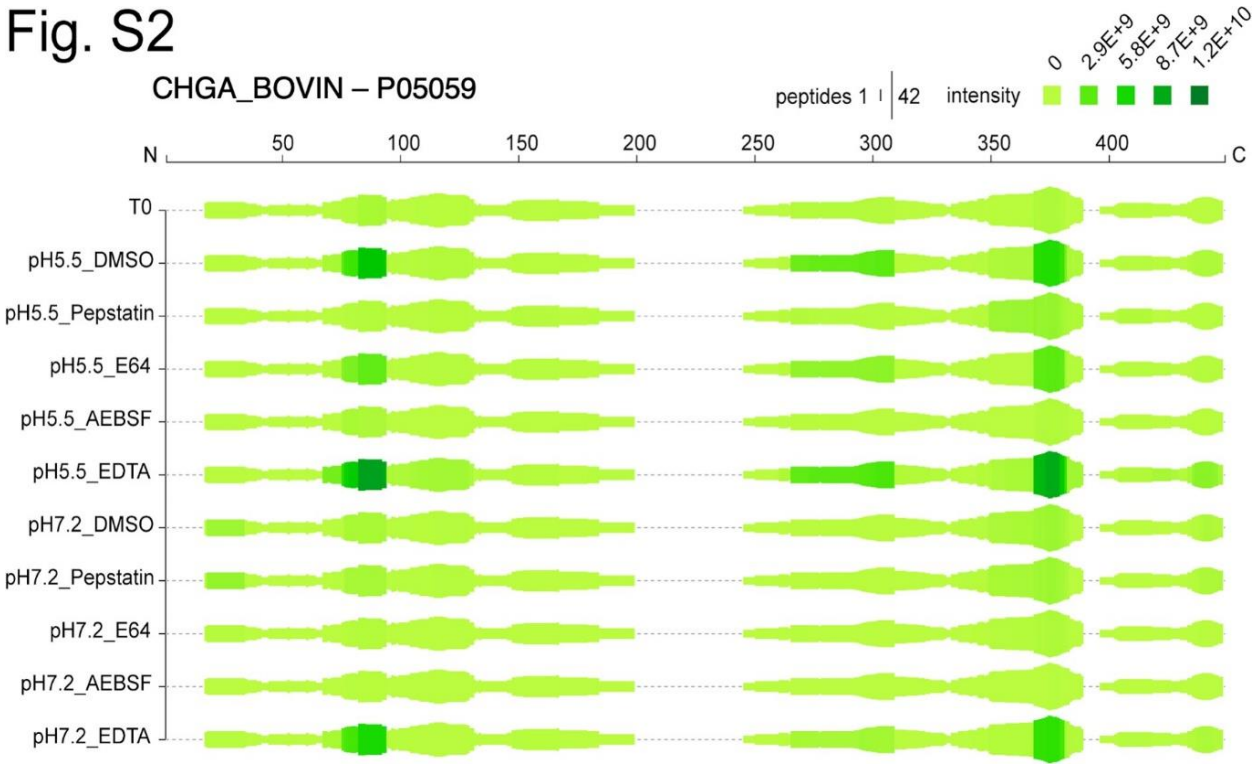

Figure 5.S2 CHGA-derived neuropeptidomes at pH 5.5 and pH 7.2, in the presence of pepstatin, E64c, AEBSF, and EDTA protease inhibitor.

Fig. S3

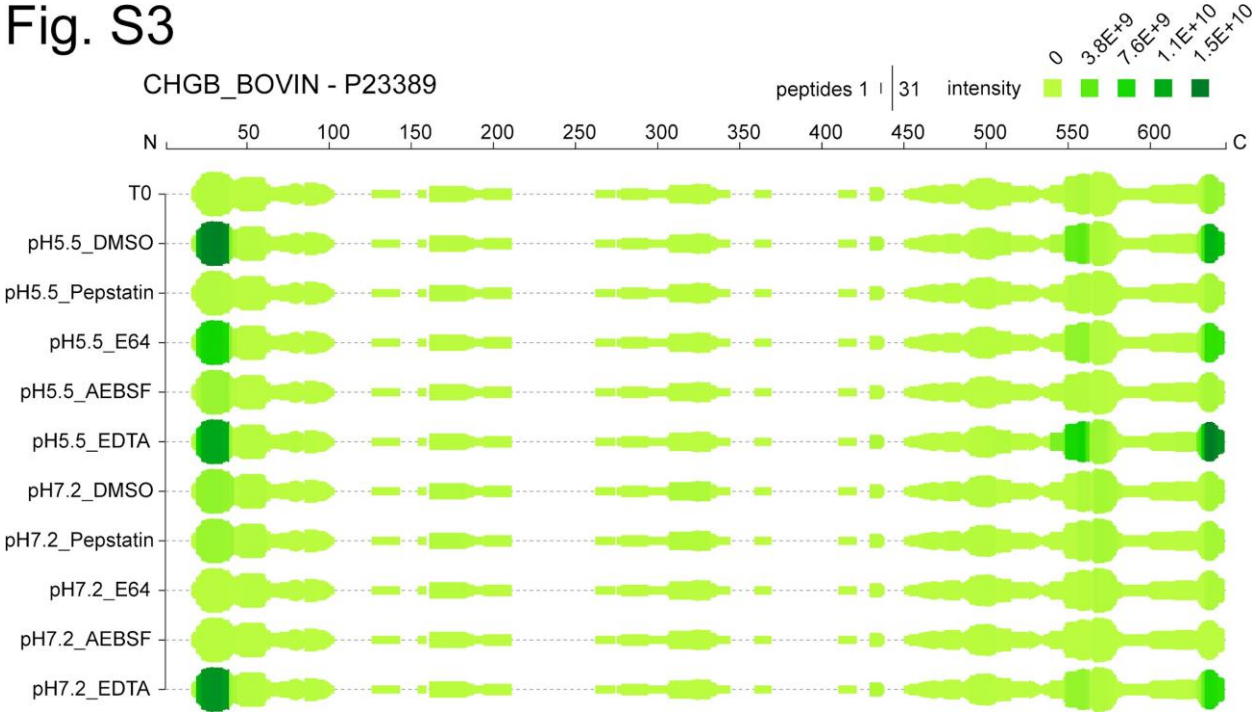

Figure 5.S3 CHGB-derived neuropeptidomes at pH 5.5 and pH 7.2, in the presence of pepstatin, E64c, AEBSF, and EDTA protease inhibitors.

Fig. S4

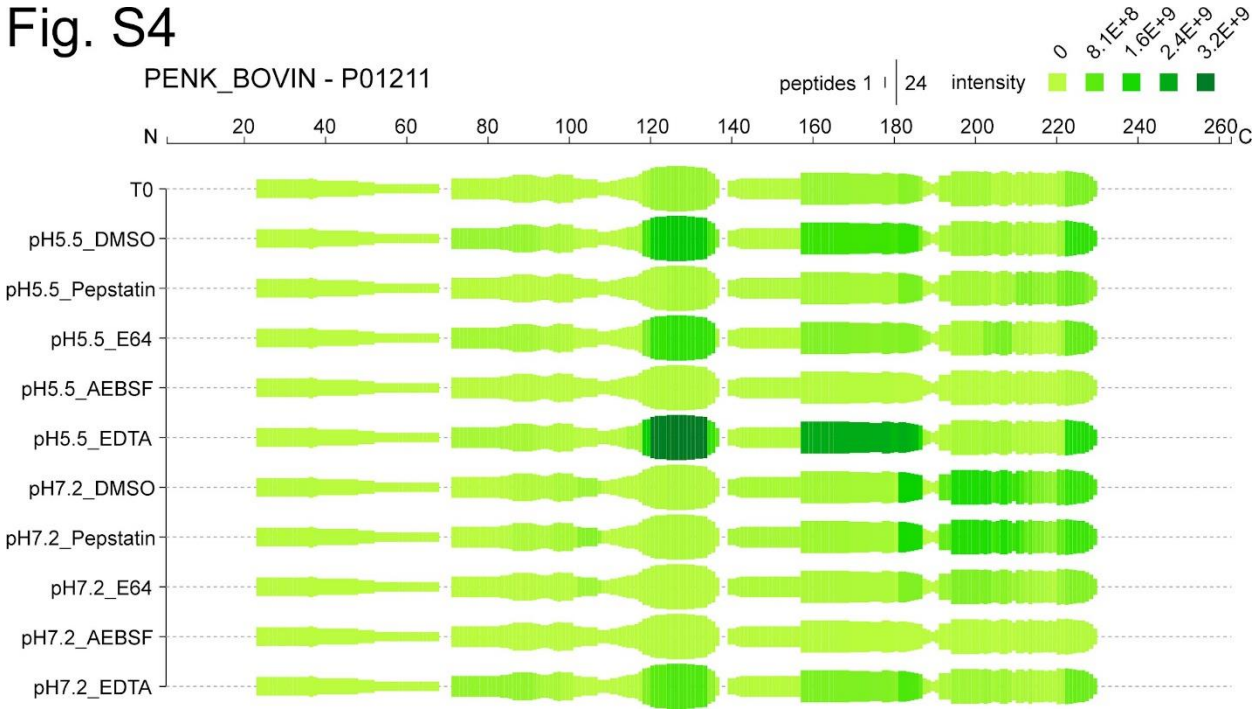

Figure 5.S4 PENK-derived neuropeptidomes at pH 5.5 and pH 7.2, in the presence of pepstatin, E64c, AEBSF, and EDTA protease inhibitors.

Fig. S5

Figure 5.S5 SCG3-derived neuropeptidomes at pH 5.5 and pH 7.2, in the presence of pepstatin, E64c, AEBSF, and EDTA protease inhibitors.

Fig. S6

Figure 5.S6 SCG2-derived neuropeptidomes at pH 5.5 and pH 7.2, in the presence of pepstatin, E64c, AEBSF, and EDTA protease inhibitors.

Fig. S7

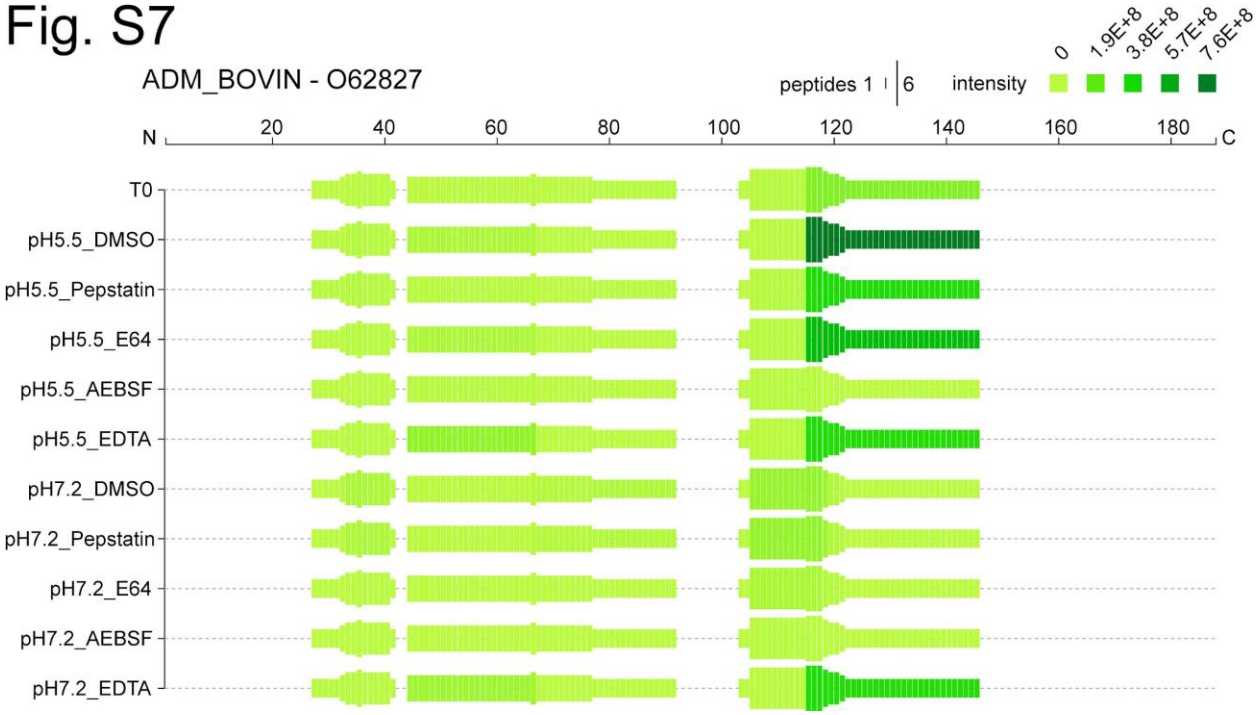

Figure 5.S7 ADM-derived neuropeptidomes at pH 5.5 and pH 7.2, in the presence of pepstatin, E64c, AEBSF, and EDTA protease inhibitors.

Fig. S9

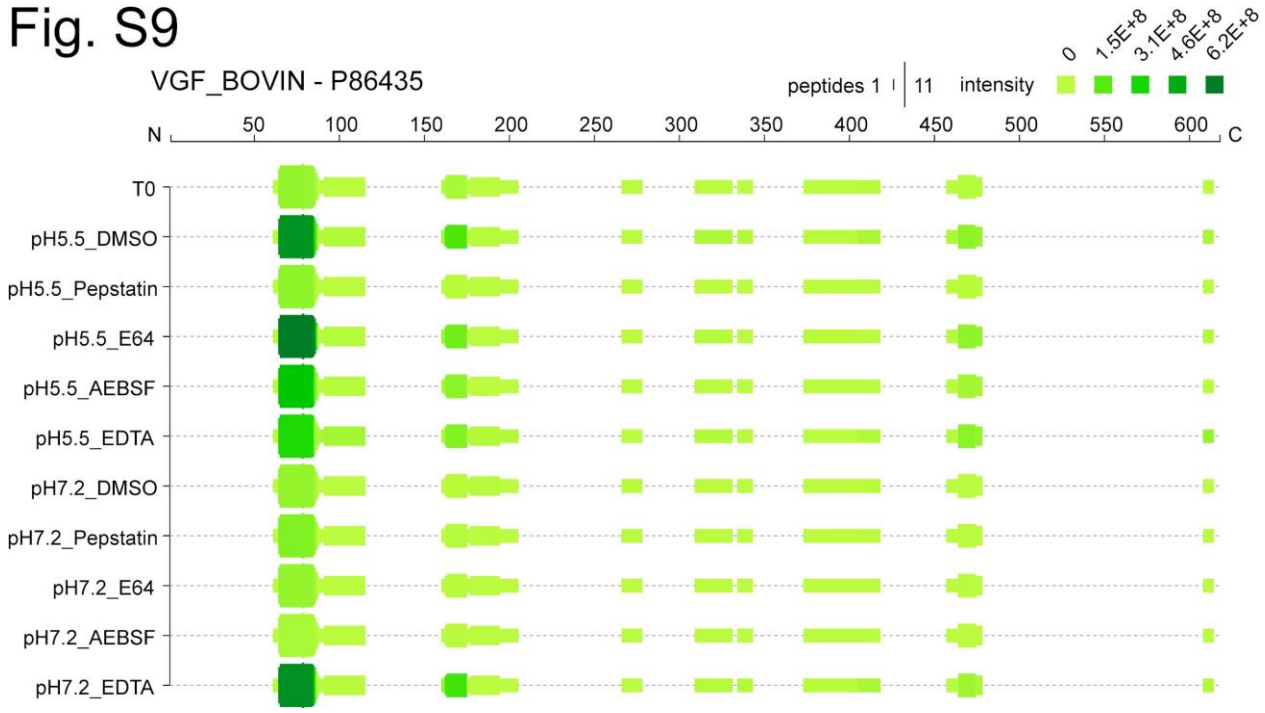

Figure 5.S9 VGF-derived neuropeptidomes at pH 5.5 and pH 7.2, in the presence of pepstatin, E64c, AEBSF, and EDTA protease inhibitors.

Fig. S10

Figure 5.S10 SCG5-derived neuropeptidomes at pH 5.5 and pH 7.2, in the presence of pepstatin, E64c, AEBSF, and EDTA protease inhibitors.

Fig. S8

Figure 5.S8 PCSK1N-derived neuropeptidomes at pH 5.5 and pH 7.2, in the presence of pepstatin, E64c, AEBSF, and EDTA protease inhibitors.

Fig. S11

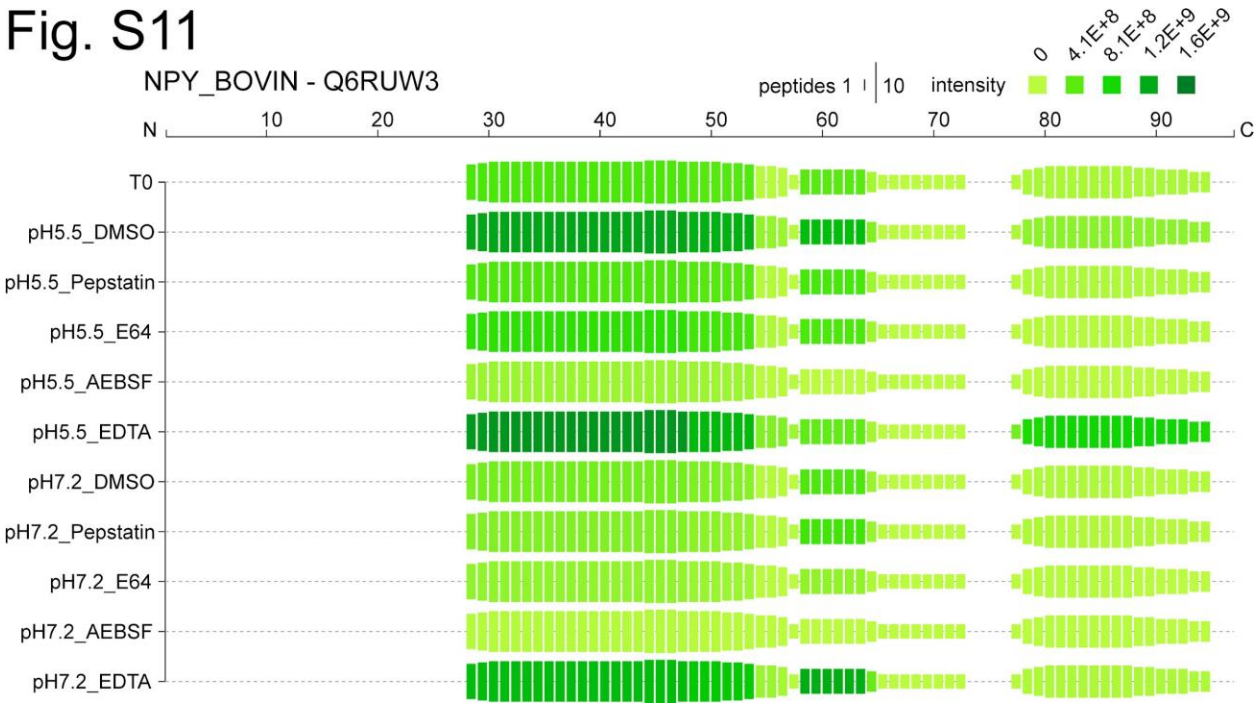

Figure 5.S11 NPY-derived neuropeptidomes at pH 5.5 and pH 7.2, in the presence of pepstatin, E64c, AEBSF, and EDTA protease inhibitors.

Fig. S12

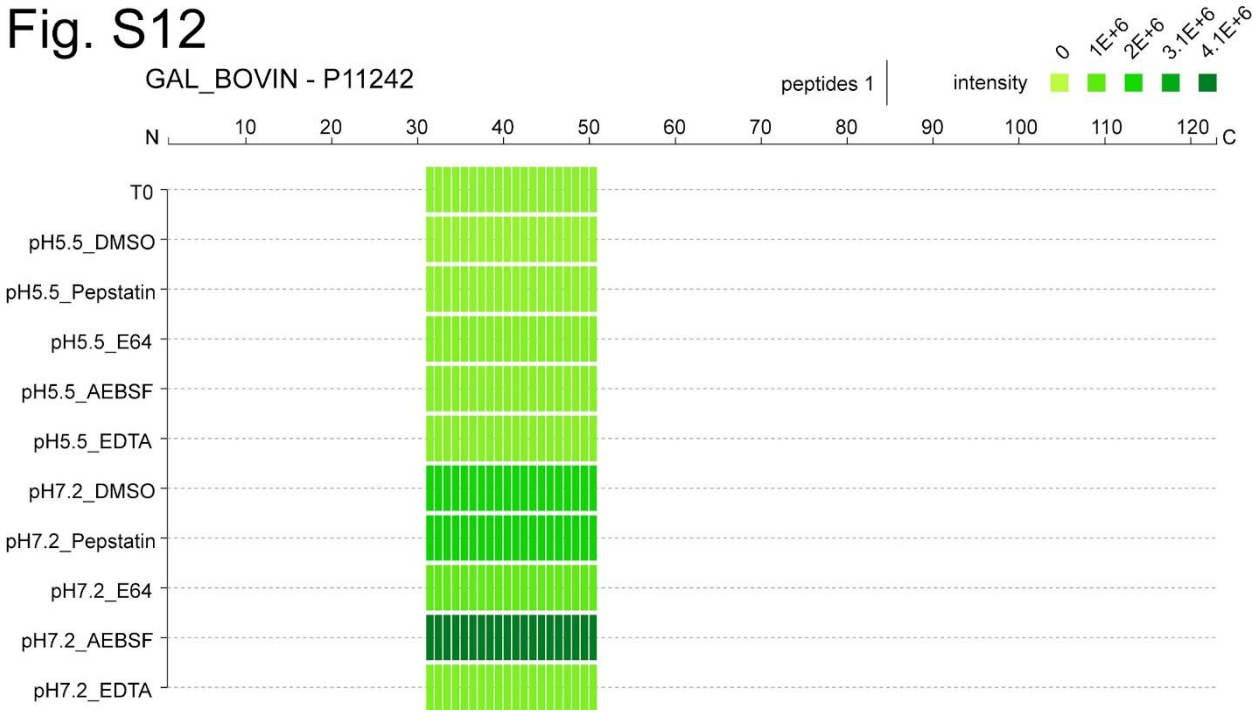

Figure 5.S12 GAL-derived neuropeptidomes at pH 5.5 and pH 7.2, in the presence of pepstatin, E64c, AEBSF, and EDTA protease inhibitors.

Fig. S13

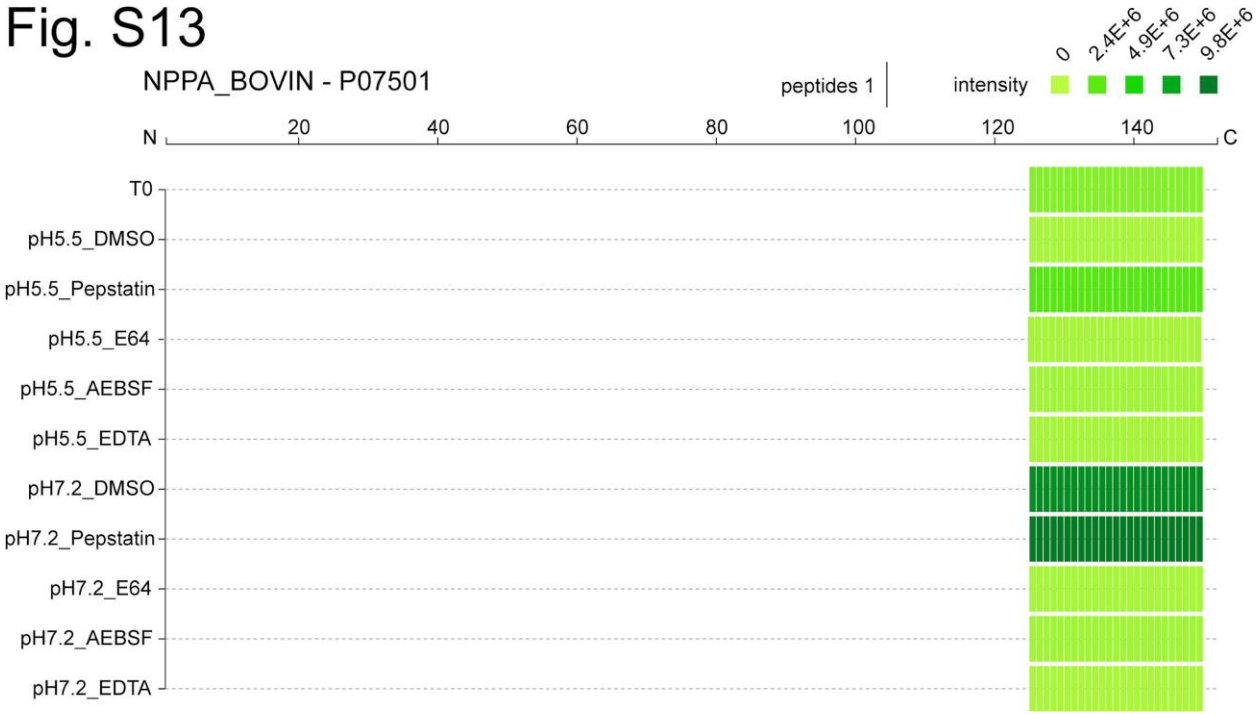

Figure 5.S13 NPPA-derived neuropeptidomes at pH 5.5 and pH 7.2, in the presence of pepstatin, E64c, AEBSF, and EDTA protease inhibitors.

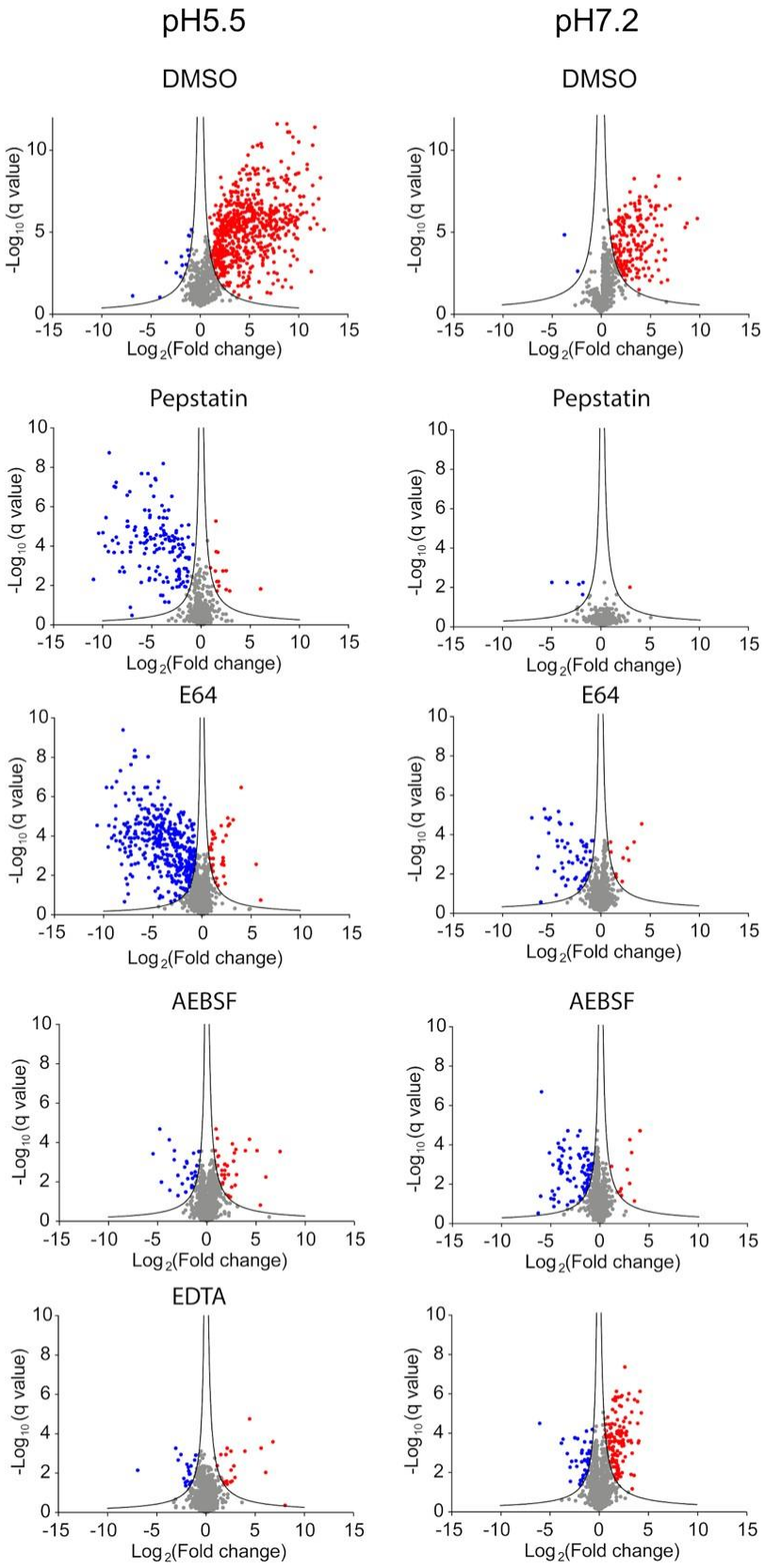

Figure 5.S14 Volcano plots of peptidomics analysis of CG neuropeptidomes generated at pH 5.5 and pH 7.2 in the presence of DMSO (control), pepstatin, E64c, AEBSF, or EDTA.

5.6 References

1. Gupta, N., Bark, S. J., Lu, W. D., Taupenot, L., O'Connor, D. T., Pevzner, P., and Hook, V. (2010) Mass spectrometry-based neuro- peptidomics of secretory vesicles from human adrenal medullary pheochromocytoma reveals novel peptide products of prohormone processing. J. Proteome Res. 9 (10), 5065−75.

2. Podvin, S., Bundey, R., Toneff, T., Ziegler, M., and Hook, V. (2015) Profiles of secreted neuropeptides and catecholamines illustrate similarities and differences in response to stimulation by distinct secretagogues. Mol. Cell. Neurosci. 68, 177−185.

3. Goldstein, D. S. (2010) Adrenal responses to stress. Cell. Mol. Neurobiol. 30 (8), 1433−40.

4. Nankova, B. B., and Sabban, E. L. (1999) Multiple signalling pathways exist in the stress-triggered regulation of gene expression for catecholamine biosynthetic enzymes and several neuropeptides in the rat adrenal medulla. Acta Physiol. Scand. 167 (1), 1−9.

5. Livett, B. G., Marley, P. D., Wan, D. C., and Zhou, X. F. (1990) Peptide regulation of adrenal medullary function. J. Neural. Transm. Suppl. 29, 77−89.

6. Kim, T., Gondré-Lewis, M. C., Arnaoutova, I., and Loh, Y. P. (2006) Dense-core secretory granule biogenesis. Physiology 21 (2), 124−33.

7. Winkler, H., and Fischer-Colbrie, R. (1998) Regulation of the biosynthesis of large dense-core vesicles in chromaffin cells and neurons. Cell. Mol. Neurobiol. 18 (2), 193−209.

8. Zhang, X., Bao, L., and Ma, G. Q. (2010) Sorting of neuropeptides and neuropeptide receptors into secretory pathways. Prog. Neurobiol. 90 (2), 276−83.

9. Merighi, A. (2018) Costorage of High Molecular Weight Neurotransmitters in Large Dense Core Vesicles of Mammalian Neurons. Front. Cell. Neurosci. 12, 272.

10. Kastin, A. J., and Pan, W. (2010) Concepts for biologically active peptides. Curr. Pharm. Des. 16 (30), 3390−3400.

11. van den Pol, A. N. (2012) Neuropeptide transmission in brain circuits. Neuron 76 (1), 98−115.

12. Hook, V., Funkelstein, L., Lu, D., Bark, S., Wegrzyn, J., and Hwang, S. R. (2008) Proteases for processing proneuropeptides into peptide neurotransmitters and hormones. Annu. Rev. Pharmacol. Toxicol. 48, 393−423.

13. Romanova, E. V., and Sweedler, J. V. (2015) Peptidomics for the discovery and characterization of neuropeptides and hormones. Trends Pharmacol. Sci. 36 (9), 579−86.

14. Buchberger, A., Yu, Q., and Li, L. (2015) Advances in Mass Spectrometric Tools for Probing Neuropeptides. Annu. Rev. Anal. Chem. 8, 485−509.

15. Hook, V., Lietz, C. B., Podvin, S., Cajka, T., and Fiehn, O. (2018) Diversity of Neuropeptide Cell-Cell Signaling Molecules Generated by Proteolytic Processing Revealed by Neuropeptidomics Mass Spec- trometry. J. Am. Soc. Mass Spectrom. 29 (5), 807−816.

16. Gupta, N., Bark, S. J., Lu, W. D., Taupenot, L., O'Connor, D. T., Pevzner, P., and Hook, V. (2010) Mass spectrometry-based neuro- peptidomics of secretory vesicles from human adrenal medullary pheochromocytoma reveals novel peptide products of prohormone processing. J. Proteome Res. 9 (10), 5065−75.

17. Seidah, N. G., and Prat, A. (2002) Precursor convertases in the secretory pathway, cytosol and extracellular milieu. Essays Biochem. 38, 79−94.

18. Borges, R., Pereda, D., Beltrán, B., Prunell, M., Rodríguez, M., and Machado, J. D. (2010) Intravesicular factors controlling exocytosis in chromaffin cells. Cell. Mol. Neurobiol. 30 (8), 1359−1364.

19. Loh, Y. P., Tam, W. W., and Russell, J. T. (1984) Measurement of delta pH and membrane potential in secretory vesicles isolated from bovine pituitary intermediate lobe. J. Biol. Chem. 259 (13), 8238−45.

20. Winkler, H., and Westhead, E. (1980) The molecular organization of adrenal chromaffin granules. Neuroscience 5 (11), 1803−1823.

21. Zabłocki, K., Szczepanowska, J., and Duszyński, J. (2005) Extracellular pH modifies mitochondrial control of capacitative calcium entry in Jurkat cells. J. Biol. Chem. 280 (5), 3516−21.

22. Wu, M. H., Urban, J. P., Cui, Z. F., Cui, Z., and Xu, X. (2007) Effect of extracellular pH on matrix synthesis by chondrocytes in 3D agarose gel. Biotechnol. Prog. 23 (2), 430−4.

23. Munteanu, R. E., Staňica, L., Gheorghiu, M., and Gáspár, S. (2018) Measurement of the Extracellular pH of Adherently Growing Mammalian Cells with High Spatial Resolution Using a Voltammetric pH Microsensor. Anal. Chem. 90 (11), 6899−6905.

24. O'Donoghue, A. J., Eroy-Reveles, A. A., Knudsen, G. M., Ingram, J., Zhou, M., Statnekov, J. B., Greninger, A. L., Hostetter, D. R., Qu, G., Maltby, D. A., Anderson, M. O., Derisi, J. L., McKerrow, J. H., Burlingame, A. L., and Craik, C. S. (2012) Global identification of peptidase specificity by multiplex substrate profiling. Nat. Methods 9 (11), 1095−100.

25. Lapek, J. D., Jr, Jiang, Z., Wozniak, J. M., Arutyunova, E., Wang, S. C., Lemieux, M. J., Gonzalez, D. J., and O'Donoghue, A. J. (2019) Quantitative Multiplex Substrate Profiling of Peptidases by Mass Spectrometry. Mol. Cell Proteomics 18 (5), 968−981.

26. Maffioli, E., Jiang, Z., Nonnis, S., Negri, A., Romeo, V., Lietz, C.B., Hook, V., Ristagno, G., Baselli, G., Kistler, E. B., Aletti, F., O'Donoghue, A. J., and Tedeschi, G. (2020) High-Resolution mass Sspectrometry-based approaches for the detection and quantification of peptidase activity in plasma. Molecules 25, 4071.

27. Bibo-Verdugo, B., O'Donoghue, A. J., Rojo-Arreola, L., Craik, C. S., and Garcia-Carreno, F. (2016) Complementary proteomic and biochemical analysis of peptidases in lobster gastric juice uncovers the functional role of individual enzymes in food digestion. Mar. Biotechnol. 18, 201−214.

28. Ivry, S. L., Sharib, J. M., Dominguez, D. A., Roy, N., Hatcher, S.E., Yip-Schneider, M. T., Schmidt, C. M., Brand, R. E., Park, W. G., Hebrok, M., Kim, G. E., O'Donoghue, A. J., Kirkwood, K. S., and Craik, C. S. (2017) Global Protease Activity Profiling Provides Differential Diagnosis of Pancreatic Cysts. Clin. Cancer Res. 23 (16), 4865−4874.

29. Paoletti, A. C., Parmely, T. J., Tomomori-Sato, C., Sato, S., Zhu, D., Conaway, R. C., Conaway, J. W., Florens, L., and Washburn, M. P. (2006) Quantitative proteomic analysis of distinct mammalian Mediator complexes using normalized spectral abundance factors. Proc. Natl. Acad. Sci. U. S. A. 103 (50), 18928−33.

30. Schechter, I. (2005) Mapping of the active site of proteases in the 1960s and rational design of inhibitors/drugs in the 1990s. Curr. Protein Pept. Sci. 6 (6), 501−12. 31. Melzer, I. M., Fernandez, S. B. M., Bösser, S., Lohrig, K., Lewandrowski, U., Wolters, D., Zörnig, M., et al. (2012) The Apaf-1- binding protein Aven is cleaved by Cathepsin D to unleash its anti- apoptotic potential. Cell Death Differ. 19 (9), 1435−1445.

31. Impens, F., Colaert, N., Helsens, K., Ghesquière, B., Timmerman, E., De Bock, P. J., Chain, B. M., Vandekerckhove, J., and Gevaert, K. (2010) A quantitative proteomics design for systematic identification of protease cleavage events. Mol. Cell Proteomics 9 (10), 2327−2333.

32. Choe, Y., Leonetti, F., Greenbaum, D. C., Lecaille, F., Bogyo, M., Brömme, D., Ellman, J. A., and Craik, C. S. (2006) Substrate profiling of cysteine proteases using a combinatorial peptide library identifies functionally unique specificities. J. Biol. Chem. 281 (18), 12824−12832.

33. Grimwood, B. G., Plummer, T. H., Jr, and Tarentino, A. L. (1989) Carboxypeptidase H: a regulatory peptide-processing enzyme produced by human hepatoma Hep G2 cells. J. Biol. Chem. 264 (26), 15662−15667.

34. Vidmar, R., Vizovišek, M., Turk, D., Turk, B., and Fonović, M. (2017) Protease cleavage site fingerprinting by label-free in-gel degradomics reveals pH-dependent specificity switch of legumain. EMBO J. 36 (16), 2455−2465.

35. Biniossek, M. L., Nägler, D. K., Becker-Pauly, C., and Schilling, O. (2011) Proteomic identification of protease cleavage sites characterizes prime and non-prime specificity of cysteine cathepsins B, L, and S. J. Proteome Res. 10 (12), 5363−5373.

36. Ji, L., Wu, H. T., Qin, X. Y., and Lan, R. (2017) Dissecting carboxypeptidase E: properties, functions and pathophysiological roles in disease. Endocr. Connect. 6 (4), R18−R38.

37. Vidak, E., Javorsěk, U., Vizovišek, M., and Turk, B. (2019) Cysteine cathepsins and their extracellular roles: shaping the micro- environment. Cells 8 (3), 264.

38. Khavrutskii, I. V., Compton, J. R., Jurkouich, K. M., and Legler, P. M. (2019) Paired Carboxylic Acids in Enzymes and Their Role in Selective Substrate Binding, Catalysis, and Unusually Shifted pKa Values. Biochemistry 58 (52), 5351−5365.

39. Hiraiwa, M. (1999) Cathepsin A/protective protein: an unusual lysosomal multifunctional protein. Cell. Mol. Life Sci. 56 (11), 894−907.

40. Yasothornsrikul, S., Greenbaum, D., Medzihradszky, K. F., Toneff, T., Bundey, R., Miller, R., Schilling, B., Petermann, I., Dehnert, J., Logvinova, A., Goldsmith, P., Neveu, J. M., Lane, W. S., Gibson, B., Reinheckel, T., Peters, C., Bogyo, M., and Hook, V. (2003) Cathepsin L in secretory vesicles functions as a prohormone-processing enzyme for production of the enkephalin peptide neurotransmitter. Proc. Natl. Acad. Sci. U. S. A. 100 (16), 9590−5.

41. Funkelstein, L., Toneff, T., Mosier, C., Hwang, S. R., Beuschlein, F., Lichtenauer, U. D., Reinheckel, T., Peters, C., and Hook, V. (2008) Major role of cathepsin L for producing the peptide hormones ACTH, beta-endorphin, and alpha-MSH, illustrated by protease gene knockout and expression. J. Biol. Chem. 283 (51), 35652−9.

42. Funkelstein, L., Toneff, T., Hwang, S. R., Reinheckel, T., Peters, C., and Hook, V. (2008) Cathepsin L participates in the production of neuropeptide Y in secretory vesicles, demonstrated by protease gene knockout and expression. J. Neurochem. 106 (1), 384−91.

43. Beinfeld, M. C., Funkelstein, L., Foulon, T., Cadel, S., Kitagawa, K., Toneff, T., Reinheckel, T., Peters, C., and Hook, V. (2009) Cathepsin L plays a major role in cholecystokinin production in mouse brain cortex and in pituitary AtT-20 cells: protease gene knockout and inhibitor studies. Peptides 30 (10), 1882−91.

44. Minokadeh, A., Funkelstein, L., Toneff, T., Hwang, S. R., Beinfeld, M., Reinheckel, T., Peters, C., Zadina, J., and Hook, V. (2010) Cathepsin L participates in dynorphin production in brain cortex, illustrated by protease gene knockout and expression. Mol. Cell. Neurosci. 43 (1), 98−107.

45. Krieger, T. J., and Hook, V. Y. (1992) Purification and characterization of a cathepsin D protease from bovine chromaffin granules. Biochemistry 31 (17), 4223−31.

46. Graf, L., Kenessey, A., Patthy, A., Grynbaum, A., Marks, N., and Lajtha, A. (1979) Cathepsin D generates gamma-endorphin from beta- endorphin. Arch. Biochem. Biophys. 193 (1), 101−109.

47. Wei, E. Q., Kudo, T., and Inoki, R. (1990) Pharmacological and biochemical study on the mechanism of enkephalin production in rat dental pulp. J. Osaka Univ. Dent. Sch. 30, 8−30.

48. Marks, N., Berg, M. J., and Benuck, M. (1986) Preferential action of rat brain cathepsin B as a peptidyl dipeptidase converting pro-opioid oligopeptides. Arch. Biochem. Biophys. 249 (2), 489−499.

49. Marks, N., and Berg, M. J. (1987) Rat brain cathepsin L: characterization and differentiation from cathepsin B utilizing opioid peptides. Arch. Biochem. Biophys. 259 (1), 131−143.

50. Marks, N., Sachs, L., and Stern, F. (1981) Conversion of Met-enkephalin-Arg6-Phe7 by a purified brain carboxypeptidase (cathepsin A). Peptides 2 (2), 159−164.

51. Kecorius, E., Small, D. H., and Livett, B. G. (1988) Characterization of a dipeptidyl aminopeptidase from bovine adrenal medulla. J. Neurochem. 50 (1), 38−44.

52. Fricker, L. D. (2018) Carboxypeptidase E and the Identification of Novel Neuropeptides as Potential Therapeutic Targets. Adv. Pharmacol. 82, 85−102.

53. Sanman, L. E., van der Linden, W. A., Verdoes, M., and Bogyo, M. (2016) Bifunctional probes of cathepsin protease activity and pH reveal alterations in endolysosomal pH during bacterial infection. Cell Chem. Biol. 23 (7), 793−804.

54. Yadati, T., Houben, T., Bitorina, A., and Shiri-Sverdlov, R. (2020) The ins and outs of cathepsins: Physiological function and role in disease management. Cells 9 (7), 1679.

55. Blum, J. S., Fiani, M. L., and Stahl, P. D. (1991) Proteolytic cleavage of ricin A chain in endosomal vesicles. Evidence for the action of endosomal proteases at both neutral and acidic pH. J. Biol. Chem. 266 (33), 22091−22095.

56. Smeekens, S. P., Chan, S. J., and Steiner, D. F. (1992) The biosynthesis and processing of neuroendocrine peptides: identification of proprotein convertases involved in intravesicular processing. Prog. Brain Res. 92, 235−246.

57. Smeekens, S. P., and Steiner, D. F. (1990) Identification of a human insulinoma cDNA encoding a novel mammalian protein structurally related to the yeast dibasic processing protease Kex2. J. Biol. Chem. 265 (6), 2997−3000.

58. Seidah, N. G., Gaspar, L., Mion, P., Marcinkiewicz, M., Mbikay, M., and Chrétien, M. (1990) cDNA sequence of two distinct pituitary proteins homologous to Kex2 and furin gene products: tissue-specific mRNAs encoding candidates for pro-hormone processing proteinases. DNA Cell Biol. 9 (6), 415−24.

59. Shennan, K. I., Smeekens, S. P., Steiner, D. F., and Docherty, K. (1991) Characterization of PC2, a mammalian Kex2 homologue, following expression of the cDNA in microinjected Xenopus oocytes. FEBS Lett. 284 (2), 277−80.

60. Thomas, L., Leduc, R., Thorne, B. A., Smeekens, S. P., Steiner, D. F., and Thomas, G. (1991) Kex2-like endoproteases PC2 and PC3 accurately cleave a model prohormone in mammalian cells: evidence for a common core of neuroendocrine processing enzymes. Proc. Natl. Acad. Sci. U. S. A. 88 (12), 5297−301.

61. Miller, R., Aaron, W., Toneff, T., Vishnuvardhan, D., Beinfeld, M. C., and Hook, V. Y. (2003) Obliteration of alpha-melanocyte- stimulating hormone derived from POMC in pituitary and brains of PC2-deficient mice. J. Neurochem. 86 (3), 556−63.

62. Smeekens, S. P., Montag, A. G., Thomas, G., Albiges-Rizo, C., Carroll, R., Benig, M., Phillips, L. A., Martin, S., Ohagi, S., and Gardner, P. (1992) Proinsulin processing by the subtilisin-related proprotein convertases furin, PC2, and PC3. Proc. Natl. Acad. Sci. U. S. A. 89 (18), 8822−6.

63. Bailyes, E. M., Bennett, D. L., and Hutton, J. C. (2017) Proprotein-processing endopeptidases of the insulin secretory granule. Enzyme 45, 301−13.

64. Peinado, J. R., Li, H., Johanning, K., and Lindberg, I. (2003) Cleavage of recombinant proenkephalin and blockade mutants by prohormone convertases 1 and 2: an in vitro specificity study. J. Neurochem. 87 (4), 868−78.

65. Pan, H., Nanno, D., Che, F. Y., Zhu, X., Salton, S. R., Steiner, D. F., Fricker, L. D., and Devi, L. A. (2005) Neuropeptide processing profile in mice lacking prohormone convertase-1. Biochemistry 44 (12), 4939−48.

66. Miller, R., Toneff, T., Vishnuvardhan, D., Beinfeld, M., and Hook, V. Y. (2003) Selective roles for the PC2 processing enzyme in the regulation of peptide neurotransmitter levels in brain and peripheral neuroendocrine tissues of PC2 deficient mice. Neuropeptides 37 (3), 140−8.

67. Rouillé, Y., Duguay, S. J., Lund, K., Furuta, M., Gong, Q., Lipkind, G., Oliva, A. A., Jr, Chan, S. J., and Steiner, D. F. (1995) Proteolytic processing mechanisms in the biosynthesis of neuroendocrine peptides: the subtilisin-like proprotein convertases. Front. Neuroendocrinol. 16, 322−61.

68. Seidah, N. G., Sadr, M. S., Chrétien, M., and Mbikay, M. (2013) The multifaceted proprotein convertases: their unique, redundant, complementary, and opposite functions. J. Biol. Chem. 288 (30), 21473−81.

69. Wegrzyn, J. L., Bark, S. J., Funkelstein, L., Mosier, C., Yap, A., Kazemi-Esfarjani, P., La Spada, A. R., Sigurdson, C., O'Connor, D. T., and Hook, V. (2010) Proteomics of dense core secretory vesicles reveal distinct protein categories for secretion of neuroeffectors for cell-cell communication. J. Proteome Res. 9 (10), 5002−24.

70. Wegrzyn, J., Lee, J., Neveu, J. M., Lane, W. S., and Hook, V. (2007) Proteomics of neuroendocrine secretory vesicles reveal distinct functional systems for biosynthesis and exocytosis of peptide hormones and neurotransmitters. J. Proteome Res. 6 (5), 1652−65.

71. Gratzl, M., Krieger-Brauer, H., and Ekerdt, R. (1981) Latent acetylcholinesterase in secretory vesicles isolated from adrenal medulla. Biochim. Biophys. Acta, Biomembr. 649, 355−66.

72. Birinci, Y., Preobraschenski, J., Ganzella, M., Jahn, R., and Park, Y. (2020) Isolation of large dense-core vesicles from bovine adrenal medulla for functional studies. Sci. Rep. 10 (1), 7540.

73. Rappsilber, J., Mann, M., and Ishihama, Y. (2007) Protocol for micro-purification, enrichment, pre-fractionation and storage of peptides for proteomics using StageTips. Nat. Protoc. 2 (8), 1896−906.

74. Rawlings, N. D., Barrett, A. J., and Bateman, A. (2010) MEROPS: the peptidase database. Nucleic Acids Res. 38 (suppl_1), D227−D233.

75. Lysyk, L., Brassard, R., Arutyunova, E., Siebert, V., Jiang, Z., Takyi, E., Morrison, M., Young, H. S., Lemberg, M. K., O'Donoghue, A. J., and Lemieux, M. J. (2021) Insights into the catalytic properties of the mitochondrial rhomboid protease PARL. J. Biol. Chem. 296, 100383.

76. Mi, H., Muruganujan, A., Huang, X., Ebert, D., Mills, C., Guo, X., and Thomas, P. D. (2019) Protocol Update for large-scale genome and gene function analysis with the PANTHER classification system (v. 14.0). Nat. Protoc. 14 (3), 703−721.

77. Kim, Y., Bark, S., Hook, V., and Bandeira, N. (2011) NeuroPedia: neuropeptide database and spectral library. Bioinformatics 27 (19), 2772−3.

78. Xiao, Y., Hsiao, T. H., Suresh, U., Chen, H. I., Wu, X., Wolf, S. E., and Chen, Y. (2014) A novel significance score for gene selection and ranking. Bioinformatics 30 (6), 801−7.

79. Colaert, N., Helsens, K., Martens, L., Vandekerckhove, J., and Gevaert, K. (2009) Improved visualization of protein consensus sequences by iceLogo. Nat. Methods 6 (11), 786−7.

80. Manguy, J., Jehl, P., Dillon, E. T., Davey, N. E., Shields, D. C., and Holton, T. A. (2017) Peptigram: A Web-Based Application for Peptidomics Data Visualization. J. Proteome Res. 16 (2), 712−719.

5.7 Copyright Permission

CHAPTER 6 – Distinct Dibasic Cleavage Specificities of Neuropeptide-Producing Cathepsin L and Cathepsin V Cysteine Proteases Compared to PC1/3 and PC2 Serine Proteases

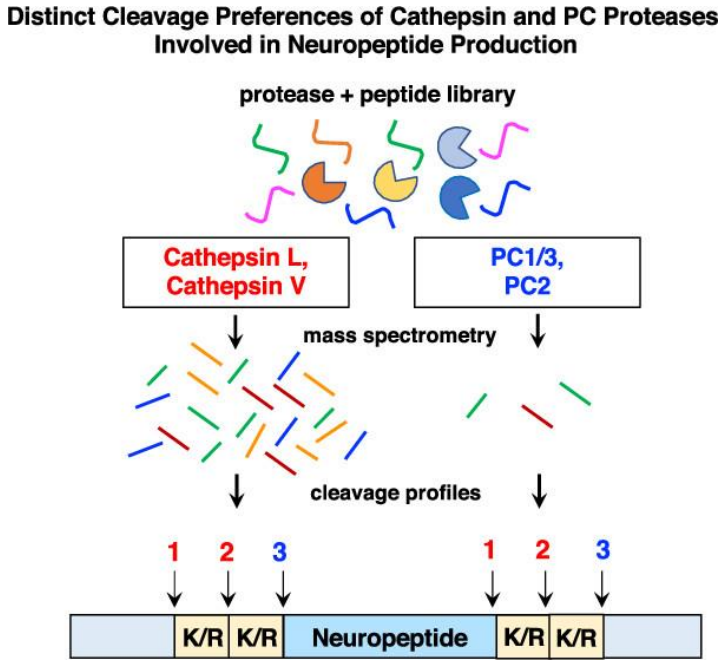

Chapter 6 Graphical Abstract. Neuropeptides, functioning as peptide neurotransmitters and hormones, are generated from proneuropeptide precursors by proteolytic processing at dibasic residue sites (i.e., KR, RK, KK, RR). The cysteine proteases cathepsin L and cathepsin V, combined with the serine proteases proprotein convertases 1 and 2 (PC1/3 and PC2), participate in proneuropeptide processing to generate active neuropeptides. To compare the dibasic cleavage properties of these proteases, this study conducted global, unbiased substrate profiling of these processing proteases using a diverse peptide library in multiplex substrate profiling by mass spectrometry (MSP-MS) assays. MSP-MS utilizes a library of 228 14-mer peptides designed to contain all possible protease cleavage sites, including the dibasic residue sites of KR, RK, KK, and RR. The comprehensive MSP-MS analyses demonstrated that cathepsin L and cathepsin V cleave at the N-terminal side and between the dibasic residues (e.g., ↓K↓R, ↓R↓K, and K↓K), with a preference for hydrophobic residues at the P2 position of the cleavage site. In contrast, the serine proteases PC1/3 and PC2 displayed cleavage at the C-terminal side of dibasic residues of a few peptide substrates. Further analyses with a series of dipeptide-AMC and tripeptide-AMC substrates containing variant dibasic sites with hydrophobic P2 residues indicated the preferences of cathepsin L and cathepsin V to cleave between dibasic residue sites with preferences for flanking hydrophobic residues at the P2 position consisting of Leu, Trp, Phe, and Tyr. Such hydrophobic amino acids reside in numerous proneuropeptides such as pro-NPY and proenkephalin that are known to be processed by cathepsin L. Notably, cathepsin L displayed the highest specific activity that was 10-, 64-, and 1268-fold greater than cathepsin V, PC1/3, and PC2, respectively. Peptide-AMC substrates with dibasic residues confirmed that PC1/3 and P2 cleaved almost exclusively at the C-terminal side of dibasic residues. These data demonstrate distinct dibasic cleavage site properties and a broad range of proteolytic activities of cathepsin L and cathepsin V, compared to PC1/3 and PC2, which participate in producing neuropeptides for cell–cell communication.

6.1 Introduction

Neuropeptides are short peptides, typically 3–40 residues in length, that are essential mediators of cell–cell signaling. They function as neurotransmitters in the nervous system and as peptide hormones in the endocrine system. (1−4) Distinct amino acid sequences of neuropeptides are key to their selective regulation of target cell receptors and neuroendocrine functions. For example, the brain neuropeptides enkephalin, β-endorphin, and dynorphin function as endogenous opioid regulators of pain relief. (5−7) Galanin regulates cognitive brain functions. (8,9) Corticotropin-releasing hormone (CRF) in the brain regulates stress and controls pituitary ACTH production involved in adrenal glucocorticoid production. (10,11) The endocrine hormones insulin and glucagon regulate glucose metabolism. (12,13) Neuropeptides are dynamic regulators of cell–cell communication for normal neuroendocrine functions, and neuropeptide dysregulation participates in human diseases. (14)

Neuropeptides are synthesized as inactive proneuropeptide precursor proteins (also known as prohormones in the endocrine system) within secretory vesicles which release active neuropeptides for cell–cell communication. (1−4,15) The inactive proneuropeptide precursors undergo proteolytic processing to generate active peptides. Within precursor proteins, neuropeptide sequences are typically flanked by the dibasic residues Lys-Arg, Arg-Lys, Lys-Lys, and Arg-Arg (K-R, R-K, K-K, and R-R) and several processing proteases have been demonstrated to cleave at such dibasic sites for neuropeptide production. These enzymes consist of cathepsin L and cathepsin V cysteine proteases (1,2) and the proprotein convertases 1/3 (PC1/3) and PC2 serine proteases. (1−3) Evidence for participation of these proteases in neuropeptide production has been shown by gene knockout of these enzymes that results in reduced production of many neuropeptides examined by biochemical and molecular cellular studies of neuropeptide

biosynthesis. (1−3) It is of interest that the cysteine protease cathepsin V is a human-specific protease (16−19) and, thus, represents a unique human-specific protease mechanism for neuropeptide production. (19)

Studies with several neuropeptide precursor-related substrates have suggested differential cleavage specificities of cathepsin L compared to PC1/3 and PC2 for dibasic residues. (1−3) Cathepsin L cleaves enkephalin-containing peptide intermediates at the N-terminal side and between dibasic residues for the production of enkephalin (20) and cleaves pro-NPY at the N-terminal side of dibasic residues for NPY production. (21) In contrast, PC1/3 and PC2 proteases cleave at the C-terminal side of the dibasic residues of proneuropeptides including proinsulin, (22−24) proenkephalin (PE), (25,26) and others. (27,28) These data suggest differential cleavage specificities at dibasic residues for these proneuropeptide processing proteases.

To evaluate the hypothesis that distinct cleavage specificities at dibasic residues may exist for cathepsin L and cathepsin V compared to PC1/3 and PC2, this study investigated the cleavage properties of these proteases by the strategy of global, unbiased multiplex substrate profiling by mass spectrometry (MSP-MS). (29,30) Furthermore, MSP-MS analyses allow evaluation of the overall protease cleavage preferences using a peptide library as a model for diverse cleavage sites. MSP-MS utilizes a library of 228 14-mer peptides designed to have maximum neighbor and near-neighbor amino acid diversity. Cleavage of any of the 2964 peptide bonds within this library can be detected and quantified by mass spectrometry. Cathepsin L and V were found to cleave at 241 and 163 sites within this peptide library, respectively, while PC1/3 and PC2 cleaved only 4 and 1, respectively. These data revealed that cathepsin L and cathepsin V cleave between and at the N-terminal side of dibasic residues, whereas PC1/3 and PC2 cleave at the C-terminal side of dibasic

residues. Analyses with a series of dipeptide-AMC and tripeptide-AMC fluorogenic substrates further demonstrated the distinct dibasic cleavage properties of these proteases. Furthermore, cathepsins L and V displayed high preferences for peptide-AMC substrates with hydrophobic residues in the P2 position adjacent to the dibasic sites. The distinct dibasic cleavage sites are important for determining the subsequent exopeptidases, aminopeptidase, and carboxypeptidases, needed for completion of neuropeptide production. Overall, the findings of this study demonstrate the different dibasic residue cleavage properties of cathepsin L and cathepsin V compared to the PC1/3 and PC2 proteases, which participate in neuropeptide production.

6.2 Results

6.2.1 MSP-MS Strategy for the Substrate Cleavage Profiling of Proneuropeptide Processing Enzymes

This study compared the dibasic cleavages of cathepsin L and cathepsin V with that of PC1/3 and PC2 that are utilized for proneuropeptide processing (Figure 6.1a). MSP-MS was conducted by incubating each of these proteases with the 228 14-mer peptide library at pH 5.5, the intravesicular pH within secretory vesicles where proneuropeptide processing occurs, (31−33) followed by nano liquid chromatography tandem mass spectrometry (nano-LC−MS/MS) to identify and quantify peptide cleavage products (Figure 6.1b). The peptide library contains numerous substrates with the dibasic residues of KR, RK, RR, and KK. Peptide cleavage sites were analyzed for the frequency of residues at the P4 to P4′ positions of the P1-↓P1′ cleavage sites. This data was used to design peptide-AMC substrates for further evaluation of cleavage sites at dibasic residue peptide sequences (Figure 6.1b).

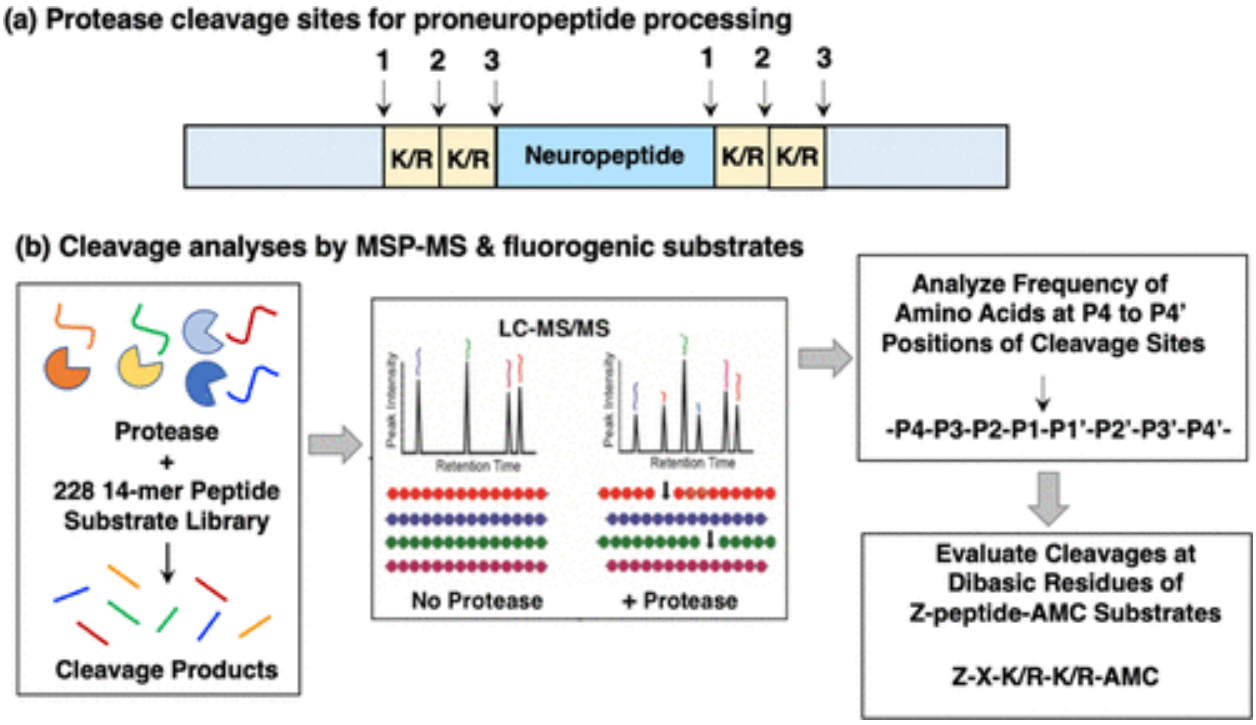

Figure 6.1 Scheme for the cleavage profiling of the proneuropeptide processing proteases cathepsin L, cathepsin V, PC1/3, ad PC2, by MSP-MS and analyses by fluorogenic peptide substrates. (a) Proneuropeptides undergo proteolytic processing at dibasic residue sites. Neuropeptides are generated from proneuropeptide precursors that require proteolytic processing at dibasic sites (K/R-K/R) to generate active neuropeptides. (b) Strategy for the cleavage profiling of cathepsin L, cathepsin V, PC1/3, and PC2 processing enzymes by MSP-MS and fluorogenic substrates. The cleavage profile properties of cathepsin L and cathepsin V cysteine proteases, combined with PC1/3 and PC2 serine proteases, were evaluated by global, unbiased multiplex substrate profiling by mass spectrometry (MSP-MS) and fluorogenic peptide-AMC substrates containing variant dibasic residue sequences. For MSP-MS, the 228 peptide library was incubated with each of the processing proteases (as described in the Methods section), and peptide cleavage products were subjected to nano-LC–MS/MS tandem mass spectrometry for identification and quantification. Peptide cleavage products were analyzed for the frequency of each of the different amino acid residues at positions P4–P4′ and at the cleaved P1↓P1′ cleavage site. Based on MSP-MS results, peptide-AMC substrates were designed to further assess the dibasic cleavage site preferences of these proteases.

6.2.2 MSP-MS Analyses of Human Cathepsin L and Cathepsin V Reveal Cleavage Sites between Dibasic Residues and at the N-Terminal Side of Dibasic Residues within Peptide Substrates

Cathepsin L and cathepsin V cleavage products were generated from the peptide library during 60 min incubation, illustrated by volcano plots showing the $\log_2$-fold change of the quantities of peptide products compared to a control assay that contained no enzyme activity

(Figure 6.2a,b). Cathepsins L and V cleaved at 241 and 163 sites within the peptide library, respectively. The endopeptidase cleavage properties of cathepsin L and cathepsin V were illustrated by the cleavages that occurred at peptide bonds of 14-mer substrates (Figure 6.2c,d). In general, cleavage sites were located between residues 2 and 12 with few peptides being cleaved between residues 1 and 2 or between residues 12 and 14 (Figure 6.2c,d). This cleavage profile indicates that cathepsins L and V have endopeptidase specificity, without exopeptidase activity for removal of N- or C-terminal residues.

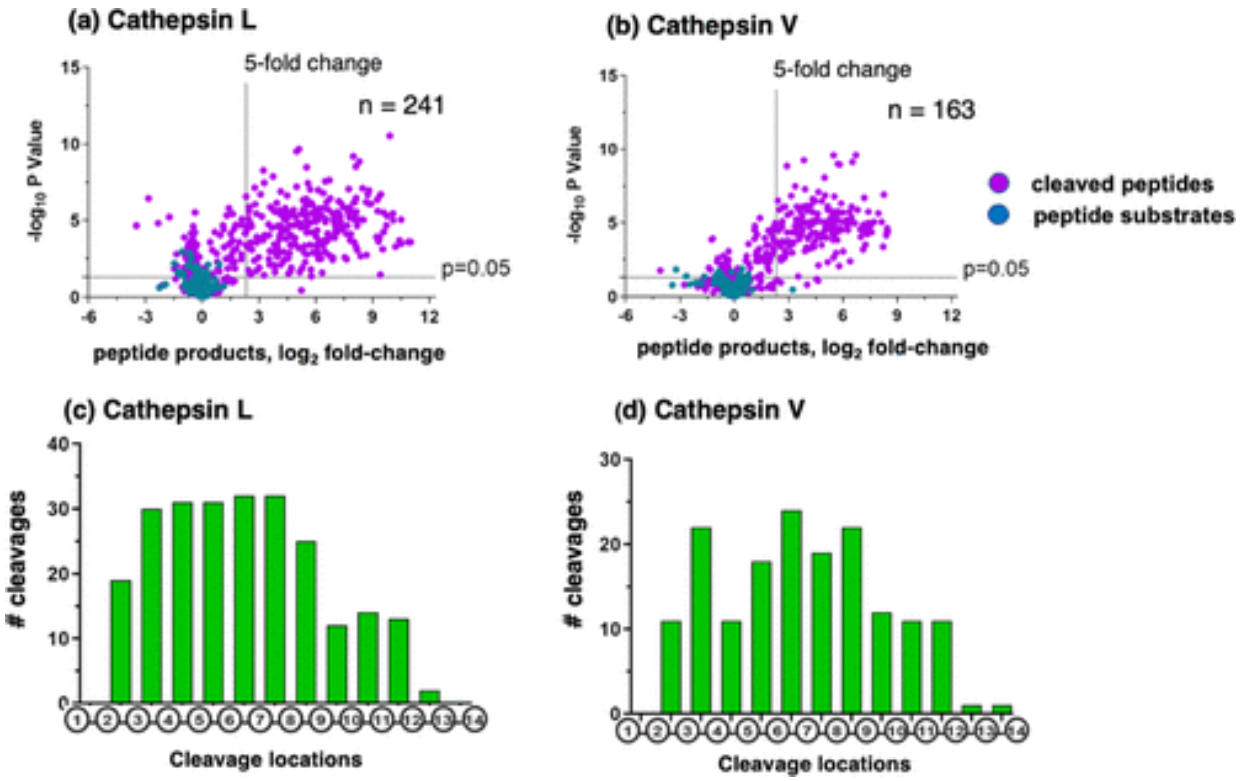

Figure 6.2 Cathepsin L and cathepsin V peptide cleavage profiling analyzed by multiplex substrate profiling by mass spectrometry (MSP-MS). (a,b) Volcano plots of cleaved peptides generated by cathepsin L (a) and cathepsin V (b). The $\log_2$ ratios of relative quantities of peptide products generated by cathepsin L or cathepsin V (60 min incubation at pH 5.5) compared to no enzyme activity controls are illustrated with $-\log_{10}p$ values. Peptide products generated with at least a 5-fold change above no enzyme activity controls and with $p < 0.05$ numbered 241 and 163 peptides in panels "a" and "b", respectively, representing 8.1 and 7.9%, respectively, of the entire number of 2964 cleavage sites among the 228 peptides of the library. Peptide sequences were analyzed for the frequencies of amino acid residues at the P4–P4′ positions of the P1–↓P1′cleavage site. (c,d) Cleavage positions of 14-mer peptide substrates for cathepsin L (c) and cathepsin V (d). The number of cleavages by cathepsin L and cathepsin V at each of the peptide bonds of the 14-mer peptide substrates are illustrated.

The frequencies of amino acid residues at P4–P4′ positions adjacent to P1–↓P1′ cleavage sites were represented by heat map and IceLogo analyses (Figure 6.3). The heat maps display the relative frequencies of residues at each of the cleavage positions as Z-scores, comparing protease cleavages with that of the reference peptide library (Figure 6.3a,b). Cathepsin L and cathepsin V displayed preferences for basic residues, Lys and Arg, at P1 and P1′ positions. Cathepsin L displayed a preference for Lys and Arg at the P1 position (Z-scores of 5.0 and 2.1, respectively) and the P1′ position (Z-scores of 2.6 and 3.0, respectively). Cathepsin V showed a preference for Lys at the P1 position (Z-score of 6.8) and some preference for Arg at the P1 position (Z-score of 0.7); at the P1′ position, cathepsin V showed preferences for Lys and Arg (Z-scores of 2.5 and 1.8, respectively). At the P2 position, both cathepsin L and cathepsin V showed strong preferences for the hydrophobic residues of Leu, Val, Phe, Trp, and Tyr.

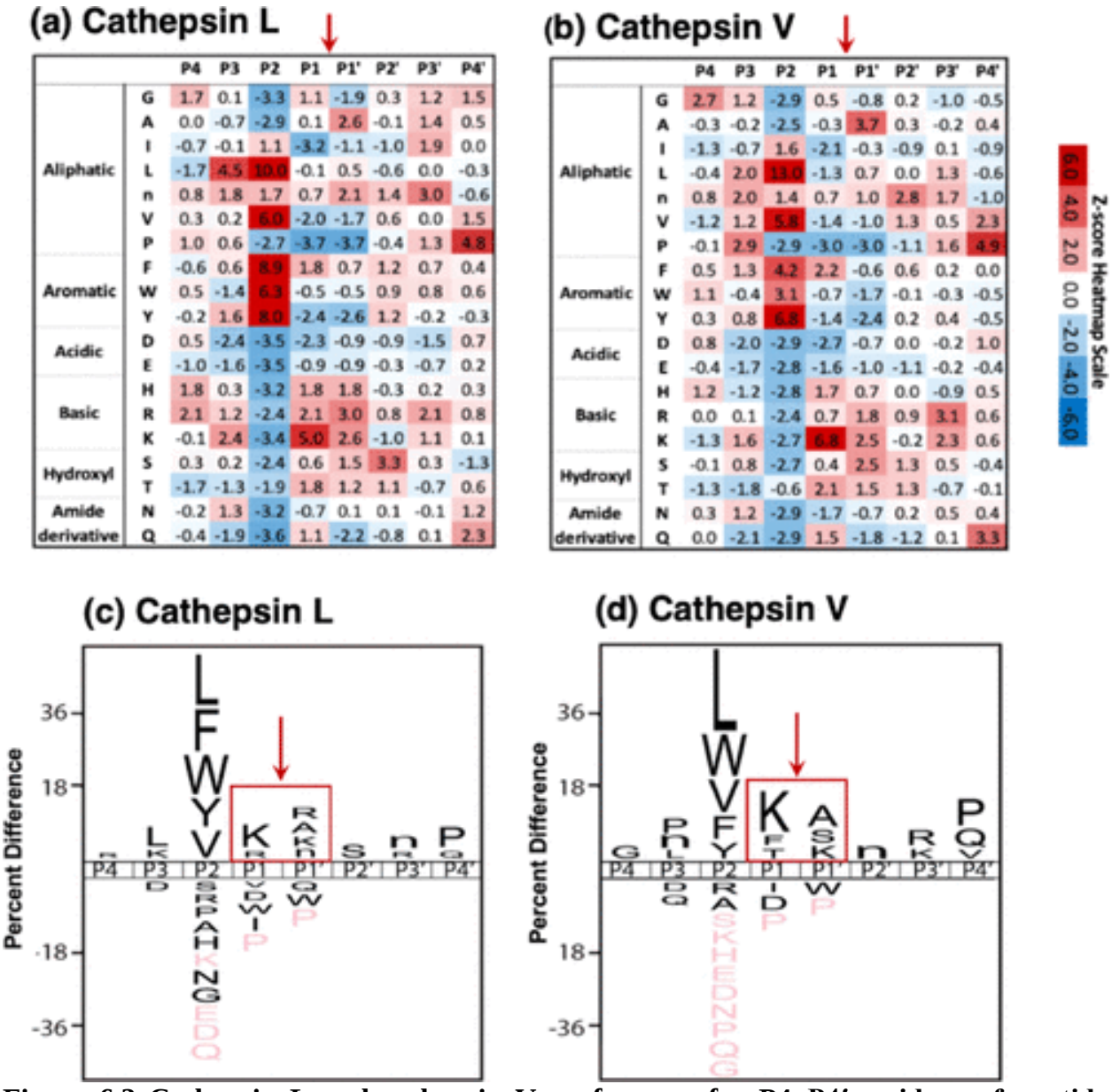

Figure 6.3 Cathepsin L and cathepsin V preferences for P4–P4′ residues of peptide cleavage sites in MSP-MS analyses. (a, b) Heat maps of amino acids preferred at cleavages sites. The peptide library cleavage data for cathepsin L (panel a) and cathepsin V (panel b) shows the frequencies of amino acid residues at each of the P4 to the P4′ positions of cleaved peptides, shown as the heat maps of Z-scores (explained in the Methods section) that compare protease cleavages with that of the reference peptide library. (c, d) IceLogo of cathepsin L and cathepsin V for preferred cleavages at P4–P4′ residues. Cathepsin L (panel c) and cathepsin V (panel d) cleavage data is illustrated by iceLogo. IceLogo shows the relative frequency of the preferred residues at the P1–↓P1′ cleavage site and at the P4–P4′ residues. Black letters above the line of P4–P4′ positions indicate preferred amino acid residues of the protease with $p < 0.05$, compared to the reference (negative data) of all possible residues at each position. Pink letters indicate residues that were never found at the indicated cleavage position.

IceLogo analyses illustrated the relative frequency of individual amino acids at P4–P4′ positions ($p < 0.05$) (Figure 6.3c,d). The cleavage of peptides by cathepsins L and V was largely driven by the P2 residue, where 62 and 63% of all cleavage sites have either Leu, Phe, Trp, Tyr, or Val at this position, respectively. Outside of the P2 position, cathepsin L frequently cleaved peptides with Lys and Arg at P1, and Lys, Arg, Ala, and norleucine (n) at P1′ while cathepsin V cleaved peptides with Lys, Phe, and Thr at P1 and Lys, Ser, and Ala at P1′. In general, these data show that cathepsin L and cathepsin V possess similar cleavage specificities, consistent with their high homology. (16−19)

Among the dibasic peptides of the library, cathepsin L cleaved between the dibasic residues of K↓R and R↓K, and at the N-terminal side of ↓KR and ↓RK dibasic sites, and the hydrophobic residues of Tyr and Trp and norleucine were present in the P2 positions of the cathepsin L dibasic cleavage sites (Table 6.1). Cathepsin V cleaved the peptides of the library at dibasic residues between K↓R, R↓K, and K↓K; furthermore, the preferred P2 residues of these cleaved peptides consisted of Tyr and Phe hydrophobic residues, as well as Ile (Table 6.1).

Table 6.1 Dibasic Residue Cleavages of Peptide Substrates by Cathepsin L and Cathepsin V Cysteine Proteases and PC1/3 and PC2 Serine Proteases[a]

protease	peptide	fold change (60 min)
cathepsin L	GnYYK↓RFnAHWVGI	142
	TPHHVNWYK↓RAPNQ	46
	EGADIWYR↓KHSHQL	5
	TPHHVNWY↓KRAPNQ	5
	LGWHAnF↓RKYPInA	124
cathepsin V	GnYYK↓RFnAHWVGI	14
	TPHHVNWYK↓RAPNQ	6
	LGWHAnFR↓KYPInA	12
	DAWAPnVIK↓KESSI	32
PC1/3	GnYYKR↓FnAHWVGI	395
	IEPPWVDSHAKR↓Nn	23
	VDYIEHKDQVRR↓nN	14
PC2	YWnSTHLAGKR↓RDW	34

[a]Dibasic peptide cleavage sites of peptide substrates are illustrated for cathepsin L, cathepsin V, PC1/3, and PC2. Cleavage sites were determined by the identification and quantification of cleaved peptide products. Cleaved peptide products analyzed were the NH_2-terminal peptide fragments, except for EGADIWR↓KHSHQL, where its COOH-terminal peptide product was identified and quantified. The fold changes of the cleaved peptide product generated at 60 min compared to 0 min controls are shown. The non-natural amino acid norleucine is indicated as lowercase "*n*."

Overall, the unbiased, global substrate cleavage profiling by MSP-MS demonstrated that cathepsin L and cathepsin V cleave between dibasic residues or at the N-terminal side of dibasic residues. In both scenarios, there is a strong preference for hydrophobic residues at the P2 position adjacent to the dibasic sites.

6.2.3 MSP-MS Analyses of PC1/3 and PC2 Indicates Cleavage at the C-Terminal Side of Dibasic Residues

MSP-MS analyses of human PC1/3 and PC2 proteases showed that PC1/3 cleaved four peptide substrates, while PC2 cleaved only one peptide, shown by Volcano plots (Figure 6.4). PC1/3 cleaved at the C-terminal side of KR↓ and RR↓ of three peptide substrates (Table 6.1). PC2 cleaved one peptide of the library, YWnSTHLAGKR↓RDW, at the C-terminal side of KR↓ residues, present within the tribasic Lys-Arg-Arg site (Table 6.1). The Gly residue at the P3 position of the KR↓ cleavage site is typical of neuropeptides that undergo C-terminal amidation. (34) The low number of peptides within the library cleaved by PC1/3 and PC2 suggests their low activity. Overall, PC1/3 and PC2 demonstrated their selectivity for cleaving at the C-terminal side of KR↓ and RR↓ dibasic residues of several substrates.

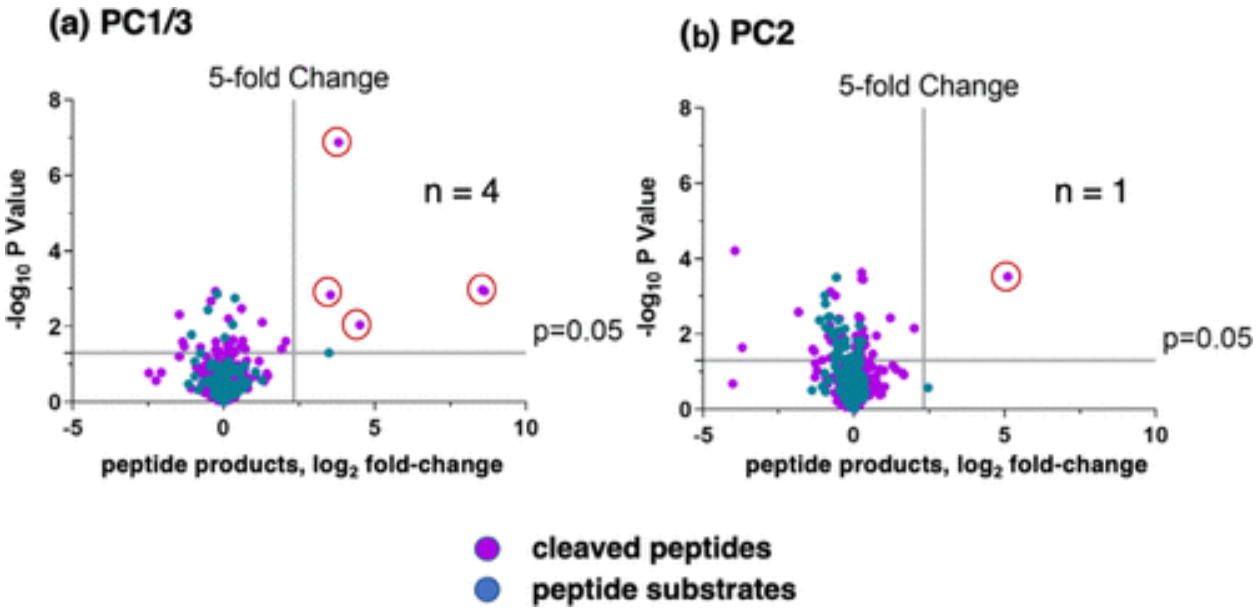

Figure 6.4 PC1/3 and PC2 cleavage profiling analyzed by MSP-MS. Volcano plots of PC1/3 (panel a) and PC2 (panel b) peptide cleavages from MSP-MS data show the $\log_2$ ratios of relative quantities of peptide products generated by PC1/3 and PC2 (60 min incubation at pH 5.5) compared to no enzyme activity controls, illustrated by $-\log_{10}p$ values. Peptide products generated with at least a 5-fold change above controls and with $p < 0.05$ were analyzed for the frequencies of amino acid residues at the P4–P4′ positions of the P1–↓P1′ cleavage site.

6.2.4 Protease Cleavage Sites Assessed with Peptide-AMC Substrates Containing Variant Dibasic Residue Sequences

The dipeptide substrates Z-K-R-AMC, Z-R-K-AMC, Z-K-K-AMC, and Z-R-R-AMC were utilized to compare cleavage at these variant dibasic residue sites by cathepsin L, cathepsin V, PC1/3, and PC2. Furthermore, tripeptide substrates were designed with Leu, Trp, Phe, Tyr, and Val adjacent to the N-terminal side of K-R sites to assess the influence of these hydrophobic residues on proteolysis at dibasic residues by cathepsin L and cathepsin V. These hydrophobic residues were frequently present at the P2 position of cathepsin L and cathepsin V cleavages of the peptide library in the MSP-MS experiments (Figure 6.3).

Cleavage at the C-terminal side of dibasic residues generates free AMC (7-amino-4-methylcoumarin) fluorescence that is quantitatively monitored (Supporting Information, Figure 6.S1). However, the cleavage between the dibasic residues of the dipeptide and tripeptide substrates, or cleavage at the N-terminal side of dibasic residues, generates nonfluorescent products. To detect these cleaved products, we used the aminopeptidase enzyme, cathepsin H, in a coupled assay to convert nonfluorescent products to fluorescent AMC (Supporting Information, Figure 6.S1). Cathepsin H hydrolyzes free N-terminal Arg and Lys residues and therefore releases the fluorescent AMC reporter. Cathepsin H does not cleave Z-peptide-AMC substrates since N-terminal residues are blocked with the Z group (benzyloxycarbonyl).

Cathepsin L cleavages of the tripeptide-AMC substrates Z-L-K-R-AMC, Z-W-K-R-AMC, Z-F-K-R-AMC, and Z-Y-K-R-AMC were readily detected following the addition of cathepsin H, but not in its absence (Figure 6.5a and Table 6.2). These findings show that cathepsin L cleaved between K-R sites, or at the N-terminal side of K-R, but not at the C-terminal side of the K-R. In contrast to tripeptide-AMC substrates, cathepsin L cleaved the dipeptide substrates Z-K-R-AMC, Z-R-K-AMC, Z-K-K-AMC, and Z-R-R-AMC at the C-terminal side of dibasic residues, since

fluorescent measurements were similar in the absence and presence of cathepsin H. These data show that cathepsin L cleavage of tripeptide substrates is controlled by the presence of the hydrophobic residues Leu, Trp, Phe, and Tyr in the P2 position, which results in the cleavage between the adjacent dibasic residues yielding an R-AMC product that can be subsequently cleaved by cathepsin H to generate fluorescent AMC. Furthermore, cathepsin L displayed the highest activity with the Z-L-K-R-AMC, Z-F-K-R-AMC, and Z-Y-K-R-AMC tripeptide substrates compared to dibasic peptides.

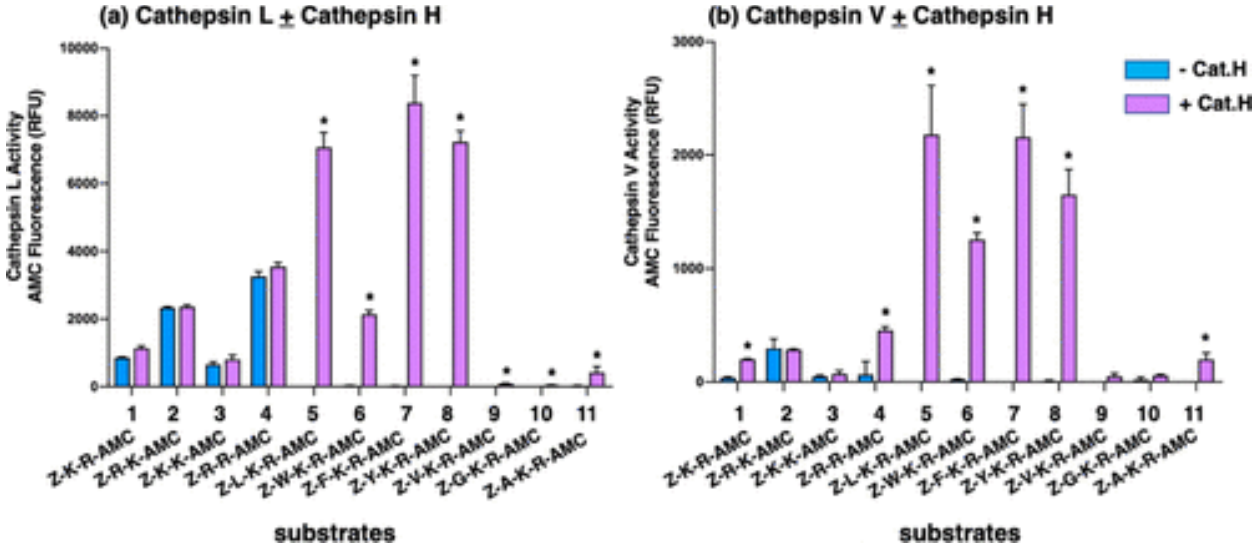

Figure 6.5 Cathepsin L and cathepsin V cleavage specificities at dibasic residue sites assessed with variant dipeptide-AMC and tripeptide-AMC substrates. Cathepsin L (panel a) and cathepsin V (panel b) were evaluated for the cleavage of dipeptide-AMC substrates containing the four dibasic variant cleavage sites KR, RK, KK, and RR and compared to the cleavage of tripeptide-AMC substrates containing the K-R with adjacent hydrophobic residues (Leu, Trp, Phe, Tyr, Val) or nonpolar residues (Gly, Ala) at the N-terminal side of the dibasic K-R site. Cathepsin L and cathepsin V were incubated with each of these substrates at 37 °C for 60 min. Then, the aminopeptidase cathepsin H or control buffer was added and incubation continued at 37 °C for another 30 min to allow conversion of basic residue-extended AMC products to free AMC for fluorometric measurement (conducted as described in the Methods section, with example shown in the Supporting Information, Figure 6.S1). Controls included incubation of cathepsin H alone with each of the substrates, which resulted in no fluorescence, indicating that cathepsin H does not remove the blocked N-terminal residues of Z-peptide-AMC substrates. Comparison of fluorescence observed in the absence and presence of cathepsin H is illustrated, with significant differences with $p < 0.05$ (student's *t*-test, $n = 3$) indicated by asterisks.

Table 6.2 Cathepsin L, Cathepsin V, PC1/3, and PC2 Cleavage of Peptide-AMC Substrates with Variant Dibasic Residues, without and with Cathepsin H Aminopeptidase Activity to Assess Processing Sites[a]

	ratio of protease activity ± cathepsin H (RFU fluorescence)			
substrate	**cathepsin L**	**cathepsin V**	**PC1/3**	**PC2**
Z-K-R-AMC	1.5	202.4	infinity, CH only	2.6
Z-R-K-AMC	1.0	1.0	1.0	0.9
Z-K-K-AMC	1.1	1.4	3.0	0.8
Z-R-R-AMC	1.1	6.8	infinity, CH only	1.5
Z-L-K-R-AMC	infinity, CH only	infinity, CH only	0.9	0.1
Z-W-K-R-AMC	73.9	48.3	0.9	1.3
Z-F-K-R-AMC	infinity, CH only	infinity, CH only	1.1	1.4
Z-Y-K-R-AMC	infinity, CH only	269	0.9	1.0
Z-V-K-R-AMC	29.7	infinity, CH only	2.9	0.7
Z-G-K-R-AMC	infinity, CH only	2.8	infinity, CH only	0.3
Z-A-K-R-AMC	26.1	infinity, CH only	1.9	1.2

[a]The ratio of each protease activity was assessed in the absence and presence of cathepsin H in coupled assays to monitor cleavages at the C-terminal side of dibasic residues compared to cleavages occurring between or at the N-terminal side of dibasic residues. The ratio of activity, indicated by the relative fluorescence of free AMC, in the presence and absence of cathepsin H is shown in this table. When AMC fluorescence was generated only in the presence of cathepsin H (CH), the table indicates "infinity, with CH only." The ratios of proteolytic activity ± cathepsin H represent data from Figures 6.5 and 6.6.

Cathepsin V cleavage of the tripeptide substrates Z-L-K-R-AMC, Z-W-K-R-AMC, Z-F-K-R-AMC, and Z-Y-K-R-AMC was prominently detected in the presence of cathepsin H, but not in the absence of cathepsin H (Figure 6.5b and Table 6.2). These data show that cathepsin V cleaved at the K-R dibasic site with a hydrophobic residue adjacent to the N-terminal side of the P1-↓P1′ cleavage site, with cleavage occurring between or at the N-terminal side of K-R residues. Among the dipeptide substrates, cathepsin V displayed lower activity. Cathepsin V cleaved Z-R-

K-AMC and Z-K-K-AMC substrates at the C-terminal side of dibasic residues but cleaved between and at the C-terminal side of the dibasic residues of Z-K-R-AMC and Z-R-R-AMC.

In contrast to cathepsin L and cathepsin V, PC1/3 and PC2 both displayed a preference for cleaving at the C-terminal side of dibasic residues within the peptide-AMC substrates (Figure 6.6 and Table 6.2). PC1/3 and PC2 displayed greater proteolysis of Z-F-K-R-AMC and Z-Y-K-R-AMC compared to the other substrates evaluated. These data illustrate differences in dibasic residue cleavage sites utilized by PC1/3 and PC2 compared to cathepsins L and V.

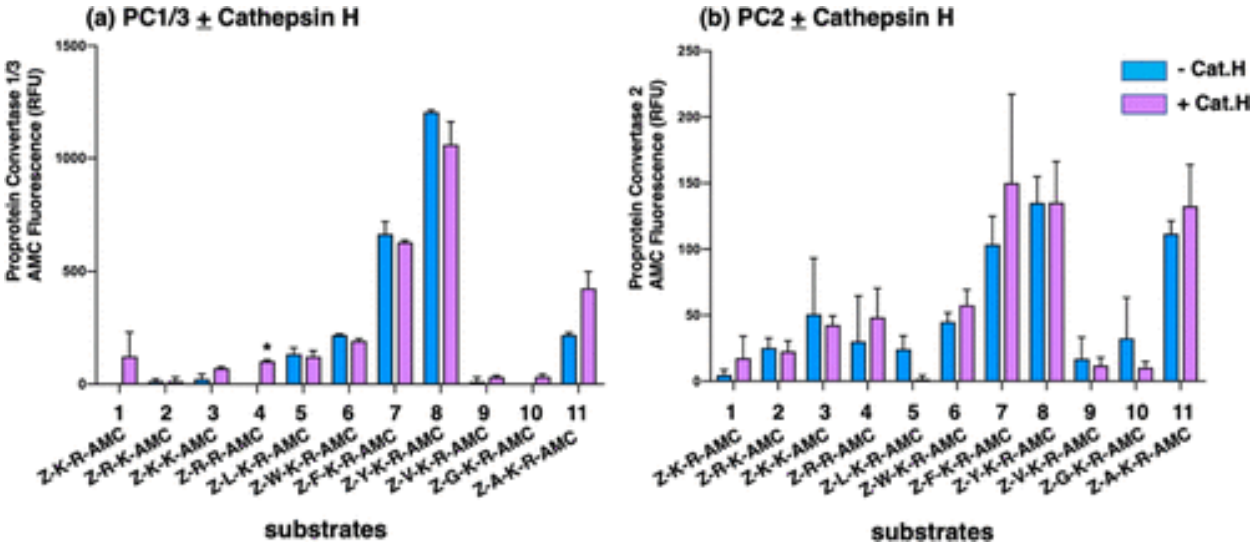

Figure 6.6 PC1/3 and PC2 cleavage properties examined with variant dipeptide-AMC and tripeptide-AMC substrates containing dibasic residue sites. PC1/3 (panel a) and PC2 (panel b) were evaluated for the cleavage of dipeptide-AMC substrates containing the four dibasic variant cleavage sites KR, RK, KK, and RR and compared to the cleavage of tripeptide-AMC substrates containing the K-R with hydrophobic residues (Leu, Trp, Phe, Tyr, Val) or nonpolar residues (Gly, Ala) at the N-terminal side of the dibasic K-R site. After incubation of PC1/3 or PC2 with each of these substrates at 37 °C for 120 min, control buffer or the aminopeptidase cathepsin H was added and incubation at 37 °C continued for another 30 min (37 °C) to allow conversion of basic residue-extended AMC products to free AMC for fluorometric measurement. Comparison of fluorescence observed in the absence and presence of cathepsin H is illustrated and included evaluation of significant differences with $p < 0.05$ (Student's *t*-test, $n = 3$).

6.2.5 Broad Range of Proteolytic Activities of Cathepsin L, Cathepsin V, PC1/3, and PC2

A broad range of proteolytic activities for these proteases was observed (Table 6.3). Cathepsin L was the most active protease, shown by its high specific activity compared to the

lower specific activities of cathepsin V, PC1/3, and PC2 that were 10, 1.5, and 0.07%, respectively, compared to cathepsin L (100%) when assayed with their standard substrates of Z-Phe-Arg-AMC for cathepsins L and V, (35,36) and substrate pGlu-Arg-Thr-Lys-Arg-AMC for PC1/3 and PC2. (37) This rank order of high to low specific activity of cathepsin L to cathepsin V, PC1/3, and PC2 is consistent with the high to low number of cleavages by each of these proteases in MSP-MS assays (Figures 6.2 and 6.4). In addition, the same rank order of high to lower specific activities of these four proteases was observed by assay of these proteases with the Z-Tyr-Lys-Arg-AMC substrate (Table 6.3). The wide range of specific activities may represent the differing activity of each of these proteases for peptide processing.

Table 6.3 Specific Activities of Cathepsin L, Cathepsin V, PC1/3, and PC2[a]

protease	substrate	specific activity (pmol AMC/ng/min)
cathepsin L	Z-Phe-Arg-AMC	8.5
	Z-Tyr-Lys-Arg-AMC	3.2
cathepsin V	Z-Phe-Arg-AMC	0.88
	Z-Tyr-Lys-Arg-AMC	0.14
PC1/3	pGlu-Arg-Thr-Lys-Arg-AMC	0.132
	Z-Tyr-Lys-Arg-AMC	0.463
PC2	pGlu-Arg-Thr-Lys-Arg-AMC	0.0067
	Z-Tyr-Lys-Arg-AMC	0.0023

[a]Specific activities were measured using Z-Phe-Arg-AMC for human cathepsin L (0.04 ng/μL) and human cathepsin V (0.2 ng/μL), and using pGlu-Arg-Thr-Lys-Arg-AMC for PC1/3 (0.9 ng/μL) and PC2 (4 ng/μL) as standard fluorogenic peptide substrates commonly used to assay for these proteases. (35−37) Also, specific activities with the substrate Z-Tyr-Lys-Arg-AMC of this study were used to compare these four enzymes. Cathepsin L and cathepsin V activity with Z-Tyr-Lys-Arg-AMC required the use of cathepsin H in a coupled assay to generate AMC fluorescence (from Figure 6.5). PC1/3 and PC2 activities were the same when conducted without or without cathepsin H (from Figure 6.6) and, therefore, their activities without cathepsin H is provided for this table.

6.3 Discussion

The cysteine proteases cathepsin L and cathepsin V, combined with the serine proteases PC1/3 and PC2, participate in processing proneuropeptides at dibasic residue sites to generate active neuropeptides. In this study, the distinct cleavage specificities of cathepsin L and cathepsin V compared to PC1/3 and PC2 were demonstrated by multiplex substrate profiling mass spectrometry (MSP-MS) combined with analysis of peptide-AMC substrates with variant dibasic residue sequences. Cleavage profiling by MSP-MS showed that cathepsin L cleaved between the dibasic residues of K↓R and R↓K, and at the N-terminal side of ↓KR and ↓RK (Table 6.1). Cathepsin V cleaved between the dibasic residues of K↓R, R↓K, and K↓K. Cathepsin L and cathepsin V did not cleave at the C-terminal side of dibasic residue sites among the peptides of the library. Cathepsins L and V displayed strong preferences for the hydrophobic P2 residues of Leu, Val, Phe, and Trp adjacent to P1↓P1′ cleavage sites. PC1/3 cleaved at the C-terminal side of KR and RR sites, while PC2 only cleaved one peptide at the C-terminal side of KR within a tribasic KRR site. The differing cleavage specificities of these four proteases were confirmed with dipeptide-AMC with variant dibasic residues and with tripeptide-AMC substrates with hydrophobic residues adjacent to the N-terminal side of the K-R dibasic residue pair. Notably, a broad range of high to low levels of proteolytic activities were found for cathepsin L > cathepsin V > PC1/3 > PC2 (Table 6.3). These findings demonstrate the distinct preferences of the proneuropeptide processing enzymes cathepsin L and cathepsin V to cleave between or at the N-terminal side of dibasic residues, whereas PC1/3 and PC2 cleave at the C-terminal side of dibasic sites, with substantial differences in the levels of proteolysis (Figure 6.7).

a. Distinct Dibasic Cleavage Site Properties of Cathepsin L and Cathepsin V, Compared to PC1/2 and PC2 Proteases

Protease	Dibasic Cleavage Site(s)	Relative Proteolytic Activity MSP-MS	peptide-AMC
Cathepsin L	1, 2	1.0	1.0
Cathepsin V	2	0.67	0.10
PC1/3	3	0.016	0.015
PC2	3	0.004	0.0007

b. Cleavage sites 1, 2, and 3 at dibasic residues of proneuropeptides

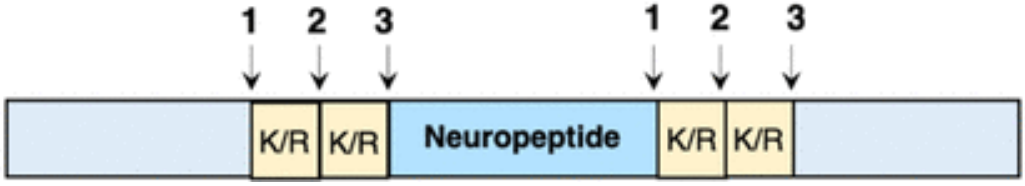

Figure 6.7 Distinct dibasic cleavage properties of cathepsin L and cathepsin V cysteine proteases compared to PC1/3 and PC2 serine proteases involved in proneuropeptide processing. (a) Information is shown for the relative proteolytic activity by the MSP-MS analyses of peptide library substrates and relative proteolytic activity observed in peptide-AMC assays using standard substrates for cathepsin L and cathepsin V (Z-F-R-AMC), and PC1/3 and PC2 (pERTKR-AMC). (b) Locations of dibasic cleavage sites (#1, 2, and 3) for each of the proneuropeptide processing proteases cathepsin L, cathepsin V, PC1/3, and PC2 are indicated.

Prior studies of cathepsin L cleavage of several proneuropeptides illustrate the presence of hydrophobic residues at the P2 position. For example, cathepsin L cleaved pro-NPY at the N-terminal side of KR within YG↓KR, with Tyr as the P2 residue (Supporting Information, Figure 6.S2). (21) With respect to enkephalin production, cathepsin L cleaved BAM-22P and peptide F proenkephalin-derived intermediates at the N-terminal side of dibasic residues of YGGFM↓RR and YGGFM↓KK with Phe at the P2 position, respectively, to generate enkephalin (YGGFM). (20) Such dibasic residue cleavages with hydrophobic P2 residues by cathepsin L and cathepsin V are predicted for processing proenkephalin, pro-CCK (cholecystokinin), and prodynorphin. (38−42)

Subsequent to cathepsin L and cathepsin V processing of proneuropeptides, intermediate peptide products will then require exopeptidase steps to remove N-terminal and C-terminal basic residue extensions by aminopeptidase and carboxypeptidase enzymes (Supporting Information, Figure 6.S4). Aminopeptidase B and cathepsin H participate as aminopeptidases for neuropeptide production. (43−45) Carboxypeptidase E (CPE) participates as an exopeptidase for the removal of C-terminal basic residues of neuropeptide intermediates in neuroendocrine tissues. (1,2)

It is notable that cathepsin V is a human-specific cysteine protease, since orthologues of human cathepsin V have not been found in mouse and many other mammalian species. (16−19) The human genome possesses the two highly homologous cathepsin V and cathepsin L cysteine proteases that are clan CA/family C1 cysteine proteases. The mouse cathepsin L possesses greater homology with human cathepsin V (74.5% protein sequence identity) compared to human cathepsin L (71.5% identify in protein sequence (19)), which supports the predicted role of cathepsin V in proneuropeptide processing as demonstrated by its processing of proenkephalin. (19) Both cathepsin V and cathepsin L are present in secretory vesicles, where neuropeptides are generated from their precursors.

The MSP-MS cleavage data of PC1/3 and PC2 parallels that of prior studies on processing proinsulin, proenkephalin, and proopiomelanocortin (POMC) proneuropeptides. PC1/3 cleaved proinsulin at the C-terminal side of Arg-Arg↓, and PC2 cleaved proinsulin at the C-terminal side of Lys-Arg↓ (22−24) (Supporting Information, Figure 6.S3). PC1/3 and PC2 cleaved proenkephalin (PE) at the C-terminal sides of multiple dibasic residues of KR↓, RR↓, and KK↓ based on mass spectrometry of peptide products (26) (Supporting Information, Figure 6.S3). In addition, PC2 cleavage at the tribasic KR↓R site shown by the MSP-MS data is consistent with

evidence for PC2 processing of the KKRR tetrabasic site of POMC to generate α-MSH. (27,46,47) It is noted that PC1/3 does not cleave RK and KK dibasic sites of POMC. (27,46,47) These data show that PC1/3 and PC2 cleave at the C-terminal side of dibasic residues of several proneuropeptides.

Subsequent to PC1/3 and PC2 processing, peptide intermediate products then require removal of C-terminal basic residues by exopeptidase carboxypeptidase E (CPE) to generate active neuropeptides (1,2) (Supporting Information, Figure 6.S4). In contrast, subsequent to cathepsin L and cathepsin V processing, aminopeptidases are needed for removal of N-terminal basic residues, and CPE is needed for removal of C-terminal basic residues to generate the mature neuropeptide.

These cysteine and serine proteases participate jointly in proneuropeptide processing, demonstrated by protease gene knockout studies. Enkephalin production utilizes cathepsin L as shown by cathepsin L gene knockout that results in the reduction of enkephalin levels in mouse brain; (20) enkephalin is also generated by PC2 as shown by reduced enkephalin brain levels in PC2 gene knockout mice. (49) POMC processing to generate ACTH, α-MSH, and β-endorphin peptide hormones utilizes cathepsin L, PC1/3, and PC2 proteases. (27,46−50) Cathepsin L gene knockout results in substantial decreases in ACTH, β-endorphin, and α-MSH derived from POMC, indicated by accumulation of POMC in the cathepsin L knockout mice. (48) PC2 gene knockout results in obliteration of α-MSH in pituitary and the brain and is accompanied by increases in ACTH and β-endorphin (1−31) consistent with these intermediates as possible substrates of PC2; (49) PC1/3 gene disruption reduces POMC processing. (50) Cathepsin L gene knockout also results in decreased production of NPY, CCK, and dynorphin neuropeptides; (21,51,52) production of these neuropeptides also involve PC2. (53−55) Numerous neuropeptides utilized PC1/3, as shown in PC1/3 null mice. (56)

Our recent study of endogenous neuropeptide production in dense-core secretory vesicles (DCSV) assessed by neuropeptidomics and MSP-MS showed that MSP-MS represented endogenous proteases involved in the production of chromaffin granule neuropeptides. (57) Thus, MSP-MS peptide library analysis of protease properties represents their neuropeptide-producing functions.

Cathepsin L had the highest specific activity compared to cathepsin V, PC1/3, and PC2 (Table 6.3). In vivo, endogenous inhibitors of cathepsin L exist in DCSV that regulate its activity. Cathepsin L is inhibited by the endogenous cystatin C protease inhibitor, (58) which is present in dense-core secretory vesicles (DCSV). (57) Cathepsin L is also inhibited by endogenous serpin type protease inhibitors present in DCSV. (59−61)

It will be of interest in future studies to gain an understanding of the coordinate roles of these cysteine and serine proneuropeptide processing proteases with the secretory vesicle proteome (57) for the production of diverse neuropeptides utilized for neuroendocrine cell–cell communication.

6.4 Methods

6.4.1 Human Recombinant-Purified Cathepsin L, Cathepsin V, PC1/3, and PC2, with Peptide Library, Peptide-AMC Substrates, and Reagents

Human recombinant proteases (with catalogue numbers indicated) were obtained from R&D Systems (Minneapolis, MN), consisting of human recombinant cathepsin L (#952-CY-010), human recombinant cathepsin V (#1080-CY-010), human recombinant PC1/3 (#2810-SE-010), and human recombinant PC2 (#6018-SE-010). Protease MSP-MS assays utilized the library of 228 14-mer peptides designed to contain all possible protease cleavage sites, as previously described (29,30) (peptides synthesized by Anaspec, Fremont, CA). Assays utilized octyl-β-

glucopyranoside (Sigma-Aldrich, Darmstadt, Germany), dithiothreitol (DTT, Promega, Madison, WI), BEH C18 packing material (Waters Corporation, Milford, MA), acetonitrile (ACN, Fisher Chemical, Pittsburgh, PA), trifluoroacetic acid (TFA, Fisher Chemical, Pittsburgh, PA), urea (Teknova, Hollister, CA), and C18 for solid-phase extraction (SPE) stage-tips (3M, Maplewood, MN). Fluorogenic proteolytic assays used the substrates Z-K-R-AMC, Z-R-K-AMC, Z-K-K-AMC, Z-R-R-AMC, Z-L-K-R-AMC, Z-W-K-R-AMC, Z-F-K-R-AMC, Z-Y-K-R-AMC, Z-V-K-R-AMC, Z-G-K-R-AMC, and Z-A-K-R-AMC from Genscript (Piscataway, NH); Z-F-R-AMC was from Bachem (Vista, CA) and pERTKR-AMC was from R&D Systems.

6.4.2 Multiplex Substrate Profiling by Mass Spectrometry (MSP-MS)

MSP-MS utilized a peptide library of 228 14-mers with diverse sequences representing all possible protease cleavage sites, synthesized as described. (29,30) The peptides of the library used for MSP-MS were designed to contain all neighbor and near-neighbor (+1 and +2) dipeptide pairs as described by O'Donoghue et al. (29) This peptide library is a universal substrate library for all proteases as well as proteases with dibasic specificity. The length of 14 residues for the peptides and cleavage products are readily detected and quantified by LC–MS/MS tandem mass spectrometry. Among the 228 peptide library, 19 peptides have neighboring dibasic amino acids, while one of these peptides has a neighboring tribasic sequence. The peptides containing KR, RK, RR, and KK sequences are shown in the Supporting Information, Table 6.S1.

Prior to incubation with the peptide library, cathepsin V was activated by incubation in 5 mM DTT, 20 mM Na-acetate pH 5.5, 1 mM ethylenediaminetetraacetic acid (EDTA), and 100 mM NaCl at 37 °C for 30 min. Cathepsin L, PC1/3, and PC2 did not require preactivation. The concentrations of each protease used for MSP-MS were determined by the incubation of cathepsin L and cathepsin V with the Z-Phe-Arg-AMC fluorogenic substrate and the incubation of PC1/3

and PC2 with pGlu-Arg-Thr-Lys-Arg-AMC, in the absence and presence of the peptide library. Diminished fluorogenic proteolytic activity in the presence of the peptide library indicated protease concentrations for peptide library incubations in MSP-MS.

Cathepsin L (0.04 ng/μL) or cathepsin V (0.16 ng/μL) was each incubated with the peptide library (0.5 μM final concentration for each of the 228 peptides) in 50 mM citrate phosphate, pH 5.5, 1 mM EDTA, 100 mM NaCl, and 5 mM DTT in a total volume of 22 μL at 37 °C. After 30 and 60 min incubation, 10 μL of aliquots were removed and added to 60 μL of 8 M urea for quenching and stored at −70 °C.

PC1/3 (3.6 ng/μL) and PC2 (5.4 ng/μL) were each incubated with the peptide library (0.5 μM final concentration for each of the 228 peptides) in 50 mM Na-acetate, pH 5.5, 5 mM $CaCl_2$, and 0.1% octyl-β-glucopyranoside (bOG); the incubation for PC2 also included 100 mM NaCl. After 30 and 60 min incubation at 37 °C, 10 μL of aliquots were removed and added to 60 μL of 8 M urea, with vortexing, for quenching; samples were stored at −70 °C.

The control "0" time condition was conducted by denaturation of each protease in 8 M urea prior to the addition of the inactive enzyme to the peptide library. Each protease MSP-MS assay condition was conducted in quadruplicate.

Samples were then prepared for LC–MS/MS by solid-phase extraction (SPE) as we have described previously. (29,30) Briefly, the samples were acidified by the addition of 40 μL 1% TFA and desalted using C18 LTS tips with peptides eluted sequentially by 50 and 80% ACN in 0.1% TFA, followed by evaporation to dryness in a Speedvac and stored at −70 °C. Prior to LC–MS/MS, samples were resuspended in 40 μL 0.1% TFA.

LC–MS/MS was performed on a Dionex UltiMate 3000 nano LC and Orbitrap Q-Exactive mass spectrometer (Thermo Fisher). Rehydration of dried samples in 0.1% trifluoracetic acid

resulted in a peptide concentration of 57 μM with respect to the 14-mer substrates of the library. For each LC–MS/MS analysis, 4 μL of the sample (equivalent to 228 pmol of starting 14-mer peptide substrates) was injected into a nano LC column (75 μm ID, 360 μm OD, 25 cm length) packed with BEH C18 (1.7 μm diameter) solid-phase material and heated to 65 °C for LC. LC was conducted with a flow rate of 0.3 μL/min using a 60 min linear gradient of 5–30% solvent B, and 15 min linear gradient of 30–85% B (solvent B = 100% ACN in 0.1% TFA) with solvent A (0.1% TFA in water). MS1 was acquired in profile mode with a 1e5 AGC target, 50 ms max injection time, 70 000 resolution (at *m*/*z* 200), and a 250–1500 *m*/*z* window. MS2 was acquired in centroid mode with a 1e5 AGC target, 50 ms max injection time, 3e2 minimum AGC target, 20 s/10 ppm dynamic exclusion, 17,500 resolution (at *m*/*z* 200), a first mass of *m*/*z* 150, and normalized HCD collision energy set to 30. Each sample was injected once.

Peptides were identified by PEAKS (v 8.5) bioinformatics software. MS/MS data files were searched against the peptide library database containing all 228 peptides. Label-free peptide quantification was performed by PEAKS; peptide identifications were assigned intensities based on the area of the precursor ion LC peak. Match-between-runs mass and retention time shift tolerances were set to 8.0 ppm and 3 min, respectively. To minimize low-quality features in the data set, data were filtered by the following criteria: (1) identified peptides with amino acid sequences that did not match to a peptide in the FDR-curated identification list were discarded and (2) PEAKS scores above 0.3 were utilized for high-quality MS/MS data. Further, to account for instrumental drift, the filtered feature list was normalized with the Loess-G algorithm by Normalyzer (http://normalyzer.immunoprot.lth.se/).

After LC–MS and bioinformatics analyses, cleavage sites were compiled for each enzyme condition and the intensities of cleaved peptides detected were compared for cathepsin L, cathepsin

V, PC1/3, and PC2 proteases. Cleaved peptide products which displayed intensity scores at least 5-fold above the 0 time control, with $p < 0.05$, were utilized for analyses of protease cleavage site frequencies and preferences.

6.4.3 Heat Map and IceLogo Analyses of Protease Cleavage Sites

The preferences of each of the proteases for amino acid residues at P4–P4′ positions of the cleavage site P1–↓P1′ of the cleaved peptides were assessed as Z-scores to evaluate the frequencies of each amino acid at each position. Z-scores were calculated by the equation $X - \mu/\sigma$, where X is the frequency of the amino acid in the experimental data set, μ is the frequency of a particular amino acid at a specific position in the reference set (control 0 time), and σ is the standard deviation. Heat maps were generated to illustrate the magnitude of the positive or negative Z-scores are depicted as color-coded gradients of blue (negative Z-score), white (zero Z-score), and red (positive Z-score).

IceLogo was used to illustrate the relative frequencies of amino acid residues at each of the P4–P4′ positions of cleaved peptides. (62) IceLogo utilizes different heights of single-letter amino acids to represent "percent difference," defined as the frequency for an amino acid appearing in the experimental data minus the frequency for an amino acid appearing in the reference peptide library MSP-MS data. Positive differences are shown above the midline, and negative differences are represented below the midline. Residues below the line shown in pink are those that never occurred at the indicated position.

6.4.4 Fluorogenic Proteolytic Assays with Variant Dibasic Residue-Containing Peptide-AMC Substrates

Cathepsin L, cathepsin V, PC1/3, and PC2 were assayed with fluorogenic dipeptide-AMC and tripeptide-AMC substrates designed to contain variant dibasic residue sequences consisting of Z-K-R-AMC, Z-R-K-AMC, Z-K-K-AMC, Z-R-R-AMC, Z-L-K-R-AMC, Z-W-K-R-AMC, Z-F-

K-R-AMC, Z-Y-K-R-AMC, Z-V-K-R-AMC, Z-G-K-R-AMC, and Z-A-K-R-AMC. After incubation of each protease with the substrates, incubation continued without and with the addition of cathepsin H to monitor cleavages within dibasic residue sites compared to cleavages at the C-termini of dibasic residues of peptide-AMC substrates (illustrated in Supporting Information, Figure 6.S1).

Cathepsin L (0.04 ng/μL) and cathepsin V (0.2 ng/μL) assays contained 5 mM citrate-phosphate buffer pH 5.5, 4 mM DTT, 1 mM EDTA, 50 mM NaCl, and 1% dimethyl sulfoxide (DMSO) with peptide-AMC substrates at 60 μM; additionally, cathepsin L assays included 0.001% bovine serum albumin (BSA). Assays were incubated at 37 °C for 60 min and AMC was monitored at excitation/emission of 360/460 nm. Cathepsin H (0.5 ng/μL, activated by the protocol provided by the manufacturer R&D Systems) was then added with 50 mM 2-(*N*-morpholino)ethanesulfonic acid (MES) buffer to adjust the pH to 6.5; incubation continued at 37 °C for 30 min, and AMC fluorescence was measured.

PC1/3 (0.9 ng/μL) and PC2 (4 ng/μL) assays contained 5 mM Na-acetate pH 5.5, 5 mM $CaCl_2$, 50 mM NaCl, 0.5% Brij-35, and 1% DMSO. Assays were incubated at 37 °C for 120 min and AMC was monitored at excitation/emission of 360/460 nm. Cathepsin H (0.5 ng/μL, activated by the protocol provided by the manufacturer R&D Systems) was then added with 50 mm MES buffer to adjust the pH to 6.5; incubation continued at 37 °C for 30 min, and AMC fluorescence was measured.

The specific activities of cathepsin L and cathepsin V were determined with the substrate Z-F-R-AMC, which is routinely used in the field for assay of these proteases. (35,36) For PC1/3 and PC2, their specific activities were assessed with the substrate pERTKR-AMC that is typically used to assay these proteases. (37)

Control assays included the incubation of substrates with cathepsin H alone which resulted in no fluorescence, indicating that cathepsin H does not remove the blocked N-terminal residues of Z-peptide-AMC substrates.

AMC standards were used to calculate enzyme-specific activities (pmol AMC/ng/min). All assays were conducted in triplicate. Mean and SD values were calculated with a comparison of conditions in *t*-tests with a significance of $p < 0.05$.

6.4.5 Data availability

LC-MS/MS files for the MSP-MS experiments can be accessed at www.massive.ucsd.edu under the dataset identifier numbers MSV000088091 (Cathepsin L and Cathepsin V) and MSV000088092 (PC1 and PC2).

6.5 Supporting Information

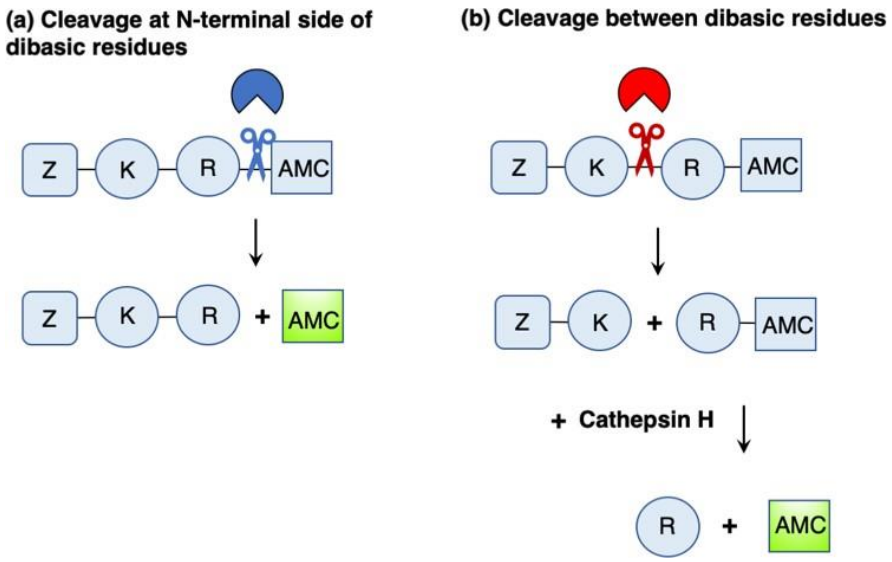

Figure 6.S1 Coupled protease assay with cathepsin H aminopeptidase activity to monitor peptide-AMC cleavages with N-terminal residue-extended AMC products.
C-terminal cleavage at dibasic residues of Z-K-R-AMC, as an example of the Z-K/R-K/R-↓AMC and Z-X-K/R-K/R-↓AMC substrates, generates fluorescent AMC monitored at excitation/emission of 360/460 nm, shown here for Z-K-R-AMC as example.
Cleavage between or at the N-terminal side of dibasic residues of Z-K-R-AMC, as an example for the Z-K/R-K/R-↓AMC and Z-X-K/R-K/R-↓AMC substrates, generates basic residue extended AMC products that are monitored by addition of the cathepsin H aminopeptidase to generate fluorescent AMC for detection and quantitation of cleaved products.

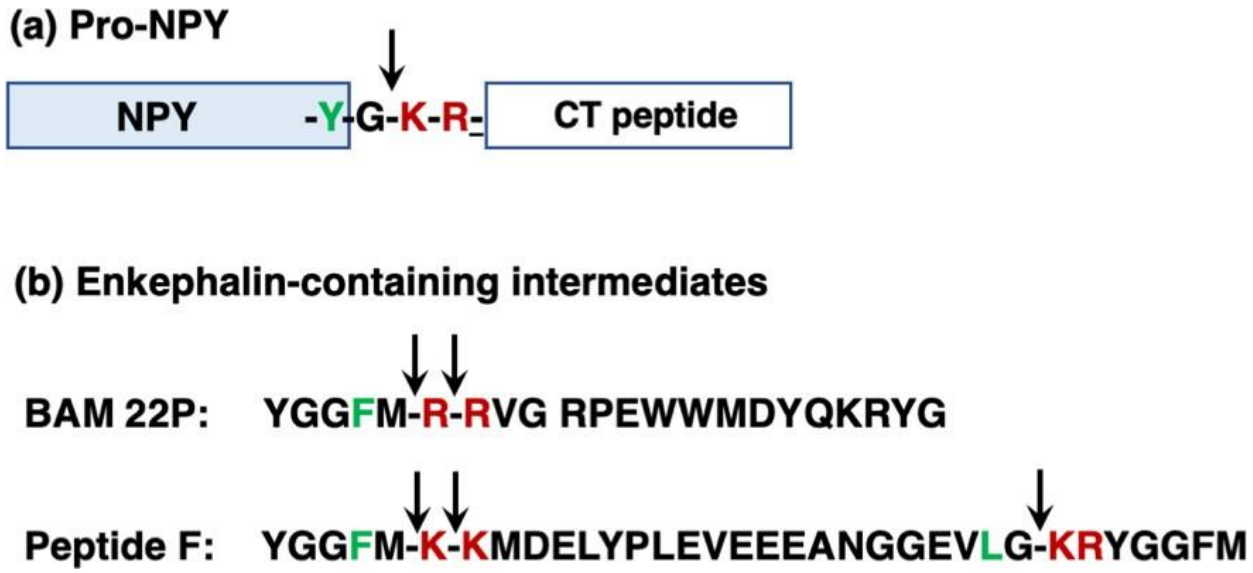

Figure 6.S2 Cathepsin L cleavage of several pro-neuropeptides at dibasic residues, between and at the N-terminal side, reported in the literature.

(a) Cathepsin L cleavage of pro-NPY. Cathepsin L cleavage of recombinant pro-NPY was determined by mass spectrometry analyses of cleavage products, as reported by our prior study of Funkelstein et al., 2008 (21). Results indicated cathepsin L cleavage at the N-terminal side of the KR (pink) processing site, with hydrophobic Tyr residue (green).

(b) Cathepsin L cleavage of enkephalin-containing intermediates BAM22P and Peptide F. Cathepsin L cleavage of BAM22P and Peptide F was determined by mass spectrometry analyses of cleavage products, as reported in our prior study of Yasothornsrikul et al., 2003 (20). Results demonstrated cathepsin L cleavage between the R↓R dibasic site, and at the N-terminal side of ↓RR with hydrophobic Tyr as P2 residue.

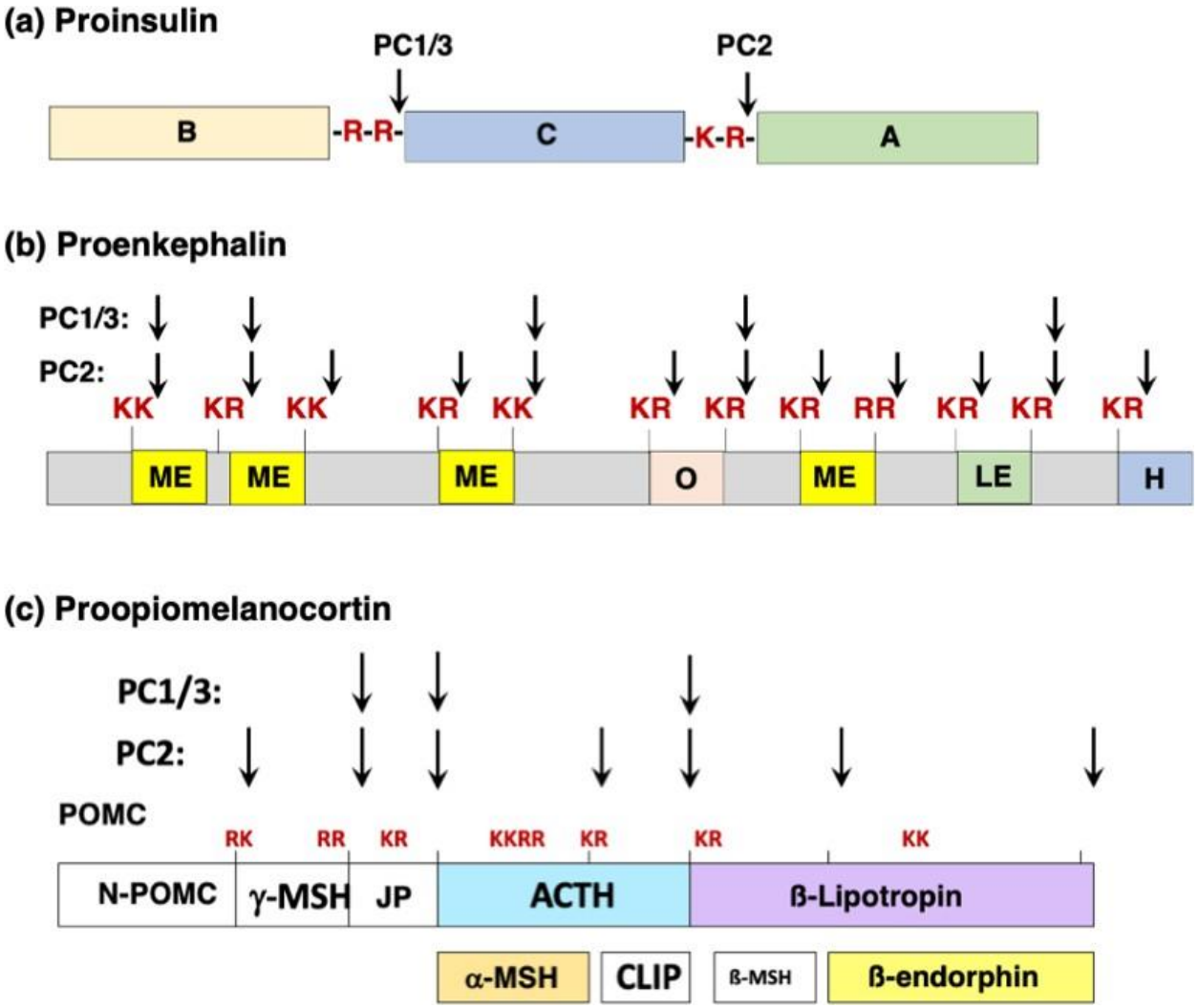

Figure 6.S3 PC1/3 and PC2 cleavage of proinsulin and proenkephalin at the N-terminal side of dibasic residues, reported in the literature.

(a) Proinsulin processing by PC1/3 and PC2. PC1/3 (human) has been demonstrated to cleave human proinsulin at the C-terminal side of RR↓ between the B and C chains, as reported by Davidson et al., 1988 (22). PC2 (human) has been shown to cleave at the COOH-terminal side of KR↓ between the C and A chains of proinsulin (22).

(b) Proenkephalin processing by PC1/3 and PC2. Processing of proenkephalin (rat) by PC1/3 and PC2 (mouse) was conducted by analyses of peptide products by MALDI-TOF, as reported by Peinado et al., 2003 (26). Arrows indicate the cleavage sites within proenkephalin by PC1/3 and PC2.

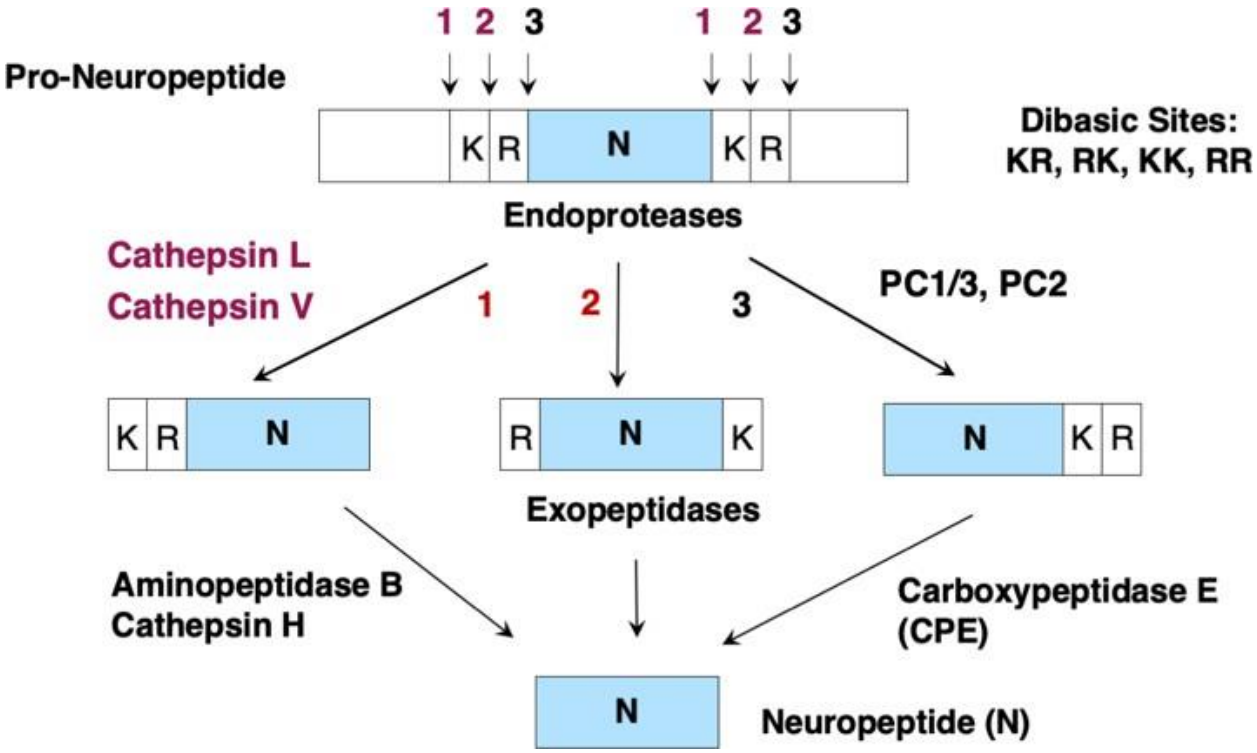

Figure 6.S4 Hypothesis for differential dibasic cleavage specificities of the cathepsin L and cathepsin V cysteine proteases, compared to the PC1/3 and PC2 serine proteases, for neuropeptide biosynthesis. Neuropeptides comprise peptide neurotransmitters and hormones. Neuropeptides are first synthesized as pro-neuropeptide precursors with dibasic residues (KR, RK, KK, and RR) flanking the active neuropeptides. The dibasic residue regions have been found to undergo proteolytic processing by cathepsin L and cathepsin V cysteine proteases (1, 2), combined with the pro-protein convertases 1 and 2 (PC1/3 and PC2) (1-3). It is hypothesized that different cleavage specificities exist for the cathepsin L and cathepsin V proteases which cleave between and at the N-terminal side of the dibasic residues, whereas the PC1/3 and PC2 serine proteases cleavage at the C-terminal side of dibasic residues. This hypothesis is supported by the findings of this study.

Table 6.S1 Dibasic residue containing peptides in the library of 228 14-mer peptides used for MSP-MS analyses[a]

	14-mers with dibasic sequence (n=19)
1	nLDKLnNWPQRRGn
2	GnYYKRFnAHWVGI
3	QnKKTLVnYNEWNL
4	LGWHAnFRKYPInA
5	GSQVFSWLNHYHRK
6	HTNKRISQWnWEIR
7	RKWQSPQVDLYDKS
8	HRRVYLTSPKAPES
9	VDYIEHKDQVRRnN
10	nEFHWRInQGKKAP
11	TPHHVNWYKRAPNQ
12	EGADIWYRKHSHQL
13	LRKDWGDIQFATAN
14	IEPPWVDSHAKRNn
15	YQLLTnNEIFRKWH
16	YWnSTHLAGKRRDW
17	DAWAPnVIKKESSI
18	ADARKYWNVHGTHQ
19	ANnQILDPDNFKRE

[a]The sequences of 14-mer peptides of the library that contain dibasic residues are shown. The library also contained one tribasic peptide.

6.6 References

1. Hook, V.; Funkelstein, L.; Lu, D.; Bark, S.; Wegrzyn, J.; Hwang, S. R. Proteases for processing proneuropeptides into peptide neurotransmitters and hormones. Annu. Rev. Pharmacol. Toxicol. 2008, 48, 393−423.

2. Hook, V.; Lietz, C. B.; Podvin, S.; Cajka, T.; Fiehn, O. Diversity of neuropeptide cell-cell signaling molecules generated by proteolytic processing revealed by neuropeptidomics mass spectrometry. J. Am. Soc. Mass Spectrom. 2018, 29, 807−816.

3. Seidah, N. G.; Sadr, M. S.; Chrétien, M.; Mbikay, M. The multifaceted proprotein convertases: their unique, redundant, complementary, and opposite functions. J. Biol. Chem. 2013, 288, 21473−21481.

4. Felig, P.; Baxter, J. D.; Frohman, L. A. Endocrinology and Metabolism, 3rd ed.; McGraw Hill, Inc.: New York, 1981.

5. Inturrisi, C. E. Clinical pharmacology of opioids for pain. Clin. J. Pain 2002, 18, S3−S13.

6. Charbogne, P.; Kieffer, B. L.; Befort, K. 15 years of genetic approaches in vivo for addiction research: Opioid receptor and peptide gene knockout in mouse models of drug abuse. Neuro- pharmacology 2014, 76, 204−217.

7. Podvin, S.; Yaksh, T.; Hook, V. The Emerging Role of Spinal Dynorphin in Chronic Pain: A Therapeutic Perspective. Annu. Rev. Pharmacol. Toxicol. 2016, 56, 511−533.

8. Steiner, R. A.; Hohmann, J. G.; Holmes, A.; Wrenn, C. C.; Cadd, G.; Juréus, A.; Clifton, D. K.; Luo, M.; Gutshall, M.; Ma, S. Y.; Mufson, E. J.; Crawley, J. N. Galanin transgenic mice display cognitive and neurochemical deficits characteristic of Alzheimer's disease. Proc. Natl. Acad. Sci. U.S.A. 2001, 98, 4184−4189.

9. Counts, S. E.; Perez, S. E.; Kahl, U.; Bartfai, T.; Bowser, R. P.; Deecher, D. C.; Mash, D. C.; Crawley, J. N.; Mufson, E. J. Galanin: neurobiologic mechanisms and therapeutic potential for Alzheimer's disease. CNS Drug Rev. 2001, 7, 445−370.

10. Dedic, N.; Chen, A.; Deussing, J. M. The CRF family of neuropeptides and their receptors mediators of the central stress response. Curr. Mol. Pharmacol. 2018, 11, 4−31.

11. Bale, T. L.; Vale, W. W. CRF and CRF receptors: role in stress responsivity and other behaviors. Annu. Rev. Pharmacol. Toxicol. 2004, 44, 525−557.

12. Holst, J. J.; Holland, W.; Gromada, J.; Lee, Y.; Unger, R. H.; Yan, H.; Sloop, K. W.; Kieffer, T. J.; Damond, N.; Herrera, P. L. Insulin and Glucagon: Partners for Life. Endocrinology 2017, 158, 696−701.

13. Reiband, H. K.; Schmidt, S.; Ranjan, A.; Holst, J. J.; Madsbad, S.; Nørgaard, K. Dual-hormone treatment with insulin and glucagon in patients with type 1 diabetes. Diabetes/Metab. Res. Rev. 2015, 31, 672−679.

14. Krieger, D. T.; Martin, J.; Brownstein, M. J. Brain Peptides; John Wiley & Sons., Inc., 1983.

15. Kim, T.; Gondré-Lewis, M. C.; Arnaoutova, I.; Loh, Y. P. Dense-core secretory granule biogenesis. Physiology 2006, 21, 124− 133.

16. Adachi, W.; Kawamoto, S.; Ohno, I.; Nishida, K.; Kinoshita, S.; Matsubara, K.; Okubo, K. Isolation and characterization of human cathepsin V: a major proteinase in corneal epithelium. Invest. Ophthalmol. Visual Sci. 1998, 39, 1789−1796.

17. Brömme, D.; Li, Z.; Barnes, M.; Mehler, E. Human cathepsin V functional expression, tissue distribution, electrostatic surface potential, enzymatic characterization, and chromosomal localization. Biochemistry 1999, 38, 2377−2385.

18. Reiser, J.; Adair, B.; Reinheckel, T. Specialized roles for cysteine cathepsins in health and disease. J. Clin. Invest. 2010, 120, 3421− 3431.

19. Funkelstein, L.; Lu, W. D.; Koch, B.; Mosier, C.; Toneff, T.; Taupenot, L.; O'Connor, D. T.; Reinheckel, T.; Peters, C.; Hook, V. Human cathepsin V protease participates in production of enkephalin and NPY neuropeptide neurotransmitters. J. Biol. Chem. 2012, 287, 15232−15241.

20. Yasothornsrikul, S.; Greenbaum, D.; Medzihradszky, K. F.; Toneff, T.; Bundey, R.; Miller, R.; Schilling, B.; Petermann, I.; Dehnert, J.; Logvinova, A.; Goldsmith, P.; Neveu, J. M.; Lane, W. S.; Gibson, B.; Reinheckel, T.; Peters, C.; Bogyo, M.; Hook, V. Cathepsin L in secretory vesicles functions as a prohormone-processing enzyme for production of the enkephalin peptide neurotransmitter. Proc. Natl. Acad. Sci. U.S.A. 2003, 100, 9590−9595.

21. Funkelstein, L.; Toneff, T.; Hwang, S. R.; Reinheckel, T.; Peters, C.; Hook, V. Cathepsin L participates in the production of neuropeptide Y in secretory vesicles, demonstrated by protease gene knockout and expression. J. Neurochem. 2008, 106, 384−391.

22. Davidson, H. W.; Rhodes, C. J.; Hutton, J. C. Intraorganellar calcium and pH control proinsulin cleavage in the pancreatic beta cell via two distinct site-specific endopeptidases. Nature 1988, 333, 93− 96.

23. Bailyes, E. M.; Shennan, K. I.; Seal, A. J.; Smeekens, S. P.; Steiner, D. F.; Hutton, J. C.; Docherty, K. A member of the eukaryotic subtilisin family (PC3) has the enzymic properties of the type 1 proinsulin-converting endopeptidase. Biochem. J. 1992, 285, 391−394.

24. Furuta, M.; Carroll, R.; Martin, S.; Swift, H. H.; Ravazzola, M.; Orci, L.; Steiner, D. F. Incomplete processing of proinsulin to insulin accompanied by elevation of Des-31,32 proinsulin intermediates in islets of mice lacking active PC2. J. Biol. Chem. 1998, 273, 3431− 3437.

25. Johanning, K.; Juliano, M. A.; Juliano, L.; Lazure, C.; Lamango, N. S.; Steiner, D. F.; Lindberg, I. Specificity of prohormone convertase 2 on proenkephalin and proenkephalin-related substrates. J. Biol. Chem. 1998, 273, 22672−22680.

26. Peinado, J. R.; Li, H.; Johanning, K.; Lindberg, I. Cleavage of recombinant proenkephalin and blockade mutants by prohormone convertases 1 and 2: an in vitro specificity study. J. Neurochem. 2003, 87, 868−878.

27. Benjannet, S.; Rondeau, N.; Day, R.; Chrétien, M.; Seidah, N. G. PC1 and PC2 are proprotein convertases capable of cleaving proopiomelanocortin at distinct pairs of basic residues. Proc Natl Acad Sci U.S.A. 1991, 88, 3564−3568.

28. Dhanvantari, S.; Seidah, N. G.; Brubaker, P. L. Role of prohormone convertases in the tissue-specific processing of proglucagon. Mol. Endocrinol. 1996, 10, 342−355.

29. O'Donoghue, A. J.; Eroy-Reveles, A. A.; Knudsen, G. M.; Ingram, J.; Zhou, M.; Statnekov, J. B.; Greninger, A. L.; Hostetter, D. R.; Qu, G.; Maltby, D. A.; Anderson, M. O.; Derisi, J. L.; McKerrow, J. H.; Burlingame, A. L.; Craik, C. S. Global identification of peptidase specificity by multiplex substrate profiling. Nat. Methods 2012, 9, 1095−1100.

30. Winter, M. B.; La Greca, F.; Arastu-Kapur, S.; Caiazza, F.; Cimermancic, P.; Buchholz, T. J.; Anderl, J. L.; Ravalin, M.; Bohn, M. F.; Sali, A.; O'Donoghue, A. J.; Craik, C. S. Immunoproteasome functions explained by divergence in cleavage specificity and regulation. eLife 2017, 18, 968−981.

31. Blackmore, C. G.; Varro, A.; Dimaline, R.; Bishop, L.; Gallacher, D. V.; Dockray, G. J. Measurement of secretory vesicle pH reveals intravesicular alkalinization by vesicular monoamine transporter type 2 resulting in inhibition of prohormone cleavage. J. Physiol. 2001, 531, 605−617.

32. Paroutis, P.; Touret, N.; Grinstein, S. The pH of the secretory pathway: measurement, determinants, and regulation. Physiology 2004, 19, 207−215.

33. Estévez-Herrera, J.; Domínguez, N.; Pardo, M. R.; González- Santana, A.; Westhead, E. W.; Borges, R.; Machado, J. D. ATP: The crucial component of secretory vesicles. Proc. Natl. Acad. Sci. U.S.A. 2016, 113, E4098−E4106.

34. Eipper, B. A.; Stoffers, D. A.; Mains, R. E. The biosynthesis of neuropeptides: peptide alpha amidation. Annu. Rev. Neurosci. 1992, 15, 57−85.

35. Boudreau, P. D.; Miller, B. W.; McCall, L. I.; Almaliti, J.; Reher, R.; Hirata, K.; Le, T.; Siqueira-Neto, J. L.; Hook, V.; Gerwick, W. H. Design of Gallinamide A Analogs as Potent Inhibitors of the Cysteine Proteases Human Cathepsin L and Trypanosoma cruzi Cruzain. J. Med. Chem. 2019, 62, 9026−9044.

36. Shah, P. P.; Myers, M. C.; Beavers, M. P.; Purvis, J. E.; Jing, H.; Grieser, H. J.; Sharlow, E. R.; Napper, A. D.; Huryn, D. M.; Cooperman, B. S.; Smith, A. B., 3rd; Diamond, S. L. Kinetic characterization and molecular docking of a novel, potent, and selective slow-binding inhibitor of human cathepsin L. Mol. Pharmacol. 2008, 74, 34−41.

37. Azaryan, A. V.; Krieger, T. J.; Hook, V. Y. Purification and characteristics of the candidate prohormone processing proteases PC2 and PC1/3 from bovine adrenal medulla chromaffin granules. J. Biol. Chem. 1995, 270, 8201−8208.

38. Horikawa, S.; Takai, T.; Toyosato, M.; Takahashi, H.; Noda, M.; Kakidani, H.; Kubo, T.; Hirose, T.; Inayama, S.; Hayashida, H.; et al. Isolation and structural organization of the human preproenkephalin B gene. Nature 1983, 306, 611−614.

39. Yoshikawa, K.; Williams, C.; Sabol, S. L. Rat brain preproenkephalin mRNA. cDNA cloning, primary structure, and distribution in the central nervous system. J. Biol. Chem. 1984, 259, 14301−14308.

40. Eberlein, G. A.; Eysselein, V. E.; Davis, M. T.; Lee, T. D.; Shively, J. E.; Grandt, D.; Niebel, W.; Williams, R.; Moessner, J.; Zeeh, J.; et al. Patterns of prohormone processing. Order revealed by a new procholecystokinin-derived peptide. J. Biol. Chem. 1992, 267, 1517−1521.

41. Goetze, J. P.; Hunter, I.; Zois, N. E.; Terzic, D.; Valeur, N.; Olsen, L. H.; Smith, J.; Plomgaard, P.; Hansen, L. H.; Rehfeld, J. F.; Balling, L.; Gustafsson, F. Cardiac procholecystokinin expression during haemodynamic changes in the mammalian heart. Peptides 2018, 108, 7−13.

42. Geijer, T.; Telkov, M.; Terenius, L. Characterization of human prodynorphin gene transcripts. Biochem. Biophys. Res. Commun. 1995, 215, 881−888.

43. Hwang, S. R.; O'Neill, A.; Bark, S.; Foulon, T.; Hook, V. Secretory vesicle aminopeptidase B related to neuropeptide processing: molecular identification and subcellular localization to enkephalin- and NPY-containing chromaffin granules. J. Neurochem. 2007, 100, 1340−1350.

44. Yasothornsrikul, S.; Toneff, T.; Hwang, S. R.; Hook, V. Y. Arginine and lysine aminopeptidase activities in chromaffin granules of bovine adrenal medulla: relevance to prohormone processing. J. Neurochem. 1998, 70, 153−163.

45. Douglas Lu, W.; Funkelstein, L.; Toneff, T.; Reinheckel, T.; Peters, C.; Hook, V. Cathepsin H functions as an aminopeptidase in secretory vesicles for production of enkephalin and galanin peptide neurotransmitters. J. Neurochem. 2012, 122, 512−522.

46. Zhou, A.; Bloomquist, B. T.; Mains, R. E. The prohormone convertases PC1 and PC2 mediate distinct endoproteolytic cleavages in a strict temporal order during proopiomelanocortin biosynthetic processing. J. Biol. Chem. 1993, 268, 1763−1769.

47. Friedman, T. C.; Loh, Y. P.; Birch, N. P. In vitro processing of proopiomelanocortin by recombinant PC1 (SPC3). Endocrinology 1994, 135, 854−862.

48. Funkelstein, L.; Toneff, T.; Mosier, C.; Hwang, S. R.; Beuschlein, F.; Lichtenauer, U. D.; Reinheckel, T.; Peters, C.; Hook, V. Major role of cathepsin L for producing the peptide hormones ACTH, beta-endorphin, and alpha-MSH, illustrated by protease gene knockout and expression. J. Biol. Chem. 2008, 283, 35652−35659.

49. Miller, R.; Aaron, W.; Toneff, T.; Vishnuvardhan, D.; Beinfeld, M. C.; Hook, V. Y. Obliteration of alpha-melanocyte-stimulating hormone derived from POMC in pituitary and brains of PC2- deficient mice. J. Neurochem. 2003, 86, 556−563.

50. Wang, L.; Sui, L.; Panigrahi, S. K.; Meece, K.; Xin, Y.; Kim, J.; Gromada, J.; Doege, C. A.; Wardlaw, S. L.; Egli, D.; Leibel, R. L. PC1/3 Deficiency Impacts Pro-opiomelanocortin Processing in Human Embryonic Stem Cell-Derived Hypothalamic Neurons. Stem Cell Rep. 2017, 8, 264−277.

51. Beinfeld, M. C.; Funkelstein, L.; Foulon, T.; Cadel, S.; Kitagawa, K.; Toneff, T.; Reinheckel, T.; Peters, C.; Hook, V. Cathepsin L plays a major role in cholecystokinin production in mouse brain cortex and in pituitary AtT-20 cells: protease gene knockout and inhibitor studies. Peptides 2009, 30, 1882−1891.

52. Minokadeh, A.; Funkelstein, L.; Toneff, T.; Hwang, S. R.; Beinfeld, M.; Reinheckel, T.; Peters, C.; Zadina, J.; Hook, V. Cathepsin L participates in dynorphin production in brain cortex, illustrated by protease gene knockout and expression. Mol. Cell. Neurosci. 2010, 43, 98−107.

53. Miller, R.; Toneff, T.; Vishnuvardhan, D.; Beinfeld, M.; Hook, V. Y. Selective roles for the PC2 processing enzyme in the regulation of peptide neurotransmitter levels in brain and peripheral neuro- endocrine tissues of PC2 deficient mice. Neuropeptides 2003, 37, 140−148.

54. Berman, Y.; Mzhavia, N.; Polonskaia, A.; Furuta, M.; Steiner, D. F.; Pintar, J. E.; Devi, L. A. Defective prodynorphin processing in mice lacking prohormone convertase PC2. J. Neurochem. 2000, 75, 1763− 1770.

55. Zhang, X.; Pan, H.; Peng, B.; Steiner, D. F.; Pintar, J. E.; Fricker, L. D. Neuropeptidomic analysis establishes a major role for prohormone convertase-2 in neuropeptide biosynthesis. J. Neurochem. 2010, 112, 1168−1179.

56. Burnett, L. C.; LeDuc, C. A.; Sulsona, C. R.; Paull, D.; Rausch, R.; Eddiry, S.; Carli, J. F.; Morabito, M. V.; Skowronski, A. A.; Hubner, G.; Zimmer, M.; Wang, L.; Day, R.; Levy, B.; Fennoy, I.; Dubern, B.; Poitou, C.; Clement, K.; Butler, M. G.; Rosenbaum, M.; Salles, J. P.; Tauber, M.; Driscoll, D. J.; Egli, D.; Leibel, R. L. Deficiency in prohormone convertase PC1 impairs prohormone processing in Prader-Willi syndrome. J. Clin. Invest. 2017, 127, 293− 305.

57. Jiang, Z.; Lietz, C. B.; Podvin, S.; Yoon, M. C.; Toneff, T.; Hook, V.; O'Donoghue, A. J. Differential Neuropeptidomes of Dense Core Secretory Vesicles (DCSV) Produced at Intravesicular and Extracellular pH Conditions by Proteolytic Processing. ACS Chem. Neurosci. 2021, 12, 2385−2398.

58. Nycander, M.; Estrada, S.; Mort, J. S.; Abrahamson, M.; Björk, I. Two-step mechanism of inhibition of cathepsin B by cystatin C due to displacement of the proteinase occluding loop. FEBS Lett. 1998, 422, 61−64.

59. Hwang, S. R.; Steineckert, B.; Yasothornsrikul, S.; Sei, C. A.; Toneff, T.; Rattan, J.; Hook, V. Y. Molecular cloning of endopin 1, a novel serpin localized to neurosecretory vesicles of chromaffin cells. Inhibition of basic residue-cleaving proteases by endopin 1. J. Biol. Chem. 1999, 274, 34164−34173.

60. Hwang, S. R.; Steineckert, B.; Toneff, T.; Bundey, R.; Logvinova, A. V.; Goldsmith, P.; Hook, V. Y. The novel serpin endopin 2 demonstrates cross-class inhibition of papain and elastase: localization of endopin 2 to regulated secretory vesicles of neuroendocrine chromaffin cells. Biochemistry 2002, 41, 10397− 10405.

61. Hwang, S. R.; Bundey, R.; Toneff, T.; Hook, V. Endopin serpin protease inhibitors localize with neuropeptides in secretory vesicles and neuroendocrine tissues. Neuroendocrinology 2009, 89, 210−216.

62. Colaert, N.; Helsens, K.; Martens, L.; Vandekerckhove, J.; Gevaert, K. Improved visualization of protein consensus sequences by iceLogo. Nat. Methods 2009, 6, 786−787.

6.7 Copyright Permission

CHAPTER 7 – CONCLUSION

7.1 Novel discoveries of cathepsin B's pH-dependent biochemical properties leads to the successful development of a neutral pH inhibitor probe of cathepsin B

We have demonstrated in my dissertation that cathepsin B (CatB) possesses unique pH dependent substrate preferences that are determined by the sequence of amino acids on the substrate, and we have uncovered structural basis for why CatB has such properties. By strategically selecting amino acid sequences preferred by CatB at either neutral or acidic pH, while simultaneously not being preferred by other cathepsins, we have successfully designed the substrate Z-Arg-Lys-AMC that can be preferably cleaved by CatB at neutral pH, without being cleaved by other related cathepsins. We then used a substrate-based inhibitor design approach to transfer these desired characteristics of the substrate into an inhibitor by replacing the AMC fluorophore with the cysteine protease reactive AOMK warhead. The AOMK warhead was chosen because it is known to irreversibly inhibit cysteine cathepsins without targeting other classes of proteases such as serine and threonine proteases. This was an especially important consideration for CatB selective inhibitor design, as there are serine proteases with similar dibasic specificity as CatB, such as PC1 and PC2, as shown in Chapter 6. Thus, although serine proteases PC1 and PC2 can cleave the substrate Z-Arg-Lys-AMC, it will not be inhibited by Z-Arg-Lys-AOMK. This approach has led to the successful rational design of the irreversible inhibitor Z-Arg-Lys-AOMK that is capable of selectively targeting CatB at neutral pH without targeting other related proteases. Future directions for this inhibitor will be to investigate CatB's extra-lysosomal role in disease pathogenesis such as Alzheimer's disease (AD) and traumatic brain injury (TBI), where CatB in the neutral pH of the cytosol due to lysosomal leakage is purported to be involved in the pathways of neuroinflammation and cell death (Figure 7.0).

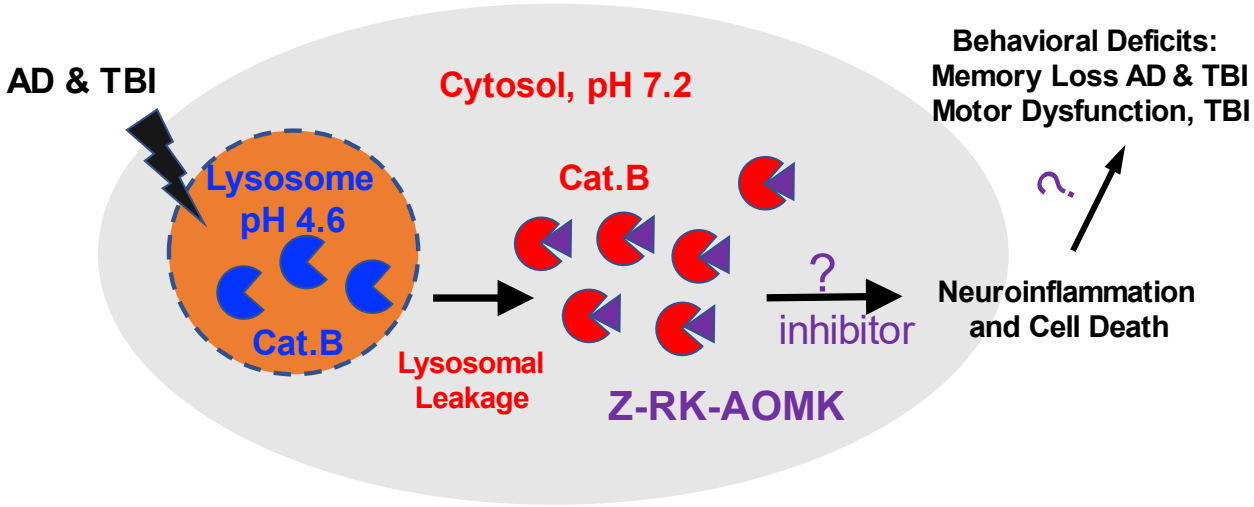

Figure 7.0 Successful Development of CatB Neutral pH-selective Inhibitor Z-Arg-Lys-AOMK. This inhibitor will be used to further study CatB's pathogenic role in the cytosol

Although we have demonstrated Z-Arg-Lys-AOMK's selectivity and potency for CatB at neutral pH in recombinant enzymes, we have not yet convincingly demonstrated its selectivity in cells. Future validation experiments include investigating this inhibitor's selectivity and potency in a cell lysate. If needed, additional modifications can be explored to improve selectivity and/or potency by using new insights gained from our recent unpublished studies that suggests that CatB significantly favors tripeptides over dipeptides, particularly by adding the amino acid norleucine to the existing scaffold Z-Arg-Lys-AOMK at its P3 position. Additionally, we recently profiled the cleavage specificity of other cathepsins by MSP-MS and found that CatB's specificity is clearly distinct from other cathepsins, shown by its preference for basic amino acids at the P2 position on the substrate that is not preferred by the other cathepsins, which gives us further confidence that the Z-Arg-Lys-AOMK inhibitor will selectively inhibit CatB in cells (Figure 7.1).

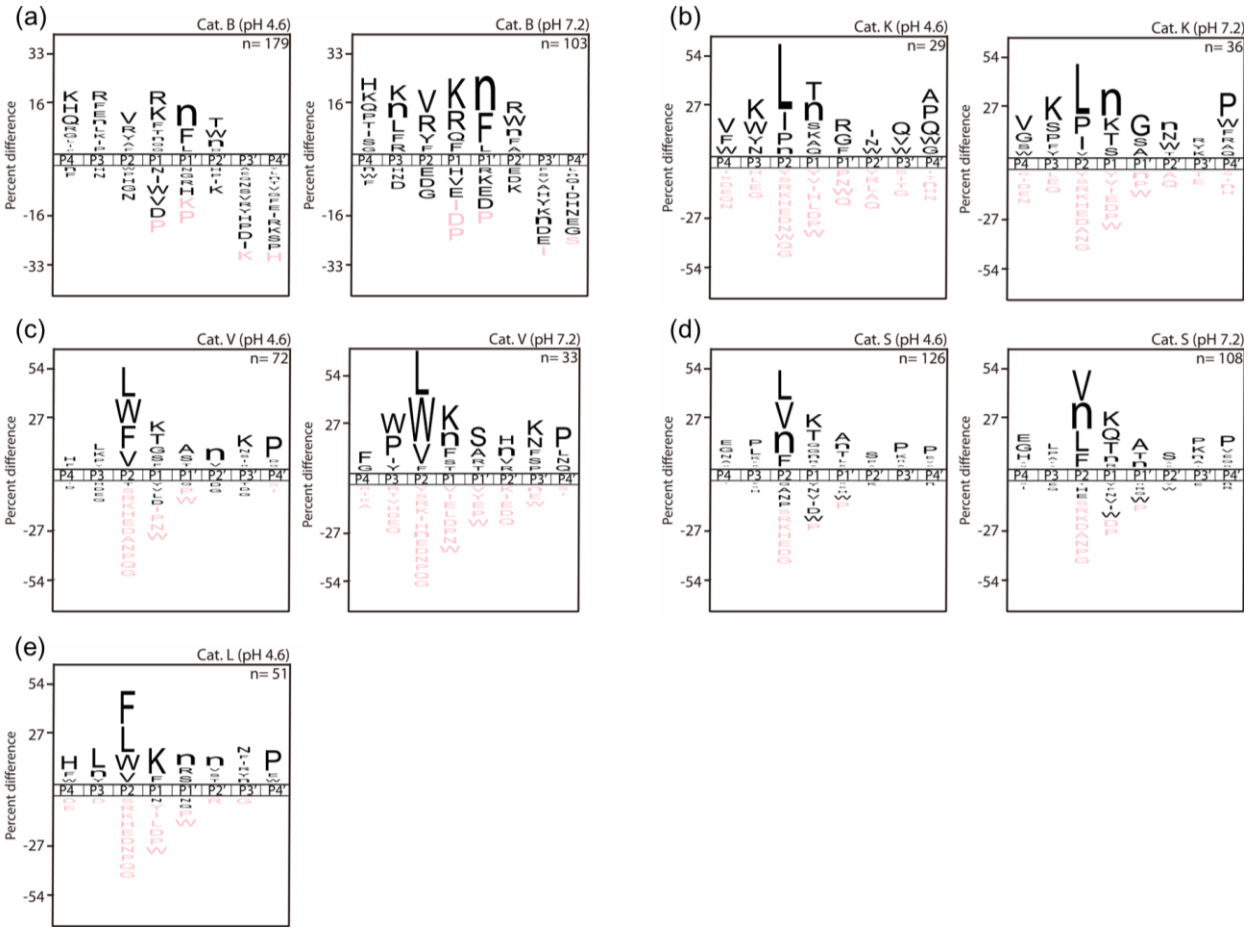

Figure 7.1 Cathepsin B, K, V, L, & S Cleavage Profiling Analysis by MSP-MS. Cathepsin B, K, V, L, & S (human, recombinant) was incubated with MSP-MS peptide library. (a) Cathepsin B at pH 4.6 and pH 7.2 (b) Cathepsin K at pH 4.6 and pH 7.2 (c) Cathepsin V at pH 4.6 and pH 7.2 (d) Cathepsin S at pH 4.6 and pH 7.2 and (e) Cathepsin L at pH 4.6 only (cathepsin L has no activity at pH 7.2). CatB show distinct preferences for P4 to P4' residues of peptide cleavage sites, particularly at the P2 position. Data shows basis for why Z-Arg-Lys-AOMK specifically inhibits CatB, as the Arg at P2 is shown to be favored by CatB but unfavored by all other related cathepsins.

7.2 Future investigations of synaptic dysfunction in human diseases

In Chapters 5 and 6, we explored the pH-dependent cleavage properties of the diverse proteases found in dense core secretory vesicles (DCSV) of neurons and showed that neuropeptides can be processed differently at the acidic environment in the secretory vesicle at pH 5.5 and the extracellular environment at pH 7.2. This further demonstrated that the different pH environment of proteases must be considered when investigating its normal functional role in cells. Interestingly, we found strong detection of activity resembling CatB in DCSV, especially when

we investigated its activity at neutral pH. Since lysosomal leakage involves the leakage of proteases, which includes CatB, we can envision how lysosomal leakage in neurons may also impact neuropeptide processing that could lead to synaptic dysfunction. This is the beginning of studies investigating how lysosomal leakage is mechanistically linked to secretory vesicle dysregulation and synaptic dysfunction observed in brain disorders in AD and TBI (Figure 1.0).

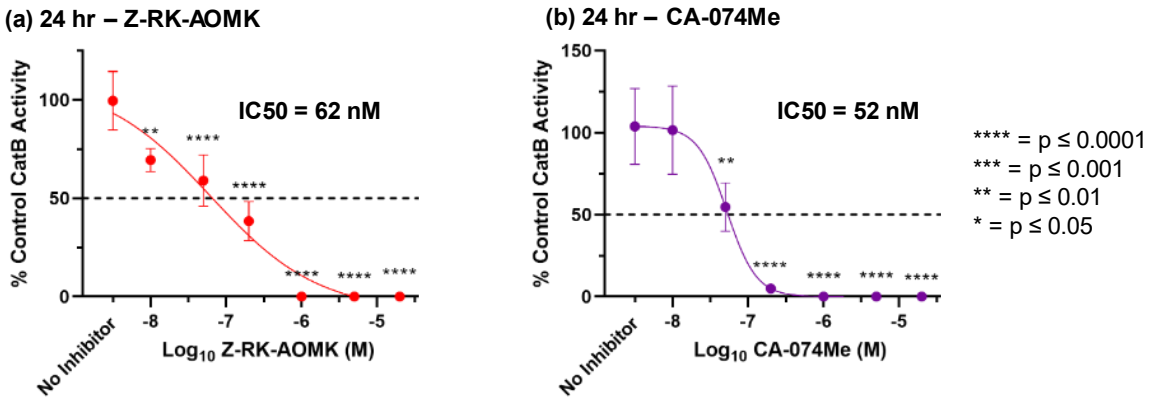

Figure 7.2 Assessing the Concentration-dependent Inhibition of Intracellular CatB in SH5Y cells using Z-Arg-Lys-AOMK and CA-074Me. (a) SH5Y cells incubated with serial diluted concentrations of Z-Arg-Lys-AOMK for 24 hours and (b) SH5Y cells incubated with serial diluted concentrations of CA-074Me for 24 hours. Error bars indicate +/- SD, n=3.

7.3 Future Investigations of Extra-lysosomal CatB

With the ample evidence that exists for CatB pathogenicity in AD, TBI, and other related diseases, this newly developed inhibitor will serve to elucidate the mechanism of how CatB might play a role in the pathogenesis of those diseases. With the validation of Z-Arg-Lys-AOMK as a selective extra-lysosomal CatB inhibitor, the role of extra-lysosomal CatB will be investigated in cellular models such as the Aβ oligomer induced lysosomal leakage models of neuronal cells in Alzheimer's disease (Figure 7.0). Preliminary cellular studies using this inhibitor demonstrated that it can selectively and potently inhibit intracellular CatB in SH5Y cells (Figure 7.2). Next would be to identify the biological substrates for CatB in the cytosol when lysosomal leakage occurs. To further aid with this endeavor, we have developed a modified version of the inhibitor, N_3-Peg_3-RK-AOMK to be used as a potentially versatile probe within cells (Figure 7.3).

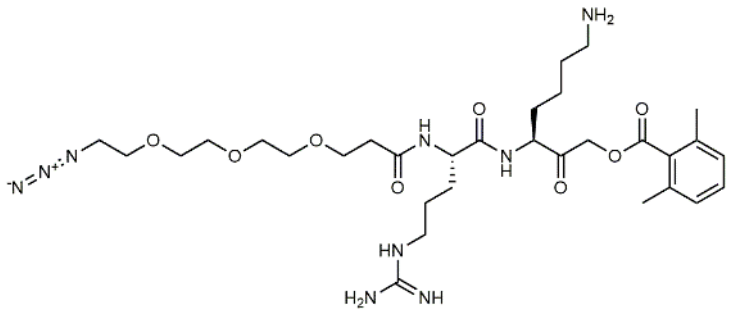

Figure 7.3 N_3-Peg_3-RK-AOMK is a Modified Version of Z-Arg-Lys-AOMK. This will be used as a versatile probe in cellular imaging of extra-lysosomal CatB when used in conjunction with fluorescent alkynes.

For visualization of CatB during lysosomal leakage, we plan to use Cy5-alkyne via copper-catalyzed click reaction to the azide group of N_3-Peg_3-RK-AOMK. This will be used as a fluorogenic activity-based probe for selective labeling of extra-lysosomal CatB in cells. Currently, we are validating the selectivity of this probe by using alkyne-beads in a cell lysate incubated with the N_3-Peg_3-RK-AOMK and using mass spectrometry to identify all the enzymes that has been covalently bound to the azide probe. We predict that mostly CatB will be identified through this approach, thus confirming its selectivity.

7.4 Future Investigations of CatB in Animal Models of AD, TBI, and Beyond

Finally, we are interested in investigating the role of CatB in animal models of neurodegenerative disease. As it was previously shown in our laboratory, gene knockout of CatB in AD and TBI mouse models greatly ameliorated the pathology commonly seen in AD and TBI such as memory loss and behavioral deficits, which has validated CatB's role in the disease pathogenesis of AD and TBI, but without a clear mechanism of how CatB is involved. Based on the lysosomal leakage hypothesis of AD and TBI disease pathogenesis, we anticipate that selective chemical inhibition of cytosolic CatB will achieve similar results (Figure 7.0). We are currently setting up the plans to evaluate our inhibitor's pharmacokinetic, pharmacodynamic, and efficacy properties in neurodegenerative mouse models. Depending on what we uncover, this can eventually lead to novel therapeutic pharmacological treatment options of AD and TBI in humans.